A thesis entitled

"A study of some electroactive, thin organic films prepared by plasma and electrochemical techniques"

submitted by

Jeffrey Graham Eaves, B.Sc. Hons (Dunelm)

a Candidate for the Degree of Doctor of Philosophy

Graduate Society,
University of Durham

April 1986

"William, it was really nothing"

(Morrissey, 1984)

MEMORANDUM

The work described in this thesis was carried out at the University of Durham between October 1982 and September 1985. Except where acknowledged by reference, this is the original work of the author and has not been submitted for any other degree.

Some of the work described in this thesis has formed the subject of the following publications:

"ESCA studies of Metal-Containing Plasma Polymers II: Plasma Polymerization of Ferrocene, Vinylferrocene and Dimethylaminomethylferrocene".

H.S. Munro and J.G. Eaves,

J.Polym.Sci., Polym.Chem.Ed., 23, (1985), 507.

and

" Electroactive Thin Films from the Anodic Electropolymerization of Iron (II) and Ruthenium (II) Tris(N-bipyridylpyrrole) Complexes"

Jeffrey G. Eaves, Hugh S. Munro and David Parker,

J.Chem.Soc.Chem.Commun., (1985), 684.

ACKNOWLEDGEMENTS

I wish to thank my supervisors, Dr. H.S. Munro and Dr. D. Parker for their help and enthusiasm and Dr. D. Parker for assistance in the syntheses described in Chapters Two and Three. Also the SERC for the provision of a research grant and the RSC for the provision of some equipment.

I am indebted to my friends and colleages in the ESCA lab., Rob Allaker, John Banks, Bill Brennan, Andy Fowler, Heiner Grünwald, Steve Johnson, Bob Short and Clare Till.

I wish to express my thanks to all the technical staff at the Chemistry Department, particularly Colin Greenhalgh, Mike and Vince (mass spectrometry), Ray and Gordon (glass-blowing) and George Rowe who maintained the ES300 spectrometer and built some of the electrical equipment used in this study. Thanks are also due to the reaction kinetics research group for the loan of their storage CRO.

I am particularly indebted to Dr. M.J. Silvester for the disclosure of his discovery of the electrode deposit derived from perfluorocyclopentene, which enabled the studies described in Chapter Five to be undertaken.

The Applied Physics Department at Durham, particularly Dr. G. Russell and Awan, were most helpful in assisting with electron microscopy and conductivity measurements. Jackie Nicol and Peter Lux recorded the FT-IR spectra described in this thesis.

I am grateful to Dr. Z.V. 'Stan' Hauptmann and Dr. Steve Johnson for discussions about electrochemistry and ESCA. Also Prof. D.T. Clark, a distant but coherent source of inspiration. Mrs. Marion Wilson typed my script.

Most of all I wish to thank my parents and Tracey for their support.

A STUDY OF SOME ELECTROACTIVE, THIN ORGANIC FILMS PREPARED BY PLASMA AND ELECTROCHEMICAL TECHNIQUES

by
JEFFREY GRAHAM EAVES

ABSTRACT

Electron Spectroscopy for Chemical Applications (ESCA) and Cyclic Voltammetry (CV) have been used to study the surface and electrochemistries of electroactive, thin organic films.

A method is developed for the preparation of such films by the synthesis of a molecule containing both an electroactive centre (ferrocene or iron (II) or ruthenium (II) trisbipyridyl) bonded to an electropolymerizable unit (pyrrole). The surface chemistries of polypyrrole, polyaniline and electrodes potentiostatted in ferrocene solutions were also investigated and results compared to previous studies where possible.

The poly-Ru(II)- and particularly the poly-Fe(II)- films are stable to electrochemical cycling between the +2 and +3 oxidation states. The poly-Fe(II)-, and probably the poly-Ru(II)-, trisbipyridyl films have charge transfer diffusion coefficients similar to those previously reported for other films containing similar redox centres. Redox conductivity has been demonstrated for an aged sample of the poly-Fe(II)- film.

Electroactive films, prepared by two different methods of plasma polymerization of substituted ferrocene monomers are described. In each case the ferrocene/ferricenium electroactivity is degraded by repeated potential cycling. The incorporation of ferrocene into a plasma polymer does not necessarily produce an electroactive film.

A preliminary investigation of the surface and electrochemistry of electrode deposits, prepared by cathodic reduction of perfluorocyclopentene, is described. The deposits appear similar in some respects to cathodically reduced PTFE.

CONTENTS

CHAPTER ONE

AN INTRODUCTION TO

CHEMICALLY MODIFIED ELECTRODES

1.1 Introduction

Electrode surface modification may be interpreted in many different ways. A general distinction between a 'modified-electrode' and an ordinary electrode is that a thin film of some chosen surface coating has been applied. This prevents direct contact between the uncoated electrode surface and the bulk electrolyte.[1]

Modified electrodes may be placed into two main categories: those for which the surface coating contains electrochemically reactive (electroactive) molecules (*e.g.* ferrocene,[2a] viologen,[2b] *etc.*), such that the modified electrode displays an innate electrochemical response in an inert electrolyte solution, and those for which the surface coating has no native electrochemistry (*e.g.* certain plasma polymer coatings[3]). The first class has provoked most interest both in fundamental studies of the kinetics and mechanism of charge transport in a surface immobilized film, and in its potential application to catalysis[21] and analysis.[43] The electroactive coatings may be further categorised into those which form essentially monolayer coverages and those which form multilayers, the distinction arising from the method of preparation. Electroinactive coatings may also be used in electrocatalysis[4], in biomedicine[5] and in chemical sensor devices.[3]

Some electrochemically generated conducting polymers (*e.g.* polypyrrole, polythiophene) may also be distinguished from the electrochemically reactive coatings. Although they exhibit intrinsic electrochemical reactions corresponding to net oxidation or reduction of the polymer film, such behaviour

is not the prime focus of study. Surface modification of polypyrrole coated electrodes with electroactive molecules has been achieved[6,7] as has polymerization of pyrrole monomers with redox active substituents.[2b,8-10] These coatings fall clearly into the electroactive class.

The systematic investigation of modified electrodes was initiated in 1975 by Murray and coworkers who used silane chemistry to covalently attach amine molecules to the surface hydroxyl groups of SnO_2 electrodes.[11] Comprehensive reviews of the work completed since 1975 have been published.[1,12-15]

1.2 Preparation of modified electrodes

The surface coating of electrodes can be performed in at least three distinct ways:

1. By direct chemical bonding to the electrode surface.
2. By adsorption.
3. By multilayer film (usually polymer) deposition.

The classifications of methods (1) and (2), chemical bonding and adsorption, are used in accordance with common practice in the modified electrode literature.[1,12-15] It is acknowledged however, that the attachment of a monolayer to a surface by a chemical bond may otherwise be termed chemisorption and that the evaporation of a high molecular weight polymer onto a surface is often referred to as film-casting and not adsorption.

All the coatings studied in this work have been produced by two variants of method (3); namely plasma and electrochemical 'polymerization'. Only a brief description of

methods (1) and (2) is given below, however many examples of the use of these methods have been documented.[1,12,13,15]

1.2.1 Chemical Bonding

The first recognized report of a deliberately chemically modified electrode described the use of covalent bond formation to link molecules to an electrode surface.[11]

The chemical bonding method makes use of the hydroxyl groups present on the surface of metals, metal oxides and elemental semiconductors, and on the variety of oxygen functionalities which may be induced on carbon surfaces (*e.g.* by oxygen glow-discharge treatment), in forming covalent links. Three of the most successfully applied bond forming reactions are outlined below.

(A) Silanization

The reaction of organosilanes with the surfaces of silica or alumina particles had been used prior to 1975 for the improvement of chromatographic column performance. The reaction may be represented as:

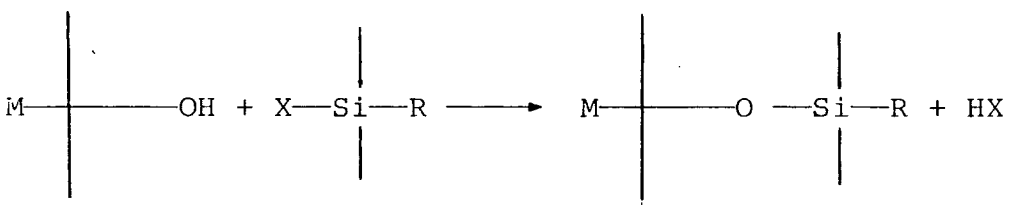

M = Metal or Semiconductor

X = OH or Cl

R = *e.g.* amine, electroactive molecule.

Trihalosilanes were found to be the most reactive and give rise to the possibility of silicon binding to as many as three surface sites in monolayer formation. Alternatively,

if small amounts of water are present in the reaction medium, polymeric multilayers may be formed. The R group may be an electroactive molecule (*e.g.* ferrocene[16]), or may itself be functionalizable. If R is an amine for example, then an electroactive molecule may be bound by amide formation.

(B) Reaction with cyanuric chloride

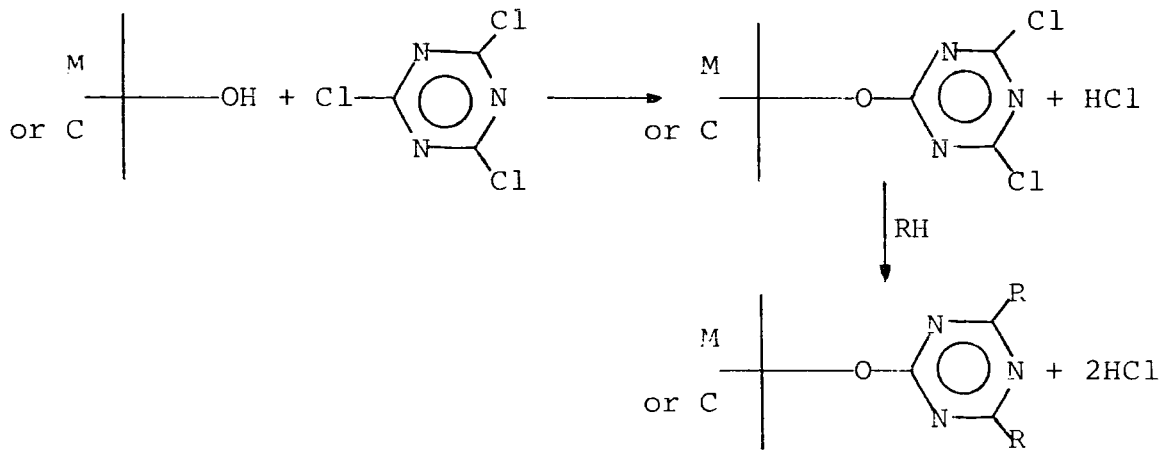

RH = electrochemically reactive amine or alcohol.

This method of preparation has apparently been most successful with carbon electrodes.[12,17]

(C) Amide bonding to oxidized carbon electrodes

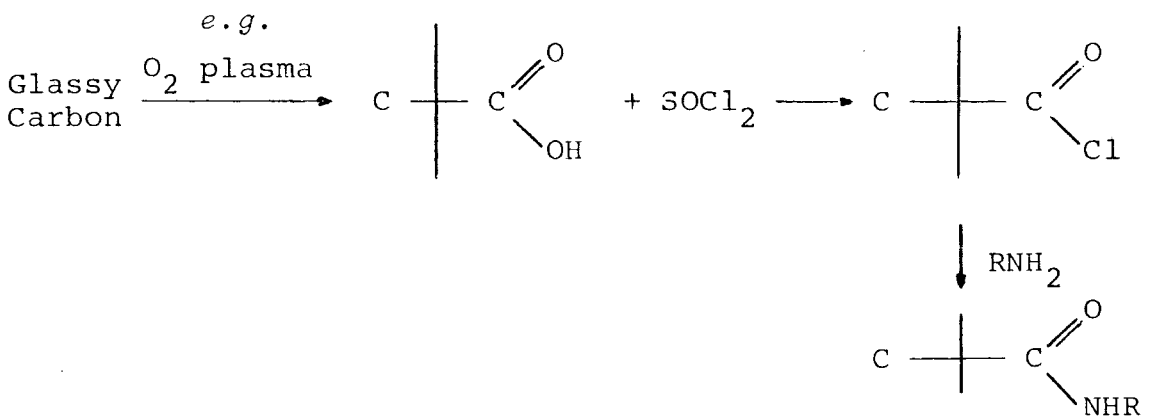

RNH_2 = electrochemically reactive amine, *e.g.* tetra-(aminophenyl)porphyrin.[18]

1.2.2 Adsorption

Adsorption onto an electrode surface from solution is the simplest way to prepare a modified electrode. The adsorbed species is most commonly polymeric (*e.g.* polyvinylferrocene,[19] polyvinylpyridine[20]) and adheres to the electrode by a combination of chemisorption and low solubility in the chosen electrolyte solution. Once adsorbed onto the electrode surface a polymer may be cross-linked to further reduce its solubility.[21] In addition to passive adsorption (*e.g.* dip or spin coating) by solvent evaporation, preferential adsorption of the oxidized form of a polymer from solution has been demonstrated in the electro-adsorption of polyvinylferrocene.[19]

1.2.3 Polymer multilayer deposition

(A) Plasma Polymerization

(i) Plasma Chemistry

A plasma is a partially ionized gas consisting of neutral molecules, atoms, radicals, ions, excited states of these species, metastables (excited states with significant lifetimes) and electrons. A plasma is an extremely reactive medium. A true plasma is electrically neutral, a condition which is met when the gas discharge volume is greater than the Debye length (λ_D) which defines the distance over which a charge imbalance may exist.[22,23] This criterion is invariably satisfied in the laboratory experiment. The excited states may decay by photon emission and in general plasmas are intense sources of electromagnetic radiation, particularly in the ultraviolet spectral regions. In

addition a smaller output of visible light gives rise to the characteristic colour of a given plasma and hence the name 'glow-discharge'.

Plasmas may be categorized by their electron temperature and electron density[22] as shown in Figure 1.2.1. Two classes of plasma may be defined: the 'hot' or equilibrium plasma in which the electron and gas temperatures are approximately the same ($>5\times10^{3}$K) and the 'cool' or non-equilibrium plasma for which the electron temperature is far greater than the gas temperature. There is a distribution of electron energies in the plasma and, if Maxwellian, the average electron energy is given by $4kT/\pi$, where T is the electron temperature and k is the Boltzmann constant.[26] Thus for a 'typical' non-equilibrium plasma with an electron density of *ca.* 10^{10} cm^{-3} and an average electron energy of 1eV, the electron temperature is *ca.* 9,100K whilst the gas temperature is little above ambient. It is this feature which makes the glow discharge suitable for chemical reactions involving organic molecules since the electron energies available (typically 1-10eV, see Figure 1.2.2) are sufficient to cleave molecular bonds but the gas temperature is low enough to prevent thermal decomposition. The use of the glow discharge plasma in organic synthesis has been reviewed.[24,25]

In the laboratory a glow discharge is conveniently obtained by the application of an electric field to a gas at low pressure (10^{-1} - 10^{-2} torr). Most often a vacuum line is used giving a dynamic flow of gas into and out of the discharge region. The power input to sustain the plasma may be D.C., A.C. (low frequency) or radiofrequency (R.F.).

PLASMAS FOUND IN NATURE AND IN THE LABORATORY

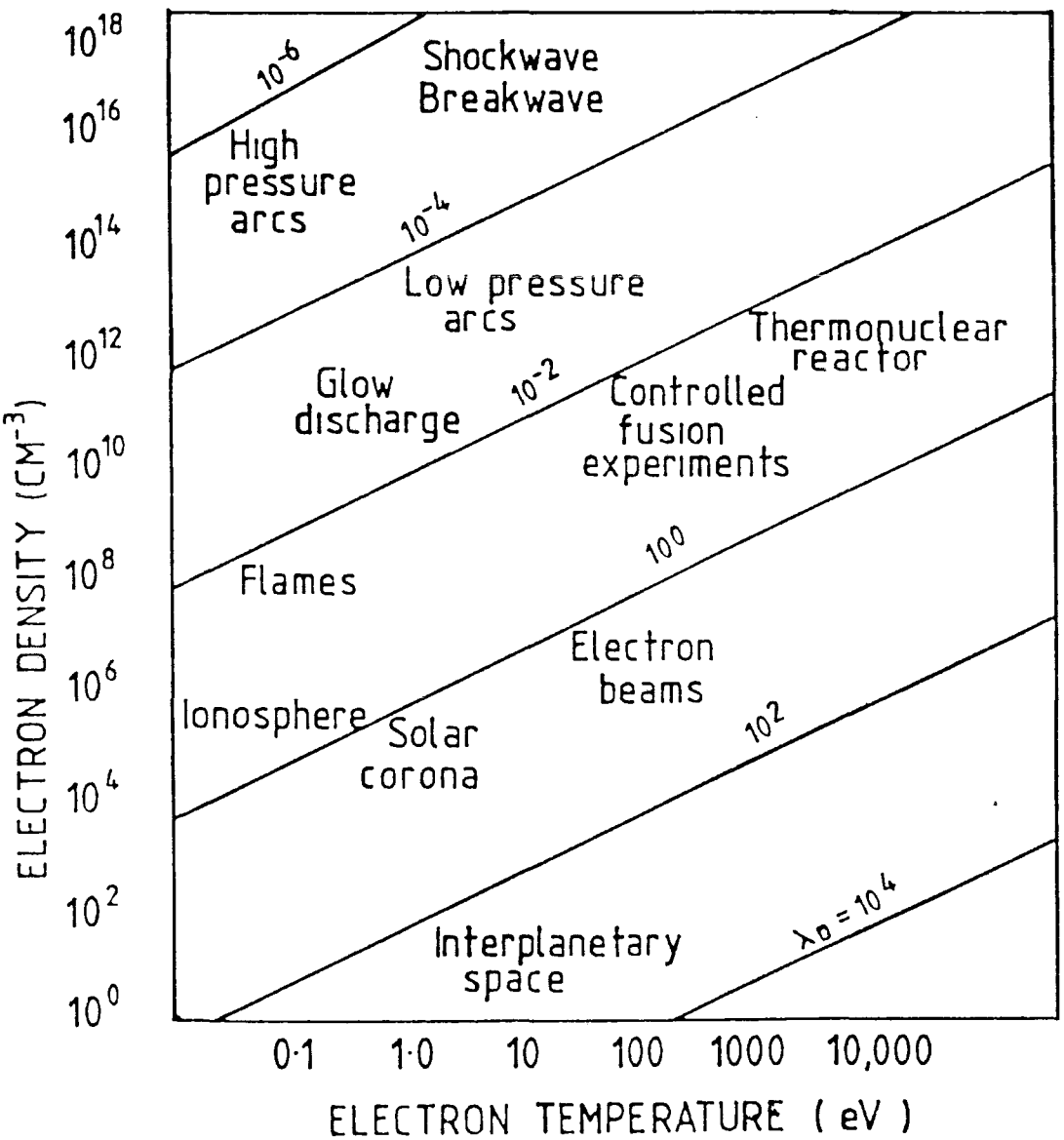

FIGURE 1.2.1 Categorization of plasmas by electron temperature and electron density.

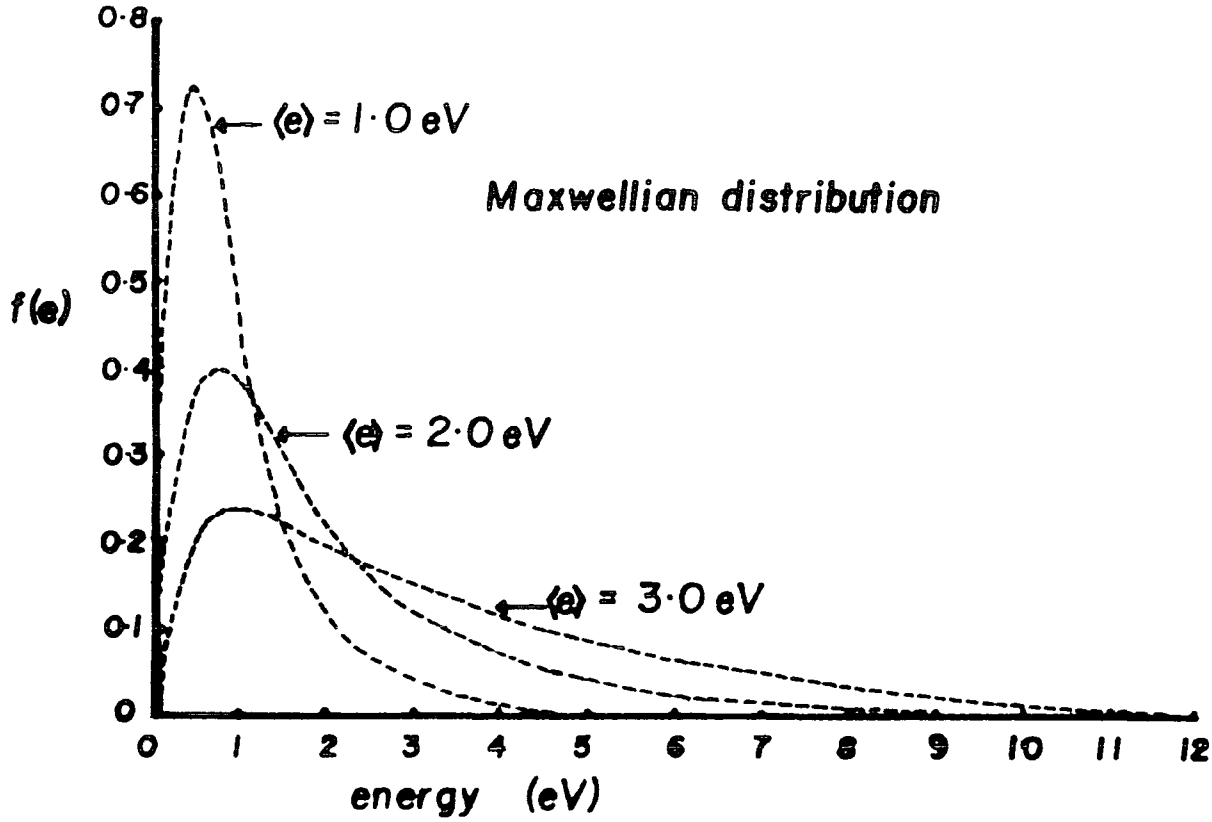

FIGURE 1.2.2 Maxwellian distributions of electron energies in a 'typical' plasma.

For R.F. power sources (>1 MHz) the power may be coupled to the plasma reactor by an externally placed coil (inductive coupling) or pair of electrodes (capacitive coupling), thereby preventing the interaction of the plasma with the metal electrodes which would otherwise lead to sputtering or etching from and/or deposition onto the electrode surfaces.

Following gas phase ionization (natural or induced) electrons are accelerated by the applied electric field and gain enough energy to produce further ionization *e.g.* $e^- + Ar \longrightarrow 2e^- + Ar^+$. Electron impact ionization is thought to be the most important process in maintaining the glow-discharge.[26] Many types of particle interaction are possible in a plasma, such as electron-atom, electron-molecule, metastable-atom, giving rise to several ionization, excitation, recombination and deexcitation processes.[22,23]

(ii) Plasma Polymerization

(a) Introduction

Plasma polymer is the generic name given to the thin films which invariably form on any substrate placed in the glow-discharge of almost any organic or organometallic vapour. These films are thin (sub-micron, thicker films are cracked) and typically are highly cross-linked, insoluble, adherent and pin-hole free. Plasma polymerization is a means of generating novel materials and not a novel method for the preparation of conventional polymers. Two general phenomena of plasma polymerization which illustrate this statement are:

(1) A plasma polymer most often bears little chemical resemblance to the 'monomer' from which it was formed. This dissimilarity is usually a result of rearrangement and/or elimination reactions in the plasma phase. For example plasma polymerized perfluorobenzene contains CF_3, CF_2 and quaternary C centres as well as CF groups.[27]

(2) 'Monomers' which do not form conventional polymers may be plasma polymerized, *e.g.* saturated hydro-[28] and fluorocarbons.[27]

(b) Mechanism

The detailed mechanism of plasma polymerization is incompletely understood and may vary with plasma conditions as well as choice of monomer. Certain relevant features may be identified:

(1) It was stated in the previous section that electron impact ionization is the most important step in creating and sustaining the plasma. However, ionization is not necessarily the primary

step in plasma polymerization. Typical bond dissociation energies of organic compounds lie well below their ionization energies and so bond cleavage occurs far more frequently than ionization. The concentration of radicals in a plasma has been estimated to be typically 10^5-10^6 times that of ions.[29] This ratio gives no information about the relative reactivities of ions and radicals but in certain cases the amount of polymer formed is too great for ions to be solely responsible.[30]

(2) An important characteristic of plasma polymers is that they contain large quantities of trapped free radicals. In principle these radicals could be generated as a consequence of the plasma polymerization process itself or by the action of the plasma on the deposited film. Non-polymerizing gas plasmas induce unpaired spins in glass samples, as has been demonstrated using esr spectroscopy,[23] so the latter possibility may not, *a priori*, be ruled out. By comparing the esr signals from glass substrates coated with plasma polymers with the signals from the glass substrates after removal of the polymers, Yasuda[23] has shown that most of the trapped radicals are produced as a direct consequence of the plasma polymerization process.

(3) The inadequacies of classical polymer growth mechanisms (step or chain growth) in explaining the growth of plasma polymers has been highlighted and a rapid step growth mechanism has been proposed by Yasuda to rationalize plasma polymer formation.[23]

(c) Variation of the plasma parameters

The variable parameters in the plasma polymerization experiment are the discharge power (W) and the monomer flow rate (F). A critical wattage has been defined by Yasuda (essentially the minimum power input for polymerization under 'full glow' conditions) and it has been emphasised that this critical wattage depends both on the flow rate and on the nature of the monomer, in particular on its molecular weight (M). Thus, in order to compare plasma conditions for different monomers a composite parameter, W/FM, which is a measure of the energy input per unit mass, should be considered and not simply the power input, W.[23]

(d) Competitive ablation and deposition

So far only deposition from a plasma has been considered, however plasmas are also commonly used to remove or 'ablate' material from a surface. The removal process may be purely physical, *e.g.* the cleaning of a carbon electrode in an inert gas plasma,[31] when it is referred to as sputtering, or may involve the formation of a new and volatile compound when the term plasma-etching is preferred, *e.g.* the etching of silicon in a CF_4 plasma.[32] The combined processes of ablation and polymerization are not independent and, particularly in the case of a perfluorocarbon plasma, loss of deposited material may be a significant process. The overall deposition process is thus the result of competitive ablation and polymerization (CAP).

(e) Characterization

Plasma polymer films are ultra-thin, adherent and highly insoluble, these properties are desirable for a coating material but make characterization by standard techniques, such as transmission infra-red and solution n.m.r. spectroscopies, difficult. ESCA(Electron Spectroscopy for Chemical Applications), also termed X-ray photoelectron spectroscopy, has been shown to be an excellent tool for the analysis of plasma polymer structure, especially for films produced from fluorocarbons since the chemical shift range allows for identification of CF_3, CF_2 and CF groups.[27,33] For plasma polymers produced from organometallics ESCA may be used to determine the oxidation state(s) of the metal.[34] Other characterization techniques are listed in Section 1.4.

There is a growing awareness of the need to characterize the plasma phase more completely than has been done previously and this has led to a branch of research commonly referred to as 'plasma diagnostics'. One of the aims of plasma diagnostic research is to identify the precursor species to polymer formation. Mass spectrometry has been used both to study ions formed in the plasma and to study effluent gas from the plasma using post-plasma ionization.[23] Unfortunately analysis of the data obtained does not straightforwardly lead to identification of the precursor species since any species detected in abundance may owe their high concentration to an inertness toward, rather than an importance in, plasma polymerization. Optical emission spectroscopy has also been used as a plasma diagnostic tool but to some extent the same problem applies.

(f) Plasma polymers as electrode coatings

Electrode coatings prepared by plasma polymerization include both categories defined in Section 1.1.

(1) Electrochemically active coatings

Only plasma polymers produced from ferrocene or substituted ferrocene monomers have shown electrochemical activity which may be associated with that of the monomer.[12] Ferrocenes are thus unusual in that a significant amount of monomer structure remains intact in the plasma polymer.

Electroactive films have been produced by the partitioning of redox active ions into pre-deposited plasma polymer films. Doblhofer has used plasma copolymerization of ammonia and allylamine to give a film of high amine content. This film strongly partitioned hexacyanoferrate ions from solution to produce an electrochemically active coating.[35]

(2) Electrochemically inactive coatings

Griggs and coworkers have used electrodes coated with plasma polymerized propylene films as oxygen sensors.[3] The polarographic response for oxygen reduction at a coated microplatinum electrode at different oxygen concentrations showed only very small changes over a three month period, whereas uncoated freshly cleaned electrodes gave an unstable response.

Yasuda has studied the suitability of plasma polymerized methane films for possible use as microelectrode insulators in neurophysiology. The film adhesion was tested by subjecting the coated electrode to continuous cyclic voltammetry.[5]

In summary plasma polymerization is a general method for the production of thin films but the mechanism of film formation usually involves rearrangement or fragmentation of a significant number of the monomers. Plasma polymerization may not, therefore, be generally applied to the production of films with electroactivity characteristic of the monomer unless discharge conditions can be found which limit the amount of monomer disruption. It is possible that such conditions may be obtained by copolymerization. For example it has been demonstrated that the plasma rearrangement of perfluorobenzene to yield a polymer containing CF_3 and CF_2 groups as well as CF can be inhibited by copolymerization with either tetramethyltin [36a] or benzene (C_6H_6),[36b] to give a deposit containing CF as the only major fluorocarbon component.

(B) Electrochemical Polymerization

The rationale behind the production of electrochemically active films by electrochemical polymerization is to synthesise a monomer which contains an electroactive molecule bound to an electropolymerizable unit, such that polymerization may be induced at the electrode surface by either oxidation or reduction. The electropolymerizable units which have been used with the greatest success are substituted vinyl compounds, pyrroles, anilines (or phenanthrolines) and, to a lesser extent, phenols.[1,12] One of the advantages of the electrochemical polymerization method is that the amount of material deposited may be easily controlled by the amount of charge passed during electrolysis.

(i) Vinyl Compounds

(a) Reductive Polymerization

In 1981 Murray and coworkers reported the reductive electropolymerization of a series of ruthenium and iron complexes with vinylpyridine (vpy) and vinylbipyridine (vbpy) ligands.[37] It was known that polymerization of 4-vinylpyridine could be anionically initiated[38] and thus it was reasoned that complexes such as $[Ru(bpy)_2(vpy)_2]^{2+}$ (bpy=4,4´ bipyridine), for which reduction is ligand rather than metal centred,[37] could be polymerized by electrochemical reduction. Polymerization of $[Ru(bpy)_2(vpy)_2]$,$^{2+}$ $[Ru(vbpy)_3]^{2+}$, $[Ru(bpy)_2(vpy)Cl]^{+}$, $[Ru(bpy)_2(vbpy)]^{2+}$ and $[Fe(vbpy)_3]^{2+}$ was successfully initiated by reduction and produced coated electrodes which showed an electrochemical response characteristic of the monomers. The deposits were found to be mechanically stable and insoluble in common organic solvents and concentrated nitric acid.[39] Significant effects on the deposition process were found by alteration of the deposition conditions.[40] It was noted:

(1) that deposition by reductive cycling led to more even film formation than reduction at constant negative potentials;

(2) that the amount of polymer deposited increased with (a) monomer concentration, (b) number of ligands substituted with vinyl groups, (c) number of reductive cycles, and (d) extent of reduction (by one or two electrons per monomer).

It was stated[40] that in most cases the one electron

reductions correspond to radical anion formation at the bipyridine ligands, *e.g.*

$$[Ru(bpy)_2(vpy)_2]^{2+} \xrightarrow{e^-} [Ru(bpy)(bpy^{\cdot-})(vpy)_2]^{+}$$

Thus in some instances it was reasoned that the vinyl containing ligand would not be the first to be reduced, for example bipyridine is reduced at a less negative potential than vinylpyridine.[40] Murray considered that polymerization was initiated by radical anion formation at a vinyl group,[39] but that this could be formed either by direct reduction of the vinyl substituted ligand (*e.g.* $[Ru(vbpy)_3]^{2+}$) or by indirect reduction.[40] In the latter case it was proposed that an intramolecular redox equilibrium would provide a small concentration of the thermodynamically less favoured oxidation-state isomer with the added electron localised on the vinyl ligand, *e.g.*

$$[Ru(bpy)(bpy^{\cdot-})(vpy)_2]^{+} \rightleftharpoons [Ru(bpy)_2(vpy)(vpy^{\cdot-})]^{+}$$

Not surprisingly the deposition efficiency was found to be higher for the direct reduction cases. A mechanistic scheme for deposition was proposed which allowed for classical chain growth polymerization *via* radical or anionic initiation or deposition *via* successive hydrodimerization steps or *via* radical coupling dimerization followed by chain growth polymerization. Both pure anionic polymerization following dimerization of the initially created radical anion and concomitant radical and anionic chain growth, under conditions where dimerization does not take place, have previously been proposed as the mechanism for the reductively electroinitiated polymerization of vinyl compounds in solution.[41] It was concluded that hydrodimerization was not the only mechanism for

deposition since some deposit was formed even for those complexes which contained only one vinyl ligand and for which only one hydrodimerization is possible inevitably yielding a soluble product. By performing a copolymerization experiment with two similar complexes, each with two vinyl ligands, one of which did not polymerize on its own, Murray concluded that hydrodimerization was mainly responsible for deposition of complexes with multiple vinyl ligands since very little of the non-homopolymerizing complex was incorporated in the deposit.

It was suggested that the main reason for the very low deposition obtained with monovinyl complexes was not the inability to deposit *via* hydrodimerization but rather that linear chain growth would require very close approach of the bulky bipyridine complexes.[39,42] In contrast complexes with two or more vinyl ligands have the opportunity to form branched chain polymers allowing for greater spatial separation of the individual complexes.

Polymerization efficiency for two electron reduction, defined as the number of polymerized monomer molecules deposited on the electrode surface, divided by the number of monomers reduced, varied between 0.04%, for indirect reduction of a monomer with one vinyl ligand, to 103%, for direct reduction of a monomer with two vinyl ligands.[40] Efficiency as low as even 103% would indicate that chain propagation was negligible in deposition. However, this figure takes no account of polymer formed in solution which was observed, but not quantified, in certain circumstances especially at long reduction times. In contrast in a study

of the reductively electroinitiated, solution polymerization of acrylonitrile Funt and Williams[41] found that for each one electron monomer reduction over three polymer molecules of molecular weight 4000 were produced. Defining polymerization efficiency as above this means that (3x4000)÷53 molecules of acrylonitrile were polymerized for each one reduced, an efficiency of 22,500%. A comparison of polymerization efficiencies for deposition by cycling the electrode potential, where initiation is possible only for part of the electrolysis time, to that by reduction at constant potential was not reported.

Murray has now described the successful deposition of more than thirty different electroactive films by electrochemical reduction of substituted vinyl compounds.[37,40,43] In addition both copolymerizations and successive depositions, to give bilayer films with rectifying properties[37,44] (see Section 1.3), have been reported.

(b) Oxidative polymerization

There are a few reports of the preparation of modified electrodes by the oxidative electrochemical polymerization of vinyl compounds. Spiro and Macor found that several metal complexes of protoporhyrin IX, the most ubiquitous naturally occurring porphyrin which has two vinyl groups conjugated to the porphyrin π system, could be deposited by electrochemical oxidation but not by reduction.[94,95] The deposited films displayed stable oxidative electrochemistry, characteristic of the monomer, in dichloromethane. In aqueous solution oxidative attack of the porphyrin caused rapid loss

of electroactivity. Films of up to approximately 1500 monolayer equivalents could be deposited. From the following observations the authors suggested that the mechanism of film formation was radical cation initiated vinyl polymerization:

(1) No film formation was observed for metallated complexes of mesoporphyrin IX which differs from protoporphyrin IX only in having ethyl groups in place of the vinyl groups.

(2) Cobalt (II) protoporphyrin IX undergoes two successive one electron oxidations. The first is metal centred (Co(II)/Co(III)) whilst the second corresponds to porphyrin ring radical cation formation. If the electrode potential is held at the level for Co(II)/Co(III) oxidation no film is formed but an increase to the radical cation forming potential results in deposition.

(3) Film deposition continues for some minutes after the electrolysis is terminated, consistent with chain growth polymerization.

(4) Manganese (III) protoporphyrin IX does not form a homopolymer on electrolysis but does form *ca.* 20% of a co-deposit with Nickel (II) protoporphyrin IX from a solution containing a 1:1 mixture of the two monomers. This result is also consistent with a chain growth mechanism.

Resonance Raman spectra for a Nickel (II) protoporphyrin IX film suggested that 50% of the vinyl groups were saturated, thus it would seem that linear polymers are formed with a low degree of crosslinking.

Polymerization efficiency, defined as the number of polymerized monomers deposited on the electrode surface divided

by the number of monomers oxidized, was found to be close to 100%, independent of monomer concentration. As previously described this value does not take account of solution polymerization but is not consistent with a chain growth mechanism.

The oxidative electrochemical polymerization of 4,4´-dibromo-4´´-vinyl triphenylamine has been reported by Moutet.[45] The vinyl group is necessary for polymerization since no deposit was formed with a saturated (hydrobrominated) derivative of the same compound. A polymer was also formed in solution and it was assumed that radical cation formation led to the deposition of a 'polystyrene-like' polymer. No estimate of polymerization efficiency or characterization of the solution polymer was given. The polymer modified electrode showed oxidative electrochemistry typical of the monomer.

Electrochemical oxidation of an isomeric mixture of all three isomers of divinylbenzene was found to produce only a passivating film of approximate maximum thickness 70Å, as determined by X-ray photoelectron spectroscopy.[46] Similarly it has been reported that vinylferrocene does not electrochemically polymerize upon oxidation.[47] It is apparent that several factors are important for successful deposition from vinyl monomers, the same is true for aniline and pyrrole monomers and this subject is addressed below.

(ii) Anilines

The anodic electrochemical deposition of a polyaniline film was first described by Letheby in 1862.[48]

Adams *et al* proposed that the final product of electro-oxidation in aqueous sulphuric acid was an eight unit oligomer emeraldine sulphate, evidence included comparison with chemically synthesized emeraldine.[49]

The conductivity of polyaniline films is highly dependent on the preparation conditions, particularly the nature of the solvent and the pH of the electrolyte solution. The conductivity of films prepared in aqueous acid is approximately 10^{-3}-10^{-1} Ω^{-1} cm^{-1} whilst that of the films prepared in neutral or basic aqueous solution or basic non-aqueous solution is approximately 10^{-15}-10^{-13} Ω^{-1} cm^{-1}.[50,51] In an infra-red spectroscopic investigation Oyama *et al* concluded that deposits prepared in aqueous acid contained only para N-C linkages between the monomers.[50] Films prepared in neutral or basic aqueous electrolyte were deemed to be linked both by N-C and N-N bonds and it was apparent that the N-C bonds were meta (1,3) disposed.[50]

Mechanistically it seems likely that under neutral or basic conditions the oligomer forms by radical coupling following one electron oxidation to give a radical cation and subsequent proton loss from nitrogen.[52] In acidic media it seems more probable that the radical cation itself is a coupling species.[49]

Murray reasoned that metal complexes with aromatic amine ligands such as 3- or 4-aminopyridine (3- or 4-NH_2py) or 5-amino-1,10-phenanthroline (5-NH_2phen) should form electro-active deposits upon electrooxidation. Successful deposition was achieved for several such complexes (*viz.* $[Ru(bpy)_2(3\text{- or } 4\text{-}NH_2py)_2]^{2+}$, $[Ru(bpy)_n(5\text{-}NH_2phen)_{3-n}]^{2+}$

where n = 0, 1, 2) from neutral or basic non-aqueous electrolyte solution.[53] The films retained the electrochemistry characteristic of the monomers.

Cyclic voltammetry showed two closely spaced oxidation waves, the first of which was associated with (irreversible) amine oxidation and the second with Ru(II)/Ru(III) oxidation. If during deposition the electrode potential was cycled only up to the amine oxidation value the maximum thickness of film which could be deposited corresponded to approximately nine molecular layers. Extension of the potential scan to the Ru(II)/Ru(III) wave gave films of up to 500 molecular layers. The explanation of this phenomenon lies in the mechanism by which a coated electrode 'communicates' with the electrolyte solution. Once a metal electrode has become coated with a few monolayers of film some means must exist for electron transfer through the film in order that more monomer may take part in electropolymerization. There are two mechanisms by which this may occur.

(1) The growing film is sufficiently electronically conducting that it behaves rather like a metal electrode and presents little or no Ohmic barrier to electron transfer (*e.g.* polypyrrole, polythiophene).

(2) The depositing film possesses 'redox conductivity'[112] associated with the electroactive centres pendant to the polymerizable groups.

This second mechanism may be used to rationalize the electrode potential dependent deposition behaviour described above. Film formation is initiated but not sustained by amine oxidation since nine monolayers have sufficient Ohmic

resistance to prevent electronic conduction from the metal electrode to the monomer solution and thus prevent further deposition. If the potential limit of the oxidation is increased to the Ru(II)/Ru(III) level then oxidation of ruthenium sites may travel through the film to the solution where any species with an oxidation potential lower than that of Ru(II)/Ru(III), for example the polymerizable amine, will be oxidized. The idea is outlined in Figure 1.2.3.

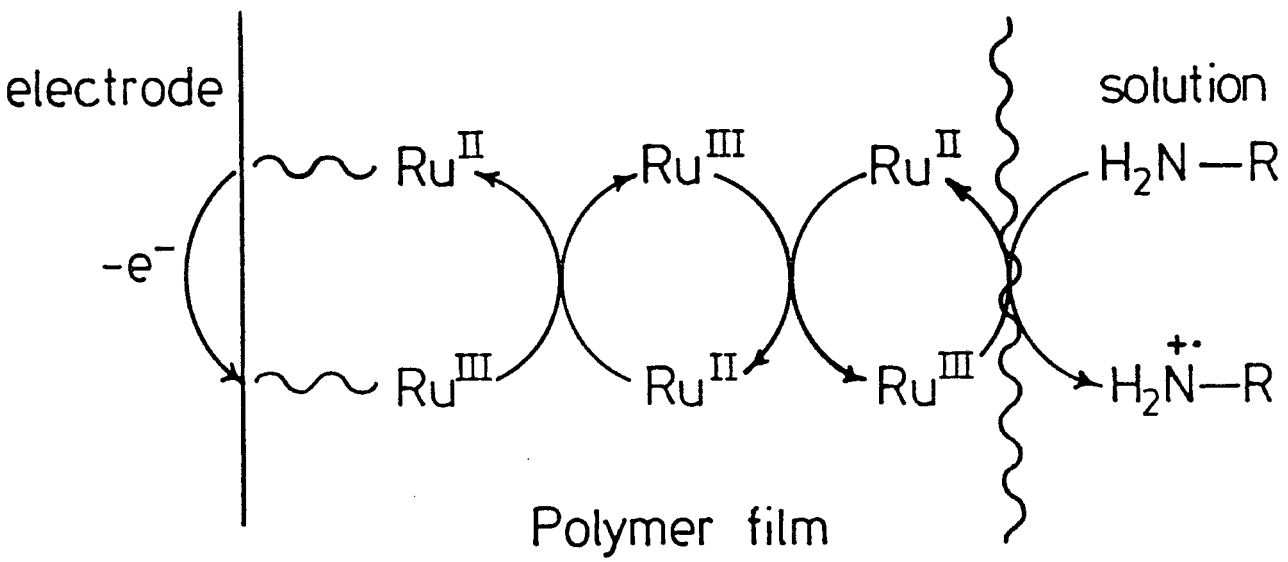

FIGURE 1.2.3 Schematic of redox conductivity

Redox conductivity is considered further in Section 1.3.

Permeation of monomer through the growing film to the electrode surface may also be of some importance in sustained film growth.

A similar redox conduction mechanism is required to explain the sustained film growth of the vinyl compounds described by Murray *et al.*[40]

(iii) Pyrroles

(a) Pyrrole

Electrochemically polymerized pyrrole is one of the most easily prepared conducting polymers and was first studied by Dall'Olio *et al.*[54] Diaz and Street have published several reports on the conductivity, electrochemistry and surface chemistry of polypyrrole, and their variation with preparation procedure.[55-59,61-67] Polypyrrole is formed electrochemically on an anode surface by an overall two electron oxidation of the monomer. Further partial oxidation of the polymer itself occurs during deposition, to give the conducting form of the polymer which has a dark appearance and is 'doped' with the anion of the electrolyte solution. The film conductivity is dependent upon the preparation conditions, particularly the electrolyte anion, but may be as high as *ca.* $10^2\ \Omega^{-1}\ cm^{-1}$ for films grown in tetrabutylammonium perchlorate solution.[55] Polypyrrole does not show metal-like conductivity since resistivity increases at decreased temperature.[56] The polymer may be reduced or 'undoped' at potentials fractionally negative of zero volts (referenced to the saturated Calomel electrode) to give an insulating, yellow coloured form which is highly sensitive to oxygen.

The proton loss is evident from a decrease in solution pH as polymerization proceeds.

The initial step in polymer formation is one electron oxidation of the monomer to yield a radical cation. The radical cation may dimerize and the dimer successively lose two protons generating a dipyrrole. Preferential oxidation of the dimer may then occur and the resultant radical cation may couple with a further pyrrole radical cation and hence build up a polymer. The sequence of reactions may be similar to those outlined below.

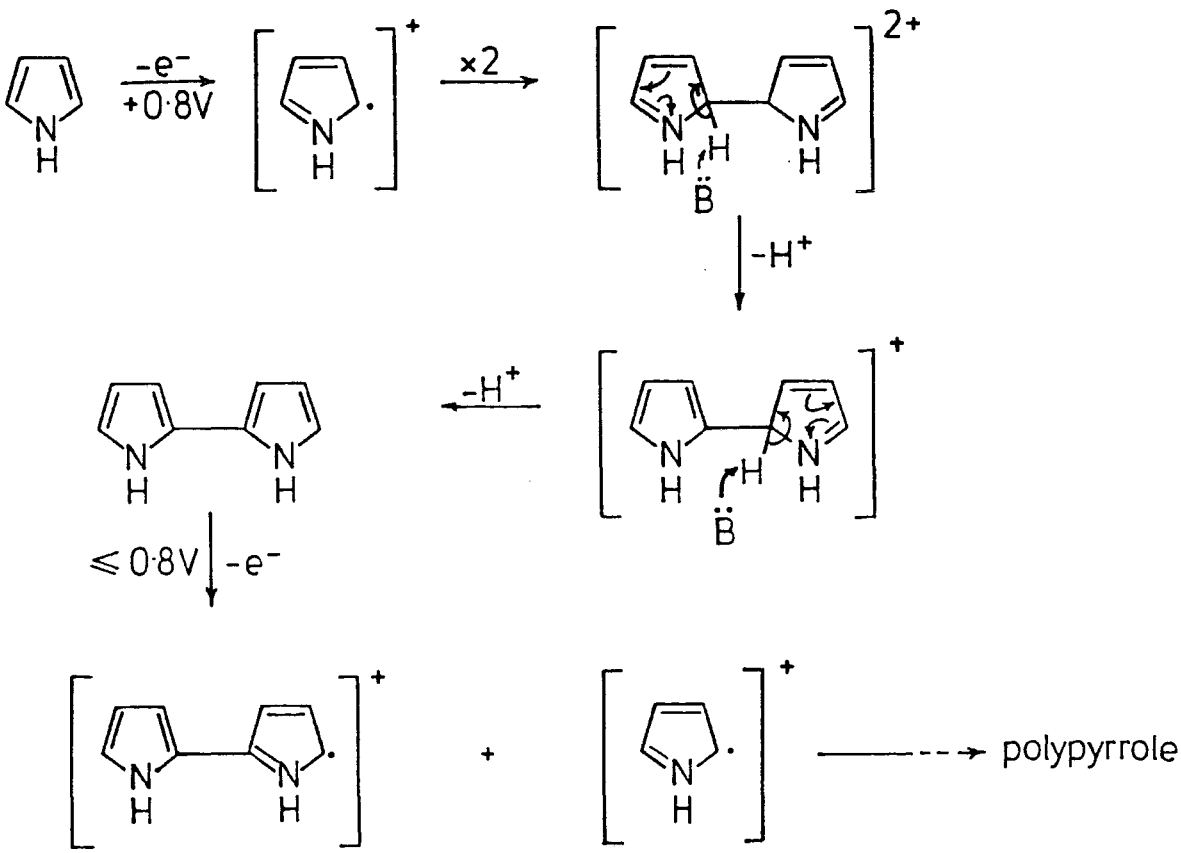

Possible mechanism for polypyrrole formation.

As the size of the polymer unit increases the oxidation reaction tends towards two electrons per monomer, the coulometrically determined value.[57] As stated above, the polymer itself is further oxidized to a level of one positive charge for every three (in perchlorate electrolyte) or four (in tetrafluoroborate electrolyte) pyrrole rings. These oxidation

levels were determined from ESCA[58] or elemental analysis[59] studies of the anion content of the dry films. Using a chemical redox titration technique, Murray has shown that the charge contained in a polypyrrole electrode is dependent upon the electrode potential and thus that there is no fundamentally unique pyrrole/counterion ratio for a working polypyrrole electrode in solution.[60]

It was initially thought that polypyrrole was a linear polymer with the ideal structure, shown below, containing only α-α´ linkages.[61]

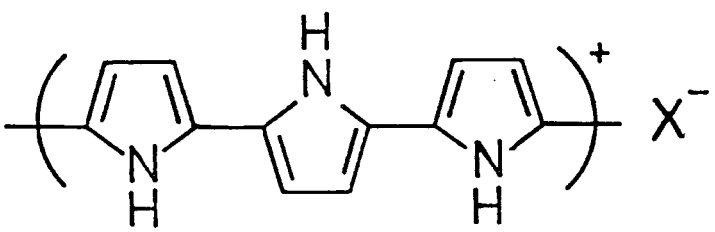

It is now generally accepted that there are some α-β linkages in the polymer[62] and that some of the carbon atoms may be saturated since elemental analysis consistently gives a higher than expected hydrogen content.[57,59b]

β,β´-dimethylpyrrole may be electrochemically polymerized to give a polymer which, although poorly crystalline, is more ordered than polypyrrole itself. The higher structural order presumably results from enforced α,α´ polymer bonding.[63]

Blocking the α positions of pyrrole apparently prevents electrochemical polymerization and Street has concluded that a linear α-α´ bonded polymer is still the best model for polypyrrole.[57]

Because of its low solubility the molecular weight of polypyrrole may not easily be determined. Street has estimated the molecular weight for poly-β,β´-dimethylpyrrole by exchanging the α hydrogens for tritium and determining the amount of tritium in the polymer on combustion.[64] If the assumption is made that the only tritium atoms are located at the ends of linear polymer chains then molecular weights of about 100,000 are obtained for poly-β,β´-dimethylpyrrole perchlorate. This value corresponds to roughly 750 pyrrole units. If, during the polymerization, a proton is not eliminated from the α carbon atom a saturated site forms in the polymer and 100,000 will be an underestimate of the molecular weight. In such a circumstance Street considers that 750 may be the number of uninterrupted conjugated pyrrole units.

In contrast, ultraviolet photoelectron spectra for polypyrrole and poly-β,β´-dimethylpyrrole show a valence density of states which may be explained by very short conjugation lengths (dimer or trimer) but do not preclude the possibility of much larger segments of linear, conjugated polymer.[65]

The mechanical properties of polypyrrole may be improved by polymerization in toluenesulphonate electrolyte[66] or by electrochemically incorporating polypyrrole within the matrix of another polymer whose mechanical properties are superior to those of polypyrrole, *e.g.* polyvinylalcohol.[67a] The electrochemical synthesis of a graft copolymer from pyrrole and a pyrrole functionalized polystyrene has also been reported.[67b]

Commercial applications for polypyrrole have been proposed[68a] and the technology for large scale, continuous

electrochemical film formation using a cylindrical roller anode has been patented.[68b]

(b) N-substituted pyrroles

There are several reports of electrochemical polymerization of N-alkylpyrroles.[69] Conductivity and anion dopant concentration for the polymers generally decrease with increasing size of the N-alkyl substituent.[69a] The decrease in conductivity is thought to be due to the enforced loss of planarity in the poly-N-alkylpyrrole chain.[59b]

N-alkylation of pyrrole provides a convenient means of attaching an electroactive molecule to an electropolymerizable one, pyrrole. This has been achieved and electroactive polymers have now been formed from pyrrole N-substituted with nitrophenyl,[70] 4,4´-bipyridinium (viologen),[2b] ferrocene (see Chapter Two) and pyridyl and bipyridyl complexes of ruthenium and iron (see Chapter Three).[8-10]

The same restrictions on sustained film growth as discussed previously for anilines apply to N-substituted pyrroles. In the case of N-nitrophenylpyrrole the electrochemical redox switching (doping/undoping) reaction typical of polypyrrole is clearly seen in a cyclic voltammogram of the coated electrode.[70] Moreover the dry conductivity of poly N-nitrophenylpyrrole is 10^{-3} Ω^{-1} cm^{-1}, the same value as that for poly N-methylpyrrole, and sustained film grown is possible because of this reasonably high electrical conductivity. The same is probably true for viologen N-substituted polypyrrole since cyclic voltammetry shows the reversible polypyrrole oxidation reaction although no conductivity value has been reported.[2b]

The poly-iron(II)tris(N-bipyridylpyrrole) film described in Chapter Three of this work has low electrical conductivity and does not show the 'polypyrrole-like' redox switching. It is likely that for this polymer sustained growth is achieved by a redox conduction electron transfer mechanism analogous to that described for the aminopyridine and aminophenanthroline complexes of ruthenium but with Fe(III) centres oxidizing further monomer at the polymer/solution interface. Supporting evidence for a redox conduction mechanism is presented in Chapter Three.

N-substitution of the monomer, though perhaps the simplest, is not the only way to prepare a derivatized, electrochemically active polypyrrole film. Preformed polypyrrole films have been surface functionalized with tetrathiofulvalene[6] and ferrocene.[7] A lower concentration of electroactive species is necessarily obtained using post functionalization and it appears that the electrochemistry is less ideal than for polymers formed from N-substituted monomers.

1.3 Electrochemical Behaviour

The electrochemical behaviour of a modified electrode, both the inherent electrochemistry of the coating and its effect on the electrochemistry of solution species, is of prime importance.

Several electrochemical techniques have been used to study modified electrodes (*e.g.* rotating disc electrolysis,[71,72] differential pulse voltammetry,[73] spectroelectrochemistry[74]) however only cyclic voltammetry (CV) and chronoamperometry have been used in this work and thus the discussion below is

limited mainly to the application of these two techniques.

An important objective in the design of chemically modified electrodes is that the coating should show the same chemical and electrochemical properties as the species from which it was prepared. From the many electroactive coatings which have now been studied by cyclic voltammetry it is clear that the formal electrode potential ($E^{\ominus}$) for electron transfer between oxidized and reduced states in the films is the same as the formal potential for analogous species in solution.[75]

It is also important that the electrochemical response for the coating (*e.g.* the CV wave) should be stable to repetition of the electrochemical experiment. As a measure of this stability it is common to report the number of CV cycles required to cause a quoted loss, if any, in signal. This may however be erroneous since if only either the oxidised or reduced form is indefinitely stable in the electrolyte medium then the time spent in the unstable form is the important parameter in defining the stability. In such a case the number of cycles required to cause a fixed amount of degradation in signal will depend both on the extent of the potential sweep and on the sweep rate.

The ideal CV behaviour for a multilayer modified electrode[12] (*i.e.* peak splitting = OmV, peak width (FWHM) = 90.6/n mV, peak current (i_p) is proportional to sweep rate (ν); see Figure 1.3.1a),[†] in which the kinetics of charge transport are rapid in relation to the experimental time scale, is almost never found. So long as the charge transfer kinetics

---

[†] n is the number of electrons transferred in the overall electrode reaction.

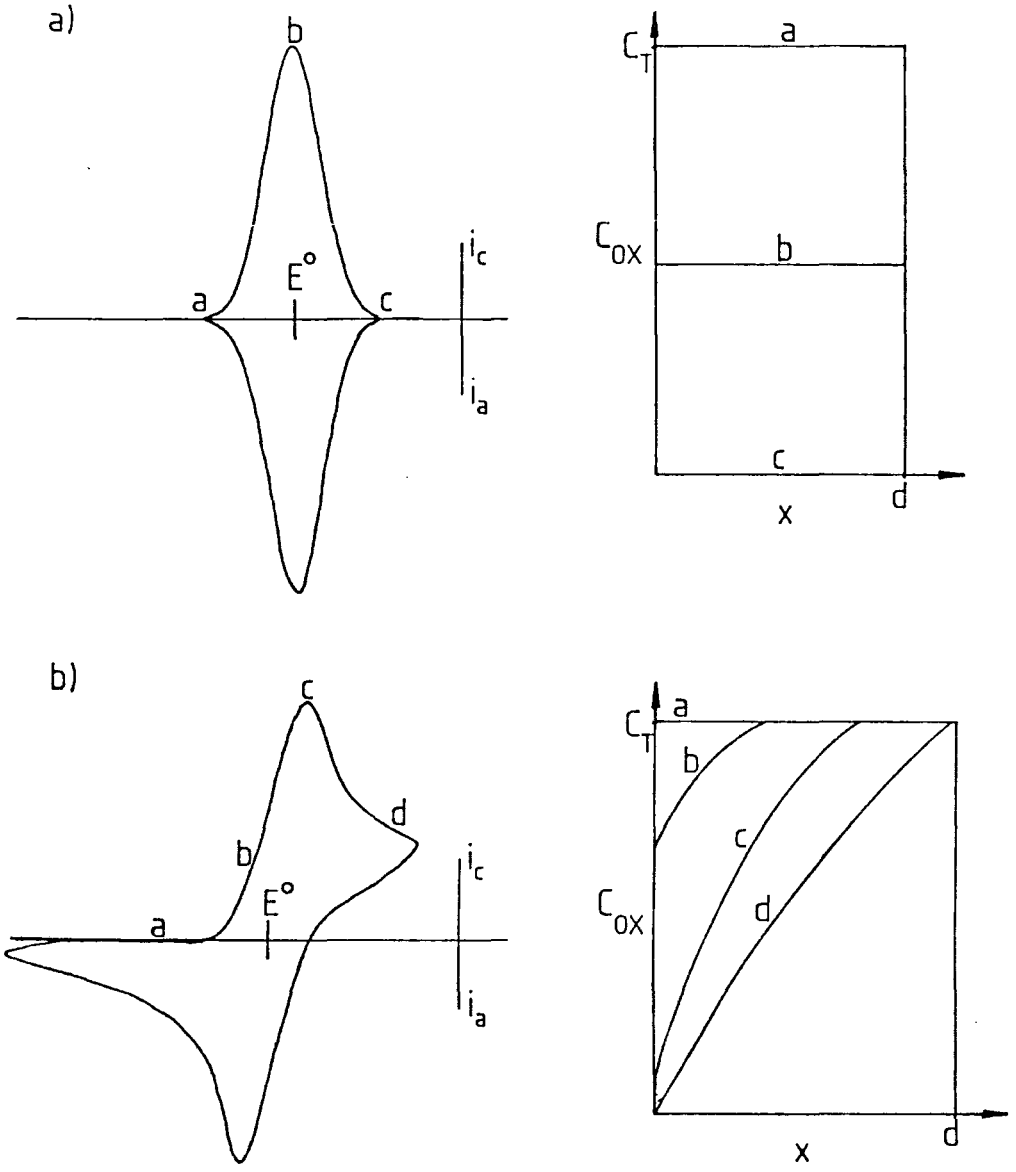

FIGURE 1.3.1 (a) Ideal CV for a surface immobilized redox species when charge transfer kinetics are rapid compared to the experimental timescale.

(b) CV for surface immobilized redox species when charge transfer kinetics are slow compared to the experimental timescale.

In both cases concentration/distance curves are shown for various points on the CVs.

C_{OX} = Concentration of oxidized redox sites

C_T = total concentration of redox sites

X = distance away from electrode surface

d = thickness of film containing redox species.

are rapid, i_p varies linearly with ν but small peak splittings of *ca.* 20-40mV, which do not inrease with sweep rate, are common. Peak widths usually exceed 90.6/n mV but whether this is due to a distribution of species in the film each with slightly different $E^{\ominus}$ values or to interactions between neighbouring redox centres is not clear.[76,77]

An example of a reversible one electron reduction of redox centres in an electrochemically reactive, multilayer polymer film may be represented:

$$O^+ + e^- \rightleftharpoons R$$

Electron transfer to redox sites in the film proceeds outwards from the electrode surface to the film-electrolyte solution interface. Only redox centres in contact with the electrode surface are reduced by direct electron transfer from the electrode. Further redox centres in the film are reduced by electron exchange with neighbouring inner centres and the reaction proceeds to establish the equilibrium ratio of oxidized and reduced sites given by the Nernst equation at the applied potential. In other words, charge propagates through the film by a redox conduction or electron hopping mechanism[12,78] and is driven by a concentration gradient. The rate at which the equilibrium is established depends upon the rate of charge transfer between the redox centres. The rate determining step in the reaction may be (a) the electron exchange reaction itself, (b) segmental motions of the polymer chains in order to bring sites close enough for electron exchange, or (c) motion of charge compensating ions, necessary to preserve electroneutrality, within the film. All of these processes are diffusion-like[10] and so a diffusion coefficient (D) may be associated with the overall rate of charge transport.

The CV behaviour for a film undergoing the reduction reaction outlined above will depend upon the film thickness (d), the diffusion coefficient (D) and the experimental time scale (τ, ν is inversely proportional to τ). So long as $\frac{D\tau}{d^2} >> 1$ then all the redox centres throughout the film are in equilibrium with the electrode potential and the concentration of oxidized and reduced sites is at all times given by the Nernst equation for the whole film. This is the case of rapid charge transfer with respect to the experimental time-scale when the ideal, 'monolayer-like' CV behaviour mentioned above is to be expected. A symmetrical peak shape, centred at $E^{\ominus}$, is expected which results from the tradeoff between a rise in current, as the electrochemical rate constant increases with increasing potential and a decrease in current as the concentration of unreduced sites is diminished (see Figure 1.3.1a).

If $\frac{D\tau}{d^2} << 1$ then the behaviour is rather like that for a solution phase species, *i.e.* i_p is proportional to $\nu^{\frac{1}{2}}$ and a CV peak with a 'diffusional tail' arises (see Figure 1.3.1b) as the current follows the changing concentration gradient at the electrode surface as the potential is swept. Ideally, for the reversible reaction, the peak splitting is 59mV, experimental values are often greater than this but whether this is due to slow electron transfer at the electrode-film interface (quasi-reversibility)[79] or uncompensated film resistance or from other effects is not clear.[12,77,80]

Electrode coatings of the same film may thus show different CV behaviour depending on the relative magnitudes of D, d and τ. A transition from 'monolayer-like' to 'solution-

phase like' behaviour may be brought about by decrease in temperature[81] (with decrease in D) or increase in film thickness[82] at constant sweep rate or range of sweep rates.

Various methods have been employed to measure the value of the charge transfer diffusion coefficient, D. One way is to record CVs for a film under conditions where $\frac{D\tau}{d^2} \ll 1$ over a range of sweep rates and use the Randles-Sevcik equation to determine $D^{\frac{1}{2}}C$, where C is the concentration of surface bound redox sites.[81] If the film thickness is known C may be estimated and a value for D determined.

A preferred method is to use potential step chronoamperometry. In this technique the equilibrium distribution of oxidized and reduced sites in the film is disturbed by the rapid application of an electrode potential. Following the 'voltage-jump' current flows in order to re-establish equilibrium at the new electrode potential. At short times after the voltage is applied the condition $\frac{D\tau}{d^2} \ll 1$ is satisfied and the current decays according to the Cottrell equation,[12,81] from which $D^{\frac{1}{2}}C$ and hence D may be estimated. At longer times $\frac{D\tau}{d^2} \gg 1$, since the film is not infinitely thick. However following the treatment for thin layer cells[83,84] an equation for current decay in a film of finite thickness may be derived. Good agreement between theory and experiment, even after longer times following the voltage-jump, may thus be obtained.[76,81]

Albery *et al*[76] have measured D for the thionine coated electrode and found the value to be *ca.* 10^{-13} cm^2 s^{-1} at low pH, D was found to decrease with increase in size of electrolyte counter ion at low pH, as would be expected if counter ion motions were rate determining. Murray *et al* determined

D at low temperatures for plasma polymerized vinylferrocene coated electrodes.[81] An Arrhenius plot gave an activation energy barrier to diffusional charge transport of *ca.* 3.7kcal/mol from which a charge transport diffusion coefficient at 298K of 10^{-11}-10^{-12} cm^2 s^{-1} was estimated.

For $[Ru(vbpy)_3]^{2+}$ coated electrodes Murray *et al*[42] determined D to be *ca.* 10^{-10} cm^2 s^{-1}. It was concluded that counter ion motions were not rate limiting in this case since rotated disk electrode currents gave permeability rates for bromide ions through the film $>10^3$ times larger than the measured D.[85]

Murray and coworkers[86] have evaluated D by measuring the limiting current arising from the redox conductivity of an electroactive film. A film of $[Os(bpy)_2(vpy_2)]^{2+}$ was sandwiched between two electrodes and the redox current was measured by applying appropriate potentials to the contacting electrodes on either side of the film. The limiting current for the Os(III)/Os(II) exchange reaction for example was measured by holding the potential of one electrode at Ov and sweeping the potential at the other to beyond $E^{\ominus}$ Os(III)/Os(II) at a rate slow enough such that $\frac{D\tau}{d^2} >> 1$. Under these conditions the concentration of Os(III) sites at the reducing electrode surface is always zero and a linear concentration gradient exists between the two electrodes. The limiting current (i_L) is reached when the concentration of Os(III) sites at the oxidizing electrode is zero and is given by the expression $i_L = \frac{nFADC_T^2}{\Gamma}$ where C_T is the total concentration of electroactive sites and the other symbols have their usual meaning.[86]

Murray *et al* determined the charge transfer diffusion coefficients for all of the three exchange reactions giving rise to redox conductivity in poly$[Os(bpy)_2(vpy)_2]^{2+}$ *i.e.* Os(III)/Os(II), Os(II)/Os(I) (formally) and Os(I)/Os(O) (formally). Diffusion coeffieicnts were found to increase in the order Os(III)/Os(II)<Os(II)/Os(1)<Os(1)/Os(O) with values of approximately $8x10^{-9}$ cm^2 s^{-1}, $24x10^{-9}$ cm^2 s^{-1} and $200x10^{-9}$ cm^2 s^{-1} respectively. That the high currents measured for the Os(1)/Os(O) exchange reaction were not due to electrical conductivity was demonstrated by holding both contacting electrodes negative of $E^{\ominus}$ Os(1)/Os(O) with a small potential difference between them, much smaller currents were then observed.

Values of D measured for the same film by both chronoamperometry and from sandwich electrodes agreed to within a factor of 2.[86]

Murray *et al* have exploited the potential dependent redox conductivity in the preparation of bilayer electrodes with uni-directional conductivity and charge trapping properties.[37,43,87] The principle of the bilayer electrode is outlined below and schematically in Figure 1.3.2. An electrode is coated with two redox polymers, one on top of the other such that there is no contact between the electrode surface and the outer film. Communication between the outer film and the electrode surface can only take place at potentials around $E^{\ominus}$ of the inner film. An example of a bilayer electrode with poly-$Ru(vbpy)_3^{2+}$ as the inner layer and a vinylferrocene polymer at the outer layer is shown in Figure 1.3.2b. $E^{\ominus}$ Ru(II)/Ru(III) is greater than $E^{\ominus}$ ferrocene/ferricenium.

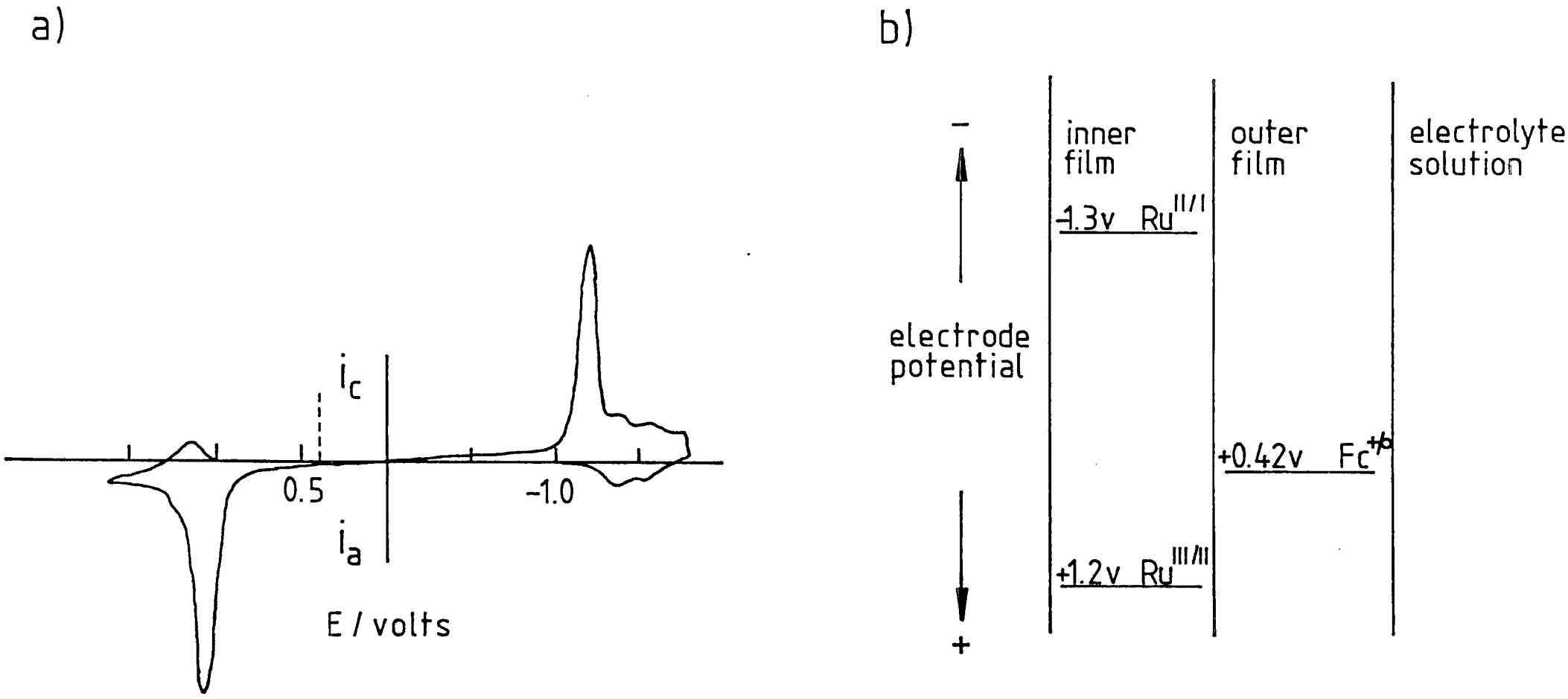

FIGURE 1.3.2 (a) CV and (b) schematic representation of a bilayer electrode consisting of an inner film of poly-$Ru(vvpy)_3^{2+}$ and an outer film of a vinylferrocene polymer. In Figure 1.3.2(a) the ferrocene $E^{\ominus}$ is indicated by a broken line.

If, in a cyclic voltammogram for this bilayer electrode, the potential is increased from a value negative of both film oxidation potentials then, when $E^{\ominus}$ ferrocene/ferricenium is reached no current flows to oxidize the outer film since the inner film will not permit redox conduction at this potential. At a potential near $E^{\ominus}$ [Ru(II)/Ru(III)] the inner film becomes redox conducting and the ferrocene film is oxidized in a current spike (see Figure 1.3.2.a), Ru(II) is also oxidized to Ru(III). On a return potential sweep Ru(III) is reduced to Ru(II) and the inner film becomes redox insulating again before $E^{\ominus}$ ferrocene/ferricenium is approached and thus the ferricenium state becomes 'trapped' in the outer film. The outer film can only be reduced back to the ferrocene state at a potential near $E^{\ominus}$ Ru(II)/Ru(I) when the inner film again becomes redox conducting and capable of reducing any contacting species with $E^{\ominus}$ less negative than Ru(II)/Ru(I) (see Figure 1.3.2). The persistence of the trapped state is dependent upon the difference in oxidation potentials for the two films. If the difference is very small the thermodynamically disfavoured back reaction will allow the trapped state to slowly decay.

An application of bilayer electrodes to trace analysis of oxidants in solution has been demonstrated.[43] The bilayer was made from an inner film of poly $Ru(vbpy)_3^{2+}$ and an outer film of an electrochemically polymerized vinyl substituted diquat (vdq). The Ru(II)/Ru(I) and Ru(I)/Ru(0) reduction potentials are both cathodic of the $vdq^{2+}/vdq^{+\cdot}$ and $vdq^{+\cdot}/vdq^{o}$ reduction potentials thus vdq^{2+} is reduced to vdq^{o} in a current spike near the Ru(II)/Ru(I) potential. The vdq^{o}

state is trapped on reversing the potential sweep and is only oxidized back to vdq^{2+} at the Ru(II)/Ru(III) wave. Any trace oxygen in solution will slowly oxidize trapped vdq^{o} to vdq^{2+} and, if a second potential sweep to Ru(II)/Ru(I) is performed, the amount of vdq^{o} which has been oxidized (untrapped) by solution species may be estimated.

Similar potential dependent 'communication' through a single layer of redox polymer film may be demonstrated with electroactive species in solution. In principle, two pathways exist for electron transfer, either diffusion of the solution species through the film or by redox conduction through the film. In the first case electron transfer will occur at the electrode surface and at the normal redox potential of the solution species. In the second case electron transfer takes place at the redox polymer - solution interface and at, or near the redox potential of the film. This has been demonstrated with a $[Ru(bpy)_2(vpy)_2]^{2+}$ film and with $[Ru(bpy)_2pyCl]^{+}$ or ferrocene as solution species, both of which may be oxidized at potentials less positive than the film Ru(II)/Ru(III) $E^{\ominus}$.[39,88] The relative importance of the two electron transfer pathways varies with film thickness with the redox conduction mechanism dominating at high film coverages. It was found that higher electrode coverages were required to block ferrocene diffusion than $[Ru(bpy)_2pyCl]^{+}$ and this result indicates a possible method for selective electrochemical oxidation of one species from a solution containing several species of similar $E^{\ominus}$ on the basis of size and/or charge discrimination.[85]

1.4 Characterization

Several non-electrochemical techniques have been applied to the study of modified electrodes. In the case of plasma and electrochemically polymerized films the usefulness of standard analysis methods is limited by the fact that the films are very thin and thus present only a short path length for transmission spectrophotometric techniques. Moreover the films are usually highly insoluble which precludes their analysis by several standard methods.

It was realized at an early stage[11] that ESCA, with its capability to detect monolayer thicknesses, is an excellent tool for the study of modified electrodes. Some of the features of ESCA which have been used to advantage in the study of modified electrodes are listed in Table 1.4.1 whilst a more complete discussion of the technique is given in the Appendix.

TABLE 1.4.1

Applicable to any chemical element

Non destructive

Small sampling area (*ca.* 0.5 cm^2) required

Ability to determine film thickness in the range 0 to *ca.* 75Å - using conventional X-ray sources[89]

Determination of oxidation state of transition metal compounds[10,34,90]

Discrimination between spin paired and paramagnetic compounds[10,90]

Qualitative information on film conductivity from sample charging measurements[91]

Attenuation of total reflectance (ATR) infra-red spectroscopy using multiple reflection, is useful for the study of thin films. Since the infra-red radiation is made to pass through the film several times the sensitivity is higher than for transmission. Coupling of the ATR technique with a Fourier transform (F.T.) infra-red spectrometer provides a distinct advantage in sensitivity for a given acquisition time.

Other techniques which have been used to study modified electrodes are listed in Table 1.4.2.

TABLE 1.4.2

Elemental analysis[40]

Secondary ion massspectrometry (SIMS)[92]

Auger electron spectroscopy (AES)[93]

Scanning electron microscopy[29]

Resonance Raman spectroscopy[94]

Uv/visible absorption spectrophotometry[76]

Transmission infra-red spectroscopy[53]

1.5 Applications

The potential application of modified electrodes to selective oxidation or reduction[85] and to trace analysis in solution[43] were mentioned above.

The catalysis of electrochemical reactions in solution, which are often slow at the uncoated electrode (*e.g.* oxygen reduction[21,96] and electron transfer involving biological molecules)[4] has been one of the aims of modified electrode research. Successful electrocatalysis has been reported

using both electroactive[21,34,96,97] and electroinactive[4] coatings; some of this work has been reviewed.[1,12,13,15,98]

Some interesting applications of electroactive films exist as coatings for semiconductor photoelectrodes used in solar conversion cells.[12]

Upon illumination with light of energy greater than or equal to the semiconductor band gap an electron-hole pair is created in the semiconductor surface depletion layer. For an n-type semiconductor photoanode the holes migrate to the surface and, in the case of n-Si, are thermodynamically capable of oxidizing the semiconductor itself. This process, which renders the cell useless, is called photocorrosion.

Wrighton[99] has shown that a surface coating of a ferrocene on n-Si will compete effectively with photocorrosion for the photogenerated holes and thus extend the working lifetime of the cell. The ferricenium thus created must be reduced back to ferrocene by some species in solution in order that the process may be repeated.

For photocorrosion protection the electroactive coating should be transparent to the irradiation for maximum efficiency. Electroactive films containing efficient chromophores may however, be used to 'sensitize' large band gap semiconductor photoelectrodes which could otherwise utilize only a small fraction of incident solar radiation. If the film absorbs light of longer wavelength than the semiconductor and the energy levels of the ground and excited state of the chromophore straddle the conduction band of an n-type semiconductor then, upon illumination, injection of holes into

the conduction band will take place thus sensitizing the semiconductor.[103] Bard and coworkers[100] have reported the sensitization of n-SnO_2 electrodes by $Ru(bpy)_3^{2+}$ contained in a Nafion surface coating.

1.6 Project aims

The main aim of the work presented in the following chapters is to prepare 'polymeric', organic or organometallic, electroactive electrode coatings. Two methods of preparation have been employed, namely plasma and electrochemical polymerization. The redox activity of the films and in particular its stability is, whenever possible, correlated to changes in the surface chemistry.

In Chapters Two and Three the electropolymerizability of pyrrole is combined with the redox activity of ferrocene and iron and ruthenium trisbipyridyl in order to prepare redox active films from novel N-substituted pyrrole monomers.

Chapter Four presents an extension of previous work concerning the preparation of redox active deposits from plasma polymerized vinylferrocene. The surface chemistry and redox activity of plasma polymers derived from several substituted ferrocenes have been studied as a function of the plasma conditions. The preparation of the first redox active plasma deposits derived from substituted ferrocenes other than vinylferrocene is described.

In Chapter Five the preparation of conducting deposits derived from the electrochemical reduction of octafluorocyclopentene is described. Most electrochemically prepared,

conducting deposits result from monomer oxidation, *e.g.* polypyrrole,[56] polythiophene,[102] polyaniline[49] and polyphenylene.[101] This work represents an interesting example of cathodic electrodeposition.†

† For all of the deposits studied in this work the application of standard techniques of polymer characterization is hampered by the insolubility of the materials formed. The word 'polymer' is used frequently in this thesis to describe insoluble films which often bear chemical resemblance to the soluble 'monomers' from which they were derived. However, no inference about the molecular weights of the materials should be drawn from the use of this word.

REFERENCES (Ch.1)

1. W.J. Albery and A.R. Hillman; Royal Society of Chemistry, Annual Reports C, (1981), 377.

2. R.J. Nowak, F.A. Schultz, M. Umana, R. Lam and R.W. Murray; Anal.Chem., 52, (1980), 315.

2b. G. Bidan, A. Deronzier and J-C. Moutet; J.Chem.Soc. Chem.Commun., (1984), 1185.

3. P.H. Wu, P.B. Griggs and E.W. Hellmuth; Polym.Mater.Sci. Eng., 49, (1983), 676.

4. M.J. Eddowes and H.A.O. Hill; J.Am.Chem.Soc., 101, (1979), 4461.

5. M.F. Nichols, A.W. Hahn, W.J. James, A.K. Sharma and H.K. Yasuda; Biomaterials, 2, (1981), 161.

6. A.F. Diaz, W.-Y. Lee, J.A. Logan and D.C. Green, J.Electroanal.Chem., 108, (1980), 377.

7. M. Velazquez-Rosenthal, T. Skotheim and J. Warren; J.Chem.Soc.Chem.Commun., (1985), 342.

8. G. Bidan, A. Deronzier and J-C. Moutet; Nouv.J. de Chimie, 8, (1984), 501.

9. S. Cosnier, A. Deronzier and J-C.Moutet; J.Electroanal. Chem., submitted 1985.

10. J.G. Eaves, H.S. Munro and D. Parker; J.Chem.Soc.Chem. Commun. (1985), 684.

11. P.R. Moses, L. Wier and R.W. Murray; Anal.Chem., 47, (1975), 1882.

12. R.W. Murray, Chapter 3 in "Electroanalytical Chemistry", vol.13, Ed. A.J. Bard, Dekker, New York (1984).

13. R.W. Murray; Acc.Chem.Res., 13, (1980), 135.

14. D.R. Rolison; Proc.Electrochem.Soc., 84, (1984), 222.

15. K.D. Snell and A.G. Keenan; Chem.Soc.Rev., 8, (1979),259.

16. M.S. Wrighton, M.C. Palazotto, A.B. Bocarsly, J.M. Bolts, A.B. Fischer and L Nadjo; J.Am.Chem.Soc., 100, (1978),7264.

17. D.C.S. Tse, T. Kuwana and G.P. Royer; J.Electroanal.Chem., 98, (1979), 345.

18. C.P. Jester, R.D. Rocklin and R.W. Murray; J.Electrochem. Soc., 127, (1980), 1979.

19a. A. Merz and A.J. Bard, J.Am.Chem.Soc., 100, (1978), 4379
b. P.J. Peerce and A.J. Bard, J.Electroanal.Chem., 112. (1980), 247.

20a. N. Oyama and F.C. Anson, J.Am.Chem.Soc., 101, (1979), 739.
b. N. Oyama and F.C. Anson; J.Electrochem.Soc., 127,(1980),247.

21. P.M. Hoang, S. Holdcroft and B.L. Funt, J.Electrochem.Soc., 132, (1985), 2129.

22. A.T. Bell, Chapter 1 in "Techniques and Applications of Plasma Chemistry", Ed. J.R. Hollahan and A.T. Bell, John Wiley, New York (1974).

23. H. Yasuda, "Plasma polymerization", Academic Press, London (1985).

24. H. Suhr, Chapter 2 in ref. 22.

25. H. Suhr, Plasma Chem.Plasma Process., 16, (1983), 194.

26. B. Chapman, "Glow discharge processes", John Wiley, New York, (1980).

27. D.T. Clark and D. Shuttleworth, J.Polym.Sci.Polym.Chem. Ed., 18. (1980), 27.

28. H. Yasuda and T. Hirotsu; J.Polym.Sci.Polym.Chem. Ed., 16, (1978), 743.

29. H. Kobayashi, M. Shen and A.T. Bell, J.Macromol.Sci.Chem., A8, (1974), 1354.

30. E. Kay, J. Coburn and A. Dilks in Top.Curr.Chem.No. 94, Ed. S. Veprek and N. Venugoplan, Springer-Verlag, Berlin, (1980).

31. N. Oyama, A.P. Brown and F.C. Anson; J.Electroanal.Chem., 87, (1978), 435.

32. D. Flamm, V. Donnelly and D. Ibbotson; J.Vac.Sci.Technol. B1, (1983), 23.

33a. D.T. Clark and D. Shuttleworth, J.Polym.Sci.Polym.Chem.Ed., 16, (1978), 1093.
b. D.T. Clark and D. Shuttleworth, *ibid*, 17, (1979), 1317.
c. D.T. Clark and D. Shuttleworth, *ibid*, 18, (1980), 407.
d. D.T. Clark and M.Z. Abrahman, *ibid*, 19, (1981), 2129.
e. D.T. Clark and M.Z. Abrahman, *ibid*, 19, (1981), 2689.
f. D.T. Clark and M.Z. Abrahman, *ibid*, 20, (1982), 691.
g. D.T. Clark and M.Z. Abrahman, *ibid*, 20, (1982), 1717.
h. D.T. Clark and M.Z. Abrahman, *ibid*, 20, (1982), 1729.
i. D.T. Clark and M.M. Abu-Shbak, *ibid*, 21, (1983), 2907.
j. D.T. Clark and M.M. Abu-Shbak, *ibid*, 22, (1984), 1.
k. D.T. Clark and M.M. Abu-Shbak, *ibid*, 22, (1984), 17.

34. M.F. Dautartas and J.F. Evans, J.Electroanal,Chem., 109, (1980), 301.

35. K. Doblhofer and I. Eiselt, Thin Solid Films, 118, (1984), 181.

36a. H.S. Munro and C. Till, Thin Solid Films, in press.
b. H.S. Munro and C. Till, in preparation.

37. H.D. Abruna, P. Denisevich, M. Umana, T.J. Meyer and R.W. Murray, J.Am.Chem.Soc., 103 (1981), 1.

38. R. Kalir and A. Zilkha, Eur.Polym.J., 14. (1978). 557.

39. H.D. Abruna, J.M. Calvert, P. Denisevich, C.D. Ellis, T.J. Meyer, W.R. Murphy, R.W. Murray, B.P. Sullivan and J.L. Walsh, Chapter 8 in "Chemically Modified Surfaces in Catalysis and Electrocatalysis", Ed. J.S. Miller, ACS Symp.Ser. 192, (1982).

40. J.M. Calvert, R.H. Schmehl, B.P. Sullivan, J.S. Facci, T.J. Meyer and R.W. Murray, Inorg.Chem. 22, (1983), 2151.

41. B.L. Funt and F.D. Williams; J.Polym.Sci., A2, (1964),865.

42. P. Deniserich, H.D. Abruna, C.R. Leidner, T.J. Meyer and R.W. Murray, Inorg.Chem., 21, (1982), 2153.

43. K. Willman and R.W. Murray, J.Electroanal.Chem., 133, (1982), 211.

44. P. Denisevich, K. Willman and R.W. Murray, J.Am.Chem.Soc., 103, (1981), 4727.

45. J-C. Moutet, J.Electroanal.Chem., 161, (1984), 181.

46. H.D. Finklea and R.S. Vithanage, J.Electroanal.Chem., 161, (1984), 283.

47. B.R. Shaw, G.P. Haight and L.R. Faulkner, J.Electroanal. Chem., 140. (1982), 147.

48. H. Letheby, J.Chem.Soc., 15, (1862), 161.

49. D.M. Mohilner, R.N. Adams and W.J. Argersinger, J.Am.Chem. Soc., 84, (1962), 3618.

50. T. Ohsaka, Y. Ohnuki, N. Oyama, G. Katagiri and K.Kamisako, J.Electroanal.Chem., 161, (1984), 399.

51. A. Volkov, G. Tourillon, P. Lacaze and J. DuBois, J. Electroanal.Chem., 115, (1980), 279.

52. M. Breitenbach and K.H. Heckner, J.Electroanal.Chem., 29, (1971), 309.

53. C.D. Ellis, L.D. Margerum, R.W. Murray and T.J. Meyer, Inorg.Chem., 22, (1983), 1283.

54. A. Dall'Olio, G. Dascola, V. Varacca and V. Bocchi, Comptes Rendus Acad.Sci.Ser.C., 267, (1968), 433.

55. M. Salmon, A.F. Diaz, A.J. Logan, M. Krounbi and J. Bargon, Mol.Cryst.Liq.Cryst., 83, (1982), 265.

56. A.F. Diaz, J.I. Castillo, J.A. Logan and W. Lee, J.Electroanal.Chem., 129, (1981), 115.

57. G.B. Street in 'Handbook of Conducting Polymers', Ed. T. Skotheim, Dekker, New York, in press 1986.

58a. P. Pfluger and G.B. Street, J.Chem,Phys.80, (1984), 544.
b. W.R. Salaneck, R. Erlandsson, J. Prejza, I. Lundström and O. Inganas, Synthetic Metals, 5, (1983), 125.

59a. G.B. Street, T.C. Clarke, R.H. Geiss, W-Y. Lee, A. Nazzal, P. Pfluger and J.C. Scott, J,de Physique Colloq., C3, (1983), 599.
b. G.B. Street, T.C. Clarke, M. Krounbi, K. Kanazawa, W. Lee, P. Pfluger, J.C. Scott and G. Weiser, Mol.Cryst.Liq.Cryst., 83, (1982), 253.

60. B.J. Feldman, P. Burgmayer and R.W. Murray, J.Am.Chem.Soc., 107, (1985), 872.

61. A. Diaz, J.M. Vasquez-Vallejo and A. Martinez-Duran, IBM J.Res. Develop., 25, (1981), 42.

62. T.C. Clarke, J.C. Scott and G.B. Street, IBM J.Res.Develop, 27, (1983), 313.

63. R.H. Geiss, G.B. Street, W. Volksen and J. Economy, IBM J. Res. Develop, 27, (1983), 321.

64. A. Nazzal and G.B. Street, J.Chem.Soc.Chem.Commun., (1984), 83.

65. P. Pfluger, U.M. Gubler and G.B. Street, Solid State Commun., 49, (1984), 911.

66. A.F. Diaz and B. Hall, IBM J. Res.Develop, 27, (1983).342.

67a. S.E. Lindsey and G.B. Street, Synthetic Metals, 10,(1984),67.
b. A.I. Nazzal and G.B. Street, J.Chem.Soc.Chem.Commun. (1985), 375.

68a. Chemical and Engineering News, 63, No.35, (1985), 20.
b. H. Naarmann, G. Koehler and J. Schlag, Chem.Abstr.100: 93546d, (1984), Patent.

69a. A.F. Diaz, J. Castillo, K.K. Kanazawa, J.A. Logan, M. Salmon and O. Fajardo, J.Electroanal.Chem., 133, (1982), 233.
b. M.G. Cross, D. Walton, N.J. Morse, R.J. Mortimer, D.R. Rosseinsky and D.J. Simmonds, J.Electroanal.Chem., 189 (1985), 389.

70. M. Salmon, A. Diaz and J. Goita, Chapter 5 in ref. 39.

71. W.J. Albery, A.W. Foulds, K.J. Hall and A.R. Hillman, J.Electrochem.Soc., 127, (1980), 654.

72. T. Ikeda, C.R. Leidner and R.W. Murray, J.Am.Chem.Soc., 103, (1981), 7422.

73. A.P. Brown and F.C. Anson, Anal.Chem., 49, (1977), 1589.

74. R.J. Mortimer and D.R. Rosseinsky, J.Chem.Soc., Dalton Trans., (1984), 2059.

75. J.R. Lenhard, R. Rocklin, H. Abruna and R.W. Murray, J.Am.Chem.Soc., 100, (1978), 5213.

76. W.J. Albery, M.G. Boutelle, P.J. Colby and A.R. Hillman, J.Electroanal.Chem., 133, (1982), 135.

77. P.J. Peerce and A.J. Bard, J.Electroanal.Chem., 114, (1980), 89.

78. F.B. Kaufman and E.M. Engler, J.Am.Chem.Soc., 101, (1979), 547.

79. Southampton electrochemistry group; "Instrumental Methods in Electrochemistry", Ellis Horwood, Chichester, (1985), p.188.

80. I. Rubinstein and A.J. Bard, J.Am.Chem.Soc., 102 (1980), 6641.

81. P. Daum, J.R. Lenhard, D. Rolison and R.W. Murray, J.Am. Chem.Soc., 102, (1980), 4649.

82. P.K. Ghosh and A.J. Bard, J.Electroanal.Chem., 169, (1984), 113.

83. p.408 in ref. 79.

84. D.M. Oglesby, S.H. Omang and C.N. Reilly, Anal.Chem., 37, (1965), 1312.

85. T. Ikeda, R. Schmehl, P. Denisevich, K. Willman and R.W. Murray, J.Am.Chem.Soc., 104, (1982), 2683.

86. P.G. Pickup, W. Kutner, C.R. Leidner and R.W. Murray, J.Am.Chem.Soc., 106, (1984), 1991.

87. P. Denisevich, K.W. Willman and R.W. Murray, J.Am.Chem. Soc., 103, (1981), 4727.

88. C.D. Ellis, W.R. Murphy and T.J. Meyer, J.Am.Chem.Soc., 103, (1981), 7480.

89. M. Umana, P. Denisevich, D.R. Rolison, S. Nakahama and R.W. Murray, Anal.Chem., 53, (1981), 1170.

90. M. Umana, D.R. Rolison, R. Nowak, P. Daum and R.W. Murray, Surf.Sci., 101 (1980), 295.

91. R. Lazzaroni, S. Dujadrin, J-P. Boutique, C. Mousty-Desbuquoit, J. Riga and J. Verbist, Mol.Cryst,Liq.Cryst., 118, (1985), 249.

92. M.R. Ross, Ph.D. Thesis, Univ. of Minnesota, Minneapolis, USA, (1981).

93. J.A. Bruce and M.S. Wrighton, J.Am.Chem.Soc., 104, (1982), 74.

94. K.A. Macor and T.G. Spiro, J.Am.Chem.Soc., 105, (1983),5601.

95. K.A. Macor and T.G. Spiro, J.Electroanal.Chem.163, (1984), 223.

96a. J.P. Collman, P. Denisevich, T. Konai, M. Marrocco, C. Koval and F.C. Anson, J.Am.Chem.Soc.,102, (1980), 6027.
b. R.A. Bull, F-R. Fan and A.J. Bard, J.Electrochem.Soc., 130, (1983), 1636.

97. R.D. Rocklin and R.W. Murray, J.Phys.Chem., 85,(1981), 2104.

98a. R.W. Murray, Phil.Trans.Roy.Soc.Lond., A302,(1981), 253.
b. W.J. Albery, *ibid*, 221.

99. M.S. Wrighton, Chapter 7 in ref. 39.

100. M. Krishnan, X.Zhang and A.J. Bard, J.Am.Chem.Soc., 106, (1984), 7371.

101. M. Satoh, K. Kaneto and K. Yoshino, J.Chem.Soc.Chem. Commun., (1985), 1629.

102. K. Kaneto, Y. Kohno, K. Yoshino and Y. Inuishi, J.Chem. Soc.Chem.Commun., (1983), 382.

103. K. Rajeshwar, P. Singh and J. DuBow, Electrochimica Acta, 23, (1978), 1133.

CHAPTER TWO

A STUDY OF ELECTRODE DEPOSITS OBTAINED FROM PYRROLE, ANILINE, FERROCENE AND A PYRROLE SUBSTITUTED FERROCENE

2.1 Electropolymerization of anilines

2.1.1 Introduction

Despite the early discovery of the aniline blacks,[1] few systematic studies of polymeric or oligomeric electrode coatings derived from the electrooxidation of aniline have been reported.[2-7] From the published work it is clear that the nature of the deposit formed varies greatly with the solvent/electrolyte system used and particularly with pH.[6] From the results of an infra-red spectroscopic study, Oyama *et al*[6] postulated that the conducting polyaniline film produced from aqueous sulphuric acid was para (1,4) linked, whilst insulating polymers produced from neutral or basic solution were linked by N-N bonds as well as meta (1,3) N-C bonds.

Diaz and Logan[3] noticed that polyaniline formed from sulphuric acid solution could be electrochemically switched between an oxidized, blue coloured form and a reduced, transparent yellow form, in a manner analogous to that for polypyrrole. In contrast to polypyrrole however, both the oxidized and reduced forms of the film were found to be conducting. This observation led Diaz and Logan to speculate that the switching reaction was associated with proton addition and elimination at nitrogen rather than oxidation and reduction of a conjugated polymer chain.

Kitani *et al*[7] discovered that the conductivity of polyaniline films formed from aqueous sulphuric or perchloric acid was drastically decreased by immersion in alkaline solution. The authors also noted the formation of a

white precipitate when a film of polyaniline, formed from aqueous sulphuric acid solution, was electrochemically reduced in the presence of barium chloride. Elemental analysis of oxidized, reduced and alkali treated samples of polyaniline, deposited from sulphuric acid solution, gave sulphur stoichiometries of 1.13, 0.81 and 0.16 respectively, for each C_6N_1 unit. These results led the authors to conclude that SO_4^{2-} or HSO_4^- anions were associated with an N protonation/deprotonation reaction and, to a lesser extent, with a 'polypyrrole-like' oxidation/reduction process.

The only ESCA results which have been reported for polyaniline are for films formed in basic acetonitrile solution, when binding energies for C_{1s}, N_{1s} and O_{1s} were presented,[4] and surface elemental ratios for films deposited in aqueous sulphuric acid.[5] An ESCA study of polyaniline films produced in acidic and neutral media was therefore undertaken to complement the reported elemental analysis and infra-red results.

2.1.2 Results and Discussion

The polyaniline films formed from both hydrochloric and sulphuric acid solutions were green after drying and were approximately one millimetre thick. These films adhered well to the electrode but on removal were powdery. The film in pH7 solution had a bronze metallic lustre and was much thinner, probably one micron or less. In all cases the electrolysis current was observed to decrease with time, as film deposition proceeded, but for the neutral solution this decrease was much more rapid.

The C_{1s}, N_{1s}, O_{1s} and, where relevant, Cl_{2p}, S_{2p} or P_{2p} core level ESCA spectra for polyaniline films grown from 1M HCl, 1M H_2SO_4 and pH7 solutions are shown in Figure 2.1.1, a, b and c respectively. Corresponding binding energies are given in Table 2.1.1 and compared to those of Volkov *et al*[4] for polyaniline prepared in basic acetonitrile solution by potentiostatic growth at +1.0v *versus* Ag^0/Ag^1 reference electrode. Surface elemental stoichiometries are presented in Table 2.1.2, and compared to those of Hernandez *et al*[5] for films grown in 0.1M H_2SO_4 by cycling the working electrode potential between -0.2 and +0.8V *versus* sodium chloride saturated calomel electrode. The elemental analysis stoichiometries for polyaniline films potentiostatically grown in 0.1M H_2SO_4 reported by Kitani *et al*[7] are also given for comparison.

From the results presented several points may be highlighted:

1. Only for the film produced in H_2SO_4 was a high anion incorporation observed. For the film formed in the buffer solution no phosphorus containing species at all could be detected. The S_{2p} binding energy is characteristic of sulphate. The high sulphate incorporation is in qualitative agreement with the elemental analysis but in disagreement with the ESCA results of Hernandez *et al*. Two possible explanations for this disparity are:

(a) that the potential cycling method used by Hernandez *et al* leads to a lower anion incorporation level, or

(b) that the films studied by Hernandez *et al*, which were approximately 500nm thick, had lost the anion before analysis. Anomalous anion incorporation levels have

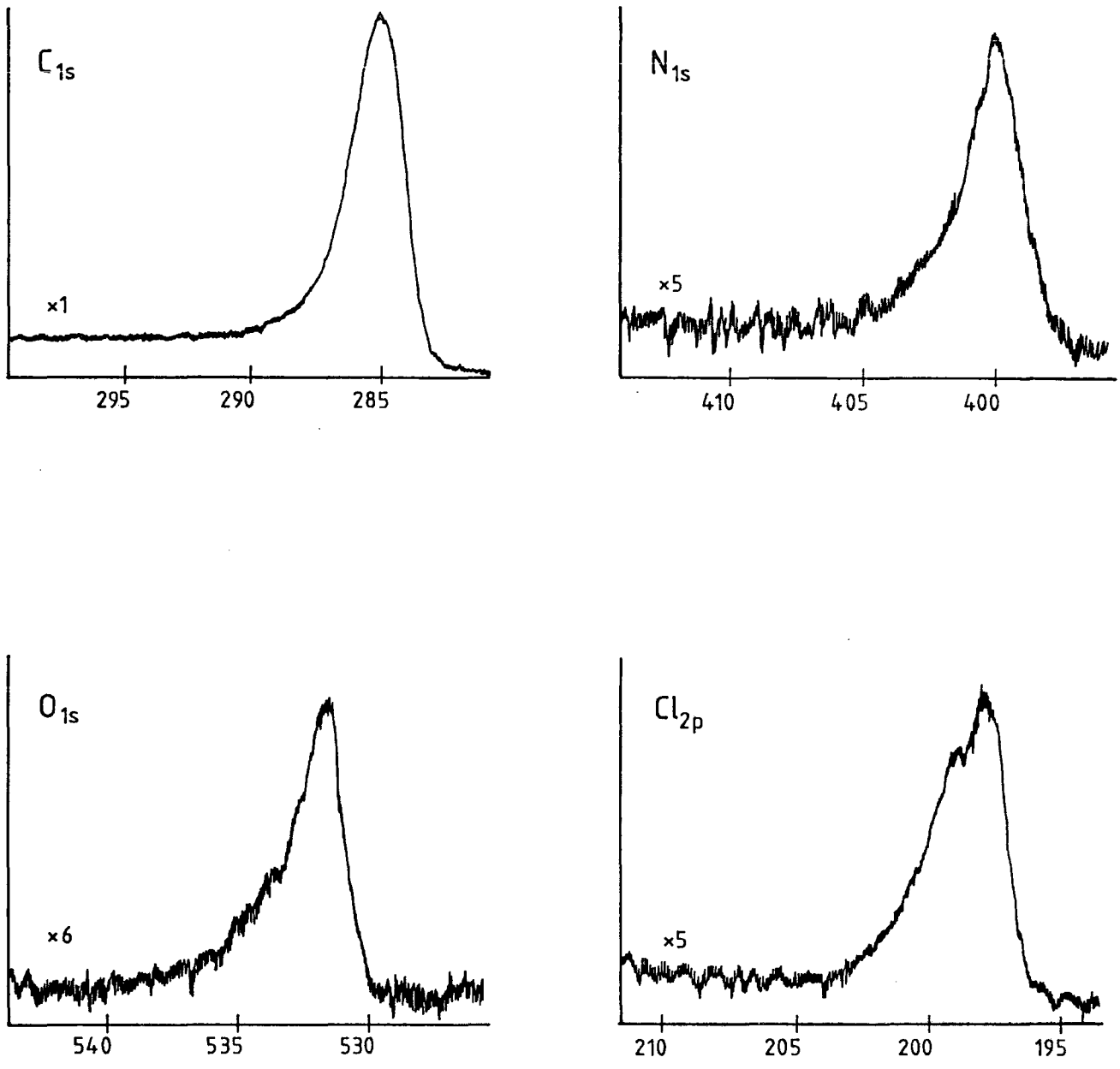

FIGURE 2.1.1.a ESCA spectra for a polyaniline sample formed from HCl solution. Binding energies in eV.

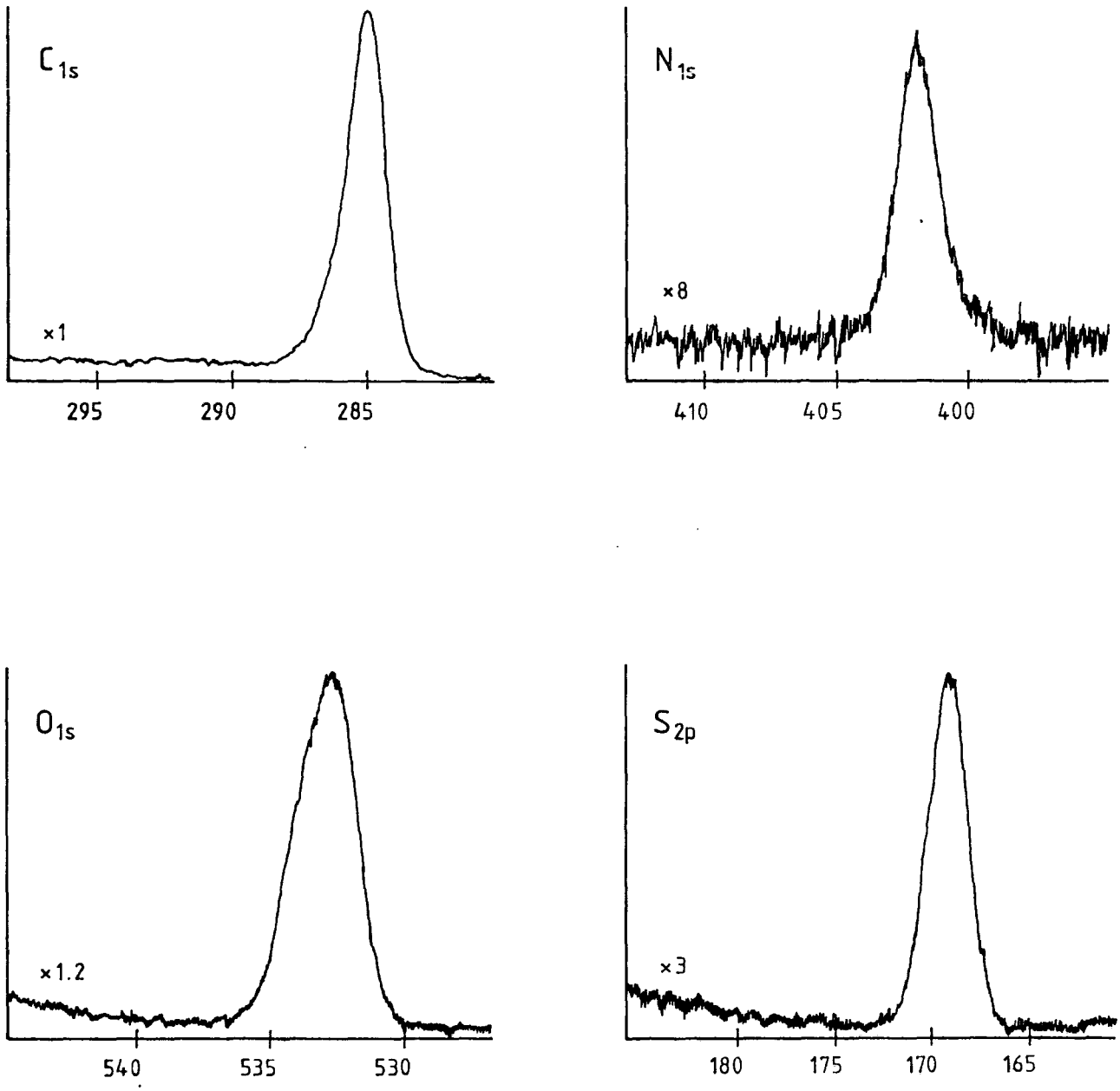

FIGURE 2.1.1.b ESCA spectra for a polyaniline sample formed from H_2SO_4 solution. Binding energies in eV.

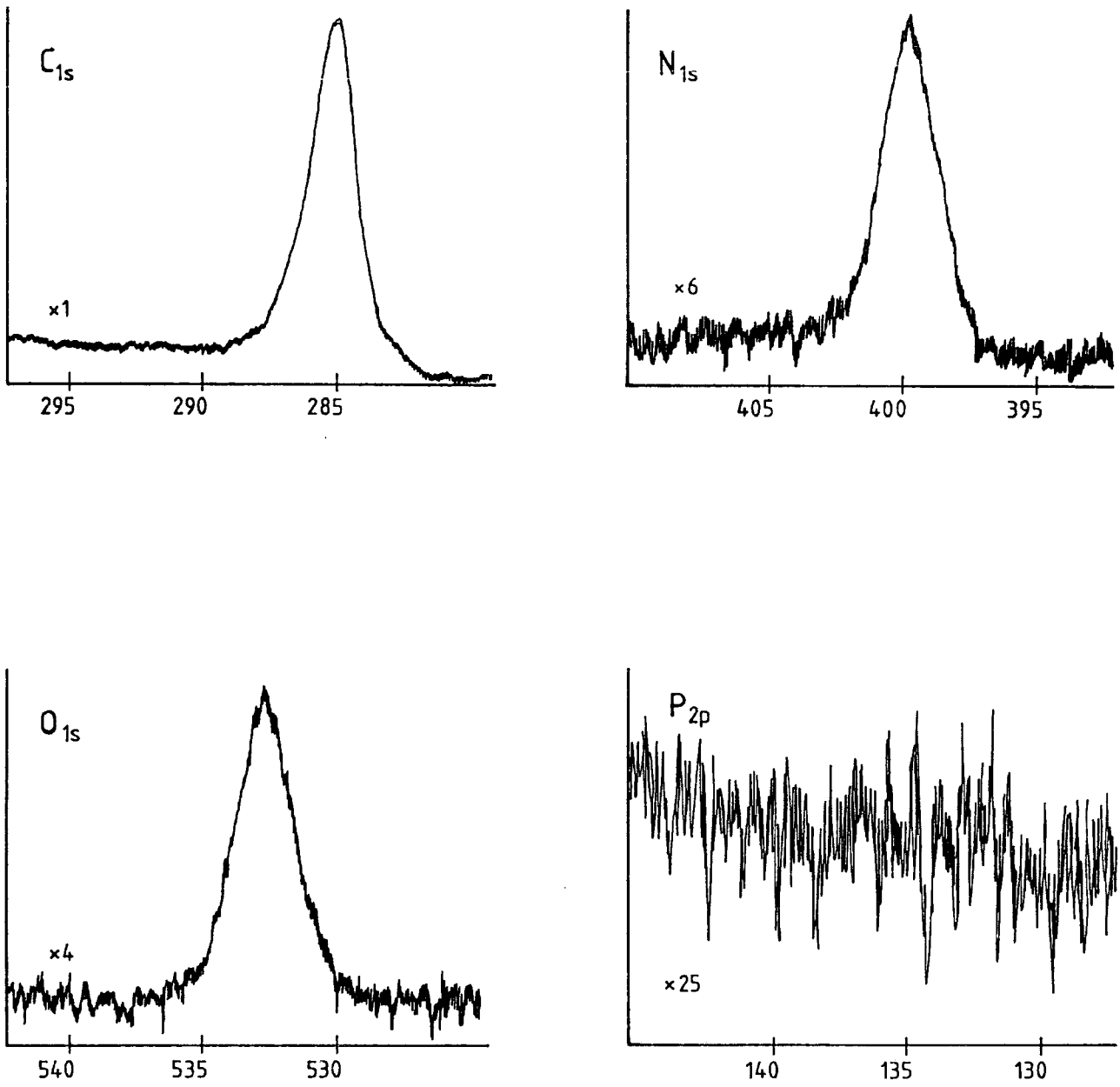

FIGURE 2.1.1.c ESCA spectra for a polyaniline sample formed from pH7 buffer solution. Binding energies in eV.

TABLE 2.1.1 Binding energies (in eV) for polyaniline deposits[a]

Electrolyte	N_{1s}	$Cl_{2p_{3/2}}$	$S_{2p_{3/2}}$	Ref.
1M H_2SO_4(aq.)	402.0	-	169.2	this work
1M HCl (aq.)	400.0	199.0	-	this work
pH7 buffer (aq.)	399.9	-	-	this work
0.1M $NaClO_4(CH_3CN)$	399.9	-	-	4

a. Relative to C_{1s} at 285.0 eV

TABLE 2.1.2 Surface and bulk stoichiometries for polyaniline deposits

Electrolyte	Stoichiometry	Ref.
1M H_2SO_4 (aq.)	$C_6N_{0.64}S_{1.5}O_{4.8}$[a]	this work
1M HCl (aq.)	$C_6N_{1.0}Cl_{0.6}O_{0.6}$[a]	this work
pH7 buffer (aq.)	$C_6N_{0.8}O_{0.8}$[a]	this work
0.1M H_2SO_4 (aq.)	$C_6N_{0.66}S_{0.02}O_{0.70}$[a]	5
0.1M $HClO_4$ (aq.)	$C_6N_{0.97}(ClO_4)_{1.14}$[b]	7
0.1M H_2SO_4 (aq.)	$C_6N_-(SO_4)_{1.13}$[b]	7

a. Surface stoichiometries derived from ESCA peak areas.

b. Bulk stoichiometries derived from elemental microanalysis.

been observed for very thin films of electrochemically prepared polypyrrole.[8] It seems unlikely that the acid concentration difference between the Hernandez study and the present work is the reason for the disparity since the elemental analysis results[7] were also for films formed from 0.1M H_2SO_4.

If the sulphur containing species were SO_4^{2-} then both the elemental analysis and the present ESCA results would indicate that a positive charge of greater than 2+ resides on each polymerized aniline unit. Kitani *et al*[7] obtained a similar anion incorporation level when using perchloric acid electrolyte ($C_6N_{0.97}Cl_{1.14}$) and speculated that the anion in polyaniline formed from H_2SO_4 may be HSO_4^-.

2. The nitrogen content is consistently low for the surface compared to the bulk, Hernandez *et al* speculated that this may be due to some unknown surface degradation process, but surface hydrocarbon contamination will also decrease the nitrogen to carbon ratio.

3. The N_{1s} binding energy for the sample prepared in H_2SO_4 solution is significantly higher than for any of the other samples which all have N_{1s} binding energies of 400.0eV±0.3eV. This result, in combination with the high anion content, suggests that only for the sulphuric acid grown sample is positive charge localized on the nitrogen atoms and therefore, following Kitani *et al*, that the nitrogen atoms are all protonated. For a model compound with unit positive charge on a nitrogen atom, tetrabutylammonium perchlorate (TBAP) the N_{1s} binding energy was found to be

402.2eV which agrees well with the suggestion of a single positive charge localized on each nitrogen atom of the sulphuric acid grown film.

The difference in the films formed in sulphuric and hydrochloric acid is difficult to rationalize, however a significantly higher rate of film formation has previously been noted in sulphuric acid compared to hydrochloric.[7]

4. In all the polyaniline C_{1s} spectra a step in the 'background' level in going from the low to high binding energy side of the peak is observed. This feature has previously been observed in ion beam degraded polymers[9,11a] and plasma polymers[10] and is an indication of electron delocalization in structurally disordered systems. These spectra may be compared to the C_{1s} spectrum of polyethylene, where no step is observed[11] and to polystyrene where a discrete shake up satellite is found.[11] Hutton[9] found a linear increase in the step height with C/H ratio in a series of polycyclic aromatic compounds. For all the polycyclic aromatics studied distinct shake up features could be discerned over the step feature.[9]

2.1.3 2,3,5,6 Tetrafluoroaniline

Theoretical studies on polyfluoroacetylene and polydifluoroacetylene led Fukui *et al* to conclude that these polymers, if synthesized, would have higher intrinsic electronic conductivities than polyacetylene.[12] There are few reports of the synthesis of fluorinated conducting polymers however preliminary results described by Ahmad and Feast have shown that a fluorinated analogue of poly(1,6-heptadiyne) has

an intrinsic conductivity 10^7 times greater than the hydrocarbon polymer.[13]

Pedlar *et al* reported the electrochemical oxidation of pentafluoroaniline, in a solution of potassium acetate in acetone/water, to give two products namely decafluoroazobenzene and octafluorophenazine.[14] Similar oxidation of p-methoxy-tetrafluoroaniline gave analogous, methoxy substituted products.[14c] 2,3,5,6-Tetrafluoroaniline which, with a para hydrogen, may in principle form a 1,4 linked polymer or oligomer, as well as the azobenzene and phenazine products, was not studied by Pedlar *et al*.

Electrolysis of 2,3,5,6-tetrafluoroaniline in acetonitrile-TBAP solution or in methanol-sulphuric acid produced no deposit on the electrode but yielded an intensely red coloured solution which was not analysed but is assumed to arise from products analogous to those obtained by Pedlar *et al*. Electrolysis in the acetonitrile-hydrochloric acid system produced little colouration in solution but a thin, bronze coloured film was deposited onto the electrode surface.

The results of ESCA analysis for the film are shown in Figure 2.1.2 A fluorine to nitrogen elemental ratio of 3.9 was obtained which strongly suggests that the film is either an adsorbed azobenzene (11) or a polyaniline, both of which require a fluorine to nitrogen ratio of 4.0. A phenazine product (1) would require a fluorine to nitrogen ratio of 3.0.

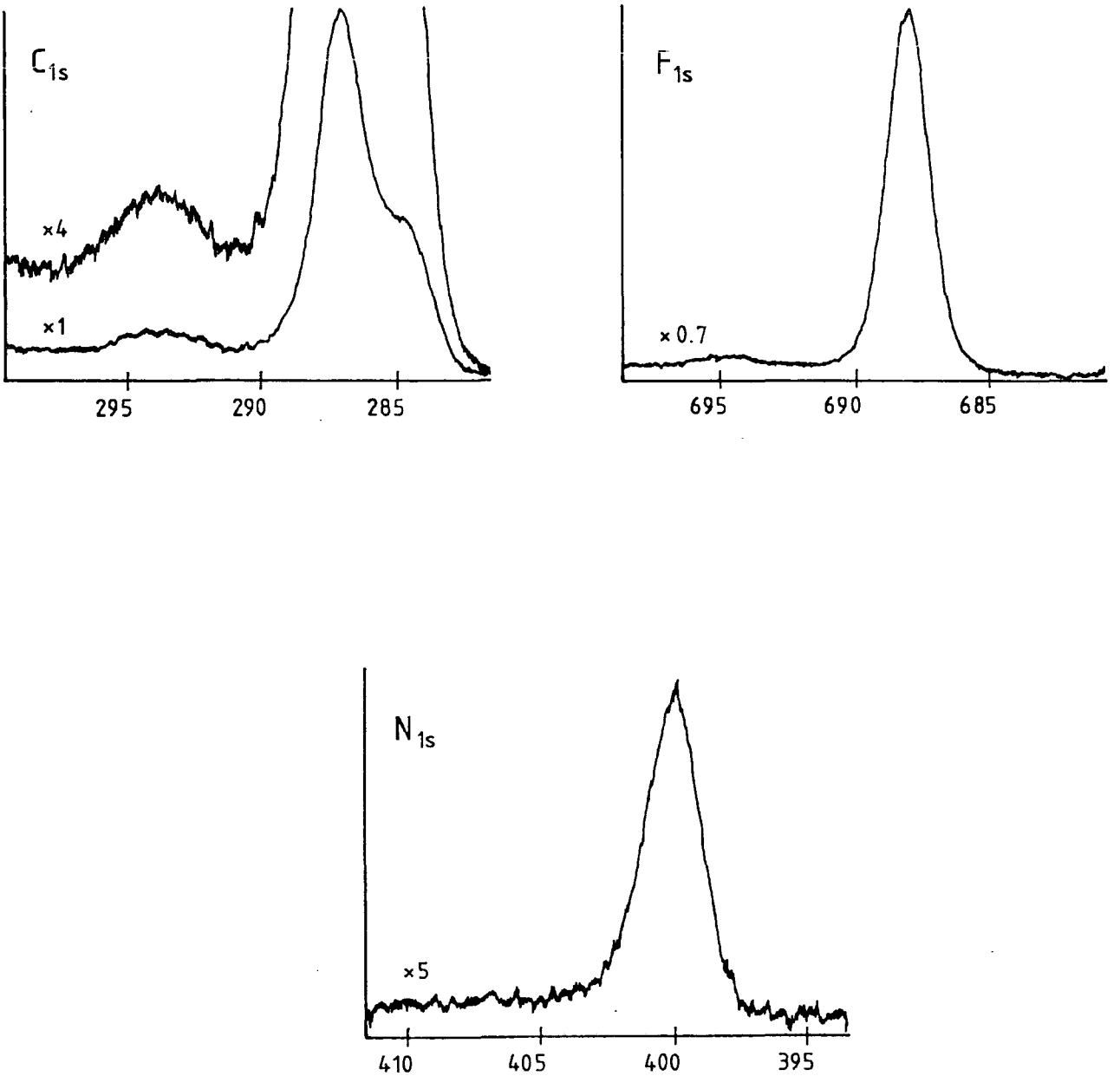

FIGURE 2.1.2 C_{1s}, F_{1s} and N_{1s} core-level ESCA spectra for the deposit formed by electrolysis of 2,3,5,6-tetrafluoroaniline in CH_3CN/HCl solution. Binding energies in eV.

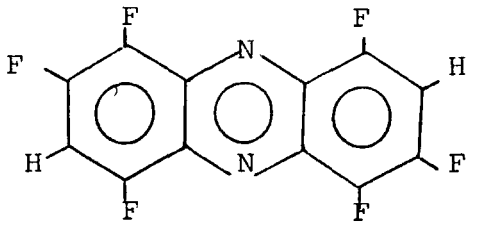

(1)

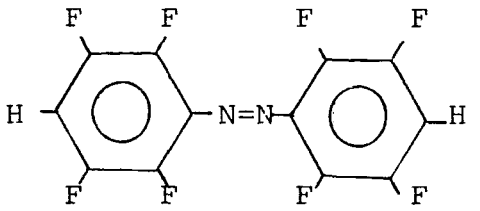

(11)

The carbon to fluorine ratio was 1.9. At first sight this seems to suggest that the film is an adsorbed phenazine (1) which would have a C/F ratio of 2.0 and not the other possible products both of which have a C/F ratio of 1.5. Excessive carbon was found in the polyaniline spectra described in the previous section. The most likely cause of this excess is surface hydrocarbon contamination and thus an observed C/F ratio of 1.9 from the present spectra is not inconsistent with an adsorbed azobenzene (11), or polymeric product.

Discrete shake up satellites may be observed in both the C_{1s} and F_{1s} spectra which contrast, the broad, featureless background steps seen in the polyaniline C_{1s} spectra. This suggests a different and perhaps more localized conjugation in the tetrafluoroaniline film.

In further contrast to the deposits obtained from aniline, the film formed from tetrafluoroaniline was soluble in acetone, suggesting that it was not a polymer.

2.1.4 Conclusions

Polyaniline films formed in different aqueous electrolyte solutions have different surface chemistries. Films formed in sulphuric acid solution have a higher anion content and a higher N_{1s} binding energy than films formed in the other electrolyte solutions used. In agreement with previous work[7] these results suggest that the nitrogen atoms in polyaniline films formed in sulphuric acid solution are protonated.

There is no evidence to suggest that a polymer or large oligomer is formed from the electrooxidation of 2,3,5,6 tetrafluoroaniline under any of the experimental conditions used.

2.2 Electropolymerization of Pyrrole

2.2.1 Introduction

Salaneck *et al*[15] and Pfluger and Street[8] have published reports devoted to the ESCA analysis of oxidized polypyrrole films electrochemically prepared from 0.1M solutions of pyrrole in tetrafluoroborate,[8,15], perchlorate[8] and hexafluorophosphate[8] electrolyte solutions.

The results may briefly be summarized as follows:

1. Asymmetric C_{1s} lineshapes were observed for all doped oxidized samples. This asymmetry was much greater than for electrochemically undoped (reduced) samples, and could not therefore be associated solely with the chemical shift of C-N carbons. Salaneck *et al* interpreted the asymmetry

as evidence for metal-like character in polypyrrole whereas Pfluger and Street ascribed the origin of the asymmetry to inequivalent pyrrole units in a disordered film.

2. Broad shake up satellites or step features were observed in the C_{1s} spectra of doped samples, whereas distinct shake up satellites were found for electrochemically undoped polypyrrole.[15a]

3. Salaneck *et al* observed a single N_{1s} peak whereas Pfluger and Street found a multicomponent N_{1s} peak broadened to the high binding energy side of the main component.

4. Pfluger and Street found a pyrrole unit to perchlorate anion ratio of 3:1 and both Pfluger and Street and Salaneck *et al* found a pyrrole to tetrafluoroborate ratio of 4:1. In a later publication Salaneck *et al* found, from a study of several samples, that the pyrrole to tetrafluoroborate ratio, determined by ESCA, varied between 4:1 and 10:1.[15b]

5. Salaneck *et al* also found that a sample of tetrafluoroborate doped polypyrrole which was subjected to one complete switching cycle (*i.e.* electrochemical reduction followed by reoxidation) in tetrabutylammoniumtetrafluoroborate (TBAT) electrolyte contained no boron and negligible fluorine, but a large amount of oxygen. This observation indicated that the tetrafluoroborate anion was not reincorporated upon reoxidation but was replaced by an oxygen containing anion. Storage in various controlled atmospheres was also found to induce loss of incorporated tetrafluoroborate and increase in oxygen content over a period of days.

In Section 2.5 and Chapter Three of this work pyrrole has been used as an electropolymerizable unit, covalently bound to electroactive molecules, to produce modified electrodes which have been studied by ESCA. It thus seemed essential to first characterize the parent material, polypyrrole by ESCA, particularly since some disagreement exists in published work regarding the N_{1s} lineshape and surface dopant concentration.

2.2.2 Results and Discussion

The C_{1s}, N_{1s} and where relevant Cl_{2p} and F_{1s} spectra for polypyrrole perchlorate and polypyrrole tetrafluoroborate are shown in Figure 2.2.1, a and b, respectively, binding energies of the main components are given. Surface elemental compositions are also given in Figure 2.2.1. B_{1s} spectra were not recorded since the 1s level for boron has a low cross-section to photoionization by MgKα radiation. In the elemental compositions given in Figure 2.2.1 one boron atom has been associated with four fluorine atoms. The validity of this procedure has been demonstrated by both Salaneck *et al*[15] and Pfluger and Street,[8] who recorded B_{1s} spectra for polypyrrole tetrafluoroborate and found the binding energy to be correct for BF_4^- and fluorine to boron ratios of 3.8 and 3.6 respectively.

The Cl_{2p} binding energy in Figure 2.2.1 for polypyrrole perchlorate is consistent with a ClO_4^- anion and the oxygen to chlorine elemental ratio of 4.4:1, although higher than the expected value, is in good agreement with that found by Pfluger and Street.[8]

$C_{5.4}N_1Cl_{0.35}O_{1.52}$

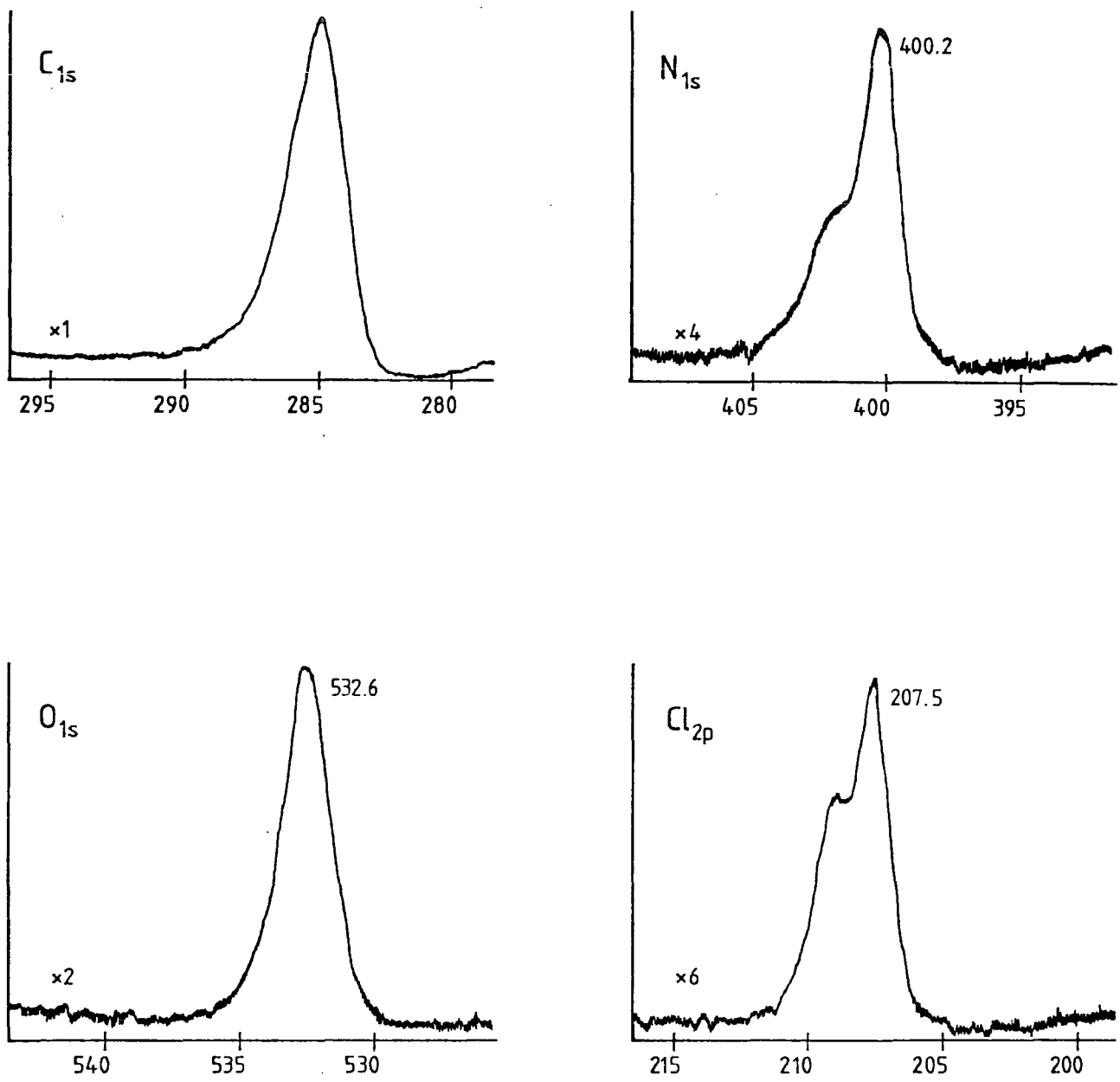

FIGURE 2.2.1.a. ESCA spectra for polypyrrole formed from TBAP electrolyte solution. Binding energies in eV.

$C_{5.9}N_1B_?F_{0.64}$

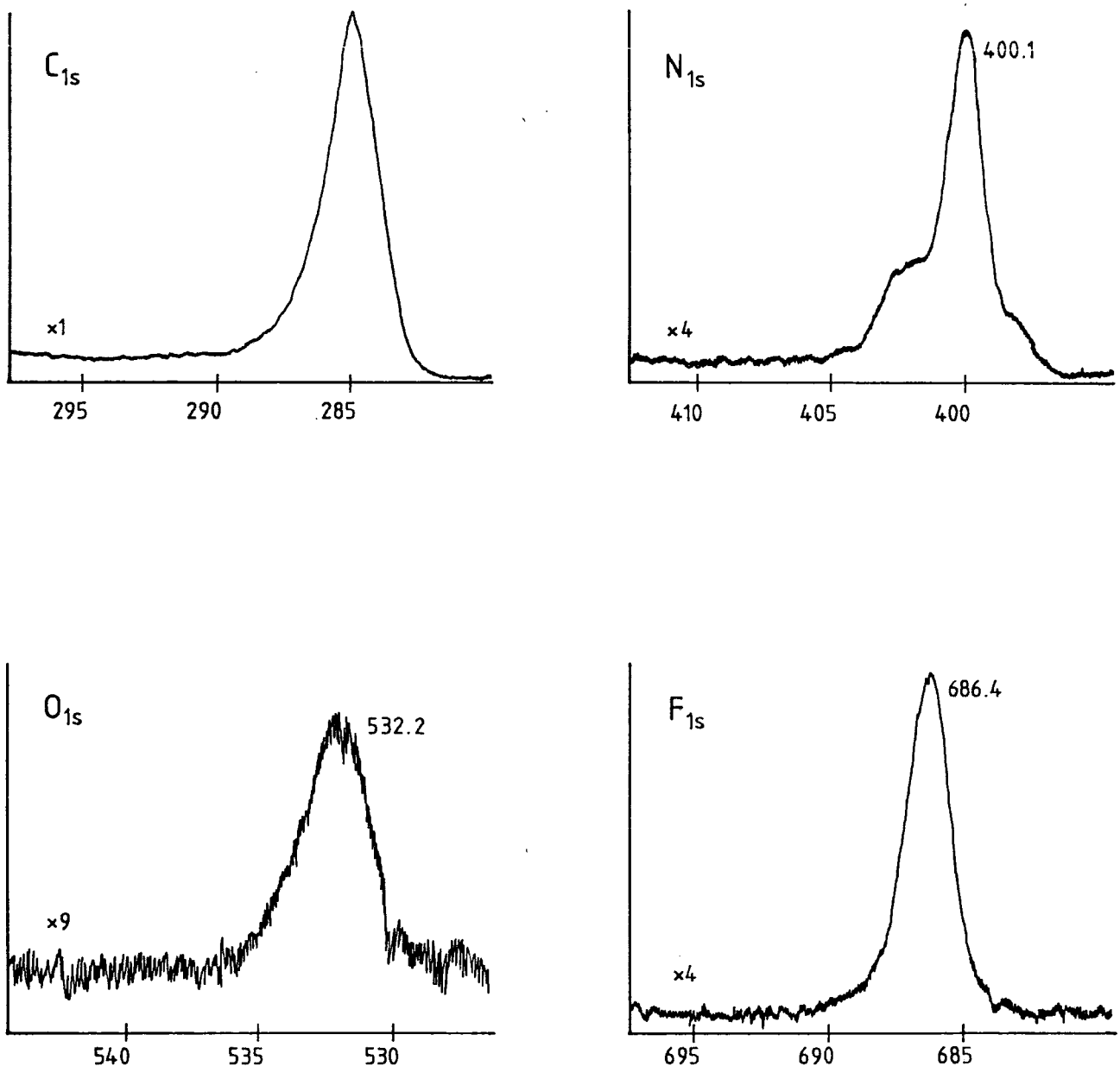

FIGURE 2.2.1.b. ESCA spectra for polypyrrole formed from TBAT solution. Binding energies in eV.

The carbon to nitrogen ratio is consistently greater than 4:1, probably as a result of some surface hydrocarbon contamination. The doping level given in Figure 2.2.1 is therefore calculated from the nitrogen to chlorine and nitrogen to fluorine elemental ratios, assuming the anions to be ClO_4^- and BF_4^- respectively.

The ESCA results for polypyrrole perchlorate are in good agreement with elemental analysis[16] in that a doping level of approximately one ClO_4^- anion for every three pyrrole units is obtained. For polypyrrole tetrafluoroborate a much lower doping level of approximately one BF_4^- anion for every six pyrrole units was found by ESCA compared to one to four found by elemental analysis.[16] This discrepancy has been noted previously by Salaneck.[15b]

It is clear that the N_{1s} spectra in Figure 2.2.1 for both polypyrrole tetrafluoroborate and polypyrrole perchlorate are not single peaks but are broadened to the high binding energy side of the main component. This result is in agreement with the N_{1s} spectra published by Pfluger and Street but not those of Salaneck *et al*. Furthermore the spectra in Figure 2.2.1 contrast with the N_{1s} spectra of the polyanilines reported in Section 2.1.2 where, regardless of the binding energy, single component peaks were observed. For the polypyrrole tetrafluoroborate sample a small peak at 398.2eV is observed. This feature has previously been noted in samples of polypyrrole which have been electrochemically undoped then reoxidized either chemically or electrochemically,[17] but has not been observed for as grown, oxidized films before. The origin of the peak is unknown

but, from a comparison of N_{1s} binding energies of known compounds, Pfluger *et al*[17] suggested that it may be due to a structure such as (111), resulting from deprotonation and bond rearrangement.

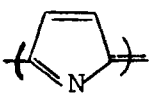

(111)

For the high binding energy shoulders the most obvious conclusion to draw is that they are associated with the oxidative doping of the polypyrrole chains. No correlation between the amount of oxidized nitrogen, seen in the N_{1s} spectrum, and the anion doping level has previously been reported. In order to investigate this possibility more fully two more samples of polypyrrole tetrafluoroborate were prepared, one as for the original sample but by cycling the electrode potential between 0 and +1.2V, and the other as for the original sample but from a 0.1M solution of pyrrole.

Curve fitted N_{1s} spectra are shown in Figure 2.2.2 together with the percentage of the total N_{1s} signal which arises from the components centred at a binding energy greater than 401eV (Column A). The percentage oxidation, predicted from the doping level, and derived from the nitrogen to chlorine and nitrogen to fluorine elemental ratios is given in Column B. The N_{1s} spectrum obtained for the sample produced by cycling the electrode potential is similar to Figure 2.2.2b and is not shown. If every oxidized nitrogen atom is associated with one electrolyte dopant anion the figures in Columns A and B of Figure 2.2.2 should agree.

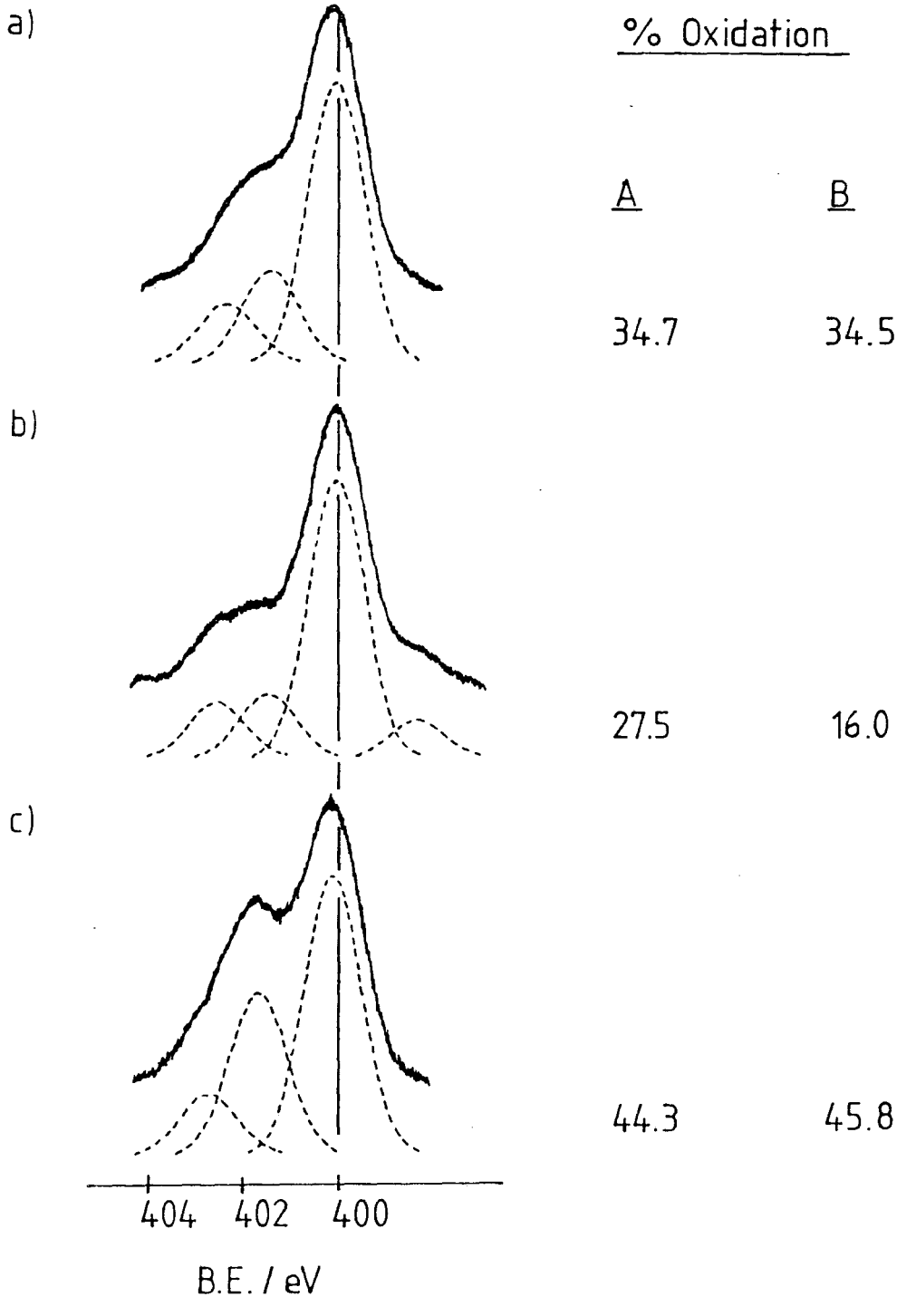

FIGURE 2.2.2 Curve fitted N_{is} spectra for polypyrrole samples. The samples were formed by CPE at +1.0V from:

(a) $5x10^{-3}$Mpyrrole/0.1M TBAP,

(b) $5x10^{-3}$M pyrrole/0.1M TBAT,

(c) 0.1M pyrrole/0.1M TBAT.

The spectra were fitted to Gaussian peak shapes. The position, intensity and peak width (FWHM) of the main component is unambiguous. The position and intensity of the other peaks were then optimized to give the best fit to the experimental spectrum maintaining the same FWHM as the main component.

Retention of peak FWHM was not favoured by Pfluger and Street who chose to curve fit the oxidized nitrogen environment to two peaks each of more than twice the main peak FWHM.[8] Whilst this approach has some merit, since increasing the positive charge on a nitrogen atom will decrease the N_{1s} core-hole lifetime and hence broaden the peak, the effect must have been grossly overestimated by Pfluger and Street. For a model compound (TBAP), having unit positive charge on nitrogen, the FWHM obtained on the ES300 was only 13% broader than the average FWHM of the main N_{1s} component for the polypyrrole films. Retention of peak FWHM for all components thus seems more appropriate.

From the data in Figure 2.2.2, it is clear that anion dopant concentration increases with the percentage of high binding energy nitrogen to the total N_{1s} signal. For the sample prepared from 0.1M pyrrole in TBAT an unusually high anion concentration was found but this agrees very well with the N_{1s} spectrum shown in Figure 2.2.2c. Good agreement is also found for the polypyrrole perchlorate sample (Figure 2.2.2a). For the sample prepared from $5x10^{-3}$M pyrrole in TBAT the oxidation level given by the N_{1s} spectrum exceeds the level predicted by the anion concentration (Figure 2.2.2b). The same is true for the sample of polypyrrole tetrafluoroborate formed by potential cycling where

23.2% of the total N_{1s} signal arises from oxidized components, whereas the amount of fluorine detected is sufficient for only 16% of the pyrrole units to be associated with tetrafluoroborate anions. These results may constitute quantitative evidence for anion replacement by oxygen containing species. Low levels of oxygen, sufficient to account for the discrepancy between the two methods of calculation, were detected for these samples. The amount of oxygen detected for the highly oxidized sample of polypyrrole tetrafluoroborate (Figure 2.2.2c) was insignificant. Surface deficiency of tetrafluoroborate for immediately analysed samples has previously been noted[15b] but not quantified in this manner.

Some caution should be exercised in comparing the oxidation levels obtained by the two methods of calculation described above. The ratio of component peak areas for the N_{1s} spectra gives directly the fraction of oxidized nitrogen atoms. It does not, however, say anything about the oxidation state or fractional positive charge on the nitrogen atoms. The most obvious method of analysis would be to associate different degrees of fractional positive charge to the two high binding energy N_{1s} components. Pfluger and Street followed this procedure and ascribed charges of $^1/_6$ + and $^1/_2$ + to components centred at 400.6eV and 402.8eV respectively. This is wholly inconsistent with a binding energy of 402.2eV for the N_{1s} spectrum of TBAP found by the same authors.[8]

The high binding energy component peaks used in Figure 2.2.2 were centred at 401.6±0.2eV and 402.8±0.2eV.

For the percentage of oxidized nitrogen to equal the total percentage doping level all the polypyrrole positive charge must be located on nitrogen and the average charge on the oxidized nitrogen atoms must be unity. For tetraalkylammonium cations, with a single positive charge on nitrogen, binding energies varying between 401eV[18] and 402.6eV[8] have been reported. It thus seems possible that both high binding energy components in the N_{1s} spectra of Figure 2.2.2 represent a unit positive charge, but that they may arise from nitrogen atoms which are chemically inequivalent (*e.g.* protonated or doubly bonded to carbon) or in structurally inequivalent sites. Supporting evidence for this hypothesis may be found in Figures 2.2.2a and c. In Figure 2.2.2a the area ratio of the 401.6eV peak to the 402.8eV is 1.6, in Figure 2.2.2c this ratio is 2.7. In both cases good agreement between the two methods of calculation of the percentage of polymer oxidation is found, this would not be expected if the two high binding energy components arose from nitrogen atoms bearing different degrees of positive charge.

Using the relative component peak areas and associated fractional charges given by Pfluger and Street,[8] the percentage oxidation predicted by their lineshape analysis would be 16.7%, in poor agreement with the perchlorate doping level of approximately 33%. From C_{1s} lineshape analyses positive charge was considered not to be associated with carbon atoms by Pfluger and Street.[8]

The C_{1s} spectra of polypyrrole perchlorate and polypyrrole tetrafluoroborate are similar and all but superimpose when compared. This situation contrasts with the

corresponding N_{1s} spectra (Figures 2.2.2a and b) discussed above and may be taken as evidence that positive charge is not localised on the carbon atoms.

The step feature noticed for the polyanilines is also observed in the C_{1s} spectra of the polypyrroles. A quantitative measure of this feature is given by the height of the step above the horizontal background on the low binding energy side of the peak (Δh) divided by the height of the main peak above the same background (h) as shown in Figure 2.2.3. For a perfectly horizontal background on the high binding energy side of the peak it is not important where, on the binding energy axis, the value of Δh is measured from. However, in the case of the polyaniline film prepared in pH7 buffer solution a shake up feature may be observed on the step and so all values of Δh were measured at a point 6.1eV removed from the centre of the peak. This is a point at which the step height is zero for the C_{1s} spectrum of high density polyethylene. The results are presented in Table 2.2.1 and compared to those for the polyaniline spectra and those obtained by Hutton[9] for pyrene and coronene.

Whilst Hutton has shown a linear increase in $\Delta h/h$ with C/H ratio for polycyclic atomatics it is clear that there is no simple relationship between bulk electronic conductivity and $\Delta h/h$, since the largest relative step height is found for the sample of polyaniline formed in neutral solution which is known to be insulating.[6]

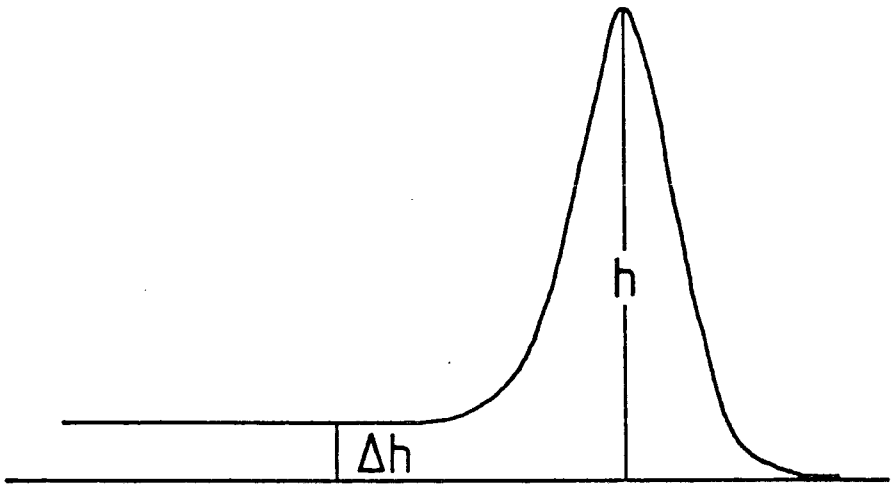

FIGURE 2.2.3

TABLE 2.2.1 C_{1s} step heights ($^{\Delta h}/_{h}$)

Sample	$^{\Delta h}/_{h}$	Ref.
PP, CPE-CH_3CN/TBAT	0.07	this work
PP, CPE-CH_3CN/TBAP	0.07	this work
PAn, CPE-H_2SO_4 (aq.)	0.05	this work
PAn, CPE-HCl (aq.)	0.10	this work
PAn, CPE-pH7 (aq.)	0.11	this work
Pyrene	*ca.* 0.06	9
Coronene	*ca.* 0.07	9

PP = Polypyrrole

PAn = Polyaniline

CPE = Controlled Potential Electrolysis.

2.2.3 Conclusions

In summary, a novel method has been presented for the determination of the degree of oxidation of polypyrrole samples which is not sensitive to anion exchange processes. The validity of the method depends upon the assumption of an average positive charge of one on the oxidized nitrogen atoms.

2.3 Electroadsorption from ferrocene solutions

2.3.1 Introduction

The previous sections have shown how ESCA may be used to study electrochemical polymers derived from pyrrole and aniline. In Section 2.5 and Chapter Three a study is presented of electroactive films produced from monomers in which pyrrole forms the electropolymerizable unit covalently bound, through the nitrogen atom, to electroactive molecules. Initially, the electrochemical deposition of redox active molecules which are commercially available was attempted. Described below is an attempt to electrochemically deposit vinylferrocene and in Section 2.4 an attempt to generate an electroactive film by electrochemical polymerization of pyrrole in the presence of vinylferrocene is described.

Bard *et al*[19] have reported the oxidative electrochemical deposition of radical initiation polymerized polyvinylferrocene from solution onto an electrode surface. The film, apparently deposited as polyvinylferricenium, displayed electrochemistry characteristic of ferrocene. In contrast,

it is reported[20,21] that monomeric vinylferrocene does not surface electropolymerize in either the ferrocene or ferricenium state to an electrochemically detectable extent. Since, in principle, as little as one monolayer of surface deposited electroactive film should be electrochemically detectable, it seems likely that either vinylferrocene forms no electrodeposit at all, or that a thin deposit is formed which has no electroactivity, ESCA is ideally suited to resolve this ambiguity.

2.3.2 Results and Discussion

A platinum electrode potentiostatted in the vinylferrocene solution was found by ESCA to be coated with a film, containing only iron, carbon and oxygen in detectable levels (hydrogen is not detectable by ESCA), which was not thick enough to obscure the Pt_{4f} signal of the underlying electrode. The film thickness, calculated from the attenuation of the Pt_{4f} signal compared to clean platinum as described in the Appendix, was found to be 43Å. A film of polyvinylferrocene of this thickness should show a detectable cyclic voltammetric ferrocene/ferricenium wave, none was found as previously reported.[21] The non appearance of a CV wave, however, does not prove that the deposit does not contain ferrocene or ferricenium. It is possible that the film is not electrochemically active for some other reason such as an impermeability to solvent.

Only one broad $Fe_{2p_{3/2}}$ signal was detected by ESCA and this had a binding energy of 711.5eV (*c.f.* Figure 2.4.1) showing that all of the iron in the film was in the +3 oxidation state.

It will be shown in Section 2.5 that electro-oxidative deposition (at +1.3V) of an electroactive, ferrocene containing film leaves the reduced state, ferrocene, in the film and not ferricenium, the oxidized form. This result, together with the fact that no ClO_4^- anions were found in the vinylferrocene deposit, suggests that this deposit did not contain ferricenium but rather some irreversibly oxidized species.

Lane and Hubbard[22] have studied the ability of vinyl compounds to adsorb on platinum electrode surfaces and so ferrocene was also studied here in order to assess the importance of the vinyl group in the electrodeposition from vinylferrocene. ESCA results for an electrode potentiostatted in the ferrocene solution were qualitatively identical to those for vinylferrocene. From the attentuation of the Pt_{4f} substrate signal the film thickness was calculated to be 46Å which, within the experimental error, is the same as the thickness of the film obtained from vinylferrocene.

A control experiment with vinylferrocene, in which no electrolysis was performed but the electrode was allowed to stand in solution for twice the normal time, showed no ESCA detectable iron signal indicating that passive adsorption of vinylferrocene, under these conditions, is negligible.

2.4 Electrochemical codeposition of vinylferrocene and pyrrole

2.4.1 Introduction

Vinylferrocene may be polymerized by radical initiation[23] and divinylferrocene has been polymerized by cationic initiation.[24] In the preceding section it was demonstrated that vinylferrocene may not be oxidatively polymerized on an electrode surface. This does not mean that vinylferrocene may not be copolymerized or simply codeposited with another monomer which does undergo oxidative electropolymerization. Pyrrole was chosen as the monomer to attempt the codeposition with vinylferrocene since it is easily electropolymerized and the homopolymer has been well studied.[25] Previous, successful attempts to incorporate foreign molecules into polypyrrole deposits have used the doping mechanism to incorporate sulphonated metalloporphyrins[26] and phthalocyanines[27], RuO_4^{2-} and derivatised polymers[29] as dopant anions in the polypyrrole film. Few electrochemical copolymerizations with pyrrole have been reported.[30]

2.4.2 Results and Discussion

Seven samples were studied, formed at potentials between +0.7V and +0.9V *versus* SCE. In each case a golden coloured film was deposited on the electrode surface and a brown precipitate formed in solution. ESCA and CV results for the films are summarized below.

1. No systematic variation in surface elemental composition with deposition potential was found.

2. The average carbon to nitrogen elemental ratio was 14.0 with mininum and maximum values of 10.6 and 18.4. The average value is approximately twice that for the polypyrrole samples described in Section 2.2.

3. N_{1s} spectra were centred around 400eV but were broadened to the high binding energy side. The signal to noise ratio was not sufficiently good to allow any estimate of the degree of oxidation by curve fitting the N_{1s} spectral envelope. In some spectra no Cl_{2p} signal was detected whilst in others a very small signal was observed. High oxygen levels were found, the average carbon to oxygen ratio being 2.5.

4. The average carbon to iron ratio was 17.4 with minimum and maximum values of 11.0 and 35.2. In all $Fe_{2p_{3/2}}$ spectra at least 95% of the total integrated intensity arose from photoionization of iron in the +3 oxidation state (see Figure 2.4.1). The remainder arose from iron in the +2 oxidation state having a binding energy of *ca.* 709eV and, from the peak width, could unequivocally be associated with photoionization of iron in a ferrocene environment (*vide infra*).

5. When the pyrrole concentration was increased by a factor ofthree and a deposition at +0.9V performed the spectrum of the resulting film showed no $Fe_{2p_{3/2}}$ signal and was in every other respect (elemental ratios, peak shapes) typical of a polypyrrole perchlorate spectrum as described in Section 2.2. This film was removed from the platinum electrode using Scotch tape and the inner surface analysed by ESCA, it was found to be similar to the outer surface.

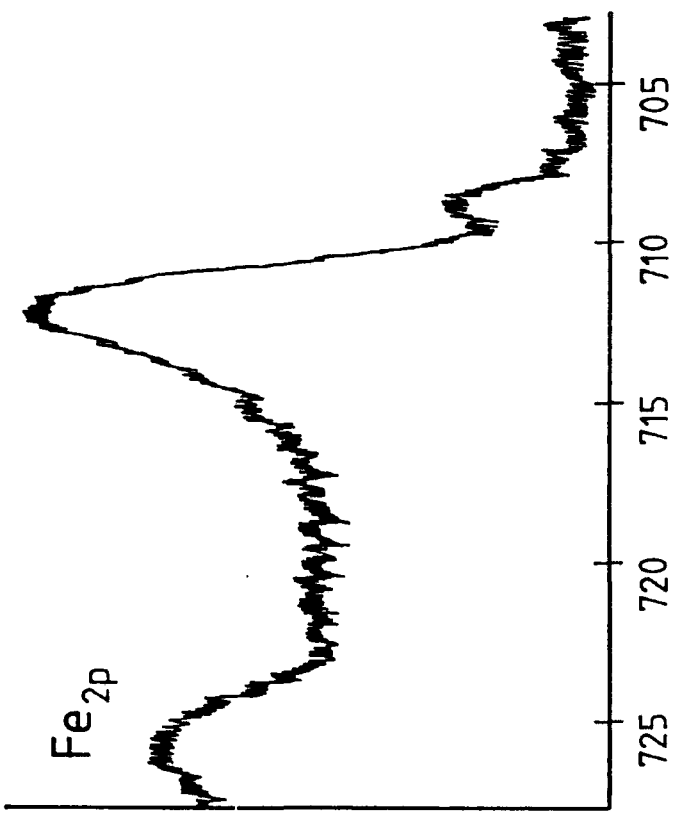

FIGURE 2.4.1

6. None of the films displayed any cyclic voltammetric response typical of ferrocene.

The higher carbon to nitrogen ratio determined for these films as compared to polypyrrole films together with the observation of a $Fe_{2p_{3/2}}$ signal shows that both carbon and iron from vinylferrocene have been incorporated into a codeposit with pyrrole. For the same reasons as given in the previous section it may be concluded that the oxidized iron found in these films is not ferricenium but some irreversibly oxidized form.

The formation of a brown precipitate from the electrolysis of ferrocene in acetonitrile solution has recently been observed by Fehlhammer and Moinet.[31] The authors did not identify the material but found it to contain iron. A comparison of mass spectra for the precipitates formed from the pyrrole/vinylferrocene experiments with mass spectra for a precipitate formed from vinylferrocene alone showed that they were identical. The spectra were not dominated by peaks typical of the ferrocene nucleus, which has a simple mass spectral pattern,[32] and could not, in isolation, be used to identify the precipitate. Moinet has suggested that the precipitate is ionic and contains the iron (VI) species FeO_4^{2-}.[33] It is difficult to rationalize the formation of this species at electrode potentials as low as +0.7V.

2.5 The electrochemical polymerization of a pyrrole substituted ferrocene

2.5.1 Introduction

In the previous sections it was demonstrated that vinylferrocene does not form a redox active deposit upon electrochemical oxidation either in the presence or absence of added pyrrole. The formation of redox active films by oxidative electrochemical polymerization of N-substituted pyrroles was first reported by Salmon *et al* [34] for p-nitrophenylpyrrole, and by Bidan *et al*[35] for pyrroles N-substituted with transition metal complexes. It thus seemed likely that ferrocene covalently bound to one or more pyrrole molecules would form a redox active electrode coating.

1,1´(3-N-pyrrolylpropyl)ferrocenedicarboxamide (1) was chosen to test this hypothesis since it could be straightforwardly synthesized from readily available precursors.

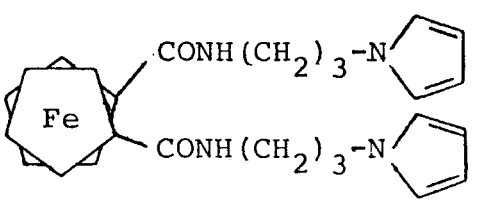

(1)

2.5.2 Results and Discussion

A single sweep cyclic voltammogram of (1) in acetonitrile solution showed the ferrocene/ferricenium wave at $E^{\ominus}$=0.78V and an irreversible oxidation peak at approximately +1.26V, which arises from pyrrole oxidation. Under the same experimental conditions the oxidation potentials of ferrocene and 1,1´(methyl)ferrocenedicarboxamide were $E^{\ominus}$=0.42V and $E^{\ominus}$=0.64V respectively.

Controlled potential electrolysis (CPE) at +1.3V, of a solution of (1) in either TBAP or TBAT electrolyte solution, produced a golden coloured film on the electrode surface.

(a) ESCA studies

The films were insoluble in common organic solvents but could be removed from an electrode by abrasion with acetone wetted tissue, as a result of less than perfect adhesion. ESCA spectra for one film are shown in Figure 2.5.1.

The $Fe_{2p_{3/2}}$ signal is a single sharp peak (FWHM=1.3eV) centred at *ca.* 708.8eV and may be contrasted with the spectrum for the codeposit of vinylferrocene and pyrrole (Figure 2.4.1). The binding energy is consistent with photoionization from iron in the +2 oxidation state. More significantly, the narrow peak width can only arise from photoionization from iron in an electron paired environment. For paramagnetic compounds peak broadening, caused by multiplet splitting (see Appendix), results as seen in Figure 2.4.1, where the peak FWHM is *ca.* 3.8eV. Since a ferrocene is the only electron paired, iron containing compound which could conceivably be deposited by oxidation of (1), the exclusive contribution to the $Fe_{2p_{3/2}}$ signal from the narrow peak may be taken as evidence that all the iron in the film is present as ferrocene. Identical $Fe_{2p_{3/2}}$ spectra were observed for films formed from solutions of (1) over 1,2,4 and 8 minute CPE deposition times. The observation of ferrocene and not the oxidized and paramagnetic form, ferricenium, may be

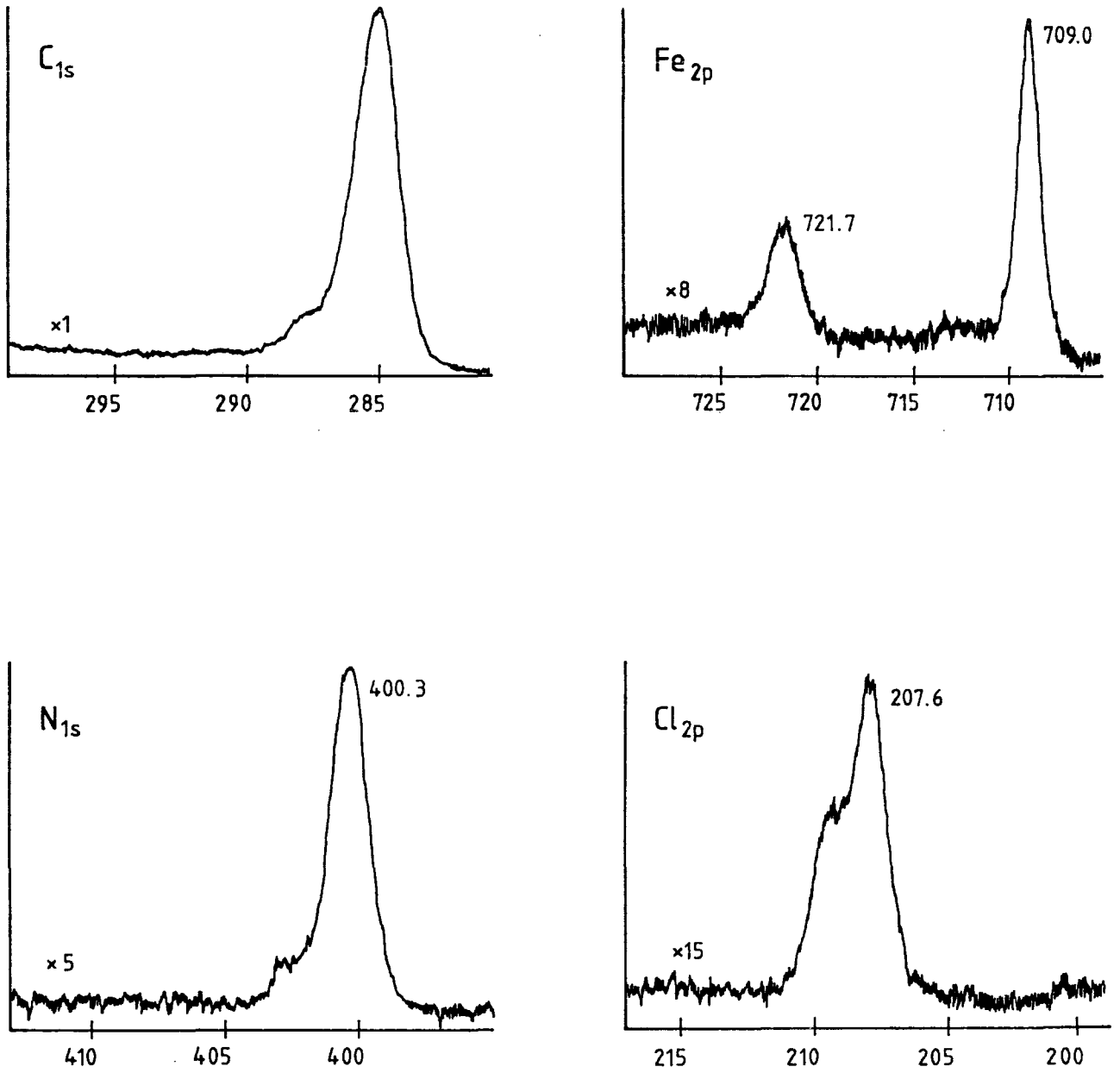

FIGURE 2.5.1 ESCA spectra for a film of poly(1) formed from TBAP solution. C_{1s}, Fe_{2p} and N_{1s} Spectra for a film of poly(1) formed from TBAT solution are similar.

rationalized in terms of rapid electron exchange between ferricenium sites in the film and solution ferrocene, after CPE, but before removal of the electrode from the cell.

That the film formed in TBAP contains perchlorate is evident from the binding energy of the Cl_{2p} signal. The film formed in TBAT contains fluorine which is assumed to arise from the tetrafluoroborate anion. The percentage anion doping level may be calculated from both the nitrogen to chlorine or fluorine elemental ratios, as for the polypyrrole samples, and the iron to chlorine or fluorine elememtal ratios. For the TBAP grown film, pyrrole chain doping levels of 39.4% and 36.8% were calculated from the nitrogen and iron ratios respectively. For the TBAT grown sample the corresponding figures are 17.6% and 18.1%. The close agreement between the two methods of calculation further suggests that (1) is electropolymerized intact. The higher incorporation of perchlorate compared to tetrafluoroborate is consistent with the polypyrrole results.

The N_{1s} spectra are different to those for polypyrrole in that little intensity at high binding energy is observed and this does not seem to vary with anion incorporation level. Curve fitting of the N_{1s} spectra is complicated by the amide nitrogens which are expected to have a small positive shift from 400eV. The main peak may nevertheless be approximated to a single Gaussian curve. The remaining intensity at higher binding energy is, for both the TBAP and TBAT grown films, only *ca.* 15% of the total. The difference in N_{1s} spectra compared to polypyrrole may be due to the N-substituent. Unfortunately no N_{1s} spectra for simple N-alkyl pyrroles have been reported.

The overall surface elemental compositions show an excess of carbon compared to that expected for poly (1). This is doubtless due to surface hydrocarbon contamination. The monomer has a C, N, Fe composition of $C_{100}N_{15.4}Fe_{3.8}$. The experimental surface stoichiometry for the TBAP grown film was $C_{100}N_{12.7}Fe_{3.4}Cl_{2.5}O_{16.4}$. For the TBAT deposited film the stoichiometry was $C_{100}N_{12.8}Fe_{3.1}F_{4.5}O_{12.8}$. In the TBAP film the oxygen level is exactly that expected for four oxygens attached to each chlorine and half of the nitrogens associated with amide bonds. For the TBAT sample an excess of oxygen was found. Oxygen was also detected in the samples of polypyrrole grown from TBAT where the tetrafluoroborate doping level was less than 20% (*vide supra*).

The high binding energy features in the C_{1s} spectra show that some of the carbon atoms are oxidized, this is to be expected since each monomer molecule contains two amide carbons. In addition, the background step, previously noted in the polypyrrole and polyaniline spectra, is present in the C_{1s} spectra of the films derived from (1). The value of $^{\Delta h}/_{h}$ is 0.05 for both TBAP and TBAT grown samples. This background step will contain a contribution from shake-up involving the localized unsaturation of the ferrocene unit.

(b) Cyclic Voltammetric Studies

Single sweep cyclic voltammograms, between-0.2V and +1.1V in monomer free solution, for electrodes modified with poly (1) deposited by CPE showed the presence of the ferrocene/ferricenium wave at 0.78V. An example of such a CV is shown in Figure 2.5.2. Also shown is the CV obtained by Skotheim *et al*[36] for a polypyrrole modified electrode to which a mono-

from ref. 36

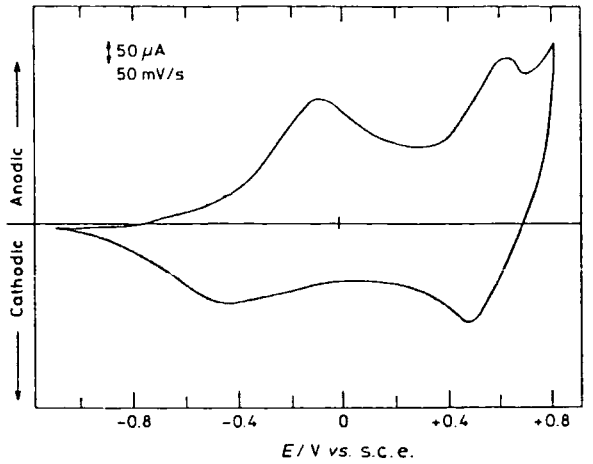

Cyclic voltammogram of a 1000 Å film of PP–ferrocene in 0.1 M Et_4NBF_4–MeCN electrolyte.

poly (1)

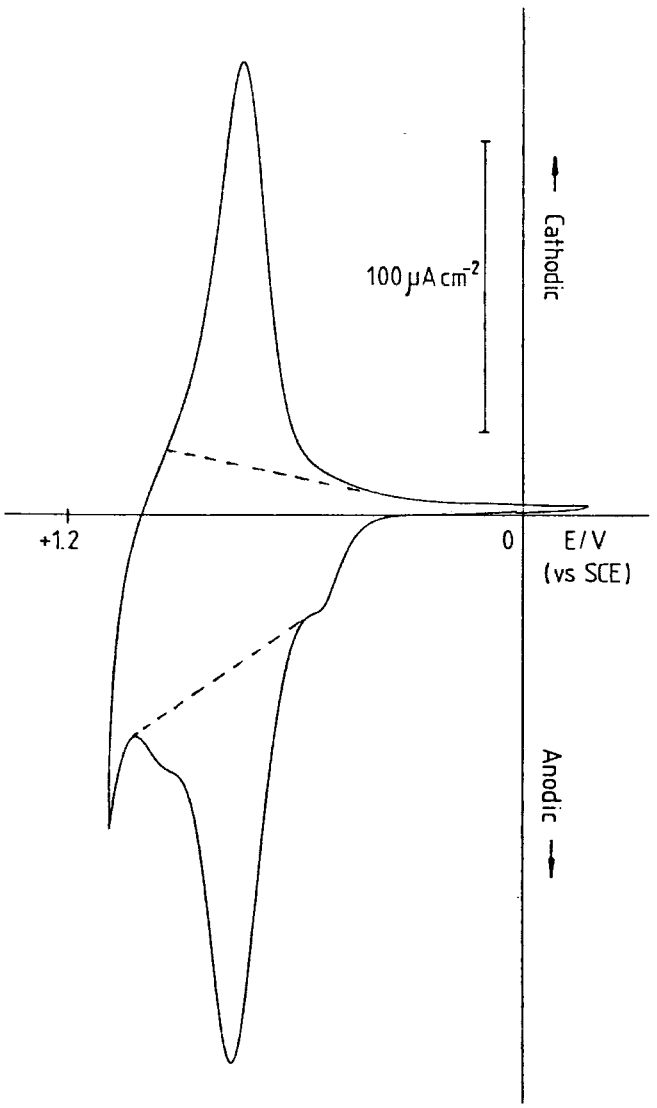

FIGURE 2.5.2 Single sweep CV (sweep rate=10mV/s) for an electrode modified with poly(1) ($\Gamma_{app} \approx 4 \times 10^{-9}$ mol cm^{-2}). The CV obtained by Skotheim *et al*[36] (see text) is also shown for comparison.

layer of ferrocene has been bound by acylation of the polypyrrole surface with ferrocenecarbonyl chloride.

At a sweep rate of 10mV/S a peak splitting of 30mV and a peak FWHM of 160mV were obtained in the CV of poly(1). The limiting peak splitting obtained by Skotheim *et al* was >170mV. This value is considerably larger than that expected for a surface immobilized, electroactive film for which charge transfer is reversible and is rapid with respect to the experimental timescale. Using the rather arbitrary background subtraction indicated in Figure 2.5.2, the ratio of anodic and cathodic peak currents for poly(1) is approximately unity. The narrow peak splitting and equality of peak heights are reasonable indications that the sweep rate is slow enough to allow all the ferrocene sites in the film to be oxidized and rereduced during one potential cycle. Under these conditions the peak area is proportional to the charge required for complete redox conversion of all ferrocene sites in the film.[37] Faraday's law may then be used to calculate the number of moles deposited on the electrode surface per unit area (Γ_{app}), as shown below.

$$\frac{\text{peak area}}{\text{sweep rate}} \quad \frac{(Js^{-1})}{(JC^{-1}s^{-1})} = q\ (C) = \Gamma_{app} nFA$$

q = total charge passed in redox reaction

n = number of electrons transferred at each redox site

F = Faraday's constant

A = geometric electrode area

Γ_{app} = apparent molar coverage

The apparent molar coverage is likely to differ from the true molar coverage since the calculated electrode area,

derived from a light microscopic measurement of electrode diameter, will be an underestimate as a result of surface roughness of the electrode. Γ_{app} also depends on the arbitrary background subtraction used. The same subtraction was performed on all CVs and so trends in molar coverage are independent of this.

Figure 2.5.3 shows the increase in Γ_{app}, determined from the area under the first anodic CV wave in monomer free solution, with the CPE time used in deposition. One solution of (1) was made in each electrolyte solution from which all the results were obtained with the same glassy carbon electrode. The gradient of the TBAT curve in Figure 2.5.3 is observed to decrease more rapidly than the TBAP curve. This information, together with the higher doping level of perchlorate compared to tetrafluoroborate, might tempt speculation that the TBAP grown film is intrinsically more electronically conducting than the TBAT.

Since the ferrocene oxidation wave in (1) is approximately 0.48V negative of the pyrrole oxidation peak it is not possible to postulate a film growth mechanism involving redox conductivity of the type described in Chapter One. It must be assumed then that the films are sufficiently electronically conducting to allow film growth up to at least an apparent molar coverage of 3.8×10^{-8} moles cm^{-2}, which was the highest coverage obtained. Using the approximation that 1 molecular layer represents a coverage of 10^{-10} mol cm^{-2}, [38] this coverage is equivalent to 380 layers. Dry state electronic conductivity measurements showed a rectifying behaviour as shown in Figure 2.5.4. Using a generous estimate of film thickness

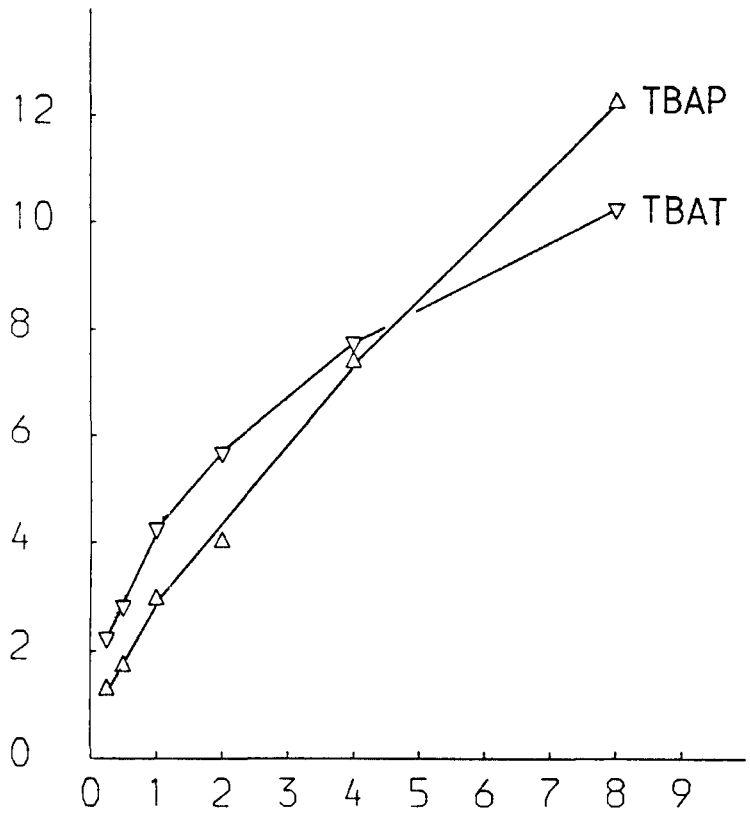

FIGURE 2.5.3 Plot of Γ_{app} (determined by single sweep CV) *versus* CPE formation time for poly(1) formed from TBAP and TBAT solutions. Ordinate: $\Gamma_{app}/10^{-9}$mol cm^{-2} Abscissa: CPE deposition time/mins.

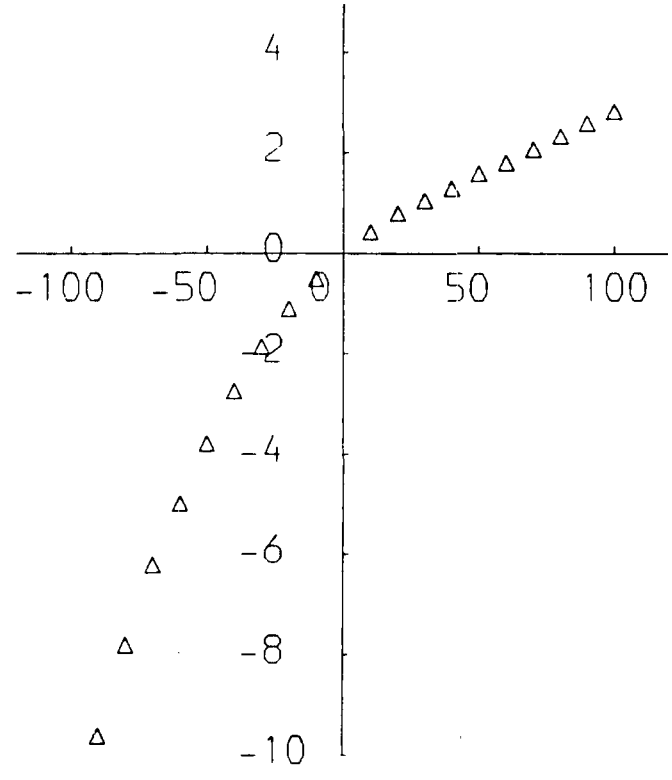

FIGURE 2.5.4 i-V plot for a poly(1). Ordinate: i(measured)/μA Abscissa: V (applied)/mV

of 10^3nm, for none of the samples tested was a conductivity greater than *ca.* $5x10^{-9}$ $(\Omega cm)^{-1}$ recorded in either voltage direction. These dry state measurements do not support the hypothesis that film growth is sustained by high electronic conductivity and leave the deposition mechanism open to speculation.

Film deposition efficiency was also calculated from the number of moles of (1) deposited, as determined by CV, divided by the number of moles of (1) oxidized during deposition, determined from the total charge passed during electrolysis and using Faraday's law:

$$q = mnF$$

where m is the number of moles oxidized and q, n and F have been previously defined.

The value of n used affects the absolute efficiency obtained but has no bearing on trends in efficiency. A value of 5.6 was used for n since at +1.3V each pyrrole is expected to undergo two electron oxidation,[39] ferrocene undergoes one electron oxidation and a doping level of 30% would require 0.6 electrons per monomer. The assignment of 30% doping to both TBAP and TBAT films is arbitrary but convenient. If the absolute doping levels determined by ESCA for the TBAP and TBAT grown films were used, the absolute efficiency for TBAT growth would be decreased by a factor of *ca.* 0.96 whilst the TBAP growth efficiency would be increased by a factor of *ca.* 1.03.

Deposition efficiency was found to be invariant with deposition time over the range one to eight minutes. This

result supports the conclusions reached from analysis of the $Fe_{2p_{3/2}}$ ESCA spectra in indicating that film deposition is the only process occurring on the electrode surface during CPE of solutions of (1) (*vide infra*). The average deposition efficiency from TBAP was found to be 6.4%±0.5%, the average value from TBAT was 8.7%±1.4%.

For CV cycles following the first, a steady decrease in peak height with cycle number was observed, as shown in Figure 2.5.5. This decay was observed regardless of the electrolyte used to grow or test the films. A plot of anodic or cathodic peak current against cycle number is a reasonable straight line, implying that the degradation process has a zero order dependence on the ferrocene concentration. Figure 2.5.6 shows zero order plots for the decay of anodic peak current for films formed over fifteen seconds and one minute CPE times. The electrodes were tested by CV between-0.2V and +1.1V in monomer free solutions of the same electrolyte as that used in the film preparation. A sweep rate of 10mV/S was used. At higher sweep rates an increase in peak splitting and a distortion of wave shape indicated that not all of the redox sites in the film were in equilibrium with the electrode potential.[37]

It is observed (Figure 2.5.6) that the rate of decay is greater at higher coverage. While this phenomenon is not explained by a simple zero order process it does not imply an increase in rate with concentration of active sites since Γ is a measure of moles per unit area and not moles per unit volume. The rate of decay was also increased by increasing

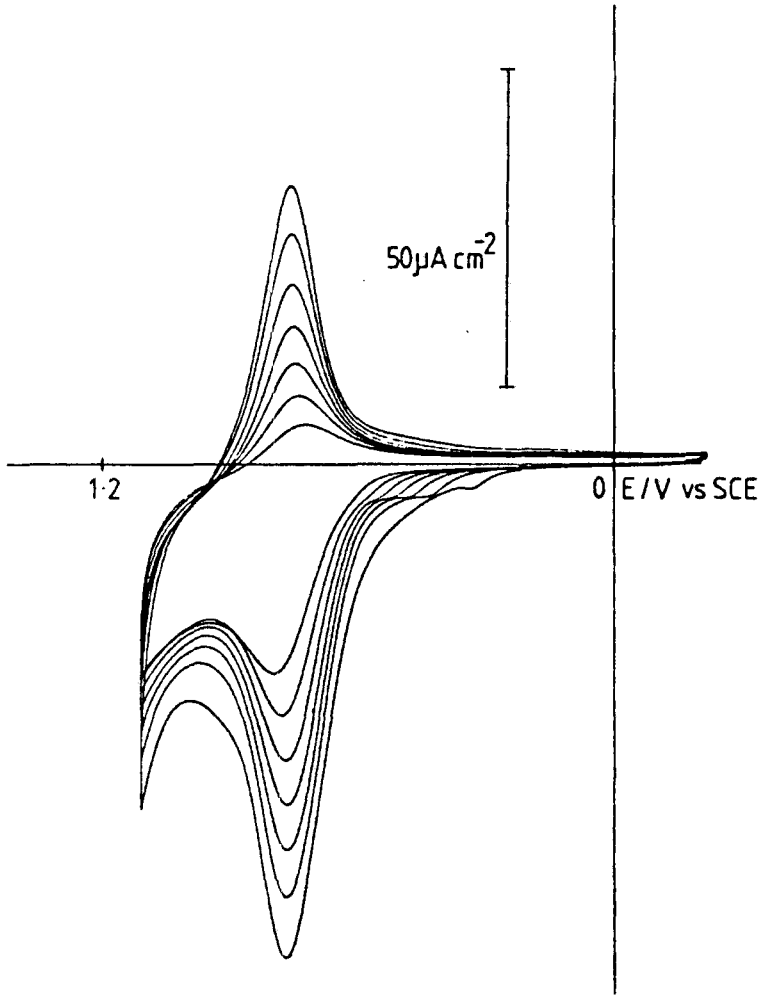

FIGURE 2.5.5 Decay of electroactivity upon repeated potential cycling (sweep rate = 10mV/s)

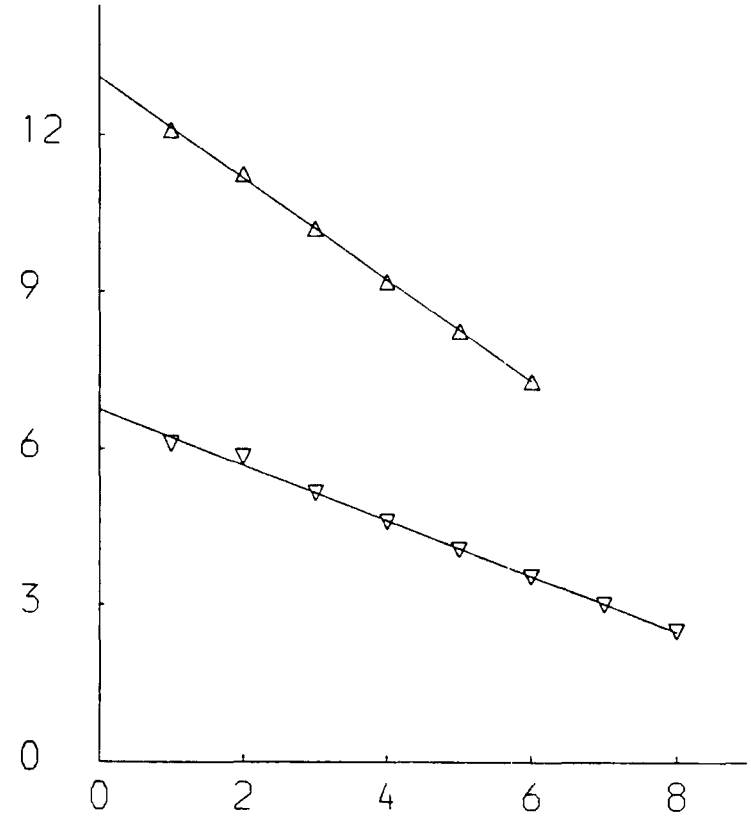

FIGURE 2.5.6 Plot of decay of peak CV current with cycle number for films of poly(1) formed over 1 min.(top) and 15 sec. CPE times. Sweep rate = 10mV/s
Ordinate: $i_p/\mu A$
Abscisssa: Cycle No.

the upper potential limit of the CV. The decay rates for the plots in Figure 2.5.6 are of the order $3x10^{-10}$ mol cm^{-2}/ cycle. The importance of dissolved oxygen, in the anodic decomposition of ferrocene or ferricenium, in certain solvents has been stressed.[31] Experiments performed in oxygen saturated solution rather than argon purged solution showed no increase in the rate of peak current decay.

When larger area platinum flag electrodes, modified with the deposit from (1), were repeatedly cycled a faint yellow turbidity could be observed in solution, implying loss of mass from the modified electrode. Four modified platinum flag electrodes which had been exhaustively cycled were examined by ESCA. The only reproducible differences between the cycled electrodes and the as grown films were a total conversion of the iron to the +3 oxidation state (*c.f.* Figure 2.4.1) and an increase in the oxygen to carbon elemental ratio of between 1.4 and 2.6 fold.

When (1) was deposited by cycling the electrode potential between -0.1V and +1.3V it was observed that the ferrocene/ ferricenium wave grew over the first few cycles but then began to degrade (Figure 2.5.7). ESCA spectra for films formed over a sufficient number of cycles such that the ferrocene/ferricenium wave became negligibly small, showed only oxidized iron (*c.f.* Figure 2.4.1). Films prepared by CPE, which were formed over longer periods of time than the total time spent in the oxidized state for the CV deposited films, showed only ferrocene environment iron.

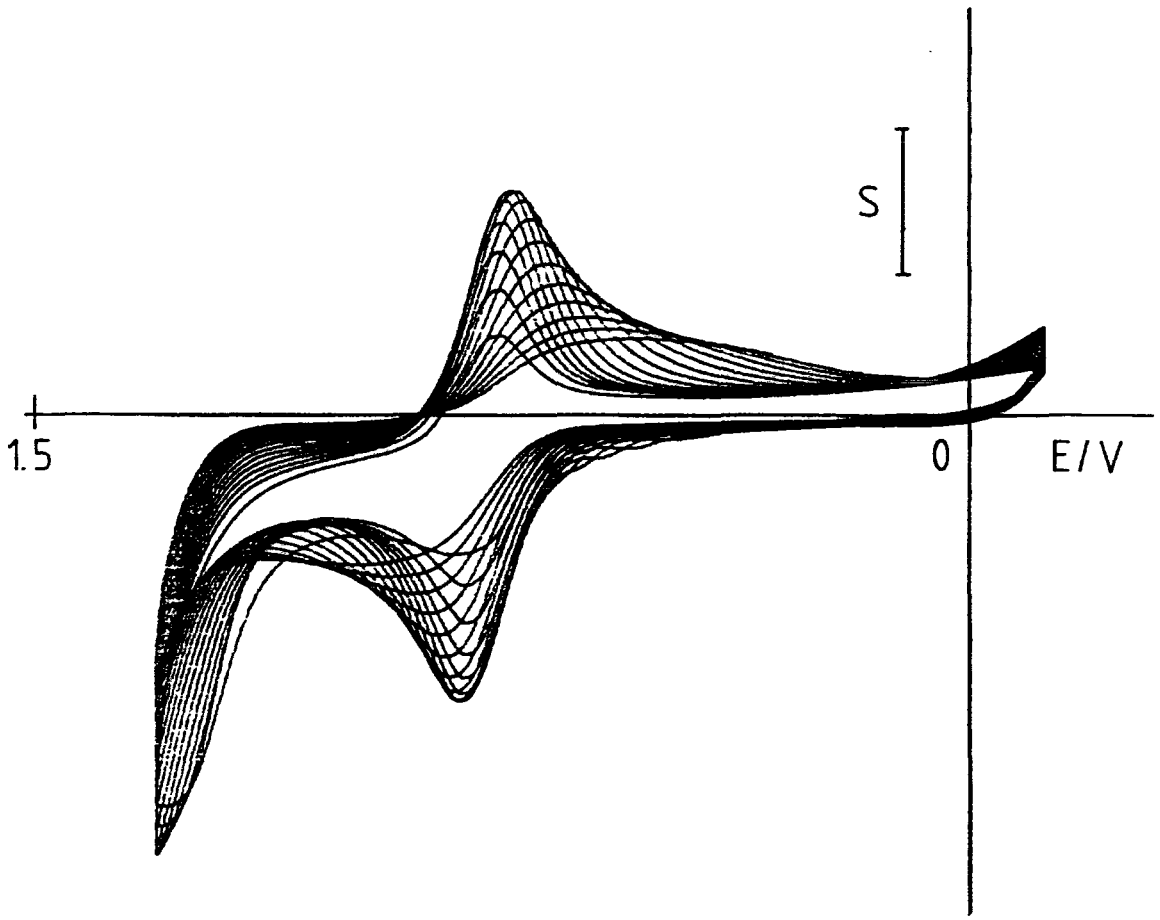

FIGURE 2.5.7 CV <u>formation</u> of poly(1) at 200mV/s. S = 200 μA cm^{-2}. Peak current increases over cycles 1→7 and then decreases on subsequent cycles. Peak splitting increases significantly after the 7th cycle.

In an attempt to assess the importance of the number of CV cycles in determining the extent of degradation, films were deposited on an electrode for the same total deposition time but over different numbers of cycles by varying the sweep rate. The amount of active film was then determined from a single sweep CV in monomer free solution at 10 mV/S. As shown in Figure 2.5.7 the degradation process is evident in the film forming CVs at higher sweep rates, when more cycles are used. The amount of active material deposited was found to decrease in the order of deposition sweep rate Γ25mV/S $\simeq$ 50mV/S > 100mV/S > 200mV/S > 400mV/S.

This trend implies that for the same preparation time the extent of degradation increases with the number of film forming cycles. This experiment is limited in its interpretation by the arbitrary total time chosen which was equivalent to two cycles at 25mV/S.

In a complementary experiment the number of film forming cycles was fixed at an arbitrary value of seven and the total deposition time varied by altering the sweep rate. The amount of active material was found to decrease in the order

Γ50mV/S $\simeq$ 100mV/S > 200mV/S > 400mV/S > 25mV/S.

Other than the 25mV/S result the trend is an increase in amount of active material deposited with deposition time. The reversal of the trend at the slowest sweep rate shows that total deposition time is also important in determing the extent of film degradation. For both the 25mV/S and 50mV/S depositions decay of peak current was observed before completion of seven film forming cycles. This experiment is again limited by the arbitrary choice of number of cycles.

The interpretations given above must be regarded with some caution for two reasons. Firstly, it is assumed that in the absence of the decay process the same amount of film would be deposited for a given deposition time regardless of sweep rate. Secondly, at higher sweep rates not all of the active sites in the film are in equilibrium with the electrode potential (*vide supra*).

Potentiostating a modified electrode formed by CPE in a monomer free solution, at +1.3V, also leads to a degradation in the amount of active material determined by single sweep CV. Performing a similar experiment in a solution of 10^{-3}M ferrocene again produces degradation.

The combined results suggest that the initial lack of any oxidized iron in films grown by CPE is due to a higher competitive rate of monomer deposition compared to degradation. The reason that films deposited by CV degrade during growth may be that in the potential range *ca.* +0.8V to +1.1V the ferrocene is oxidized and can degrade[31] but the potential is not high enough for any competitive deposition by pyrrole oxidation.

Peak current decay was also observed by Skotheim *et al*[36] for polypyrrole coated electrodes modified with a monolayer of ferrocene.

2.5.3 Polymer Structure

The low dry state conductivity of the films and the steric hindrance of the monomer might suggest that the polymer or oligomer produced by the oxidation of (1) is linked

by dimer pyrrole units as shown in Figure 2.5.8.

Figure 2.5.8

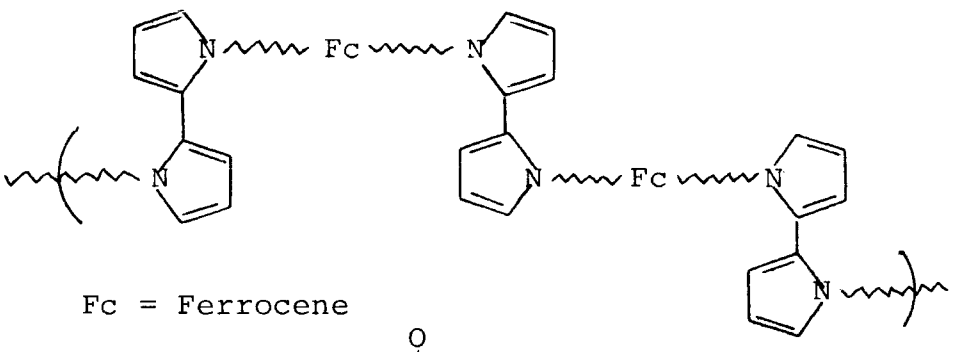

Fc = Ferrocene

N ~~~~ = N-$(CH_2)_3$-NH-C(=O)-

This structure would be formed by an overall one electron oxidation of each pyrrole and is inconsistent with the coulometric data reported by Cosnier *et al*[39] who found two electron pyrrole oxidation for monomers containing more than one sterically hindered pyrrole unit. It seems likely that longer polypyrrole segments than dimer are present in the electrode deposits formed from (1).

2.5.4 Conclusions

An electroactive film has been reported from the electropolymerization of a pyrrole substituted ferrocene. Although the electroactivity of this film is degraded by oxidative potential cycling the initial CV response is superior to that reported for a polypyrrole coated electrode surface functionalized with a ferrocene monolayer.[36]

2.6 Experimental

2.6.1 Electrochemical Experiments

A potassium chloride saturated calomel electrode (SCE) with a Vycor frit was used as reference electrode for all electrochemical experiments. Tetrabutylammonium perchlorate (TBAP, ex Fluka) and tetrabutylammonium tetrafluoroborate (TBAT, ex Aldrich) electrolytes were dried in an oven before use. All solvents were analytical reagents and, in certain cases, further purified as described in the relevant section. Other than for the aniline experiments, electrolyte solutions were 0.1M TBAP or 0.1M TBAT. Prior to any electrochemical experiment solutions were purged with argon for 15 minutes and a gentle stream of argon was maintained over the cell during the experiments. All glassware was cleaned in a hot solution of 'Micro', washed with distilled water and dried in an oven before use.

Electrode deposits were formed by controlled potential electrolysis (CPE) of the appropriate monomer - electrolyte solution using a Thompson Ministat 251 precision potentiostat and a Fluke 8000A digital multimeter to set the potential and measure the current.

For ESCA analysis films were prepared by electro-oxidation in a one compartment cell (100mL Pyrex beaker) using 30mL solutions. Platinum flags were used as anode and cathode. The flags were cut from thick foil (Johnson Matthey) and measured 7mm x 18mm, which is an ideal size for mounting onto a standard Kratos probe tip for ESCA analysis. Prior to use in film preparation the platinum electrodes

were cleaned with 'Silvo' and subsequently etched in hot concentrated nitric acid for approximately 30 minutes, washed with distilled water and dried. ESCA analysis revealed that only a very low level of carbon contamination was present on the platinum surface following this procedure and that cleanliness was not much improved by a 45 minute, 50W hydrogen plasma treatment.

For cyclic voltammetric analysis films were prepared as described above but were deposited onto Kel-F shrouded platinum (1.7mm diameter) or glassy carbon (3.1mm diameter) disc electrodes supplied by Bioanalytical Systems (BAS). These electrodes were polished with diamond and alumina pastes (BAS), washed with distilled water and dried before use. Depositions were performed in a standard 20mL BAS glass cell with Teflon cap using 10mL solutions.

Cyclic Voltammograms were recorded with a BAS CV-1B and a Linseis LY1700 chart recorder. A platinum wire counter electrode was used.

Cyclic voltammogram peak areas in cm^2 were determined using an Apple 11/e microcomputer with graphics tablet, light pen and associated software. The areas used in apparent molar coverage calculations were the average of at least five determinations.

2.6.2 ESCA analysis

After preparation films were washed in electrolyte-free solvent and then dried under nitrogen and subsequently in vacuum. Coated electrodes were mounted onto a standard Kratos probe tip using double sided 'Scotch' tape.

A Kratos ES300 electron spectrometer was used (see Appendix).

Spectra were recorded with the sample positioned at an angle of 35^{o} with respect to a plane parallel to the location of the electron analyser slits. MgKα X-radiation was used. Binding energies are quoted relative to hydrocarbon C_{1s} at 285eV and with the spectrometer calibrated as described in the Appendix. Surface elemental stoichiometries were obtained from peak area ratios corrected by the appropriate elemental sensitivity factors, experimentally determined from standard samples. An error of ±10% may be expected in the surface stoichiometries.

The ESCA spectrum of tetrabutylammonium perchlorate was obtained from material evaporated onto clean gold from acetone solution.

Curve fitting of ESCA spectra was performed manually using the graphics software of the Kratos DS300 computer system. A linear background subtraction was used. Gaussian component peaks were used exclusively and constant peak width (FWHM) was used for all components of any one core-level spectrum.

2.6.3 Polyaniline

Aniline was distilled and then stored in a refrigerator for not more than one week before use.

Polyaniline films were formed by 10 minute CPE at +1.0V from aqueous solutions which were 0.1M in aniline and either 1.0M in sulphuric acid, 1.0M in hydrochloric acid or buffered to pH7 (approximately 0.1M in each of Na_2HPO_4/NaH_2PO_4).

2.6.4 Tetrafluoroaniline

2,3,5,6 Tetrafluoroaniline (Aldrich) was used as received. Acetonitrile (Fison) was of HPLC quality.

CPEs at +1.3V for 10 minutes were performed in solutions which were all 0.1M in tetrafluoroaniline and were either 0.1M TBAP in acetonitrile, 5:1 1M aqueous HCl: acetonitrile or methanol which was 1M in H_2SO_4.

2.6.5 Polypyrrole

Pyrrole (Fluka) was distilled before use. HPLC grade acetonitrile was further dried by refluxing over P_2O_5, under a dry nitrogen atmosphere, for several hours and was then used immediately after distillation.

Controlled potential film depositions were performed in acetonitrile solutions which contained TBAP or TBAT and either 5×10^{-3}M or 10^{-1}M pyrrole. The electrolysis potential was +1.0V and its duration 10 minutes. In one case a film was formed by cycling the working electrode potential and the CV-1B was used in place of the Ministat.

2.6.6 Electrooxidation of ferrocene and vinylferrocene

Attempts to electrochemically deposit vinylferrocene (Eastman) and ferrocene (B.D.H.) were made from 4×10^{-3}M solutions in dry, argon purged acetonitrile which was 0.1M in TBAP. CPE was performed at +0.8V for 5 minutes.

The control experiment with vinylferrocene was performed in an identical manner except that the electrodes were allowed to stand in solution for ten minutes and were disconnected from the potentiostat.

2.6.7 Codeposition of vinylferrocene and pyrrole

CPEs were carried out in dry acetonitrile solutions which were 3 x 10^{-3}M in vinylferrocene, 10^{-2}M in pyrrole and 0.1M in TBAP. The electrolysis potentials used were +0.7V and +0.8 to +0.9V in 0.02V increments. The electrolysis time was 30 minutes.

The brown precipitate formed in all codeposition experiments and the brown precipitate formed from electrolysis of vinylferrocene alone were repeatedly washed with acetonitrile and centrifuged and then dried and analyzed by mass spectrometry.

2.6.8 1,1´(3-N-pyrrolylpropyl)ferrocenedicarboxamide(1)

(a) Synthesis of monomer

1,1´(3-N-pyrrolylpropyl)ferrocenedicarboxamide(1) was synthesized following the method described by Hammond *et al* for the preparation of other disubstituted ferrocenes.[40]

Triethylamine (2.5g, 0.026 mole) and N-(3-aminopropyl)-pyrrole (1.18g, 0.01 mole) were added to a solution of ferrocene-1,1´-dicarboxyllic acid chloride (3.01g, 0.01 mole) in dichloromethane (20mL) and the mixture stirred at 20°C for 16 hours. After filtering the solvent was removed under reduced pressure to yield a reddish solid which was chromatographed on neutral alumina (activity II/III), eluting with dichloromethane/methanol (1%). A clean red fraction was obtained and upon removal of solvent an orange microcrystalline solid was obtained (3.7g, 75%), which melted with decomposition at 136°C. The solid gave spectral and analytical data in agreement with the structure (1). Chemical

analysis, found C64.5%, H5.85%, N 11.2%, $C_{26}H_{30}FeN_4O_2$ requires C64.2%, H6.22%, N 11.5%. ^1H N.m.r. (Bruker WH360, $CDCl_3$, 360MHz), δ_H 6.74 (4H, dd, pyrrole CH), 6.60 (2H, broad t, NHCO), 6.18 (4H, dd, pyrrole CH'), 4.38 (4H, t, ferrocene CH), 4.33 (4H, t, ferrocene CH'), 4.03 (4H, t, CH_2N), 3.41 (4H, dt, CH_2NH), 2.08 (4H, quint., $CH_2CH_2CH_2$). Mass spectrum (VG 7070E), m/Z 486 (M^+), 485 (M^+-1), 407, 328, 271, 179.

(b) Electrodeposition

Controlled potential film depositions were conducted at +1.3V in dry acetonitrile/electrolyte solutions which were 2 x 10^{-3}M in the monomer(1). Films formed for ESCA analysis were deposited over 5 minutes electrolysis time.

In some experiments the CV-1B was used in place of the Ministat to prepare films by cycling the electrode potential between -0.1V and +1.3V. The CV-1B was also used to repeatedly voltage-cycle some of the films prepared by CPE before ESCA analysis.

In the calculation of deposition efficiency, the total charge passed during electrolysis was determined from graphical integration of the current-time response.

Conductivity measurements were performed on films deposited onto new platinum flag electrodes. 1.5mm diameter gold contacts were slowly evaporated on top of the films using an Edwards Vacuum evaporator. Film resistance measurements were taken with a base contact to the platinum electrode and a 'soft' spherical gold probe to the evaporated contact. Film resistance was determined from a plot of applied voltage

(Time Electronics 2003S D.C. voltage supply) against measured current (Keithley 414A picoammeter). Several films and several contacts for each film were tested. The film thickness was estimated from the charge passed during electrolysis, the area of the electrode, the experimentally determined deposition efficiency and using estimates of 10^{-10} mol cm^{-2} = 1 monolayer[38] and 1 monolayer = 10Å. Because of the assumptions involved the conductivity values quoted are likely to be accurate only to within an order of magnitude.

An increase in resistance with film thickness was used to test that the resistance measured was a property of the film and not of the contacts to the film.

Four point probe measurements of film conductivity, using a standard probe, were not possible since deposits thick enough to prevent film puncture, and thus short circuit, by the probe could not be grown.

REFERENCES - Chapter 2

1. H. Letheby, J.Chem.Soc., 15, (1862), 161.

2. D.M. Mohilner, R.N. Adams and W.J. Argersinger, J.Am. Chem.Soc., 84, (1962), 3618..

3. A.F. Diaz and J.A. Logan, J.Electroanal.Chem., 111, (1980), 111.

4. A. Volkov, G. Tourillon, P. Lacaze and J. DuBois, J.Electroanal.Chem., 115, (1980), 279.

5. R. Hernandez, A.F. Diaz, R. Waltman and J. Bargon, J.Phys.Chem., 88, (1984), 3333.

6. T. Ohsaka, Y. Ohnuki, N. Oyama, G. Katagiri and K. Kamisako, J.Electroanal.Chem., 161, (1984), 399.

7. A. Kitani, J. Izumi, J. Yano, Y. Hirimoto and K. Sasaki, Bull.Chem.Soc.Jpn., 57, (1984), 2254.

8. P. Pfluger and G.B. Street, J.Chem.Phys., 80, (1984),544.

9. D.R. Hutton, Ph.D. Thesis, Durham, (1983).

10. H.S. Munro and G. Grunwald, J.Polym.Sci., Polym.Chem. Ed., 23, (1985), 479.

11. a. D. Briggs, Chapter 9 in "Practical surface analysis by Auger and X-ray photoelectron spectroscopy", Eds. D. Briggs and M.P. Seah, John Wiley, Chichester (1983).

    b. A. Dilks, Chapter 5, p.315 in "Electron Spectroscopy: Theory Techniques and Applications", Vol.4, Eds. C.R. Brundle and A.D. Baker, Acad.Press, London, (1981).

12. T. Yamabe, K. Tanaka, H. Terama-e, K. Fukui, H. Shirakawa, and S. Ikeda, Synthetic Metals, 1, (1979/80), 321.

13. a. M.M.Ahmad and W.J. Feast, Polymer Commun., 25, (1984), 231.

    b. M.M. Ahmad and W.J. Feast, Mol.Cryst.Liq. Cryst., 118, (1985), 417.

14. a. A.G. Hudson, A.E. Pedlar and J.C. Tatlow; Tetrahedron Letts., (1968), 2143.

    b. A.G. Hudson, A.E. Pedlar and J.C. Tatlow; Tetrahedron, 26, (1970), 3791.

    c. A.G. Hudson, M.L. Jenkins, A.E. Pedlar and J.C.Tatlow, Tetrahedron, 26, (1970), 5781.

15. a. W.R. Salaneck, R. Erlandsson, J. Prejza, I. Lundström and O. Inganas, Synthetic Metals, 5, (1983), 125.

15. b. R. Erlandsson, O. Inganas, I. Lundström and W.R. Salaneck, Synthetic Metals, 10, (1985), 303.

16. a. G.B. Street, T.C. Clarke, M. Krounbi, K. Kanazawa, W. Lee, P. Pfluger, J.C. Scott and G. Weiser, Mol. Cryst.Liq.Cryst., 83, (1982), 253.

b. G.B. Street, T.C. Clarke, R.H. Geiss, W-Y.Lee, A.Nazzal, P. Pfluger and J.C. Scott, J.de Physique Colloq., C3, (1983), 599.

17. P. Pfluger, M. Krounbi and G.B. Street, J.Chem.Phys., 78, (1983), 3212.

18. C.D. Wagner, W.M. Riggs, L.E. Davis, J.F. Moulder and G.E. Muilenberg, 'Handbook of X-ray photoelectron spectroscopy', Perkin-Elmer Corporation, Physical Electronics Division, Minnesota, (1979).

19. a. A. Merz and A.J. Bard, J.Am.Chem.Soc., 100, (1978),4379.

b. P.J. Peerce and A.J. Bard, J.Electroanal.Chem., 112, (1980), 247.

20. H.D. Finklea and R.S. Vinthanage, J.Electroanal.Chem., 161, (1984), 283.

21. B.R. Shaw, G.P. Haight and L.R. Faulkner, J.Electroanal. Chem., 140, (1982), 147.

22. R.F. Lane and A.T. Hubbard, J.Phys.Chem., 77, (1973),1411.

23. M.H. George and G.F. Hayes, J.Polym.Sci., Polym.Letts. Ed., 11, (1973), 471.

24. J.S. Brooks, C.M. Care, S. Plimley and G.C. Corfield, Hyperfine Interact., 20, (1984), 151.

25. G.B. Street in 'Handbook of Conducting Polymers', Ed. T. Skotheim, Dekker, New York, in press 1986.

26. O. Ikeda, K. Okabayashi, N. Yoshida and H. Tamura, J.Electroanal.Chem., 191, (1985), 157.

27. R.A. Bull, F-R Fan and A.J. Bard, J.Electrochem.Soc., 131, (1984), 687.

28. R. Noufi, J.Electrochem.Soc., 130, (1983), 2126.

29. N. Bates, M. Cross, R. Lines and D. Walton, J.Chem.Soc., Chem.Commun., (1985), 871.

30. M. Velazquez-Rosenthal, T.A. Skotheim, A. Melo, M.I.Florit, and M. Salmon, J.Electroanal.Chem., 185, (1985), 297.

31. W.P. Fehlhammer and C. Moinet, J.Electroanal.Chem., 158, (1983), 187.

32. E.I. Mysov, I.R. Lyatifov, R.B. Materikova and N.S. Kochetkova, J.Organometal.Chem., 169, (1979), 301.

33. C. Moinet, private communication, (1986).

34. M. Salmon, A. Diaz and J. Goita, Chapter 5 in "Chemically Modified Surfaces in Catalysis and Electrocatalysis", ACS Symp.Ser., 192, (1982).

35. G. Bidan, A. Deronzier and J-C Moutet, Nouv.J. de Chimie, 8, (1984), 501.

36. M. Velazquez-Rosenthal, T. Skotheim and J. Warren, J.Chem.Soc.Chem.Commun., (1985), 342.

37. R.W. Murray, Chapter 3, p.205, in "Electroanalytical Chemistry", Vol.13, Ed. A.J. Bard, Dekker, New York, (1984).

38. ref. 37, p.235.

39. S. Cosnier, A. Deronzier and J-C Moutet, J.Electroanal. Chem., submitted 1985.

40. P.J. Hammond, H.P. Bell and C.D. Hall, J.Chem.Soc., Perkin Trans.I, (1983), 707.

CHAPTER THREE

THE ELECTROCHEMICAL POLYMERIZATION OF SOME PYRROLE SUBSTITUTED, TRANSITION METAL BIPYRIDYL COMPLEXES

3.1 Introduction

Iron and ruthenium trisbipyridyl complexes show well-behaved oxidative and reductive electrochemistry.[1,2] Ruthenium (11) trisbipyridyl ($Ru(bpy)_3^{2+}$) complexes have a long lived (10^2 nonosecond lifetime), luminescent excited state which is produced from the ground state by photon absorption at *ca.* 450nm. This excited state undergoes facile electron transfer with appropriate solution redox species, as outlined below for oxidative quenching.

$$Ru(bpy)_3^{2+} \longrightarrow Ru(bpy)_3^{2+*}$$

$$Ru(bpy)_3^{2+*} + A \longrightarrow Ru(bpy)_3^{3+} + A^-$$

$$Ru(bpy)_3^{3+} + A^- \longrightarrow Ru(bpy)_3^{2+} + A \quad \text{(back reaction)}$$

$$Ru(bpy)_3^{3+} + S \longrightarrow Ru(bpy)_3^{2+} + S^+$$

A supersensitizer, S, may be used to compete with the back reaction and increase the efficiency of the production of A^-.

The excited state, $Ru(bpy)_3^{2+*}$, is created by promotion of an electron from a 'metal centred', t_{2g} symmetry, d orbital to a 'ligand centred' π^* orbital. The promotion of the electron and the creation of a hole in the d orbital make the excited state species a more powerful oxidant and reductant than the ground state. In addition to homogeneous, solution phase photoinduced electron transfer reactions, $Ru(bpy)_3^{2+}$ has also been used to 'sensitize' wide bandgap semiconductors,[3] such as n-TiO_2 , by donation of the promoted electron to the semiconductor conduction band.[4,5] Such *dye sensitization* allows more of the incident light to be utilized

in solar conversion cells employing wide band gap semiconductors.[4] Two methods of sensitization with $Ru(bpy)_3^{2+}$ or derivatives of $Ru(bpy)_3^{2+}$ have been used and these may be summarized as follows:

(1) A solution of $Ru(bpy)_3^{2+}$ surrounds the photoanode with the aim of strongly adsorbing a monolayer of the dye onto the electrode surface.[4]

(2) A multilayer of $Ru(bpy)_3^{2+}$ is coated onto the photoanode and no dye is present in solution.

This second method of photosensitization has been successfully achieved with a n-SnO_2 photoanode coated with Nafion polymer containing $Ru(bpy)_3^{2+}$ cations.[5] The relative merits of the two methods have been discussed,[5] however the highest photon to current conversion so far reported (44%) was achieved using the first method.[4] Bard *et al* deduced that slow charge transport through the polymer film was the major limitation to the efficiency of the cell using the Nafion coating.[5] Rapid charge transport is necessary for efficient turnover of $Ru(bpy)_3^{3+}$ to $Ru(bpy)_3^{2+}$ at the film/solution interface if penetration of the film by the supersensitizer is negligible.

As described in Chapter One, Murray *et al* have reported the reductive electrochemical polymerization of vinyl substituted trisbipyridyl complexes of iron and ruthenium.[6,7] No photosensitization experiments using these coatings have yet been reported but it is noteworthy that the chronoamperometrically derived diffusional charge transport coefficients for the $Ru(bpy)_3^{2+}$ containing Nafion polymer and poly-

$Ru(vbpy)_3^{2+}$ are similar.[8,7]

Electron transfer from an excited state of $Fe(bpy)_3^{2+}$, produced from the ground state by photon absorption at *ca.* 530nm, has been reported.[9,10] The electron transfer efficiency is much lower than that for $Ru(bpy)_3^{2+}$ and this is believed to be due to the fact that the non-luminescent, long lived (nanosecond lifetime) excited state is not a $d\pi^*$ state, as for the ruthenium compound, but rather a lower energy dd^* state created by population of the metal-centred, e_g symmetry d orbitals.[11] It has been suggested[12] that the $d\pi^*$ states for $Fe(bpy)_3^{2+}$ may lie at energies only slightly above the dd^* states and that appropriate chemical perturbation could produce an iron trisbipyridyl complex with a $d\pi^*$ lowest energy excited state and having analogous photochemistry to $Ru(bpy)_3^{2+}$.

In Chapter Two the successful electropolymerization of 1,1´(3-N-pyrrolylpropyl)ferrocenedicarboxamide was described. The preparation of polymers from the electrooxidation of pyrrole substituted iron and ruthenium trisbipyridyl complexes in this chapter is a logical extension to this. The possible application of such polymers in photosensitization provided a further stimulus for this work.

3.2 Ligand Design

The simplest means of preparing a pyrrole substituted bipyridine ligand is by N rather than C alkylation of pyrrole.[33] 5-(N-pyrrolylmethyl)-2,2´-bipyridine (bpypyr) was chosen as the *target* ligand since for its synthesis, by nucleophilic displacement of bromine from 5-Bromomethyl-2,2´-bipyridine

by pyrrole under basic conditions, no competing elimination reaction is possible. Details of free ligand and metallated complex syntheses are given in Section 3.7.

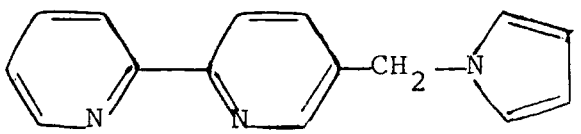

(bpypyr)

3.3 Results and Discussion - Iron(11)5-(N-pyrrolylmethyl)-2,2´-bipyridine

A single sweep cyclic voltammogram, between the potential limits -0.2 and +1.3V, of a solution of iron(11)5-(N-pyrrolylmethyl)-2,2´-bipyridine tetrafluoroborate ($Fe(bpypyr)_3^{2+}2BF_4^-$) showed one 'reversible'oxidation wave at $E^{\ominus}$=1.1V. Separate peaks for pyrrole and Fe(11)/Fe(111) oxidation were not observed. The peak anodic current was greater than the cathodic. These results suggest that the irreversible pyrrole oxidation and the reversible Fe(11)/Fe(111) oxidation takes place at the same electrode potential.

Controlled potential electrolysis at +1.3V of $Fe(bpypyr)_3^{2+}2BF_4^-$ in acetonitrile/0.1M TBAP (tetrabutylammonium perchlorate) solution produced even, red coloured electrode deposits. The deposited films were insoluble in common organic solvents but could be removed from an electrode by abrasion with solvent wetted tissue.

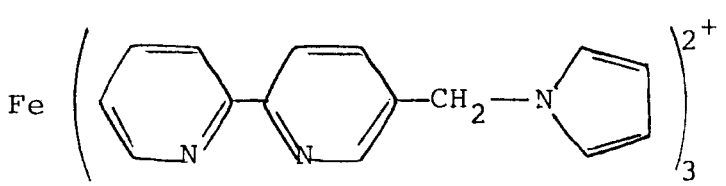

$= Fe(bpypyr)_3^{2+}$

3.3.1 ESCA Studies

The C_{1s}, N_{1s}, Fe_{2p} and Cl_{2p} ESCA spectra for a film of poly-$Fe(bpypyr)_3^{2+}$ formed in acetonitrile/TBAP solution are shown in Figure 3.3.1. The O_{1s} spectrum was featureless and is not shown.

The $Fe_{2p_{3/2}}$ signal is a single sharp peak (FWHM=1.3eV) and is centred at 709.3eV, the same binding energy as the monomer $Fe_{2p_{3/2}}$ signal. The narrow peak width is consistent with a film in which all of the iron is present in an electron paired, low spin d^6 configuration. This result constitutes unambiguous evidence that iron (ll) tris-bipyridyl remains intact upon electropolymerization. The most probable explanation for the observation of Fe(ll) and not Fe(lll), even though the electrolysis was terminated at a potential positive of the Fe(ll)/Fe(lll) oxidation, is electron exchange between Fe(lll) sites in the film and Fe(ll) species in solution after electrolysis but before removal of the electrode from the cell.

Although the film was deposited from a solution of $Fe(bpypyr)_3^{2+}2BF_4^-$ no F_{1s} signal was detected. A large Cl_{2p} signal was observed which had a binding energy consistent with ClO_4^-. The amount of oxygen detected in the film was also consistent with the ClO_4^- anion as the only oxygen containing species.

The N/Cl stoichiometry was 3.0 and the Cl/Fe stoichiometry was also 3.0. These ratios indicate that the film is oxidized to a level of one positive charge for each monomeric unit, or a polypyrrole chain oxidation level of 33%. This oxidation level is comparable to that found for

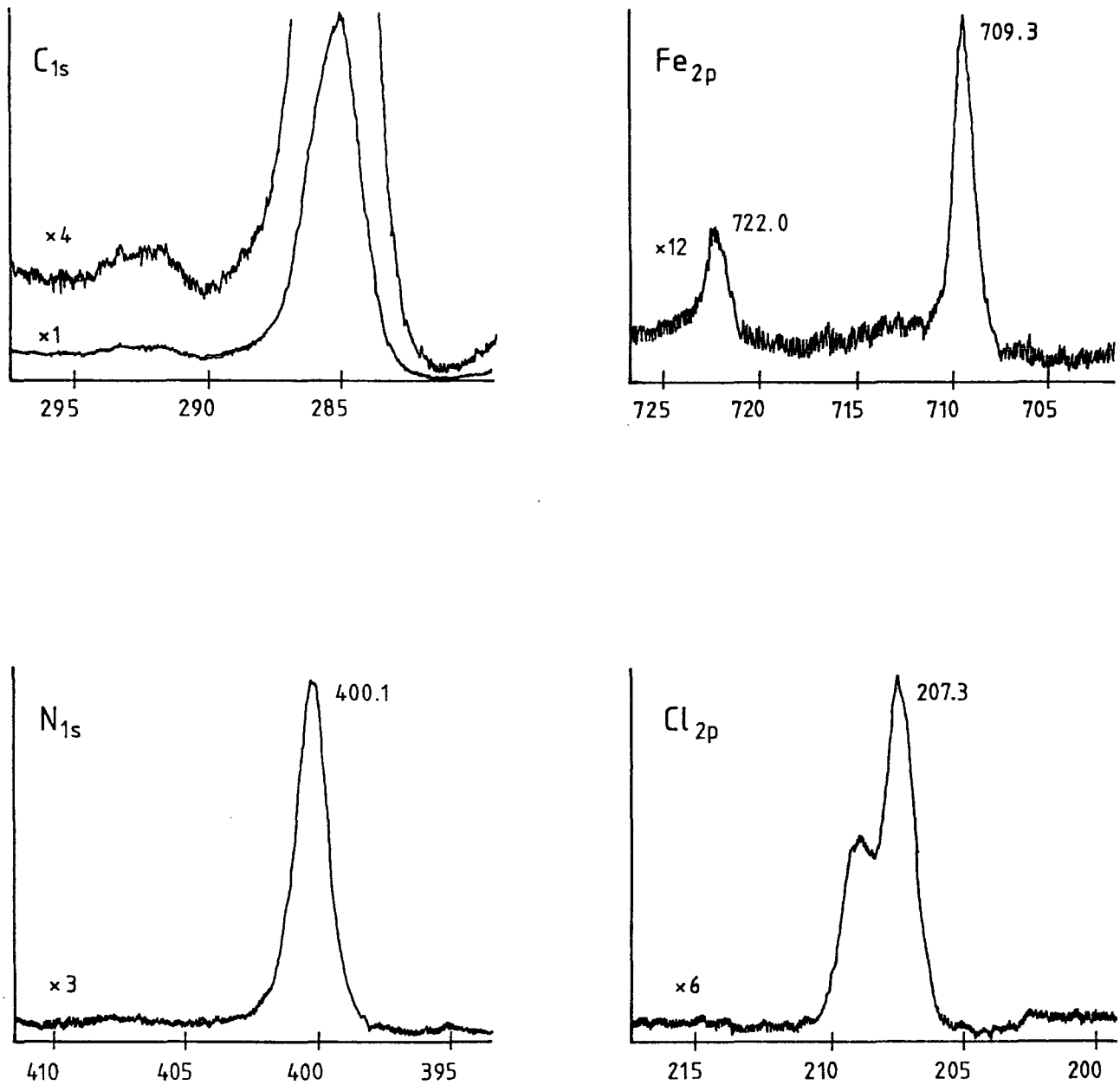

FIGURE 3.3.1 ESCA spectra. Binding energies are in eV relative to C_{1s} at 285eV.

the 1,1´-(3-N-pyrrolylpropyl)-ferrocenedicarboxamide polymer formed in TBAP solution (see Chapter Two). Since a high binding energy $Fe_{2p_{3/2}}$ peak was not observed the possibility of a d^5Fe^{3+} complex charge compensating for the dopant perchlorate may be discounted.

The N_{1s} spectrum is similar to that of the monomer. Pyrrole and bipyridyl nitrogens are not resolved and no significant intensity at high binding energy was observed, in agreement with the poly-1,1´-(3-N-pyrrolylpropyl)ferrocenedicarboxamide N_{1s} spectra.

The overall elemental composition shows an excess of carbon which is probably due to surface hydrocarbon contamination. The monomer has a C:N:Fe stoichiometry of $C_{45}N_9Fe_1$. The film grown from TBAP solution has a surface elemental composition of $C_{45}N_{7.2}Fe_{0.8}Cl_{2.4}O_{9.1}$.

Distinct shake up satellites are observed in both the C_{1s} and N_{1s} spectra. The C_{1s} spectrum is expanded by a factor of 4 in Figure 3.3.1 to show this feature more clearly. The position and intensity of the C_{1s} shake up is similar to that found for the monomer and is diagnostic of the localised unsaturation of the bipyridyl ligands.

Poly-$Fe(bpypyr)_3^{2+}$ was also deposited onto a conducting tin oxide coated Pyrex glass electrode from TBAP solution. The resulting film appeared red in transmitted light. Figure 3.3.2 shows that the visible absorption band at *ca.* 530nm, observed for monomeric $Fe(bpypyr)_3^{2+}$ in solution, is retained in the polymer film.

Controlled potential electrolysis at +1.3V of the monomer in TBAT (tetrabutylammonium tetrafluoroborate)

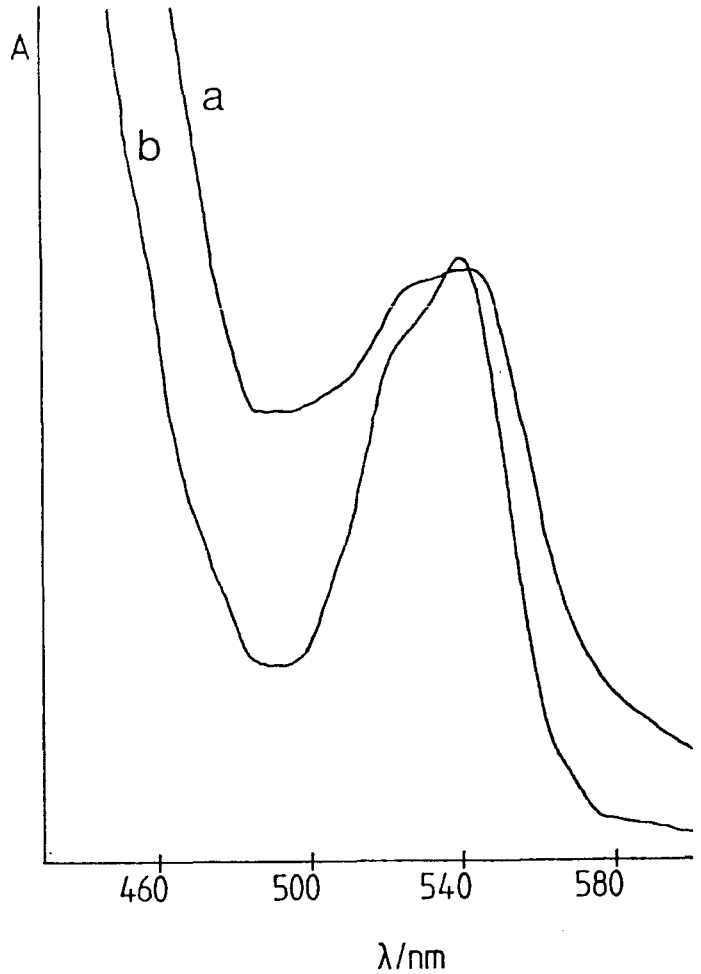

FIGURE 3.3.2 Visible adsorption spectra for (a) poly-Fe-$(bpypyr)_3^{2+}$ and (b) the monomer in CH_3CN solution.

solution produced a film similar in appearance to that formed in TBAP solution. For the same electrolysis time and monomer concentration approximately one third as much film was deposited in TBAT compared to TBAP solution. Moreover, whereas successful deposition in TBAP was entirely reproducible, several attempts to repeat deposition in TBAT failed.

The C_{1s}, N_{1s} and Fe_{2p} spectra for the film of poly-$Fe(bpypyr)_3^{2+}$ formed in TBAT are similar to those shown in Figure 3.3.1. O_{1s} and F_{1s} signals were also detected, the F_{1s} signal is assumed to arise from the BF_4^- anion. The N/F stoichiometry was 1.2 which is equivalent to 1.9 tetrafluoroborate anions per monomeric unit. The F/Fe stoichiometry was 8.4 which is equivalent to 2.1 tetrafluoroborate anions per

monomeric unit. These results show that the film formed in TBAT was not doped with BF_4^-. The overall surface stoichiometry of the film was $C_{45}N_{9.8}Fe_{0.98}F_{8.2}O_{2.9}$ in reasonable agreement with the monomer stoichiometry. The film was not analysed for boron due to the low cross-section of B_{1s} electrons to photoionization by MgKα X-rays. The detection of oxygen in the film means that the possibility of some oxygen containing species acting as a dopant anion can not rigorously be excluded.

3.3.2 Electrochemical studies

Unless otherwise stated poly-$Fe(bpypyr)_3^{2+}$ films were formed from CH_3CN/TBAP electrolyte solution.

3.3.2.1 Deposition efficiency

Cyclic voltammetry, in monomer-free electrolyte solution, of electrodes modified with poly-$Fe(bpypyr)_3^{2+}$ shows that the Fe(II)/Fe(III) redox wave is retained in the polymer film (see Figure 3.3.5, Section 3.3.2.2). Over the first five to ten CV cycles the peak currents diminish slightly, after which a stable response is observed. A similar 'break-in' phenomenon has previously been reported for other electroactive films.[13] The cyclic voltammetry of electrodes modified with films of poly-$Fe(bpypyr)_3^{2+}$ is discussed in Section 3.3.2.3. All estimates of Γ_{app} (see Chapter Two, Section 2.5.2) were derived from CVs obtained after the break-in period.

Each monomer has three pyrrole units and so the number of electrons, n, involved in the film forming

process in TBAP should be approximately 8.0. This figure takes account of the irreversible two electron oxidation of each pyrrole ring, the reversible one electron oxidation of the Fe(II)/Fe(III) couple and the oxidative doping level of one electron lost per monomer.[14] † The deposition efficiency is calculated, as in Section 2.5.2, from the ratio of the number of moles of monomer deposited on the electrode surface (determined by CV) to the number of moles of monomer oxidized. The choice of 8.0 for the value of n affects the absolute value of deposition efficiency but not trends in this efficiency. The results of a study of the variation of deposition efficiency with CPE deposition time are summarised in Table 3.3.1. Deposition efficiency for $Fe(bpypyr)_3^{2+}$ is considerably higher than that for 1,1´-(3-N-pyrrolylpropyl)-ferrocenedicarboxamide (Section 2.5.2). Table 3.3.1 shows that, unlike 1,1´-(3-N-pyrrolylpropyl)ferrocenedicarboxamide, deposition efficiency decreases with increasing deposition time. Cosnier *et al* also report a variation in deposition efficiency for pyrrole substituted ruthenium complexes with film thickness.[14]

That the decrease in deposition efficiency at longer CPE times is not caused by oxidative degradation is suggested by the fact that oxidized, paramagnetic iron species were not observed in the $Fe_{2p_{3/2}}$ ESCA spectra of films of poly-$Fe(bpypyr)_3^{2+}$ regardless of deposition time.

---

† The number of electrons lost in the oxidative polymerization was not determined experimentally. Cosnier *et al* [14] have published the results of exhaustive coulometry experiments which indicate that two electron oxidation per pyrrole ring is involved in the electrooxidative polymerization of similar pyrrole substituted ruthenium complexes.[14] It should be noted that Cosnier *et al* found considerably less than 100% current efficiency for the deposition process and for this reason the values of n reported may be invalid.

TABLE 3.3.1 Deposition efficiency for poly-Fe(bpypyr)$_3^{2+}$

CPE time/mins.	% efficiency[a]
0.5	88.5
1.0	73.6
2.0	61.8
4.0	53.3
8.0	41.5

a. For deposition onto a glassy carbon electrode at +1.3V.

The reason for the decrease in deposition efficiency is obscure. One possible explanation is a progressive change in deposition mechanism. It is possible that at short CPE times (thin films) most deposition takes place following diffusion of Fe(bpypyr)$_3^{2+}$ monomers to the growing film/electrode interface where monomer oxidation occurs and is followed by an efficient polymer incorporation process due to the encapsulation of the oxidized monomer by the growing polymer. For longer CPE times the diffusional pathway is less favourable and most monomer oxidation may take place *via* redox conduction through the growing polymer film at the film/solution interface where the formation of smaller oligomers, which may diffuse into solution, is more likely. Redox conductivity is discussed in Section 3.3.2.5.

Films of poly-Fe(bpypyr)$_3^{2+}$ were also formed by cycling the potential at an electrode between -0.2 and +1.5V. A typical CV showing film growth on a glassy carbon electrode surface is shown in Figure 3.3.3. The

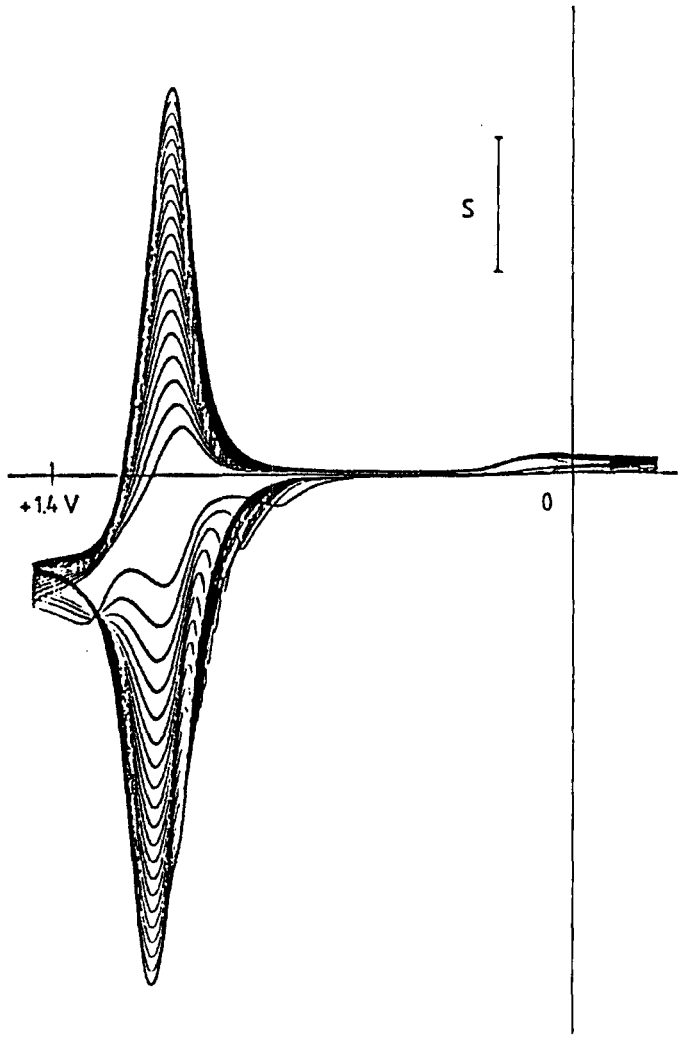

FIGURE 3.3.3 CV deposition of poly-Fe-$(bpypyr)_3^{2+}$. S = 200 μA cm^{-2} Sweep rate = 50 mV s^{-1}.

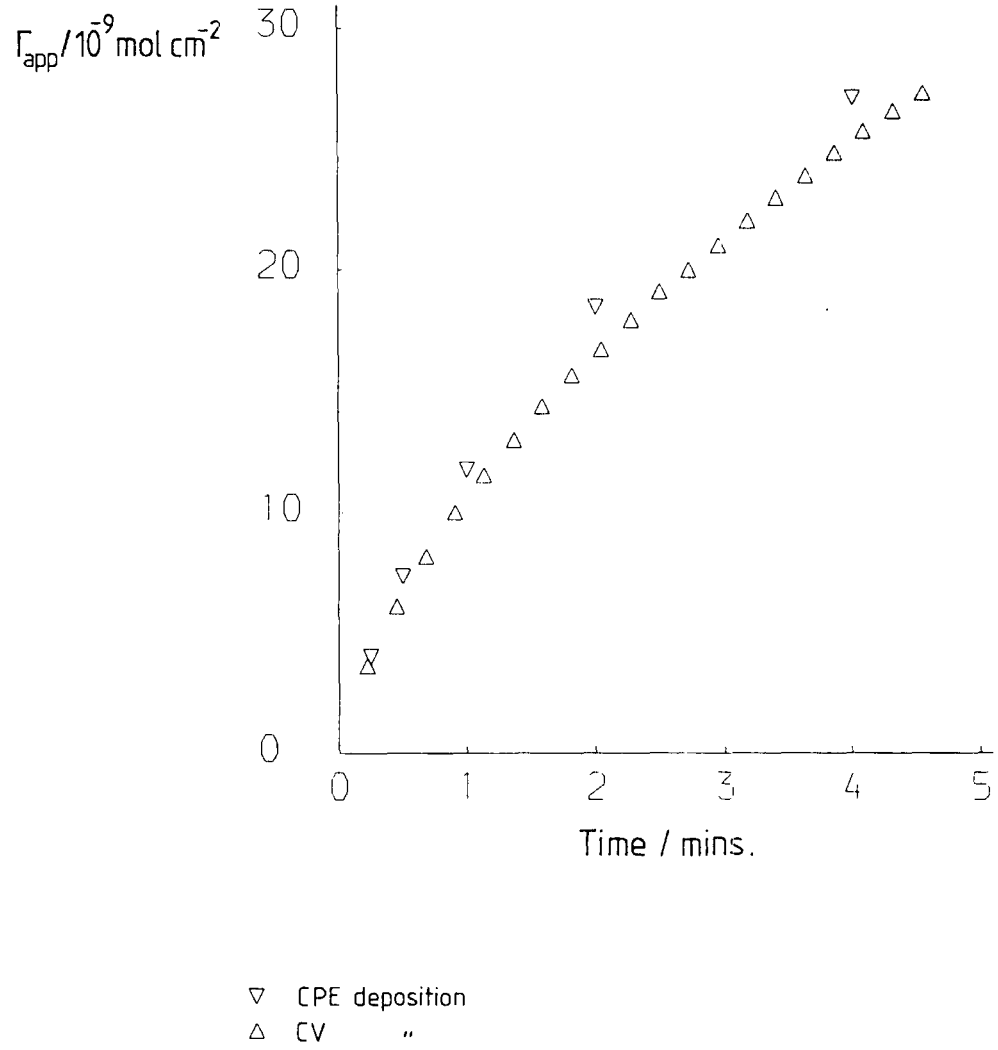

FIGURE 3.3.4 Plot of extent of poly-Fe-$(bpypyr)_3^{2+}$ deposition *versus* oxidation time (see text).

amount of poly-Fe(bpypyr)$_3^{2+}$ deposited does not increase linearly with cycle number, rather the growth rate becomes progressively slower.

If pyrrole and Fe(ll)/Fe(lll) oxidation both occur at the same potential then a much larger anodic than cathodic peak current might be expected in the CV since the oxidation leading to pyrrole polymerization is irreversible. As polymer is deposited on the electrode surface, however, the CV response will quickly become dominated by the contribution from the polymer itself, this being reversible one electron Fe(ll)/Fe(lll) oxidation/reduction. Under the experimental conditions used approximately 20-30 monolayers are deposited in the first cycle (assuming 10^{-10} mol cm^{-2} = 1 monolayer) and Figure 3.3.3 shows that the anodic and cathodic peak currents rapidly become similar in size.

Since poly-Fe(bpypyr)$_3^{2+}$ may be deposited by potential cycling, as well as by CPE, it is possible to investigate whether or not deposition continues on the electrode surface during CV at potentials less positive than $E^{\ominus}$ for Fe(ll)/Fe(lll). Figure 3.3.4 shows a plot of the apparent molar coverage (Γ_{app}), determined from CV of the modified electrode, against CPE deposition time at +1.3V. Also shown in Figure 3.3.4 is a plot of Γ_{app}, determined from 'normalised' (*vide infra*)CV peak areas, against the time spent at a potential greater than $E^{\ominus}$ for Fe(ll)/Fe(lll) for a film grown by CV. For CV growth the time spent at potentials greater than Fe(ll)/Fe(lll) $E^{\ominus}$ is approximately 20% of the total time. The peak area for each cycle in the film growth is normalised to that expected after break-in in monomer-free solvent and

electrolyte. The normalisation factor was taken from the ratio of the CV peak area in monomer free electrolyte solution after break-in, for the film after 21 growth cycles, to the CV peak area for the 21st growth cycle in the monomer solution. The validity of this normalisation depends upon the assumption that the contribution to the CV of the growing film from the monomer is small compared to that from polymer already deposited. This is the case for all but the first few cycles.

The agreement between the two curves in Figure 3.3.4 is good indicating that deposition occurs only during the period for which the monomer may be oxidized. This result is consistent with a growth mechanism similar to that delineated for pyrrole in Chapter One in which highly reactive radical cations are the only polymer building species. If a chain propagation mechanism were controlling deposition then some film formation might be expected to occur during the CV 'off' time. Figure 3.3.4 shows that this is not the case.

3.3.2.2 Stability of modified electrodes

In the CV deposition of poly-Fe(bpypyr)$_3^{2+}$ shown in Figure 3.3.3 it may be seen that there is a prepeak to the main oxidation wave. At higher cycle numbers this prepeak merges with the main wave. The origin of the prepeak is unknown but similar prepeaks have previously been observed by Bidan *et al.*[13] Figure 3.3.5 shows the first 5 cycles in the cyclic voltammogram, in monomer-free solvent and electrolyte, of a film of poly-Fe(bpypyr)$_3^{2+}$ formed over 5 CV cycles from a solution of the monomer. The initial break-in phenomenon, mentioned above, is associated almost entirely with the

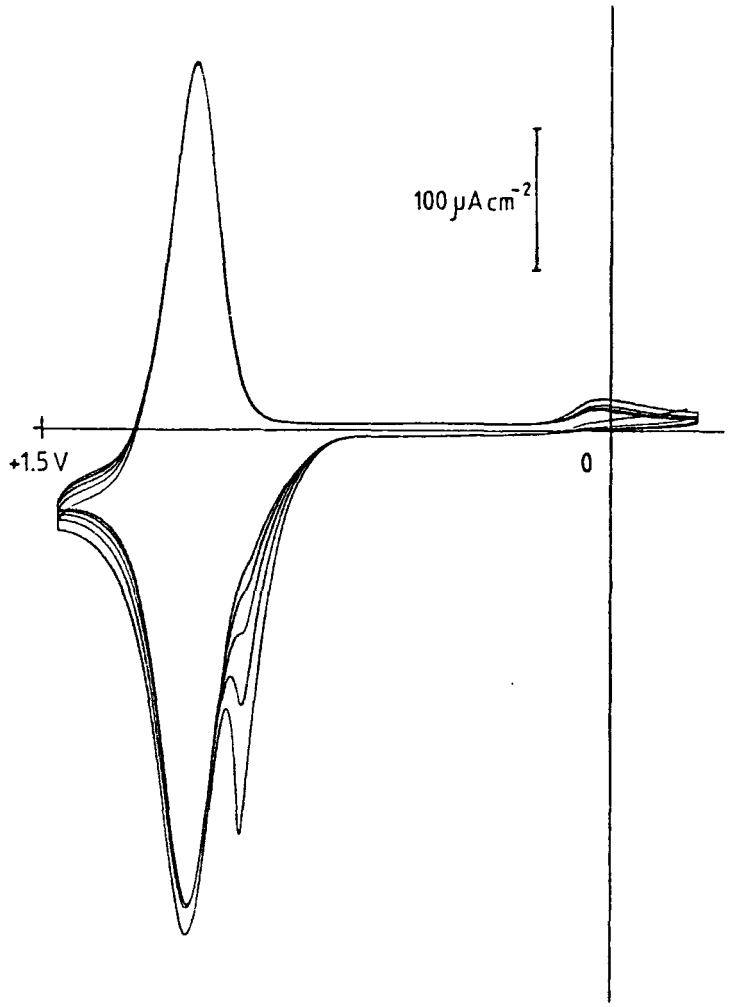

FIGURE 3.3.5 CV of poly-Fe(bpypyr)$_3^{2+}$ modified electrode in CH_3CN/0.1M TBAP. Sweep rate = 50mV s^{-1}

loss of this prepeak. Identical break-in behaviour was found for films prepared by CPE.

After break-in, films of poly-Fe(bpypyr)$_3^{2+}$ have a high degree of stability toward electrochemical cycling between the Fe(II) and Fe(III) states. For example negligible loss of integrated peak current was observed for one modified electrode after 200 cycles between -0.2 and +1.5V at 50mV/s. During this treatment the film spent approximately 46 minutes in the oxidized state. Murray *et al*[7] have reported similarly high stabilities for poly-Fe(Vbpy)$_3^{2+}$ (Vbpy=4-vinyl-4´-methyl-2,2´-bipyridine).

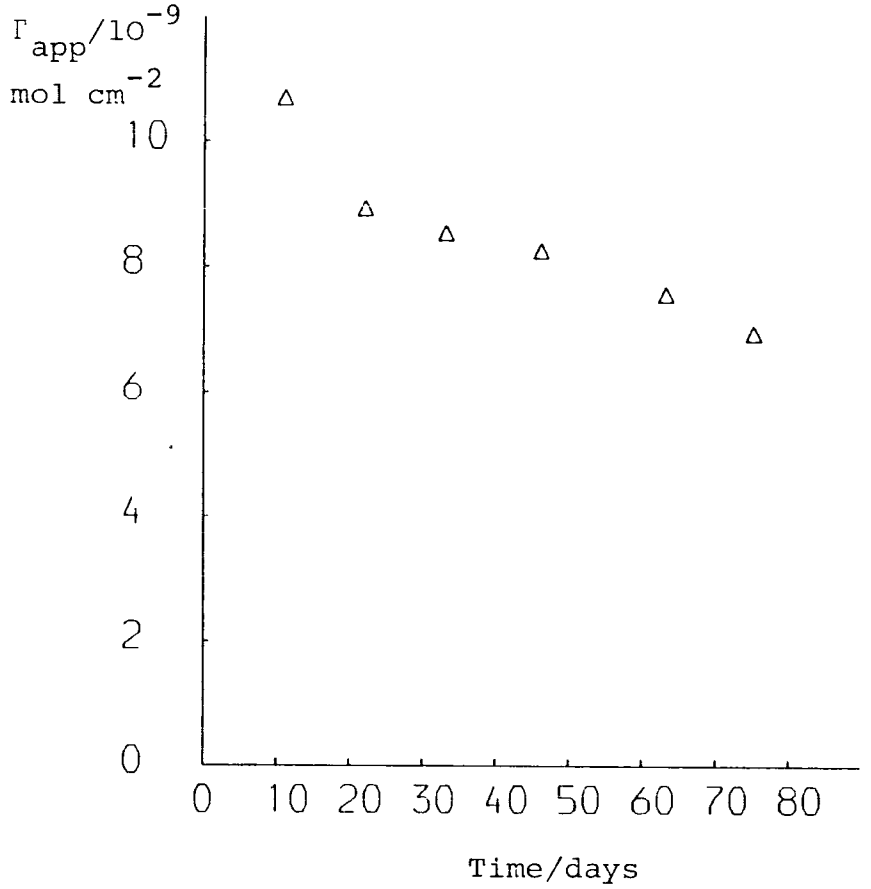

FIGURE 3.3.6 Decrease in electroactivity with storage time

The stability of a poly-Fe(bpypyr)$_3^{2+}$ modified electrode towards storage in air in the absence of light was also tested. Figure 3.3.6 shows the decrease in film electroactivity plotted as a decrease in Γ_{app}, determined from steady state CVs at 50mV/s, against the storage time in days. The film was first tested 11 days after its preparation and the usual break-in phenomenon of loss of the anodic prewave and slight loss of peak current over the first few cycles followed by a stable response was observed. For CV tests subsequent to the first, an entirely opposite initial response was found. Over the first 5 to 10 cycles the peak current grew and the peak splitting decreased from a first-cycle value of 220mV to 50mV on the third cycle and

reached a steady-state value of 35mV. The reason for this behaviour is not known but a possible explanation is the replacement of electrolyte anions in the film which have been lost during storage. This was not checked by ESCA but anion loss during storage has been reported for polypyrrole.[15]

Although there is a steady decrease in CV peak current with storage time, 66% of the electroactivity is retained 75 days after film preparation. There is no evidence that storage of the film produced any degradation of its charge transport kinetics since the CV peak splitting was the same (35mV) on each test. The peak FWHM also remained constant at 170mV.

Films of poly-$Fe(bpypyr)_3^{2+}$ show no stability toward reductive potential cycling. A potential excursion between OV and -1.7V gives rise to a large current spike at *ca.* -1.2V (Figure 3.3.7). Such current spikes have been observed for poly-$Ru(Vbpy)_3^{2+}$ [7] and similar reductively polymerized ruthenium complexes.[16] A potential scan between OV and +1.5V, following the reductive excursion, shows a large increase in the anodic wave at the Fe(ll)/Fe(lll) redox potential (Figure 3.3.7). Subsequent scans between OV and -1.7V show smaller cathodic current spikes, shifted to more negative potentials. Subsequent scans between OV and +1.5V show that all Fe(ll)/Fe(lll) electroactivity is lost (Figure 3.3.7). No film was visible on the electrode surface following this treatment. A similar loss of Ru(ll)/Ru(lll) electroactivity has been reported for electrodeposited ruthenium trisbipyridyl complexes, but only after repeated scanning to negative potentials.[7,14]

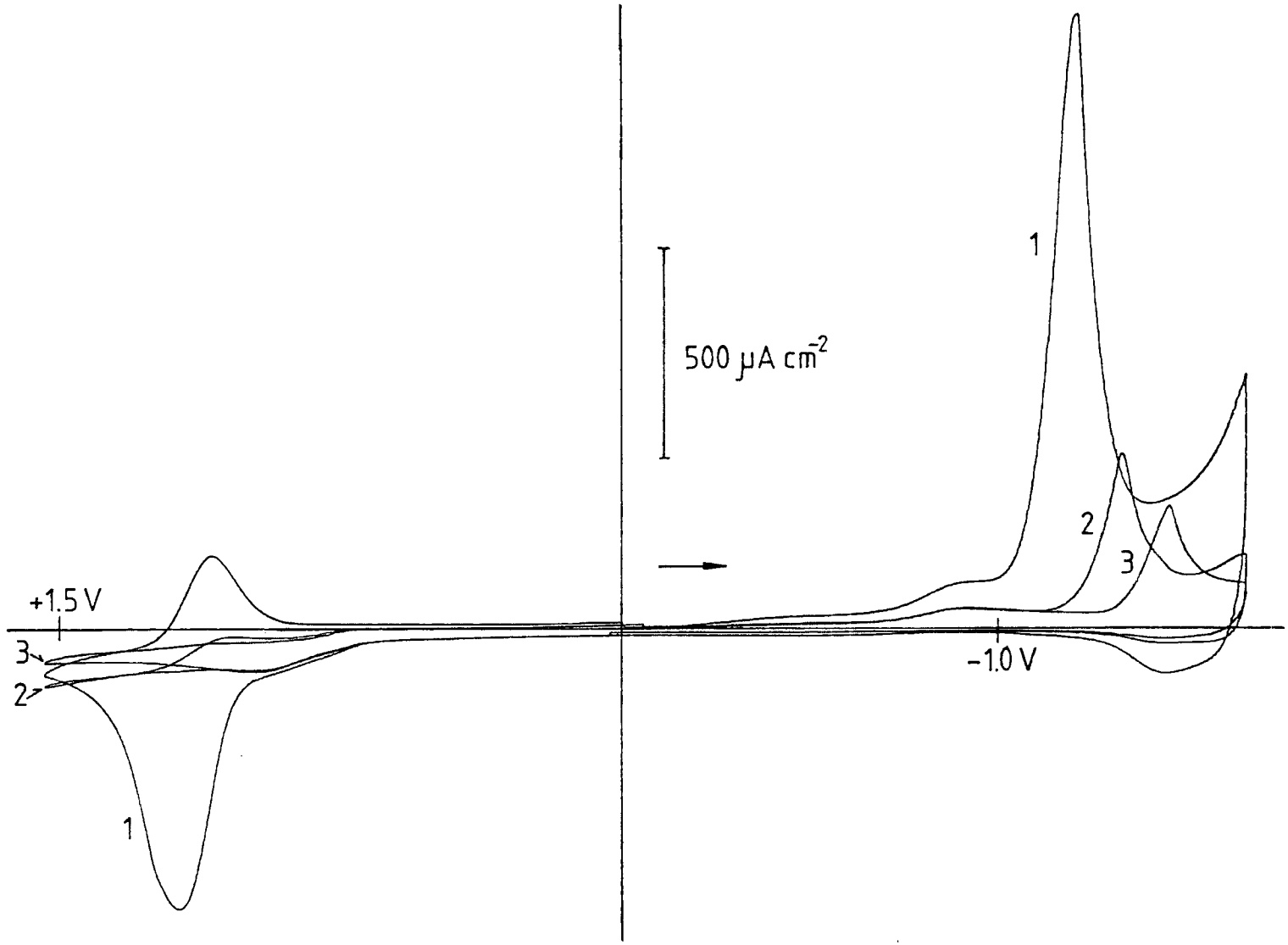

FIGURE 3.3.7 3 CV cycles (OV → -1.7V → +1.5V → OV) for a poly-Fe(bpypyr)$_3^{2+}$ modified electrode. Sweep rate = 50mV s^{-1}.

That reductive potential cycling leads to the destruction of the $Fe(bpypyr)_3^{2+}$ redox sites was confirmed by ESCA. An electrode which was cycled from OV to -1.7V then to +1.5V and back to OV showed one broead $Fe_{2p_{3/2}}$ signal centred at 711.8eV indicating that all the iron in the film had been irreversibly oxidized to the +3 oxidation state. Moreover, a large Pt_{4f} signal from the underlying electrode was detected, indicating that the remaining film was only a few nanometres thick. Since the film was initially red coloured and did not give interference patterns in visible light it must originally have been thicker than several hundred nanometres.

3.3.2.3 Cyclic voltammetry studies

Films of poly-$Fe(bpypyr)_3^{2+}$ of different thickness were prepared by varying the CPE time in a $2x10^{-3}$M solution of the monomer. Cyclic voltammograms were then recorded in monomer-free solution. Plots of anodic peak current against sweep rate are shown in Figure 3.3.8. For the thinnest film tested ($\Gamma_{app}=4x10^{-9}$ mol cm^{-2}) a linear plot up to a sweep rate of 300mV/s was obtained. This is the behaviour expected for a surface immobilized, electroactive film sufficiently thin for all of the redox sites within the film to undergo oxidation and reduction during one potential cycle, over the range of sweep rates specified (see Chapter One). Only in this linear region of peak current response to sweep rate does the peak area represent the apparent molar coverage, Γ_{app}, of the electroactive species.[17]

As film thickness is increased deviations from linearity become more pronounced and occur at slower sweep

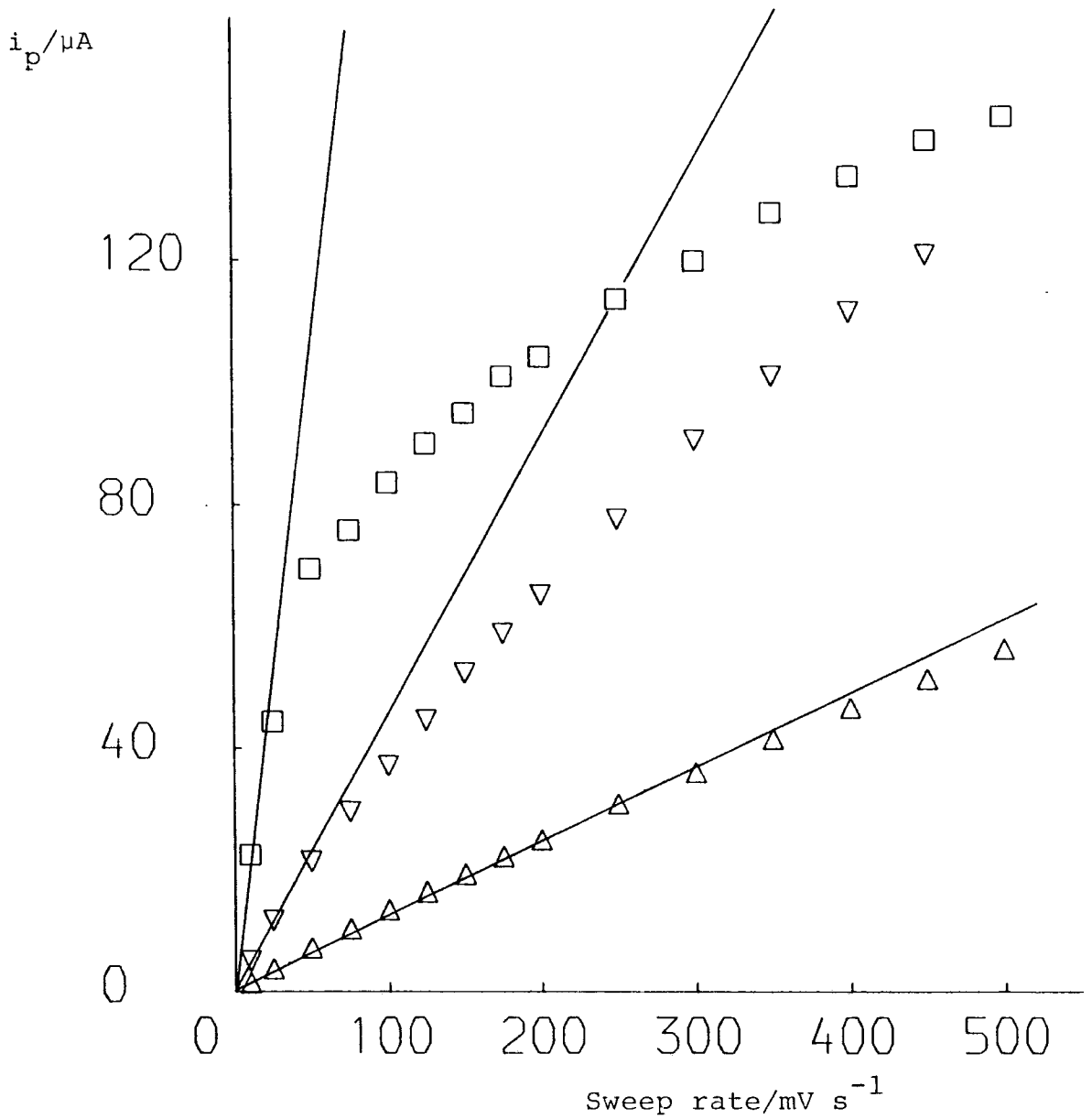

□ $\Gamma_{app} = 3.7 \times 10^{-8}$ mol cm^{-2}
▽ $\Gamma_{app} = 1.2 \times 10^{-8}$ mol cm^{-2}
△ $\Gamma_{app} = 4.0 \times 10^{-9}$ mol cm^{-2}

FIGURE 3.3.8 i_p *versus* sweep rate plots for poly-Fe-$(bpypyr)_3^{2+}$ modified electrodes for 3 film thicknesses.

rates (see Figure 3.3.8). This phenomenon is to be expected since for a given sweep rate there will be a certain film thickness beyond which the rate of charge transport through the film is insufficiently large for all of the redox sites to undergo oxidation and reduction in one cycle. This condition is fulfilled when $\frac{D\tau}{d^2} < 1$ (see Chapter One). Similar experimental results have been reported by Ghosh and Bard for $Ru(bpy)_3^{2+}$ incorporated into a host polymer film.[18]

Table 3.3.2 gives the variation of peak splitting and anodic peak FWHM with sweep rate for the films used to obtain the plots shown in Figure 3.3.8. As expected[17] (see Chapter One) the peak splitting increases for the thicker films at sweep rates corresponding to the non-linear regions of Figure 3.3.8. A loss of peak symmetry, manifested as a 'diffusional tail' (see Figure 1.3.1) accompanied the increase in peak splitting in the CVs of the thicker films. Some CV data for poly-$Fe(vbpy)_3^{2+}$, reported by Murray *et al*, are also given in Table 3.3.2 for comparison.[7]

For the film prepared over 1 minute CPE time ($\Gamma_{app}=1.2\times10^{-8}$ mol.cm^{-2}), a linear plot of peak current against the square root of sweep rate was obtained between sweep rates of 175 and 450 mV/s (Figure 3.3.9). This plot has a negative intercept on the current axis. The slope of the linear region of Figure 3.3.9 may be used to determine a value for the product $D^{1/2}C$, where C is the concentration of redox centres in the film, from the Randles-Sevčik equation:[19]

$$i_p = -(2.71\times 10^5)\ n^{3/2}\ D^{1/2}\ C\nu^{1/2}A \quad \text{at } 20^oC$$

ν = sweep rate in Vs^{-1}.

TABLE 3.3.2 Variation of CV parameters with potential sweep rate for films of poly-$Fe(bpypyr)_3^{2+}$ of varying thickness

a. Film formed by 15s CPE deposition ($\Gamma=4.0\times10^{-9}$ mol cm^{-2})

sweep rate/mVs^{-1}	peak splitting /mV	anodic peak FWHM/mV
25	10	155
50	15	155
100	15	155
200	20	160
400	30	160

b. Film formed by 1 min CPE deposition ($\Gamma=1.2\times10^{-8}$ mol cm^{-2})

25	20	170
50	20	180
100	40	170
200	50	160
400	75	170

c. Film formed by 8 min CPE deposition ($\Gamma=3.7\times10^{-8}$ mol cm^{-2})

10	30	150
25	65	160
50	90	170
100	110	190
200	130	210
400	140	205

d. Films of $poly\text{-}Fe(vbpy)_3^{2+}$ (ref.7)

20($\Gamma=1.2\times10^{-8}$ mol cm^{-2})	30	175
50($\Gamma=2.0\times10^{-8}$ " ")	40	150
100($\Gamma=2.0\times10^{-8}$ " ")	70	160

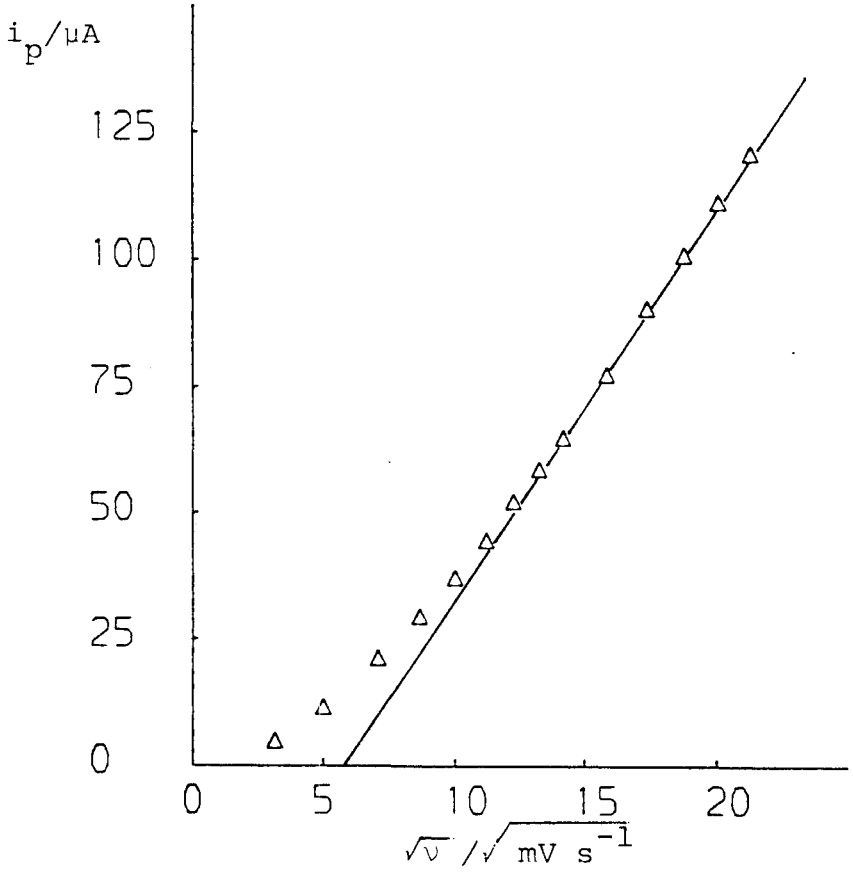

FIGURE 3.3.9

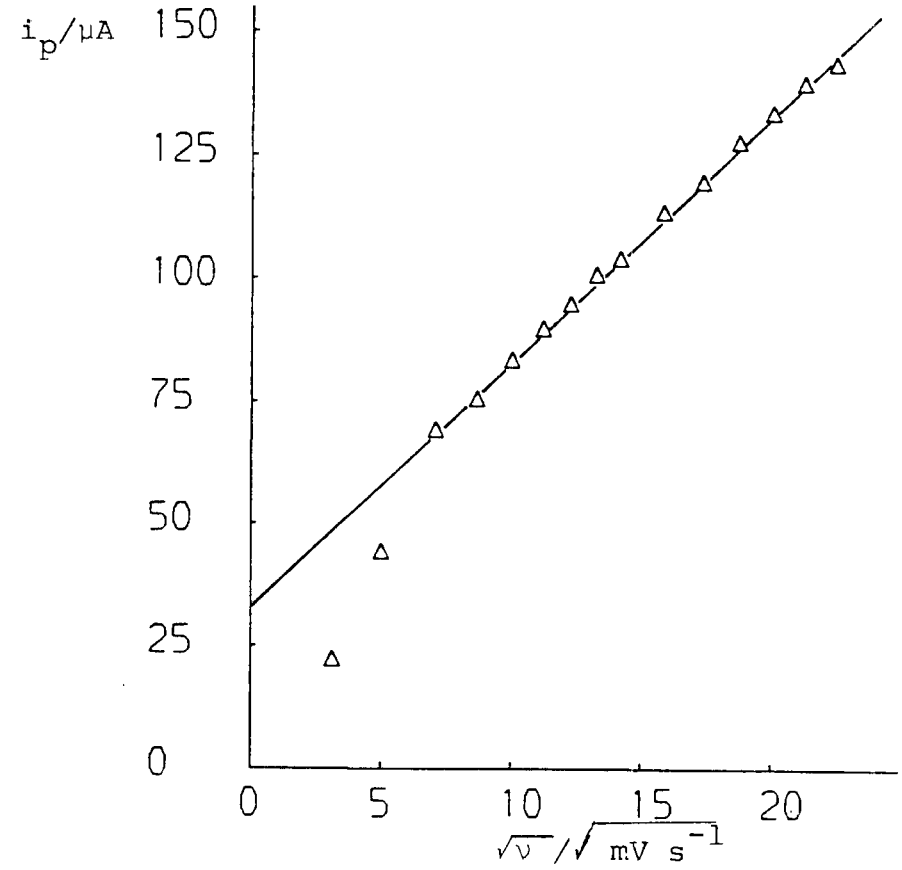

FIGURE 3.3.10

Plots of peak current *versus* $\sqrt{\text{sweep rate}}$ for poly-Fe(bpypyr)$_3^{2+}$ films.

The data in Figure 3.3.9 give a value of 1.2×10^{-8} mol cm^{-2} $s^{-\frac{1}{2}}$ for $D^{\frac{1}{2}}C$. In order to calculate D the concentration of redox sites in the film must be known. The concentration may not be determined from the apparent molar coverage since $\Gamma = cd$ and the film thickness, d, is unknown. For films of poly-$Ru(vbpy)_3^{2+}$ Murray *et al*[7] have assumed a density of 1.35g cm^{-3}. If the same density is assumed for poly-$Fe(bpypyr)_3^{2+}$ and the molecular weight of one redox site is taken as 961 then a site concentration of 1.4×10^{-3} mol cm^{-3} is obtained. This yields a value of 7.3×10^{-11} $cm^2 s^{-1}$ for D, the charge transfer diffusion coefficient. It is commonly assumed that a coverage of 10^{-10} mol cm^{-2} is roughly equivalent to one monolayer. If this were the case for poly-$Fe(bpypyr)_3^{2+}$ a concentration of 1.4×10^{-3} mol cm^{-3} would give a monolayer thickness of 7.2Å.

A plot of peak current against the square root of sweep rate for another film of poly-$Fe(bpypyr)_3^{2+}$ formed over 5 CV cycles ($\Gamma_{app} = 1.2 \times 10^{-8}$ mol cm^{-2}) was similar to Figure 3.3.9 and also gave a value of 1.2×10^{-8} mol $cm^{-2} s^{\frac{1}{2}}$ for $D^{\frac{1}{2}}C$.

For thicker films of poly-$Fe(bpypyr)_3^{2+}$ plots of peak current against sweep rate were linear but had positive intercepts on the current axis and yielded smaller values of $D^{\frac{1}{2}}C$ than the thinner films. Figure 3.3.10 shows such a plot for a film formed over 8 minutes CPE time ($\Gamma_{app} = 3.7 \times 10^{-8}$ mol cm^{-2}) which yielded a value of 7.8×10^{-9} mol $cm^{-2} s^{-\frac{1}{2}}$ for $D^{\frac{1}{2}}C$. A similar result was obtained for a film formed over 20 CV cycles.

For the film prepared over 1 minute CPE time the peak splitting increased from 50mV to 75mV over the linear region of Figure 3.3.9. For the 8 minute CPE deposited film the corresponding increase was 110mV to 145mV. The larger peak splitting for the thicker film may be caused by the increased Ohmic resistance of this film. This could also be the reason for the apparent dependence of $D^{\frac{1}{2}}C$ on film thickness.

3.3.2.4 Potential step chronoamperometry

Potential step chronamperometry may also be used to determine the product $D^{\frac{1}{2}}C$, as discussed in Chapter One.[17] In summary, the current response to the rapid application of a voltage pulse disturbing the Nernstian equilibrium in an electroactive film is expected to obey the Cottrell equation[19] at short times, t, after the application of the pulse.[22] This behaviour is predicted since charge transport through a redox active film is diffusional in nature[7,21] and at short times after the pulse the outermost 'layers' of the film will experience no change in concentration and so a 'semi-infinite' boundary condition will apply.[22]

$$i = \frac{nFD^{\frac{1}{2}}CA}{\pi^{1/2}t^{1/2}} \qquad \text{Cottrell equation}$$

At longer times after the application of the voltage pulse, the changing concentration gradient of oxidized and reduced redox sites will impinge upon the film boundary and the current-time response will no longer obey the Cottrell equation.[22] Both Murray *et al*[22] and Albery *et al*[23] have shown that experimental chronoamperometry data, for redox active electrode coatings, obey a current time

equation appropriate for thin layer cell electrochemistry at longer times after the voltage pulse. The extent of the linear region in a Cottrell plot of chronoamperometric data for modified electrodes will depend upon the magnitudes of D and d. The extent of linearity will be greatest for a small charge transfer diffusion coefficient[22a] and a thick film. Albery[24] and Murray *et al*[22b] have commented on the superiority of chronoamperometry over cyclic voltammetry for the determination of $D^{\frac{1}{2}}C$.

Figure 3.3.11 shows a i *versus* $t^{-\frac{1}{2}}$ plot, following a 0 to +1.6V potential step, for a platinum electrode coated with 1.5×10^{-8} mol cm^{-2} of poly-$Fe(bpypyr)_3^{2+}$. The slope of the linear portion of the plot yields a value of 2.8×10^{-8} mol $cm^{-2}s^{-\frac{1}{2}}$ for $D^{\frac{1}{2}}C$. It may be noticed that non-linearity is observed in the plot at short times (larger

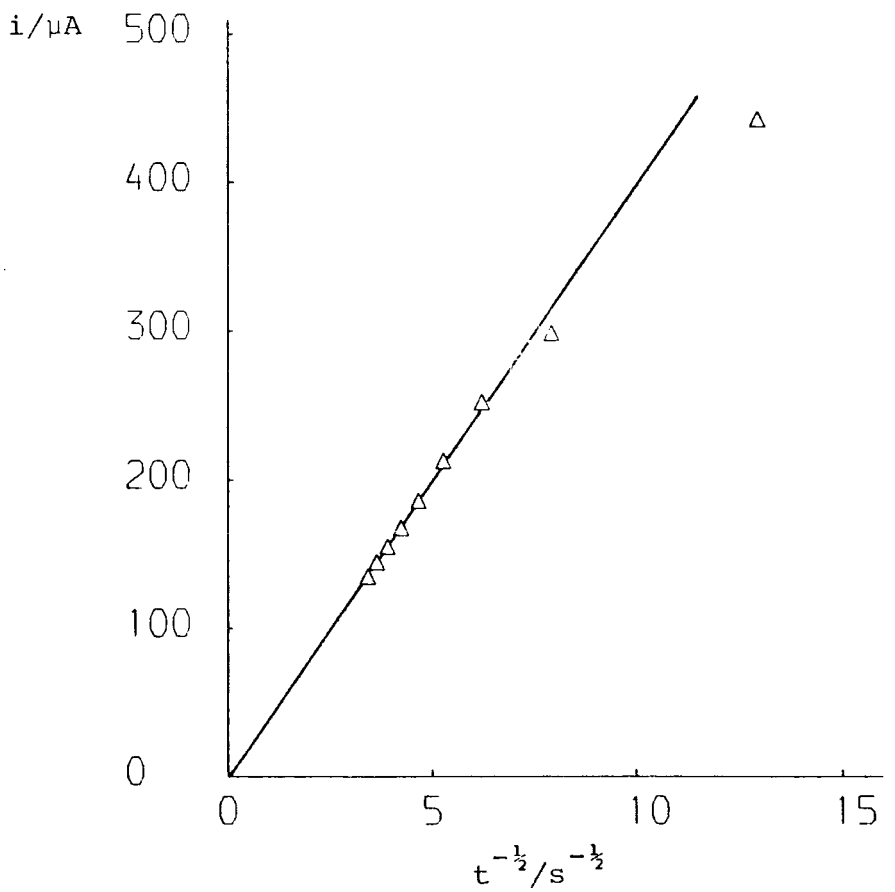

FIGURE 3.3.11

values of $t^{-\frac{1}{2}}$) but not at longer times, apparently in violation of the predicted behaviour. The absence of non-linearity at long times is probably due to the fact that the film is thick enough to prevent any change in the ratio of oxidized to reduced sites in the outermost 'layers' during the time interval recorded on the storage oscilloscope. For thinner films, deviations from linearity at longer times following the voltage pulse were observed. The curvature apparent at short times has been observed in other studies[22b] and is attributed to the Ohmic resistance of the film which causes a smaller than expected current flow. Murray *et al* have shown that linearity at short times may be obtained by increasing the concentration of the supporting electrolyte.[22b] For plasma-polymerized vinylferrocene films i *versus* $t^{-\frac{1}{2}}$ plots similar to Figure 3.3.11 were obtained by Murray *et al* in 0.5M $LiClO_4$/water, whereas linear short time plots were obtained in 1M $LiClO_4$/water. For a film of poly-$Fe(bpypyr)_3^{2+}$, 0 to +1.6V potential steps in saturated $LiClO_4$/acetonitrile solution gave rise to i *versus* $t^{-\frac{1}{2}}$ plots similar to Figure 3.3.11 and gave a $D^{\frac{1}{2}}C$ value of 2.8×10^{-8} mol $cm^{-2}s^{-\frac{1}{2}}$.

Several films of poly-$Fe(bpypyr)_3^{2+}$. deposited onto a platinum electrode to a coverage of *ca.* 1.5×10^{-8} mol cm^{-2} in each case, were individually examined by chronoamperometry. For any one film high experimental reproducibility was found (the oscilloscope traces superimposed). The agreement between $D^{\frac{1}{2}}C$ values obtained from different films was not as good, and an average value of 3.1×10^{-8} mol $cm^{-2}s^{-\frac{1}{2}}$ was obtained with maximum and minimum values of 3.4×10^{-8} and 2.3×10^{-8} mol $cm^{-2}s^{-\frac{1}{2}}$. The

assumption of a redox site concentration of 1.4M, as in Section 3.3.2.3, gives an average value of 4.9×10^{-10} $cm^2 s^{-1}$ for D.

Table 3.3.3 compares the $D^{\frac{1}{2}}C$ values derived for poly-$Fe(bpypyr)_3^{2+}$, determined from both chronoamperometry and cyclic voltammetry data, with some of those reported for some pyridyl and bipyridyl coordinated ruthenium polymers.

TABLE 3.3.3

Polymer	$\Gamma_{app}/10^{-8}$ mol cm^{-2}	$D^{\frac{1}{2}}C/10^{-8}$ mol $cm^{-2} s^{-\frac{1}{2}}$	Ref.
$Fe(bpypyr)_3^{2+}$	av.~1.5	av. 3.1[a]	this work
"	1.2	1.2[b]	" "
"	3.7	0.78[b]	" "
$Ru(vbpy)_3^{2+}$	av. 0.65	av. 2.2[a]	25
$Ru(bpy)_2(vpy)_2^{2+}$ [c]	-	3.2[a]	25

a. Determined by chronoamperometry
b. Determined by cyclic voltammetry
c. vpy = 4-vinylpyridine.

The chronoamperometrically determined $D^{\frac{1}{2}}C$ values for the three polymers listed in Table 3.3.3 are similar. The agreement between $D^{\frac{1}{2}}C$ values for poly-$Fe(bpypyr)_3^{2+}$ determined by the two methods is poorer than that previously reported for plasma-polymerized vinylferrocene films.[22a]

Chronoamperometry experiments at 5°, 20° and 35°C were performed in an attempt to determine the activation energy of the charge transfer process. The variable temperature experiment showed poor reproducibility.

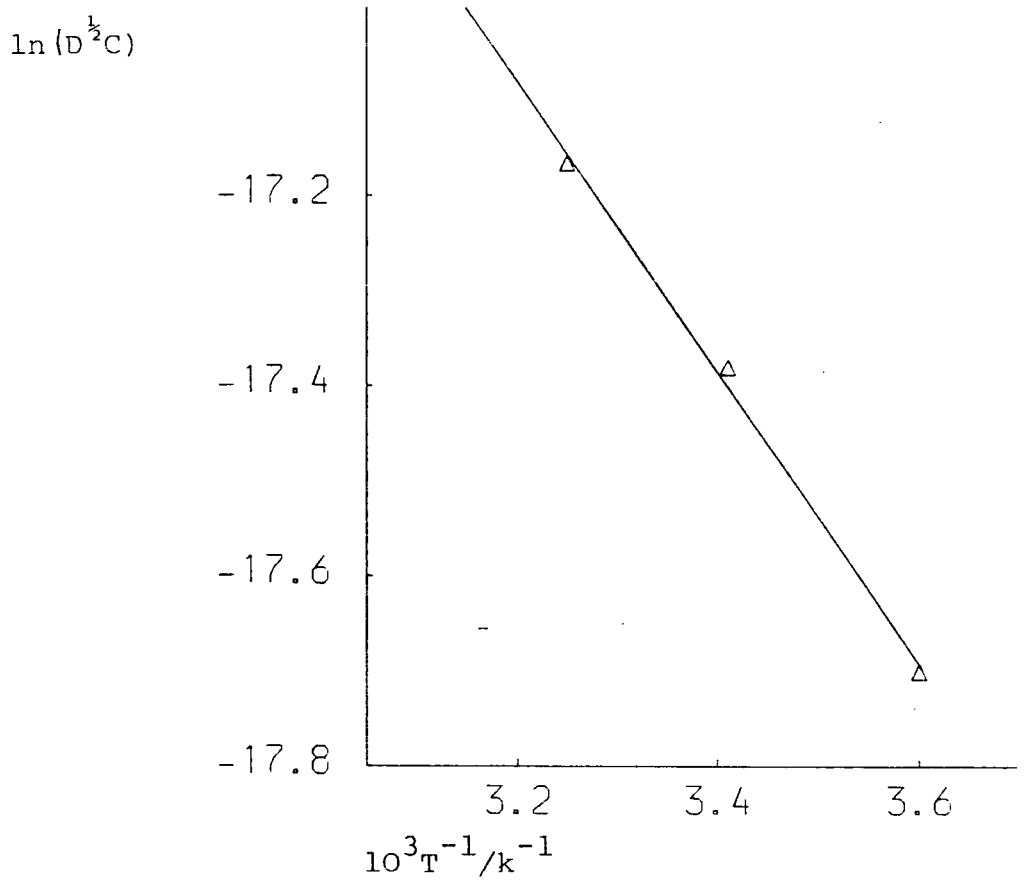

FIGURE 3.3.12

Figure 3.3.12 shows an Arrhenius plot for the data from one experiment from which an activation energy of **23.2**kJmol^{-1} was obtained. Because of the lack of experimental reproducibility this figure can only be regarded as an order of magnitude estimate, however it compares reasonably well with the value of *ca.* 15.4 kJ mol^{-1} reported by Murray *et al*[22a] for plasma polymerized vinylferrocene films.

The nature of the rate limiting process controlling the charge transport diffusion coefficient in electroactive films has been investigated [23,25] (see Chapter One), but was not examined in this study.

3.3.2.5 Cyclic Voltammetry of poly-Fe(bpypyr)$_3^{2+}$ films in the presence of solution redox species

Electrodes coated with films of poly-Fe(bpypyr)$_3^{2+}$ were examined by cyclic voltammetry in the presence of dissolved redox species. Ferrocene and 2,3-dichloro-5,6-dicyano-p-benzoquinone (DDQ) were chosen as the solution species since both show well behaved voltammetry at uncoated electrodes and undergo one electron oxidations at electrode potentials ($E^{\ominus}_{soln.}$) less positive than the Fe(ll)/Fe(lll) oxidation in poly-Fe(bpypyr)$_3^{2+}$ ($E^{\ominus}_{pol.}$). This latter criterion is necessary for any attempt to investigate the ability of the electrode coating to support redox conductivity (*vide infra*).

In principle ferrocene and DDQ may be oxidized either at the electrode/polymer interface, after diffusion through a continuous polymer film or permeation through cracks in an imperfect film, or at the polymer film/solution interface, a process which requires either redox conduction through the film (see Chapter One) or an electronically conducting film. In the case of redox conductivity mediated electron transfer, oxidation of the solution species will take place at or near $E^{\ominus}_{pol.}$. The oxidation is then expected to be very rapid and the anodic current appear as a spike since the electrode potential which 'suddenly' appears at the polymer/solution interface is in excess of that required to oxidize the solution species by an amount *ca.* ($E^{\ominus}_{pol.}-E^{\ominus}_{soln.}$). The solution oxidation is also expected to be irreversible since, on the reverse CV sweep, the polymer film is completely reduced to the Fe(ll) state and thus

becomes redox insulating before the potential at which the solution species can be reduced is reached. For electron transfer with solution species following the electronic conductivity or diffusion/permeation pathways, the oxidation will occur at or near $E^{\ominus}_{soln.}$. In these cases the reversibility of the electrochemical reaction is expected to be the same as at the uncoated electrode.

Electron transfer involving solution species at a redox polymer coated electrode at both $E^{\ominus}_{pol.}$ and $E^{\ominus}_{soln.}$ has been demonstrated by Meyer *et al*[26a] and by Murray *et al*.[26b]

Figure 3.3.13a shows a cyclic voltammogram for a solution of *ca*. 10^{-2}M ferrocene at an electrode coated with 1.2×10^{-8} mol cm^{-2} of poly-$Fe(bpypyr)_3^{2+}$. Almost all of the ferrocene oxidation occurring at the modified electrode takes place at $E^{\ominus}_{soln.}$. A small amount of ferrocene oxidation also takes place at $E^{\ominus}_{pol.}$, as may be seen in Figure 3.3.13b in which the oxidation peak around $E^{\ominus}_{pol.}$ is expanded and compared to the polymer peak in inert solvent and electrolyte. The spiked form of the ferrocene oxidation peak is apparent.

Similar results were obtained with a solution of *ca*. 10^{-3}M DDQ at an electrode coated with 1.3×10^{-8} mol cm^{-2} poly-$Fe(bpypyr)_3^{2+}$.

The electrode used for the air storage tests (Section 3.3.2.2) was also examined by CV in the presence of ferrocene and DDQ after 75 days' storage, at which time an apparent decrease in electrode coverage from

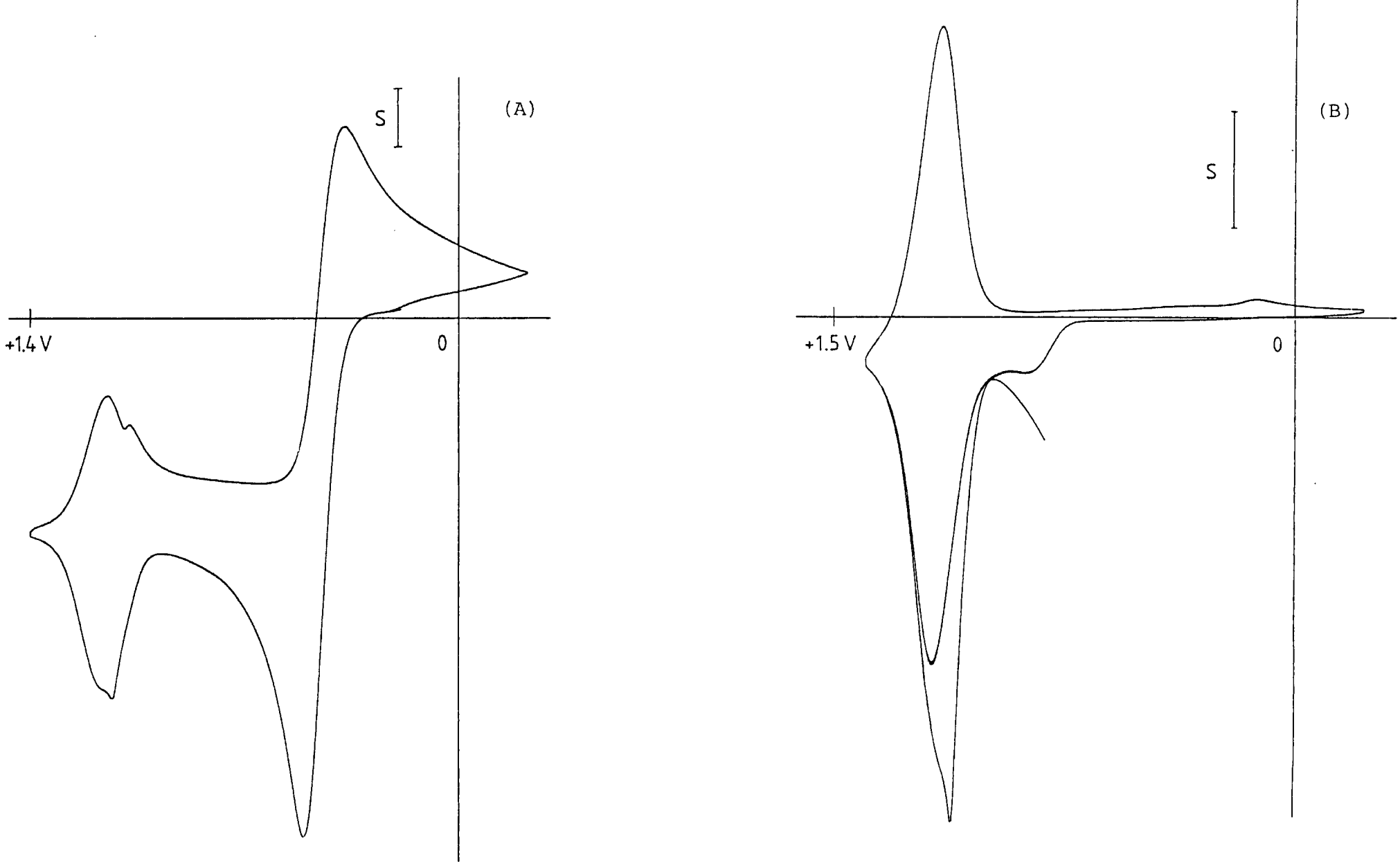

FIGURE 3.3.13a. CV of Poly-Fe(bpypyr)$_3^{2+}$ modified electrode in the presence of ferrocene in solution. S = 125μA cm^{-2}. Figure 3.3.13b - comparison of the anodic CV wave at $E^{\ominus}$pol before and after the addition of ferrocene to the electrolyte solution. S = 100μA cm^{-2}. Sweep rate = 50mV s^{-1}.

1.1×10^{-8} mol cm^{-2} (day 11) to 0.7×10^{-8} mol cm^{-2} had occurred. A voltammogram for this electrode in a solution which was *ca.* 5×10^{-3}M in ferrocene is shown in Figure 3.3.14, almost all of the ferrocene oxidation takes place near $E^{\ominus}_{pol.}$. The size of the anodic peak for the polymer in the absence of ferrocene is indicated. A similar result was obtained with a solution of *ca.* 10^{-3}M DDQ.

These results demonstrate that after 75 days' storage in air the only mechanism which exists for the oxidation of ferrocene and DDQ in solution, at an electrode coated with poly-$Fe(bpypyr)_3^{2+}$, is redox conductivity through the polymer film. It must be concluded that either:

(a) storage of the film produces some change which prevents oxidation of the solution species at $E^{\ominus}_{soln.}$, or

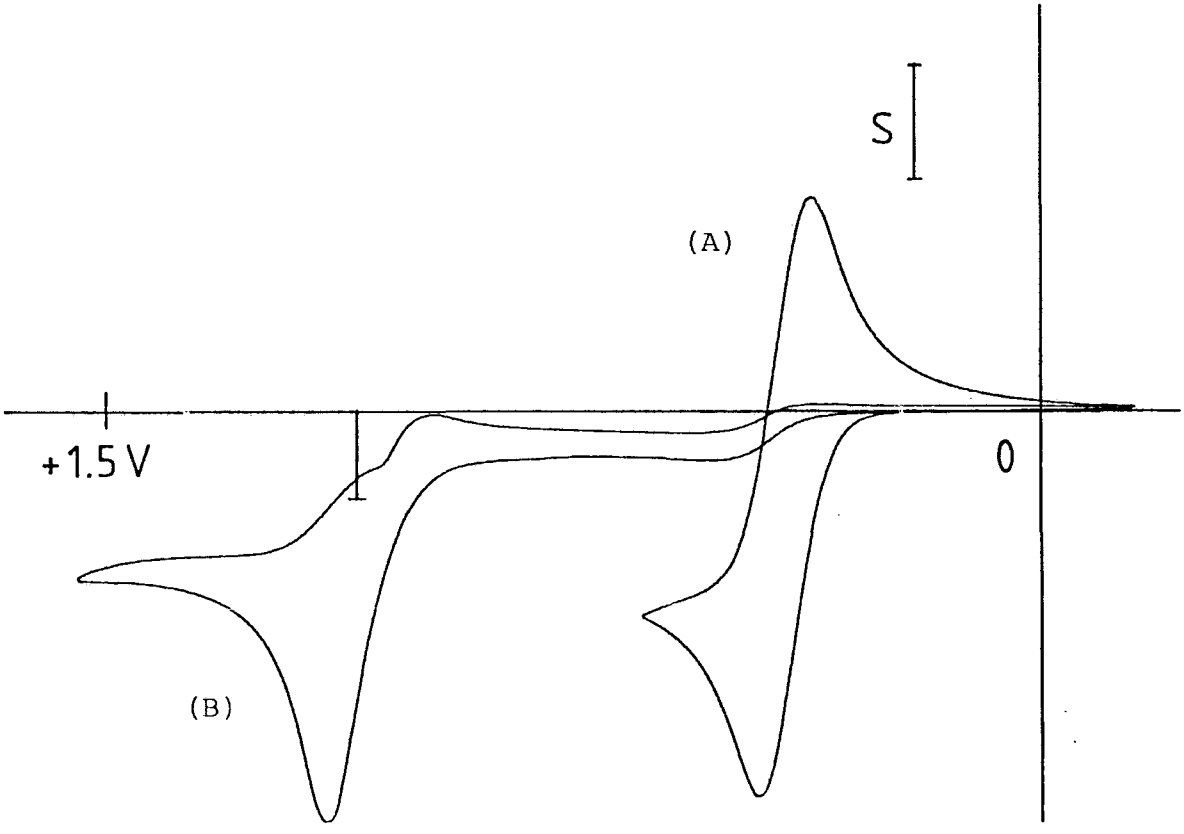

FIGURE 3.3.14 CV response for solution ferrocene at (A) an uncoated and (B) 75 day aged poly-$Fe(bpypyr)_3^{2+}$ coated electrode. S = 200μA cm^{-2}. Sweep rate = 50mV s^{-1}

(b) the films which were tested immediately after preparation were cracked or contained pinholes and that the film tested after 75 days was defect free.

Conclusion (b) may be ruled out for the following reasons:

(i) Optical microscopy of films of similar thickness to those discussed above showed that they were smooth, continuous and defect free within the resolution limit of the microscopy.

(ii) Short circuits were not found when conductivity measurements were made on films of poly-$Fe(bpypyr)_3^{2+}$ (see Section 3.3.2.6).

(iii) Although oxidation of DDQ occurred at $E^{\ominus}_{soln.}$ on a freshly prepared modified electrode, one electron reduction of DDQ was inhibited (see Figure 3.3.15). A similar selective inhibition of DDQ reduction has been observed by Nishihara and Aramaki[27] on electrodes coated with films of electropolymerized 1,1´-Bis(chloromethyl)ferrocene. Although no satisfactory explanation for this phenomenon was given by Nishihara and Aramaki it seems most unlikely that inhibition of the reduction and not the oxidation of DDQ would occur at a cracked or punctured modified electrode.

The results obtained with the freshly prepared films may then only be explained by a continuous film which either, permits diffusion of the solution redox species or, has some electronic conductivity. Although Salaneck *et al*[15] have reported a steady loss in electronic conductivity for films of polypyrrole stored in air, it seems likely that this is not the explanation for the storage induced changes found in this study for the following reasons:

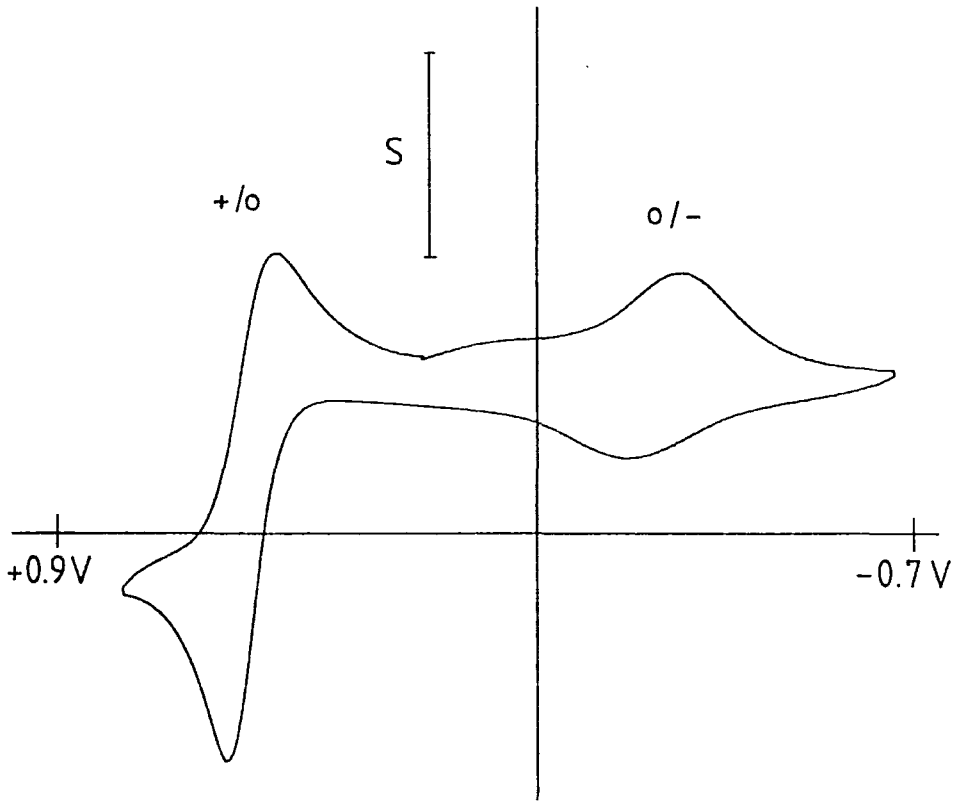

FIGURE 3.3.15 Inhibition of DDQ reduction at a coated electrode. At an uncoated electrode the $DDQ^{+/o}$ and $DDQ^{o/-}$ waves are similar S = 100μA cm^{-2}

(i) No change in the CV characteristics (peak splitting, $E^{\ominus}$, wave shape) in inert solution were observed for the 75 day aged modified electrode compared to a freshly prepared one. If a decrease in electronic conductivity large enough to produce the changes in solution species oxidation described above had occurred it is not unreasonable to expect some change in the voltammetry of the polymer itself. Loss of integrated peak current without degradation of peak splitting is not taken as evidence for this.

(ii) If films of poly-$Fe(bpypyr)_3^{2+}$ are initially sufficiently electronically conducting to permit oxidation of solution species at $E^{\ominus}_{soln.}$ then it is unlikely that a

second oxidation peak at $E^{\ominus}_{pol.}$ (see Figure 3.3.13b) would be observed since electronic and redox conductivity mediated electron transfers to solution species both occur at the film/solution interface.

Finally, since the film tested after 75 days was of a similar thickness to the immediately tested films it is not possible to explain the loss of the peak at $E^{\ominus}_{soln.}$ for the aged electrode in terms of inhibition of the diffusional pathway by a thick film.

Cosnier *et al* have very recently reported the successful electropolymerization of some pyrrole substituted ruthenium bipyridyl complexes[14] (*vide infra*). It was demonstrated that oxidation of both ferrocene and decamethylferrocene can take place at electrodes modified with one of these polymers at both $E^{\ominus}_{soln.}$ and $E^{\ominus}_{pol.}$. Oxidation at $E^{\ominus}_{soln.}$ was shown to decrease with increasing film thickness and at all thicknesses oxidation at $E^{\ominus}_{soln.}$ is greater for ferrocene than the larger decamethylferrocene. These observations strongly suggest that oxidation at $E^{\ominus}_{soln.}$ is due to diffusion of the dissolved redox species through the polymer film and not to electronic conductivity of the film. No dependence of the redox behaviour with ageing time of the modified electrode was reported.

In summary, for an electrode modified with poly-$Fe(bpypyr)_3^{2+}$ which has been aged in air the only pathway available for oxidation of ferrocene and DDQ in solution is redox conduction through the film. For a freshly prepared modified electrode it is probable that oxidation of the solution species occurs at the electrode/polymer interface following diffusion of these species through the polymer.

3.3.2.6 Conductivity

Dry state conductivity measurements were recorded for films of poly-Fe(bpypyr)$_3^{2+}$ in an identical manner to that described for poly-1,1´-(3-N-pyrrolyl-propyl)ferrocene-dicarboxamide (Chapter Two). An increase in measured resistance with film thickness indicated that the resistance was a property of the film. A typical i-V plot is shown in Figure 3.3.16. The films of poly-Fe(bpypyr)$_3^{2+}$ tested were thick enough to be coloured and did not display interference patterns with visible light. If a film thickness of 1000nm is assumed a conductivity of *ca.* 3 x $10^{-5}(\Omega cm)^{-1}$ is obtained. This value is comparable to some non-electroactive poly-N-alkylpyrroles[28] but should only be considered to be accurate to one order of magnitude because of the assumed film thickness.

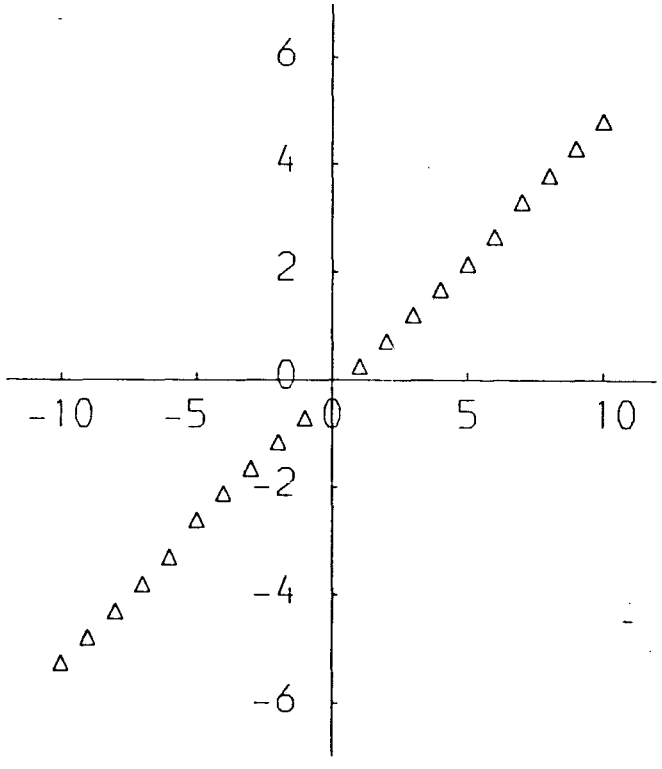

FIGURE 3.3.16 Ordinate: measured current/mA
Abscissa: applied p.d./mV

3.4 Ruthenium complexes

3.4.1 Electropolymerizability

The ruthenium analogue of $Fe(bpypyr)_3^{2+}$ may be prepared from $RuCl_3 3H_2O$. Moreover, in contrast to their iron counterparts, $Ru(bpypyr)_2(bpy)^{2+}$ and $Ru(bpypyr)(bpy)_2^{2+}$ may be readily prepared. Ruthenium trisbipyridyl complexes in which one, two and all three of the bipyridyl ligands were substituted with pyrrole were thus synthesized (see Section 3.7).

Both $Ru(bpypyr)_3^{2+}$ and $Ru(bpypyr)_2(bpy)^{2+}$ could be electrooxidatively polymerized onto the surface of an electrode by cycling the electrode potential between -0.2 and +1.6V. The films displayed Ru(II)/Ru(III) electrochemistry characteristic of the monomers. A cyclic voltammetry 'break-in' phenomenon similar to that described for poly-$Fe(bpypyr)_3^{2+}$ was observed for both films. Typical cyclic voltammograms for modified electrodes following break-in are shown in Figure 3.4.1. The 'polymerizability' of both these ruthenium monomers appears to be less than for $Fe(bpypyr)_3^{2+}$ since for similar monomer concentrations and number of film forming cycles almost 10 times as much polymer was deposited from $Fe(bpypyr)_3^{2+}$ compared to the ruthenium monomers (see Table 3.4.1).

TABLE 3.4.1

Monomer	No.of film forming CV cycles	$\Gamma_{app}/10^{-9}$mol cm^{-2}
$Fe(bpypyr)_3^{2+}$	21	27.0
$Ru(bpypyr)_3^{2+}$	19	3.7
$Ru(bpypyr)_2(bpy)^{2+}$	26	3.8

---

poly-Ru(bpypyr)$_3^{2+}$

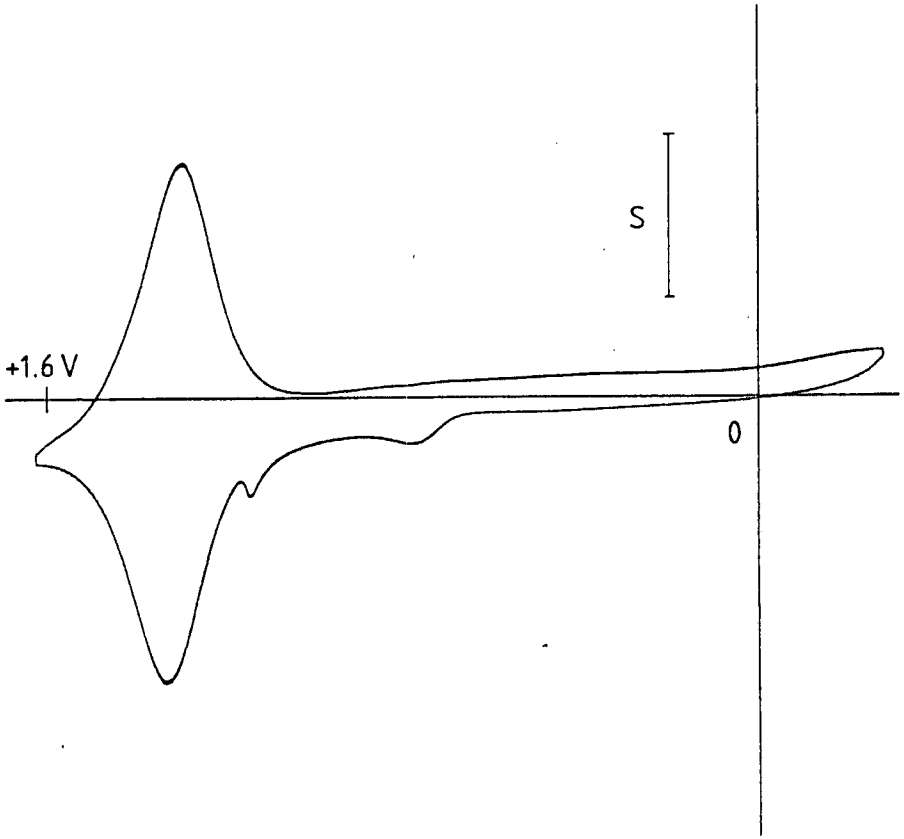

poly-Ru(bpypyr)$_2$(bpy)$^{2+}$

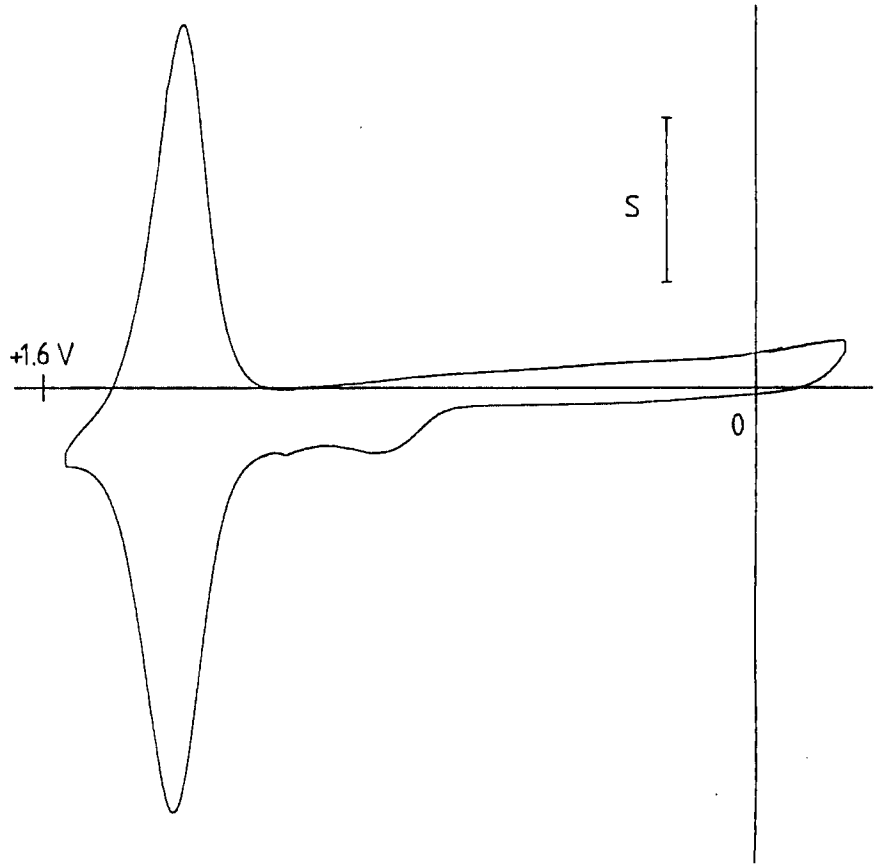

FIGURE 3.4.1 S = 25μA cm^{-2}, sweep rate = 50 mV s^{-1}

In contrast $Ru(bpypyr)(bpy)_2^{2+}$ could not be electro-oxidatively polymerized either by CV up to +1.6V or by CPE at +1.6V. During the course of this work Cosnier *et al*[14] have also prepared trisbipyridyl complexes of ruthenium of of the general formula $Ru(bpypyr')_n(bpy)_{3-n}^{2+}$

bpypyr' = 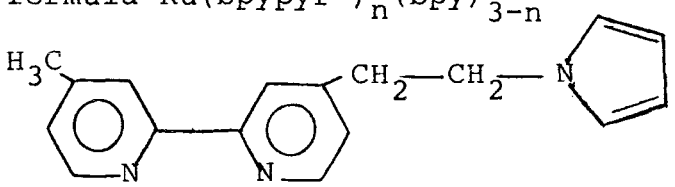

It was found that the polymerizability of the monomers decreased in the order $Ru(bpypyr')_3$ $Ru(bpypyr')_2(bpy)^{2+}$ >> $Ru(bpypyr')(bpy)_2^{2+}$. By using dichloromethane solvent Cosnier *et al* were able to increase the deposition efficiency with $Ru(bpypyr')(bpy)_2^{2+}$. In the present study attempts to deposit electroactive films from $Ru(bpypyr)(bpy)_2^{2+}$ using dichloromethane as solvent failed.

Attempts to deposit films from $Ru(bpypyr)_3^{2+}$ and $Ru(bpypyr)_2(bpy)^{2+}$ using TBAT electrolyte were unsuccessful. It was also found that after a few days storage samples of $Ru(bpypyr)_3^{2+}$ and $Ru(bpypyr)_2(bpy)^{2+}$ became inactive towards polymerization using TBAP electrolyte. No such problem was encountered with $Fe(bpypyr)_3^{2+}$.

3.4.2 ESCA studies

C_{1s} (and $Ru3d_{5/2}$), N_{1s} and Cl_{2p} spectra for poly-$Ru(bpypyr)_3^{2+}$, prepared by cyclic voltammetry in TBAP solution are shown in Figure 3.4.2. Spectra for poly-$Ru(bpypyr)_2(bpy)^{2+}$ are similar in appearance and are not shown.

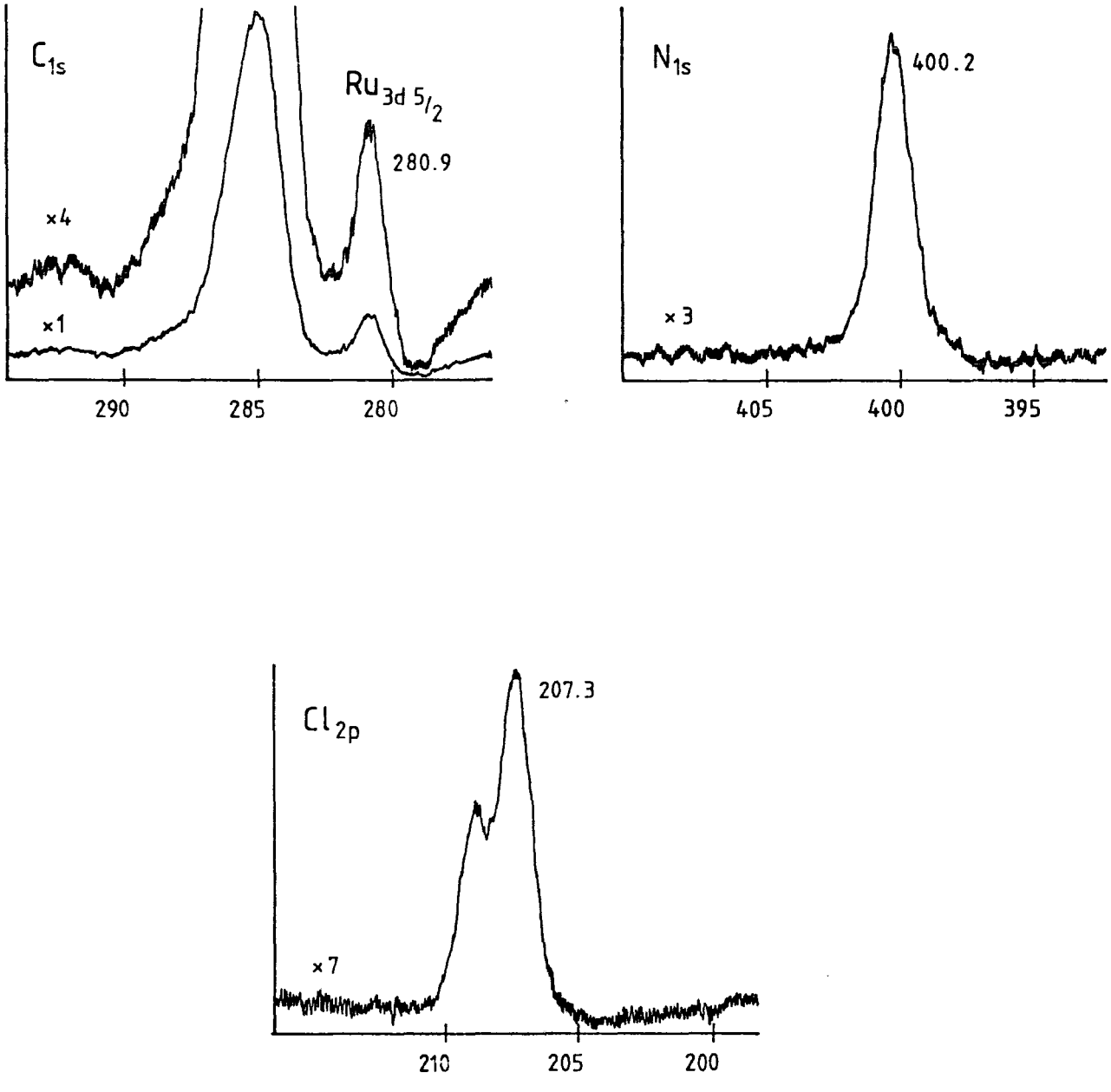

FIGURE 3.4.2 ESCA spectra for poly-$Ru(bpypyr)_3^{2+}$.
Binding energies in eV.

The $Ru_{3d_{5/2}}$ signal is a single sharp peak (FWHM=1.6eV) centred at 280.9eV, the same binding energy as the monomer. The narrow peak width is consistent with a film in which ruthenium(11) is present in a low spin d^6 configuration. This indicates that the ruthenium trisbipyridyl molecular structure is retained in the polymer film.

The deposits were prepared from $Ru(bpypyr)_3^{2+}$-$2PF_6^-$ and $Ru(bpypyr)_2(bpy)^{2+}2BF_4^-$ but no F_{1s} signal was detected in either film. Large Cl_{2p} signals with binding energies consistent with the perchlorate anion were found for both films. Oxygen was detected and in each case the oxygen to chlorine stoichiometry was 4.4 in reasonable agreement with the expected value for the perchlorate anion. For poly-$Ru(bpypyr)_3^{2+}$ the N/Cl stoichiometry was 3.2. If the polymer was undoped a N/Cl stoichiometry of 4.5 would be expected. The experimental N/Cl stoichiometry is equivalent to a polypyrrole chain oxidation level of 27%, or approximately one positive charge for each monomeric unit. The binding energy and peak width of the $Ru_{3d_{5/2}}$ signal preclude the possibility that this positive charge is associated with the metal. For poly-$Ru(bpypyr)_2(bpy)^{2+}$ the N/Cl stoichiometry was 2.7. For an undoped film a value of 4.0 would be expected. The experimental stoichiometry is equivalent to a polypyrrole chain doping level of 48%, or approximately one positive charge for each monomer in the film. The consistency of oxidation level in number of monomer units rather than percentage doping of the polypyrrole chain is surprising and requires further investigation.

Only the $^{5}/2$ component of the Ru_{3d} spin-orbit doublet is seen in Figure 3.4.2, the $^{3}/2$ component is hidden by the C_{1s} signal. For ruthenium the 3d core level is the most suitable to study since it gives the most intense signal under the experimental conditions used. The proximity of the C_{1s} signal make quantitative determinations for ruthenium inaccurate and so it is not possible to confirm the polymer doping level from the $Ru_{3d_{5/2}}$ to Cl_{2p} peak area ratios.

The C_{1s} and N_{1s} spectra are similar to those observed for poly-$Fe(bpypyr)_3^{2+}$. A shake-up satellite may be seen in the expanded C_{1s} spectrum but the signal to noise ratio is insufficiently good to discern any such feature in the N_{1s} spectrum. For both polymers a C/N stoichiometry slightly greater than that of the monomer was found. This is again probably due to extraneous hydrocarbon. The contribution of the $Ru_{3d_{5/2}}$ signal to the C_{1s} envelope may be considered insignificant.

Samples of two of the ruthenium trisbipyridyl monomers prepared by Cosnier *et al*[14] were donated by these workers for polymerization and ESCA analysis. The monomers provided were $Ru(bpypyr')_3^{2+}2BF_4^-$ and $Ru(bpypyr')_2(bpy)^{2+}2BF_4^-$.

Attempts to electrochemically deposit a film from $Ru(bpypyr')_3^{2+}$ produced only thin coatings, not thick enough to obscure the Pt_{4f} signal from the electrodes on which they were deposited. Much thicker films than this have been reported by Cosnier *et al* and it may only be assumed that some degradation of the monomer had taken place.

Thicker films were obtained with $Ru(bpypyr')_2(bpy)^{2+}$. ESCA spectra obtained for one of these films are similar in appearance to those obtained for poly-$Ru(bpypyr)_3^{2+}$ and poly-$Ru(bpypyr)_2(bpy)^{2+}$. The C_{1s} and $Ru_{3d_{5/2}}$ spectra for poly-$Ru(bpypyr')_2(bpy)^{2+}$ are shown in Figure 3.4.3. The narrow $Ru_{3d_{5/2}}$ peak width (FWHM=1.4eV) and the C_{1s} shake-up satellite confirm that the trisbipyridyl structure is retained in the polymer. The N/Cl stoichiometry was 4.1,

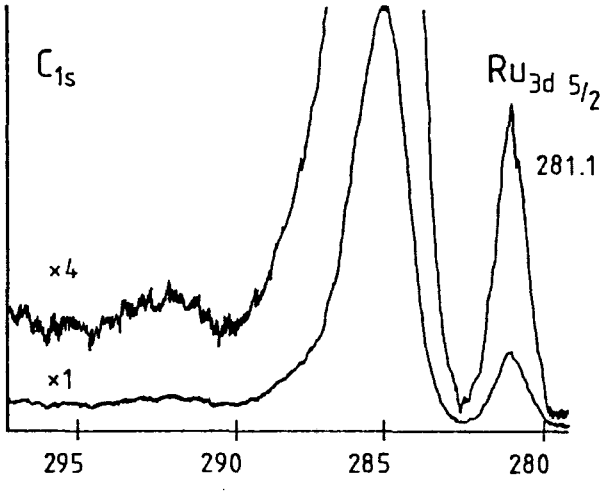

FIGURE 3.4.3 C_{1s} and $Ru_{3d_{5/2}}$ spectra for poly-$Ru(bpypyr')_2(bpy)^{2+}$ (Binding energies in eV)

for an undoped film a value of 4.0 would be expected. No F_{1s} signal was detected but the O/Cl stoichiometry was 6.5, which leaves open the (remote) possibility of some other oxygen containing species acting as dopant anion. Whether the lack of ClO_4^- dopant in the film is an inherent property of poly-$Ru(bpypyr')_2(bpy)^{2+}$ or is a consequence of ageing of

the monomer before film preparation is unclear. It was not possible to deposit films thicker than a few monolayers from this monomer using 0.1M TBAT electrolyte.

3.4.3 Electrochemical studies

3.4.3.1 Stability

Both poly-$Ru(bpypyr)_3^{2+}$ and poly-$Ru(bpypyr)_2(bpy)^{2+}$ are less stable toward electrochemical cycling between the metal +2 and +3 oxidation states than poly-$Fe(bpypyr)_3^{2+}$. For example, 9% of the integrated anodic peak current was lost after cycling a film of poly-$Ru(bpypyr)_2(bpy)^{2+}$ 56 times between -0.2 and +1.55V at 50mV/s. This corresponds to approximately 9 minutes in the Ru(III) state. Cosnier *et al* report an 8% loss in electroactivity for poly-$Ru(bpypyr')_2(bpy)^{2+}$ after 100 cycles at 100mV/s, corresponding to approximately 14 minutes in the oxidized state.[14] Oxidative stabilities both superior[7] and inferior[16] to these have been reported for other electro deposited ruthenium bipyridyl and pyridyl complexes.

No extensive study of the effect of ageing on the electrochemistry of the ruthenium containing films was conducted. It was observed, however, that for a film of poly-$Ru(bpypyr)_3^{2+}$ *ca.* 11% of the electroactivity was lost after 13 days' storage in air. The CV peak splitting and peak width were unchanged by this storage.

Both poly-$Ru(bpypyr)_3^{2+}$ and poly-$Ru(bpypyr)_2(bpy)^{2+}$ are unstable toward potential cycling between OV and -1.7V. Their behaviour is similar to that of poly-$Fe(bpypyr)_3^{2+}$ (see Figure 3.3.7) and leads to rapid degrad-

ation of Ru(II)/Ru(III) electroactivity.

3.4.3.2 Cyclic voltammetry

The CV response of films of poly-$Ru(bpypyr)_3^{2+}$ (Γ_{app} = 3.7x10^{-9}mol cm^{-2}) and poly-$Ru(bpypyr)_2(bpy)^{2+}$ (Γ_{app} = 3.8x10^{-9}mol cm^{-2}) was tested as a function of sweep rate in monomer free solution. Fig. 3.4.4 shows plots of peak anodic current against potential sweep rate. For both films the plots are linear up to a sweep rate of approximately 300mV/s. This behaviour is comparable to that for the thinnest film of poly-$Fe(bpypyr)_3^{2+}$ tested (Γ_{app} = 4.0x10^{-9}mol cm^{-2}, see Figure 3.3.8) and suggests that the magnitudes of the charge transfer diffusion coefficients, D, for all three polymers are similar. A value of D of ca. 5 x 10^{-10}cm^{2}s^{-1} for the ruthenium polymers might suggest that they should show similar photosensitization properties on n-SnO_2 photoanodes to that reported for $Ru(bpy)_3^{2+}$ incorporated in Nafion[8] (see Section 3.1).

Table 3.4.2 shows the variation in peak splitting and peak width with sweep rate for the films used to obtain the plots shown in Figure 3.4.4.

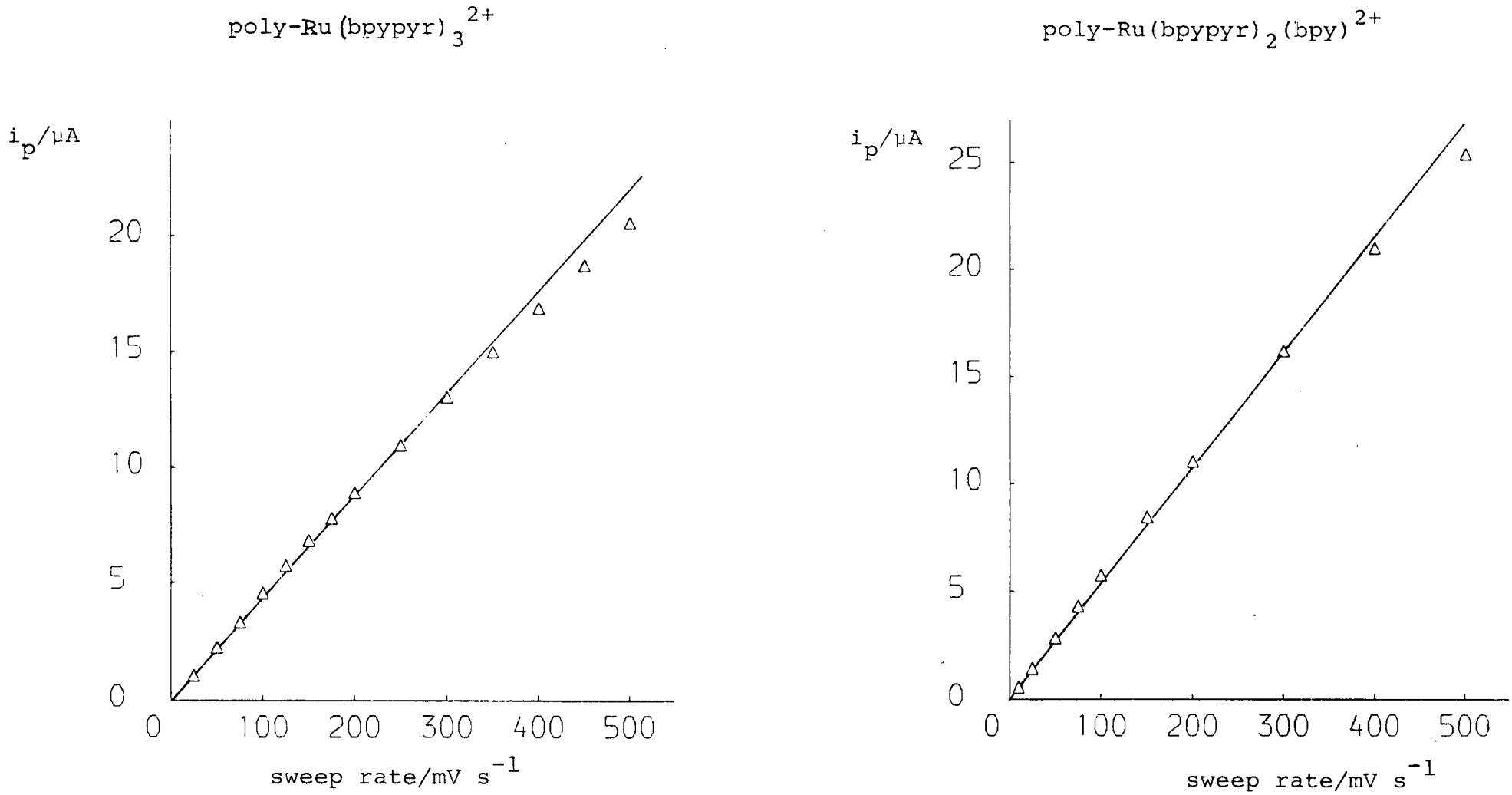

FIGURE 3.4.4 Plots of CV peak current *versus* sweep rate

TABLE 3.4.2 Variation of CV parameters with potential sweep rate for films of poly-$Ru(bpypyr)_3^{2+}$ and poly-$Ru(bpypyr)_2(bpy)^{2+}$

a. poly-$Ru(bpypyr)_3^{2+}$ ($\Gamma = 3.7 \times 10^{-9}$ mol cm^{-2})

sweep rate/ mVs^{-1}	peak splitting/ mV	anodic peak FWHM/mV
25	25	160
50	30	170
100	30	170
200	30	170
400	30	185

b. poly-$Ru(bpypyr)_2(bpy)^{2+}$ ($\Gamma = 3.8 \times 10^{-9}$ mol cm^{-2})

25	20	130
50	20	140
100	30	140
200	30	140
400	30	150

3.5 Copper complex

Copper (11) bisbipyridyl complexes ($Cu(bpy)_2^{2+}$) have reduction potentials of *ca.* OV for the Cu(11)/Cu(111) transformation. This redox reaction is accompanied by a green (Cu(11))/yellow colour change and has been exploited in the preparation of electrochromic devices.[29] There have been no reports of electrode modification by the electropolymerization of substituted $Cu(bpy)_2^{2+}$ complexes.

Attempts to electropolymerize $Cu(bpypyr)_2^{2+}$, either by CV from O to +1.6V or by CPE at +1.6V, were unsuccessful. No film was visible following electrolysis. ESCA showed that a thin, copper containing film was deposited but that its thickness was less than 50Å.

The reason for the failure of $Cu(bpypyr)_2^{2+}$ to form electrode deposits of similar thickness to those obtained with the iron and ruthenium complexes probably lies in the growth mechanism. If the growing film does not possess electronic conductivity then redox conductivity is required for sustained film growth. For the iron and ruthenium complexes the Fe(111) and Ru(111) oxidation states are capable of inducing polymerization at the film/solution interface by oxidation of the pyrrole function. For a poly-$Cu(bpypyr)_2^{2+}$ film to grow *via* a redox conductivity mechanism the Cu(111) state must be formed and be capable of oxidizing the pyrrole function of the monomer. Although Cu(111) has been characterized for some bisdiamine complexes of copper,[30] no reversible oxidation wave which could be attributed to Cu(11)/Cu(111) was observed in a cyclic voltammogram of $Cu(bpypyr)_2^{2+}$. The inability of $Cu(bpypyr)_2^{2+}$ to sustain film growth supports a

redox conductivity mechanism for film growth from the iron and ruthenium complexes. Moreover, the free ligand, bpypyr, does not form films thicker than a few nanometres upon electro-oxidation, although an irreversible oxidation peak at *ca.* +1.5V is observed in a cyclic voltammogram. This result further supports the postulation that redox conductivity is required for sustained film grown. It is noted, however, that Bidan *et al* have reported successful film growth from the electrooxidation of 1-methyl-1´-(3-pyrrolyl-1-propyl)-4,4´-bipyridinium tetrafluoroborate for which it is not possible to postulate a redox conductivity growth mechanism.[31] It is possible (see Section 3.3.2.5) that diffusion of monomer to the growing film/electrode interface is of some importance in film growth.

3.6 Conclusions

The successful electropolymerization of pyrrole substituted iron (11) and ruthenium (11) trisbipyridyl complexes to form electroactive films has been achieved. The iron containing polymer, in particular, shows a high degree of stability to Fe(11)/Fe(111) redox cycling and is reasonably stable to storage in air over a period of months. The iron complex, and probably the ruthenium complexes, have charge transfer diffusion coefficients similar to those previously reported for reductively electropolymerized films based on ruthenium trisbipyridyl. It has been unambiguously demonstrated that poly-$Fe(bpypyr)_3^{2+}$ films possess redox conductivity and it is likely that redox conductivity is the mechanism for sustained film growth of all the successfully deposited films.

3.7 Experimental

3.7.1 Monomer synthesis

Reactions were carried out under a dry argon atmosphere. Commercial solvents were distilled from an appropriate drying agent prior to use. Proton n.m.r. spectra were recorded on a Bruker WH360 (360MHz) or a Bruker WP200 (200MHz), chemical shifts are given in p.p.m. relative to $SiMe_4$ at 0 p.p.m. Mass spectra were recorded on a VG 7070E spectrometer.

3.7.1.1 Ligand synthesis

5-Bromomethyl-2-2´-bipyridine

Freshly recrystallized N-bromosaccinimide (1.96g, 11mmol) and azabisisobutyronitrile (50mg) were added to a solution of 5-methyl-2,2´-bipyridine[32] (1.7g, 10mmol) in dry tetrachloromethane (100ml) and the solution refluxed for 10 hours. The course of the reaction was monitored by ^1H n.m.r., following the disappearance of the methyl singlet at 2.4 p.p.m. and the growth of the CH_2-Br singlet at 4.46 p.p.m. After cooling to 0^oC the solution was filtered and the solvent removed under reduced pressure to yield a pale yellow oil (m/e: 250/248 (M^+), 169 (M^+-Br), 141,117) which was used directly in the next step.

5-(N-pyrrolylmethyl)-2,2´-bipyridine

Aqueous sodium hydroxide solution (50%, 10ml), tetra-n-hexylammonium bromide (50mg) and pyrrole (670mg, 10mmol) were added sequentially to a solution of 5-bromomethyl-2,2´-bipyridine (2.48g, 10mmol) in dichloro-

methane (20ml).[33] The mixture was stirred at 35°C for 8 hours, then poured into water (30ml) and extracted with water (3x20ml). After removal of solvent under reduced pressure the residue was chromatographed on neutral alumina (activity II-III, elute with toluene) to yield a colourless solid, which was washed with cold hexane (3x5ml) and dried *in vacuo*, (1.57g, 67%), mp 87-88°C. M/e (NH_3 chemical ionization): 236 (M^++1), 235, 170, 169. δ_H ($CDCl_3$) 8.68 (1H, mult, H-6′), 8.50 (1H, broad d, J 1.8Hz, H-6), 8.37 (1H, d, J 8.1Hz, H-4), 8.35 (1H, d, J 7.8Hz, H-3′), 7.81 (1H, td, J 7.8, 1.8 Hz, H-4′), 7.53 (1H, dd, J 8.2, 2.3Hz, H-3), 7.31 (1h, td, H-5′), 6.72 (2H, dd, pyrrole Hα), 6.22 (2H, dd, pyrrole Hβ), 5.15 (2H, **S**, CH_2), (see Figure 3.7.1a). Elemental analysis, found C 76.3, H 5.61, N 17.7%. $C_{15}H_3N_3$ requires C 76.6, H 5.53, N 17.9%.

3.7.1.2 Complex syntheses

The iron complex was prepared according to the literature procedure,[34] and the ruthenium complexes were prepared from $Ru(bpy)_2Cl_2.2H_2O$,[35] $Ru(bpy)Cl_4$ [36] or $RuCl_3.3H_2O$ according to established methods.[37,38] The following abbreviations are used: bpy = 2,2′-bipyridine; bpypyr = 5-(N-pyrrolylmethyl)-2,2′-bipyridine.

(a) $Fe(bpypyr)_3^{2+}2BF_4^-$

Sodium tetrafluoroborate (0.3g) and 5-(N-pyrrolylmethyl)-2,2′-bipyridine (175mg, 0.74mmol) were added to a solution of ferrous sulphate (0.2g) in water (100ml). The mixture was refluxed for 2 hours and allowed to cool to yield red crystals of the tetrafluoroborate salt, which were collected

by filtration, washed with cold water and dried *in vacuo*, (194mg, 80%).

Two diastereoisomers, *mer* and *fac* (see Figure 3.7.3),[40] each of which is chiral exist for $Fe(bpypyr)_3^{2+}$. Separate ^1H n.m.r. signals for the two diastereoisomers are expected and are observed at the pyrrole H_β, pyrrole H_α and bpypyr H-6 resonances. The *fac* isomer has C_3 symmetry and any position on one ligand is related to an identical position on the others by 120° rotations. Accordingly one signal is seen for all homotopic protons. The *mer* isomer has no symmetry and separate resonances are seen for each of the three ligands at pyrrole H_α, pyrrole H_β and bpypyr H-6 (Figure 3.7.1). M/e (fast atom bombardment, thiodiethanol matrix) 848 (M^+-BF_4), 761 (M^+-2BF_4) (see Figure 3.7.2). δ_H ($(CF_3)_2CO$) 8.75-8.60 (6H, mult., arom. CH), 8.18 (3H, mult., arom. CH), 6.88, 6.81 6.69, 6.64 (3H, S+S+S+S, H-6), 6.56, 6.52, 6.50, 6.48 (6H, dd+dd+dd+dd, pyrrole H_α), 6.01, 5.99, 5.95, 5.92 (6H, dd+dd+ dd+dd, pyrrole H_β), 5.25-5.13 (6H, mult., CH_2), see Figure3.8.1b). The relative ratio of diastereoisomers (see Figure 3.7.3) determined from integration of the signals due to H-6 and the pyrrole α and β protons is 1.8:1, *mer*:*fac*. Elemental analysis, found C, 55.8, H, 4.2, N, 12.6%. $B_2C_{45}H_{39}F_8FeN_9 \cdot 2H_2O$ requires C, 55.6; H, 4.43; N. 13.0%.

(b) $Ru(bpypyr)_3^{2+}2PF_6^-$

5-(N-pyrrolylmethyl)-2,2 -bipyridine (350mg, 1.49mmol) was added to a solution of ruthenium trichloride (111 mg, 0.42 mmol) and the solution refluxed for 45 hours in the dark when only one visible absorption band at *ca.* 450nm was discerned. The cooled solution was added dropwise with stirring to a solution of ammonium hexafluorophosphate (0.3g) in water (20ml) to yield an orange-brown precipitate. This was repeatedly washed with water and centrifuged and finally

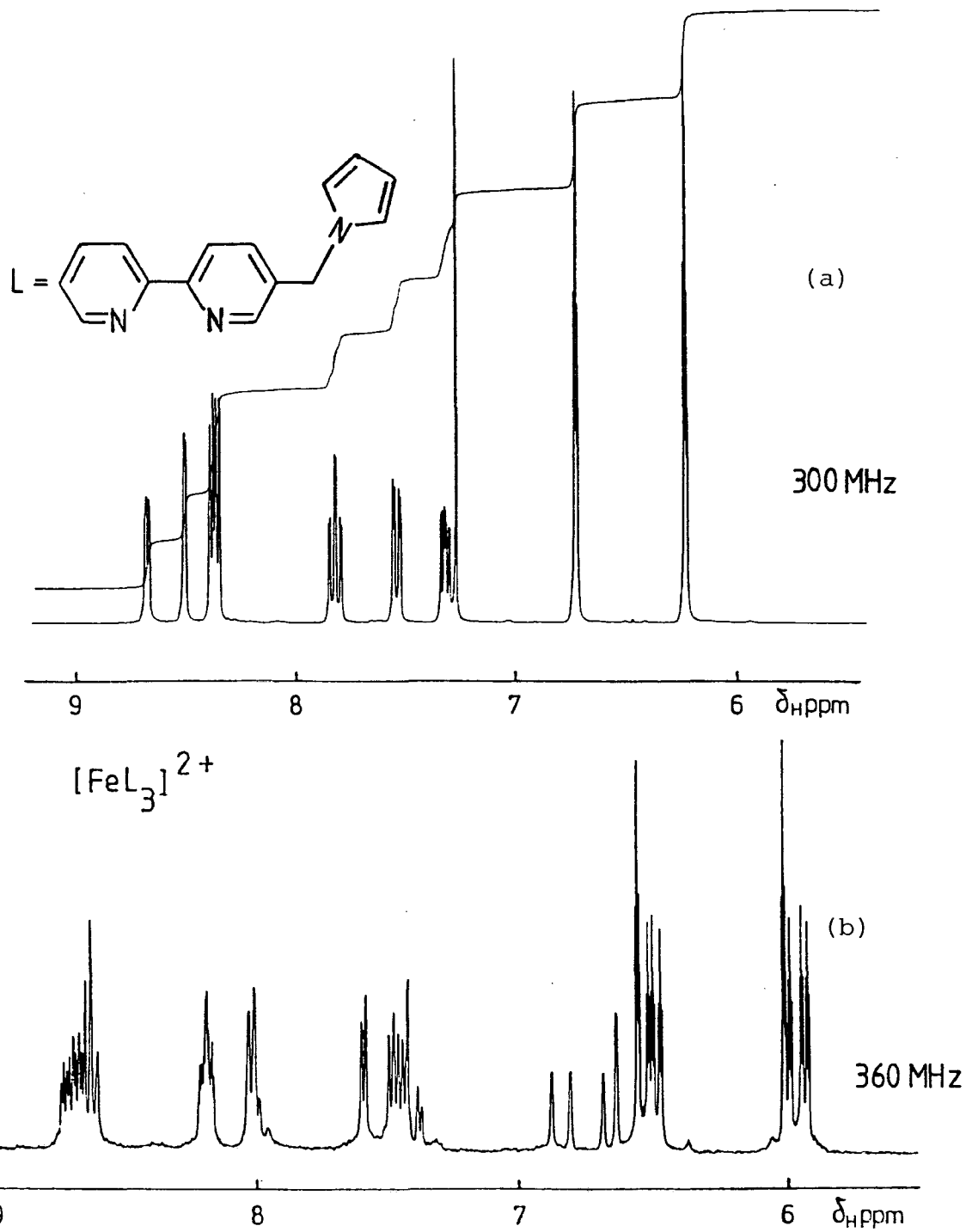

FIGURE 3.7.1a ^{1}H n.m.r. spectrum of bpypyr.

FIGURE 3.7.1b ^{1}H n.m.r. spectrum of $Fe(bpypyr)_3^{2+}2BF_4^-$

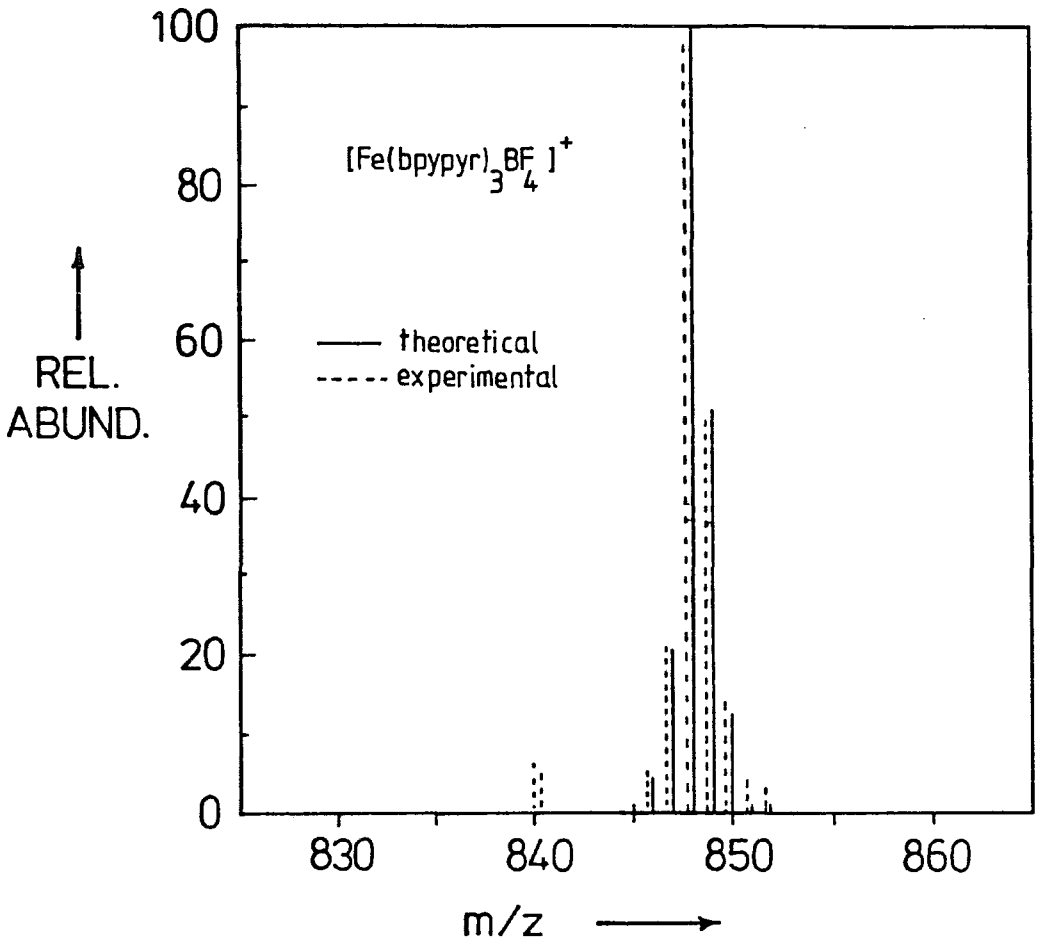

FIGURE 3.7.2 Mass Spectrum.

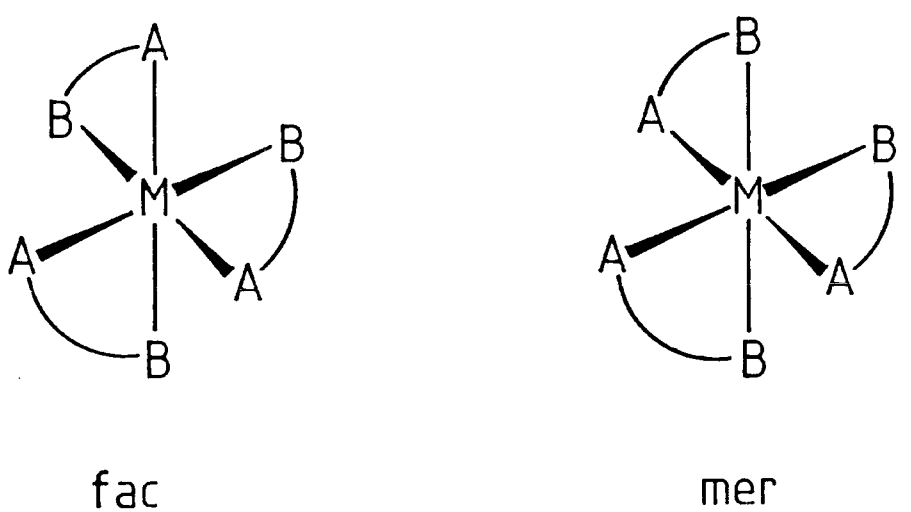

FIGURE 3.7.3 Diasterioisomers for an octahedral species $M(AB)_3$ where AB is an unsymmetrical bidentate ligand.

dried *in vacuo* (375mg, 81%). M/e (fast atom bombardment, thiodiethanol matrix) 952 (M^+-PF_6), 807 (M^+-2PF_6), δ_H ($(CD_3)_2CO$) 8.74-8.66 (6H, mult., arom. CH), 8.22-8.16 (3H, mult., arom. CH), 8.13-7.75 (6H, mult., arom. CH), 7.52-7.45 (3H, mult., arom. CH), 7.18, 7.03, 6.95, 6.75 (3H, S+S+S+S, H-6), 6.56, 6.52, 6.51, 6.48 (6H, dd+dd+dd+dd, pyrrole H_α), 6.02, 5.98, 5.94, 5.92 (6H, dd+dd+dd+dd, pyrrole H), 6.02, 5.98, 5.94, 5.92 (6H, dd+dd+dd+dd, pyrrole H_β), 5.24-5.17 (6H, mult., CH_2). The relative ratio if diastereoisomers determined as for $Fe(bpypyr)_3^{2+}$ is 3:1, *mer*:*fac*.

Elemental analysis, found C, 48.1, H, 3.93, N, 11.1%. $C_{45}H_{39}F_{12}N_9P_2$ Ru.$3H_2O$ requires C, 48.4, H, 3.66, N,11.3%.

(c) $Ru(bpypyr)_2(bpy)^{2+}2BF_4^-$

5-(N-pyrrolmethyl)-2,2´-bipyridine (90mg, 0.38mmol) was added to a solution of tetrachlororuthenium-2,2´-bipyridyl (40mg, 0.1mmol) in isopropanol (5ml) and the mixture refluxed for 6 hours in the dark. After removal of solvent under reduced pressure, the residue was dissolved in water (10ml), filtered and added to a solution of sodium tetrafluoroborate (0.3g) in water (5ml) to give an orange precipitate. This was redissolved in the minimum amount of dichloromethane (*ca.* 2ml) and added dropwise with stirring to dry ether (20ml). The orange precipitate was filtered off washed with ether (2x3ml) and dried *in vacuo* (58g, 65%). Three diastereoisomers,[40] each of which is chiral, exist for $Ru(bpypyr)_2(bpy)^{2+}$. None of the diastereoisomers possesses any symmetry element and separate signals are expected for the two bpypyr ligands in each isomer. This was observed at the pyrrole H_α and pyrrole H_β resonances. M/e (fast atom bombardment, thiodi-

ethanol matrix) 902 (M^+), 815, 728. δ_H ($CDCl_3$) 8.4-6.9 (22H, mult., arom. CH), 6.58-6.45 (4H, 6xdd, pyrrole H_α) 6.06-5.93 (4H, 6xdd, pyrrole H_β), 5.15-5.05 (4H, mult., CH_2). Elemental analysis, found C, 50.5, H, 4.31, N, 11.6%. $B_2C_{40}H_{34}F_8N_8$ Ru.$2H_2O$ requires C, 50.9, H, 4.03, N, 11.9%.

(d) $Ru(bpypyr)(bpy)_2^{2+}2ClO_4^-$

5-(N-pyrrolylmethyl)-2,2´-bipyridine (118mg, 0.5mmol) was added to a solution of $Ru(bpy)_2Cl_2.2H_2O$ [35] (260mg, 0.5mmol) in ethanol (5ml) and the mixture refluxed in the dark for 20 hours. After evaporating to dryness, the residue was redissolved in water (10ml) and a solution of lithium perchlorate (0.3g) in water (3ml) was slowly added to yield an orange precipitate. This was redissolved in dry acetone (3ml) and added dropwise onto ether (25ml) to give an orange precipitate which was dried *in vacuo* (330mg, 78%). M/e (fast atom bombardment, thiodiethanol matrix) 748 (M^+-ClO_4), 649.

δ_H ($(CD_3)_2CO$) 8.82-8.73 (6H, mult., arom. CH), 8.18 (5H, mult., arom. CH), 8.1-7.8 (6H, mult., arom. CH), 7.6 (5H, mult., arom. CH) 7.23 (1H, br.s., bpypyr H-6), 6.54 (2H, dd, pyrrole H_α), 5.04 (2H, dd, pyrrole H_β), 5.22 (2H, dd, CH_2). Elemental analysis, found: C, 48.6, H, 3.81, N, 11.6%. $C_{35}H_{29}Cl_2N_7O_8Ru.H_2O$ requires C, 48.3, H, 3.56, N, 11.2%.

(e) $Cu(bpypyr)_2^{2+}2ClO_4^-$ [39]

5-(N-pyrrolylmethyl)-2,2´-bipyridine (118mg, 0.5mmol) was added to a hot solution of copper(II) perchlorate (90mg, 0.24mmol) in ethyl acetate (15ml) and the solution heated at

60°C for 30 mins. A green-blue precipitate formed which was filtered and recrystallized from hot ethanol to give a green microcrystalline solid (311mg, 85%). M/e (fast atom bombardment, thiodiglycol) 634/632 (M^+-ClO_4), 535/533. Elemental analysis, found C, 48.9, H, 3.5, N, 11.1%. $C_{30}H_{26}Cl_2CuN_6O_8$ requires C, 49.1, H, 3.82, N, 11.5%

3.7.2 Electrochemical polymerization and analysis of modified electrodes

Electrode preparations, film depositions (by CV or CPE at +1.3V) and electrochemical experiments on modified electrodes were performed as described in Chapter Two. Unless otherwise stated all electrochemical experiments were carried out in dried, argon purged acetonitrile which was 0.1M in TBAP. Film depositions were performed from solutions which were *ca.* $2x10^{-3}$M in the relevant monomer.

For chronoamperometry experiments the Thomson Ministat 251 potentiostat was used to apply a 0 to +1.6V potential jump to the modified electrode. The current response was measured using a small resistance in series with the cell. An analog instrumentation amplifier was used to provide a differential voltage input to a Tektronix 5115 storage oscilloscope on which the transient response was displayed.

ESCA spectra and conductivity measurements were recorded as described in Chapter Two. ESCA spectra of monomers were obtained from samples evaporated onto cleaned gold from acetone solution.

Visible absorption spectra were recorded on a Pye-Unicam SP 8-100 spectrophotometer.

REFERENCES for Chapter Three

1. N. Tokel-Takvoryan, R. Hemingway and A.J. Bard, J.Am.Chem.Soc., 95, (1973), 6582.

2. T. Saji and S. Aoyagui, J.Electroanal.Chem., 58, (1975), 401.

3. K. Rajeshwar, P. Singh and J. DuBow, Electrochimica Acta, 23, (1978), 1117.

4. J. Desilvestro, M. Gratzel, L. Kavan, J. Moser and J. Augustynski, J.Am.Chem.Soc., 107, (1985), 2988 and references therein.

5. M. Krishnan, X.Zhang and A.J. Bard, J.Am.Chem.Soc., 106, (1984), 7371.

6. H.D. Abruna, P. Denisevich, M. Umana, T.J. Meyer and R.W. Murray, J.Am.Chem.Soc., 103, (1981), 1.

7. P. Denisevich, H.D. Abruna, C.R. Leidner, T.J. Meyer and R.W. Murray, Inorg.Chem., 21, (1982), 2153.

8. C.R. Martin, I. Rubinstein and A.J. Bard, J.Am.Chem.Soc., 104, (1982), 4817.

9. P.J. DeLaive, T.K. Foreman, C. Giannotti and D.G. Whitten, J.Am.Chem.Soc., 102, (1980), 5627.

10. T.K. Foreman, Ph.D. Thesis, Diss.Abstr.International B, 43, (1982), 132.

11. C. Creutz, M. Chou, T. Netzel, M. Ohumura and N.Sutin, J.Am.Chem.Soc., 102, (1980), 1309.

12. A.G. Motten, K. Hanck and M.K. DeArmond, Chem.Phys.Letts., 79, (1981), 541.

13. G. Bidan, A. Deronzier and J-C Moutet, Nouv J. de Chimie, 8, (1984), 501.

14. S. Cosnier, A. Deronzier and J-C Moutet, J.Electroanal. Chem., submitted 1985.

15. R. Erlandsson, O. Inganas, I. Lundstrom and W.R. Salaneck, Synthetic Metals, 10, (1985), 303.

16. J.M. Calvert, D.L. Peebles and R.J. Nowak, Inorg.Chem., 24, (1985), 3111.

17. R.W. Murray, Chapter 3 in "Electroanalytical Chemistry", Vol.13, Ed. A.J.Bard, Dekker, New York, (1984).

18. P.K. Ghosh and A.J. Bard, J.Electroanal.Chem., 169,(1984),113.

19. Southampton electrochemistry group, "Instrumental Methods in Electrochemistry", Ellis Horwood, Chichester, (1985).

20. Ref. 17, p.235.

21. E. Laviron, J.Electroanal.Chem., 112, (1980), 1.

22. a. P. Daum, J.R. Lenhard, D. Rolison and R.W. Murray, J.Am.Chem.Soc., 102, (1980), 4649.

b. P. Daum and R.W. Murray, J.Phys.Chem. 85, (1981), 389.

23. W.J. Albery, M.G. Boutelle, P.J. Colby and A.R. Hillman, J.Electroanal.Chem., 133, (1982), 135.

24. W.J. Albery and A.R. Hillman, Royal Society of Chemistry Annual Reports C, (1981), 377.

25. P.G. Pickup, W. Kutner, C.R. Leidner and R.W. Murray, J.Am.Chem.Soc., 106, (1984), 1991.

26. a. C.D. Ellis, W.R. Murphy and T.J. Meyer, J.Am.Chem.Soc. 103, (1981), 7480.

b. T. Ikeda, R. Schmehl, P. Denisevich, K.Willman and R.W. Murray, J.Am.Chem.Soc., 104, (1982), 2683.

27. H. Nishihara and K. Aramaki, J.Chem.Soc.Chem.Commun., (1985), 709, Fig. 2b.

28. A.F. Diaz, J. Castillo, K.K. Kanazawa, J.A.Logan, M.Salmon, and O. Fajardo, J.Electroanal.Chem., 133, (1982), 233.

29. Chemical Abstracts, 100:129946a, (1984), Patent.

30. P. Stevens, J.M. Waldeck, J. Strohl and R. Nakon, J.Am. Chem.Soc., 100, (1978), 3632.

31. G. Bidan, A. Deronzier and J-C Moutet, J.Chem.Soc.Chem. Commun., (1984), 1185.

32. T.L.J. Huang and D.G. Brewer, Can.J.Chem., 59, (1981), 1689.

33. N-C Wang, K-E Teo and H.J. Anderson, Can.J.Chem.,55,(1977),4112.

34. F.H. Burstall and R.S. Nyholm, J.Chem.Soc.,(1952), 3570.

35. B.P.Sullivan, D.J. Salmon and T.J. Meyer, Inorg.Chem., 17, (1978), 3334.

36. R.A.Krause, Inorg.Chim.Acta., 22, (1977), 209.

37. J.M. Calvert, R.H. Schehl, B.P. Sullivan, J.S. Facci, T.J. Meyer and R.W. Murray, Inorg.Chem., 22, (1983), 2151.

38. J.N. Braddock and T.J.Meyer, J.Am.Chem.Soc., 95, (1983), 3158.

39. J.R. Hall, M.R. Litzow and R.A. Plowman,Aust.J.Chem., 18, (1965), 1331.

40. K.F. Purcell and J.C. Kotz, "Inorganic Chemistry", Chapter 11, Saunders, Philadelphia (U.S.A.), (1977).

CHAPTER FOUR

SURFACE CHEMISTRY, ELECTROACTIVITY AND STABILITY OF MOFIFIED ELECTRODES PREPARED BY PLASMA POLYMERIZATION (PP) OF FERROCENE AND SUBSTITUTED FERROCENES

4.1 Introduction

In 1963 Bradley and Hammes demonstrated that vinylferrocene was efficiently polymerized in an electroded, audio-frequency (10-50kHz) plasma, with a deposition rate per unit of electrical energy input approximately twice that of styrene.[1] In 1978 Murray *et al* found that vinylferrocene formed thin, insoluble films when a charge of the monomer was placed close to a substrate in an externally coupled, radio-frequency (r.f.) argon plasma.[2] The films obtained by this deposition process, hereafter called 'argon plasma polymerization' or 'argon PP' for brevity†, were electrochemically active, showing ferrocene-like cyclic voltammetry (CV) similar to coatings of conventionally polymerized vinylferrocene. Subsequently, Dautartas *et al* demonstrated that the deposit formed from a r.f. plasma of neat vinylferrocene vapour ('neat PP') also displayed ferrocene-like electroactivity.[4,5] Several reports describing the surface chemistry and electrochemistry of argon plasma polymerized vinylferrocene have since appeared.[6-16] ESCA has been used to confirm that the deposits formed by both PP methods contain iron in a ferrocene environment along with a variable amount (usually 10-40%) of iron(III).[4a,5,8,12,16] This information, together with the fact that the films contained more oxygen than iron,[4a,7] led to the conclusion that the films were not identical to conventionally polymerized vinylferrocene.

---

† The term argon PP should not be confused with argon-induced PP, which is a means of initiating polymerization of vinyl monomers in solution to yield, after a period of hours or days following termination of the plasma, ultra-high molecular weight polymers.[3]

The chemical environment of the oxygen was not defined, however it was concluded that oxygen was not directly or α-bonded to the carbon atoms of an unfragmented ferrocene nucleus since the oxidation potentials of the films, in acetonitrile, were typical of ferrocene and not oxygen functionalized ferrocenes.[4a,7]

No comparison of the surface and electrochemistries of deposits formed from vinylferrocene by the two plasma methods has been reported. Moreover, since PP is a generally applicable technique, it is perhaps surprising that no ferrocene monomer other than vinylferrocene has been reported to produce an electroactive film upon PP.

Described below is a comparative study of the deposits produced, by both Ar and neat PP, from five ferrocene monomers including vinylferrocene. The ability of a monomer to retain a proportion of intact ferrocene units upon PP was semiquantitatively monitored using ESCA. The electrochemical response of the deposits and its persistence were tested by CV of coated electrodes. The results obtained are compared to those previously obtained for vinylferrocene.

4.2 Results and Discussion

4.2.1 Introduction

The plasma deposits, produced by both methods of PP described above, obtained from five monomers, *viz.* ferrocene (CpHFeCpH, Cp = C_5H_4), vinylferrocene ($CpHFeCpCH{=}CH_2$), dimethylaminomethylferrocene (DMAMF, ($CpHFeCpCH_2N(CH_3)_2$),

ferrocenecarboxaldehyde (FCA, CpHFeCpCHO) and benzoylferrocene (BF, $CpHFeCpCOC_6H_5$), were studied. It was found that neat PP produced thin films (interference pattern in visible light) over several tens of cm^2 whereas Ar PP produced thicker films (estimated thickness $\leq 10^{-6}$m) confined to a few cm^2 close to the monomer charge. For BF no polymer was deposited using the Ar plasma method, this is perhaps a consequence of the lower volatility of this monomer.

4.2.2 ESCA Analysis

(a) Ferrocene Monomer

Ferrocene has been studied by ESCA previously[25,26] but was reinvestigated in order to rule out complications in comparing monomer and plasma polymer spectra which might otherwise arise from variation of instrumental parameters (*e.g.* spectral resolution and energy scale calibration, see Appendix).

Figure 4.2.1 shows the C_{1s} and Fe_{2p} spectra of ferrocene condensed onto clean gold at -125°C in high vacuum. The $Fe_{2p_{3/2}}$ signal is a single sharp peak (FWHM= 1.5eV) at 708.5eV relative to the C_{1s} signal arbitrarily set at 285.0eV.† The C_{1s}-$Fe_{2p_{3/2}}$ peak separation of 423.5eV compares well with the values of 423.2eV, reported by Barber *et al* for ferrocene,[25] and 423.4eV, reported by Umana *et al* for vinylferrocene.[8] The $C_{1s}/Fe_{2p_{3/2}}$ peak area ratio gave

† Although the sample was deposited onto gold which was in electrical contact with the spectrometer, the condensed film was thick enough to produce sample charging which made the C_{1s} signal appear at 286.9eV. Values ranging between 284.7[25] and 285.7eV[26] have been reported for the C_{1s} binding energy in ferrocene.

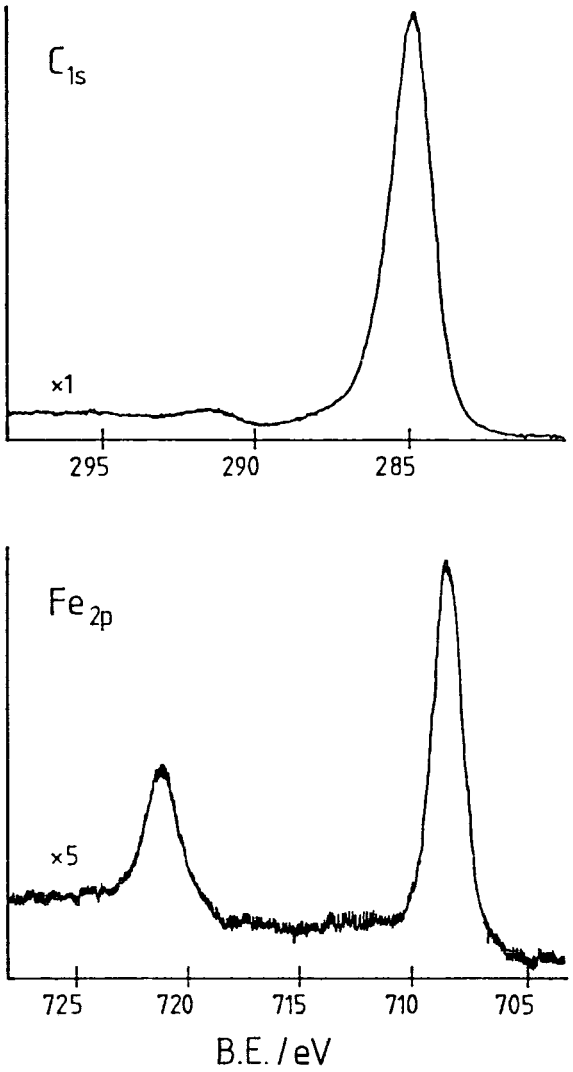

Figure 4.2.1 ESCA Spectra of Monomeric Ferrocene

an apparent C/Fe stoichiometry of 10.7. A steady increase in the $C_{1s}/Fe_{2p_{3/2}}$ peak area ratio was observed on leaving the sample in front of the spectrometer X-ray window over a period of *ca.* 1 hour. This increase arises from high vacuum transfer of hydrocarbon material from the warm window to the cold probe.

A shake-up satellite may be discerned in the C_{1s} spectrum.

Monomeric DMAMF was similarly analyzed by ESCA. $Fe_{2p_{3/2}}$ (FWHM = 1.5eV) and N_{1s} (FWHM = 2.0eV) binding energies of 708.6 and 399.9eV were found.

(b) Plasma polymers

Figure 4.2.2 shows C_{1s} and $Fe_{2p_{3/2}}$ spectra for plasma polymers produced from the five monomers and prepared by both neat and Ar PP. O_{1s} spectra were largely featureless and are not shown. The plasma polymers derived from DMAMF gave small N_{1s} signals centred at *ca.* 400eV; these signals were considerably broader than that for the monomer. This supports the suggestion, drawn from infra-red analysis (*vide infra*), that rearrangement of the N function has taken place.

The ESCA spectra for plasma polymers deposited by both neat and Ar PP are similar, for the same monomer. Table 4.2.1 gives surface elemental stoichiometries and $Fe_{2p_{3/2}}$ binding energies for the plasma polymers including He plasma polymerized vinylferrocene, for which the spectra were qualitatively similar to the Ar plasma deposit. All the plasma deposits contain iron, most of which (50-90%) is usually present in a ferrocene environment. Some Fe(III) is also present. The dominance of ferrocene environment iron over Fe(III) is indicated by the greater integrated signal intensity of the narrow peak at 708.5-709eV compared to the broader peak at higher binding energy. Vinylferrocene is thus not unique in its ability to form a plasma polymer with a significant retention of ferrocene structure. For neat plasma polymerized BF only, the Fe(III) signal is greater than the ferrocene signal.

For all the plasma polymers other than that formed from BF, a reasonable agreement between the monomer and

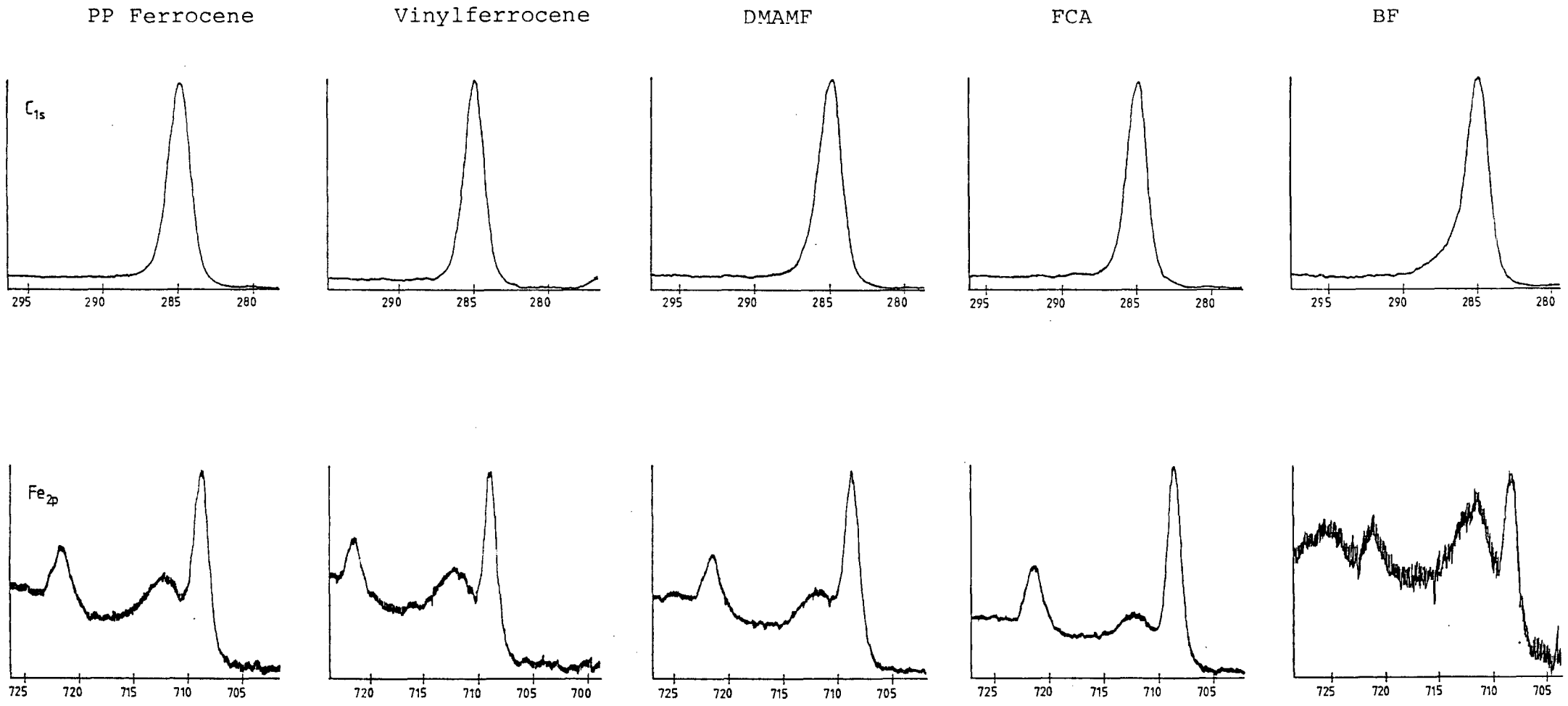

FIGURE 4.2.2 C_{1s} and Fe_{2p} ESCA Spectra for <u>neat</u> plasma polymerized ferrocenes

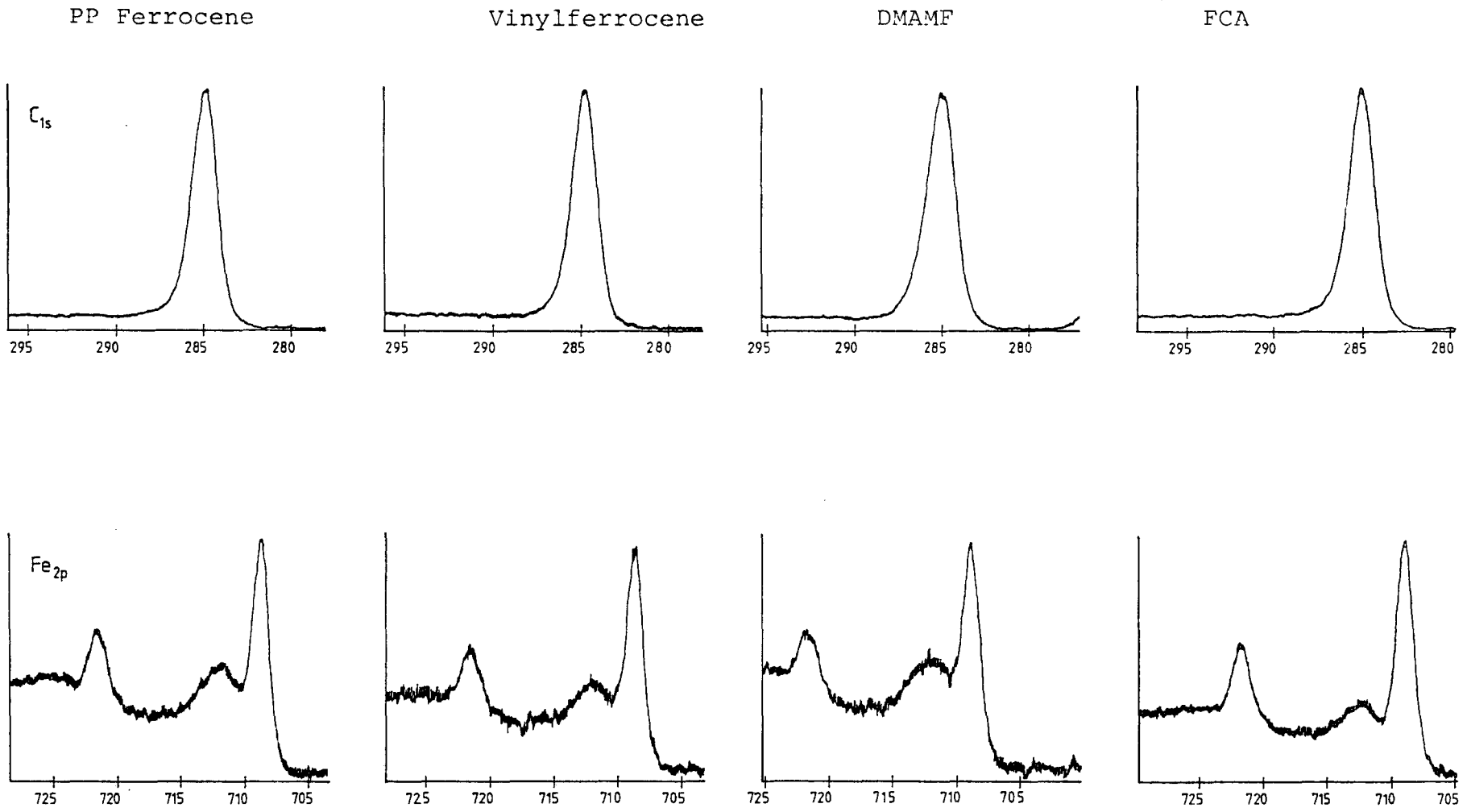

FIGURE 4.2.2 (contd.) C_{1s} and Fe_{2p} ESCA Spectra for Ar plasma polymerized ferrocenes

TABLE 4.2.1 ESCA data for plasma polymers

Monomer	PP method	'Ferrocene' $Fe_{2p_{3/2}}$ binding energy/eV	C:Fe:O(:N) stoichiometry	C_{1s} $\Delta h/h$ [a]
Ferrocene	Neat	708.8	$C_{10.5}FeO_{1.7}$	0.06
"	Ar	708.8	$C_{12.4}FeO_{1.8}$	0.06
Vinylferrocene	Neat	708.9	$C_{13.4}FeO_{1.9}$	0.05
"	Ar	708.9	$C_{14.5}FeO_{1.4}$	0.06
"	He	708.8	$C_{12.4}FeO_{1.7}$	0.06
FCA	Neat	708.7	$C_{10.2}FeO_{2.6}$	0.06
"	Ar	708.9	$C_{12.0}FeO_{1.6}$	0.07
DMAMF	Neat	708.8	$C_{11.5}FeO_{1.6}N_{0.7}$	0.07
"	Ar	709.0	$C_{14.5}FeO_{1.8}N_{1.2}$	0.05
BF	Neat	708.5	$C_{31.6}FeO_{6.1}$	0.06
"	Ar	No polymer	-	-

a. Defined in Chapter Two.

plasma polymer C/Fe stoichiometries is found (see Table 4.2.1). Some hydrocarbon contamination is expected, but this is likely to be less significant than for the electrochemical polymers studied in Chapters Two and Three since the plasma polymers are formed by a vacuum technique and were analyzed immediately after preparation. The Ar plasma deposits contain slightly more carbon than their neat analogues. Since this is the case for deposits formed from all the monomers studied, including ferrocene, this result is not considered to be evidence for greater retention of substituent structure in the Ar deposits. The increased C/Fe stoichiometry for plasma polymerized BF compared to the monomer must be a result of

elimination of the benzoyl (or phenyl) group in the plasma phase followed by independent plasma polymerization of this fragment.

The asymmetric line shape (or step feature) seen in the C_{1s} spectra undoubtedly arises, at least in part from shake-up-like electronic transitions. Values of $^{\Delta h}/_{h}$, defined in Chapter Two, for the C_{1s} spectra are given in Table 4.2.1. The average value of $^{\Delta h}/_{h}$, 0.06, is similar to that found by Hutton[33] for the polycyclic aromatic compound Pyrene ($C_{16}H_{10}$). This asymmetry makes background subtraction somewhat arbitrary and this complicates component analysis of the C_{1s} spectrum. Nevertheless, it is possible to say that all of the plasma polymers, except that derived from BF, contain more oxygen than may be accounted for by oxygen functionalized carbon atoms. It must be concluded, therefore, that some of the oxygen in these deposits is associated with the high binding energy iron.

For plasma polymerized BF component analysis of the C_{1s} spectrum, following linear background subtraction and using Gaussian peaks to represent $-\overset{|}{\underset{|}{C}}-O$ (286.6eV), $\succ C=O$ (287.8eV) and $O-\overset{|}{\underset{|}{C}}=O$ (289eV),[27] is shown in Figure 4.2.3. This analysis indicates that *ca.* 20% of the carbon atoms are bonded to oxygen, an amount large enough to account for all of the oxygen in the film. The component analysis further indicates that most of the oxygen bound to carbon is $-\overset{|}{\underset{|}{C}}-O$ whereas in the monomer the only oxidized carbon function is $\succ C=O$.

The C_{1s} lineshapes for the plasma polymerized FCA deposits are similar to those for plasma polymerized

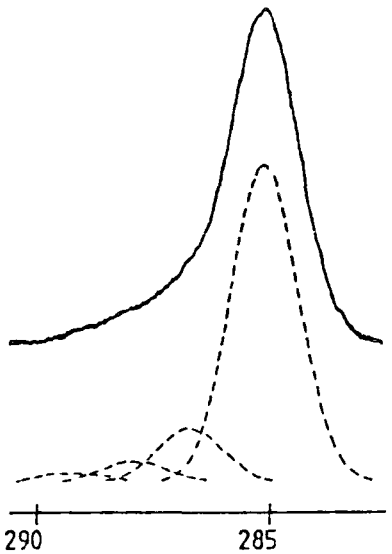

Figure 4.2.3 Curve-fitted C_{1s} spectrum for neat plasma polymerized BF

ferrocene and vinylferrocene, this suggests that the CHO function is eliminated in the plasma phase. Partial elimination of the amine function for plasma polymerized DMAMF is also suggested by the decrease in N/C stoichiometry and increase in the N_{1s} FWHM for the plasma deposits compared to the monomer.

The high binding energy (711-711.5eV, this study) broad (FWHM≈3.0eV, this study) $Fe_{2p_{3/2}}$ peaks have been shown by Murray *et al* to arise in part from ferricenium, for Ar plasma polymerized vinylferrocene.[8] Diminution of these peaks following treatment of the films with a reducing agent was taken as evidence for this.[8]

From the spectral features mentioned above it seems likely that part of the high binding energy $Fe_{2p_{3/2}}$ signal arises from irreversibly oxidized iron for the following reasons.

(1) There is generally more oxygen in the films than may be accounted for by oxygen functionalized carbon atoms. This discrepancy is more pronounced for neat PP than Ar PP.

(2) The chemical shift between the $Fe_{2p_{3/2}}$ signals of ferrocene and ferricenium has been shown by Neuse and Mzimela[36] to be only 1.6-1.8eV compared to a $Fe_{2p_{3/2}}$ peak splitting of 2.6-2.8eV in the spectra shown in Figure 4.2.2.

(3) The binding energy of the broad $Fe_{2p_{3/2}}$ peak (711.0-711.5eV) is not inconsistent with those reported for Fe_2O_3[28,29] and FeOOH.[28]

4.2.3 Infra red spectroscopic analysis

Infra red spectra of 'as deposited' films were recorded for some of the plasma polymers, *viz.* neat plasma polymerized ferrocene, vinylferrocene and DMAMF and Ar plasma polymerized ferrocene, vinylferrocene and FCA. The infra red spectrum of neat plasma polymerized ferrocene, obtained from material scraped from the reactor walls and pressed into a disc with KBr, has been reported by Phadke.[30] This spectrum was of poor quality.[30]

By Ar PP films thick enough to record high quality transmission infra red spectra, by repeated scanning and signal averaging on a microcomputer controlled, conventional double beam infra red spectrometer, could be obtained. Ar plasma polymerized films were deposited onto polished KBr windows. Neat PP did not produce films sufficiently thick

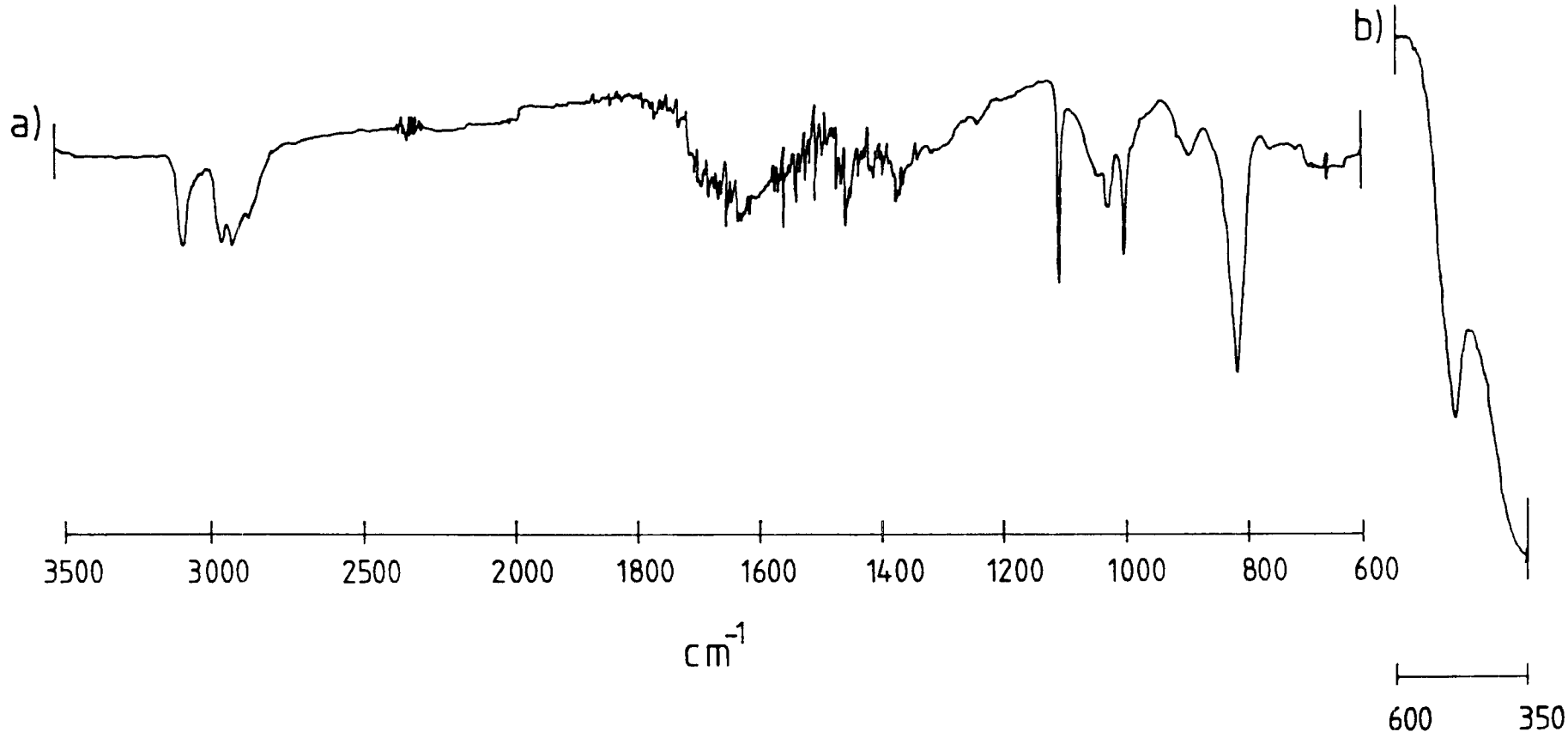

FIGURE 4.2.4 Infrared Spectrum for Ar plasma polymerized vinylferrocene

for transmission infra red studies. Instead films were deposited on cleaned Al foil and Attenuationof Total Reflection (ATR) spectra recorded on a Fourier-transform spectrometer. Some caution should be exercised in comparing the spectra for neat and Ar plasma polymers from the same monomer since different recording techniques and spectrometers were used.

All of the plasma polymers studied showed infra red bands typical of the ferrocene nucleus.[31] Figure 4.2.4 shows the spectrum for Ar plasma polymerized vinylferrocene. Table 4.2.2 lists infra red bands which were found in all the plasma polymers studied, together with the assignments given by Lippincott and Nelson for monomeric ferrocene.[31] The similarity of the deposits obtained from different monomers is emphasized by the infra red spectra of Ar plasma polymerized ferrocene, vinylferrocene and FCA which may almost be superimposed. No carbonyl band at *ca.* 1650 cm^{-1} (the band position for the monomer) was found for the FCA deposit, which supports the ESCA evidence that the CHO function is eliminated in the plasma. For neat plasma polymerized DMAMF bands typical of N-H were observed (3400 cm^{-1}, 1600 cm^{-1})[32] which indicate rearrangement of the tertiary amine function.

TABLE 4.2.2 Infra red band positions and assignments[31] for plasma polymers

position/cm^{-1} ± 5 cm^{-1}	Assignment[31]
480	antisymm. ring-metal stretch
817	CH bending ($\perp$)
1000	CH bending (∥)
1105	antisymm. ring breathing

Expanded plots of the 3400-2700 cm^{-1} region of the infra red spectra of Ar plasma polymerized vinylferrocene and ferrocene and neat plasma polymerized ferrocene are shown in Figure 4.2.5. Both aromatic or 'ferrocene environment' (>3000 cm^{-1}) and aliphatic C-H stretching bands were observed for all the deposits studied. For the plasma polymers derived from ferrocene, aliphatic C-H may arise only from fragmentation of the ferrocene nucleus. Since ESCA shows that for ferrocene the C/Fe ratio of the monomer is approximately retained in the plasma polymer it must be concluded that some of the iron present in the deposit is in neither a ferrocene nor a ferricenium environment. It is likely that non-ferrocene environment iron is also present in the other plasma polymers. The 3400-2700 cm^{-1} region of the infra red spectra is discussed further in Section 4.2.4.1.

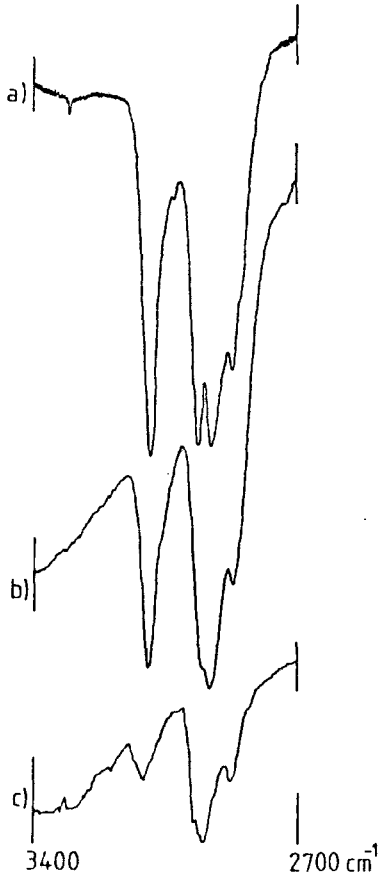

(a) Ar plasma polymerized vinylferrocene

(b) Ar plasma polymerized ferrocene

(c) Neat plasma polymerized ferrocene

FIGURE 4.2.5

4.2.4 Cyclic Voltammetry

4.2.4.1 Redox activity

Table 4.2.3 summarizes single sweep CV behaviour for the electroactive deposits, the associated voltammograms are shown in Figures 4.2.6 and 4.2.8 (Section 4.2.4.2). Although the data in Table 4.2.3 and Figures 4.2.6 and 4.2.8 show that vinylferrocene is not unique in its ability to form a plasma deposit which will display ferrocene-like electroactivity, several of the deposits which were shown by ESCA to contain a significant amount of intact ferrocene were non-electroactive. Deposits listed as non-electroactive in Table 4.2.3 gave CV responses which were smaller than the usual background currents for unmodified electrodes.

TABLE 4.2.3

Monomer	PP Method	Electro-active?	$E^{\ominus}$/V	Approximate Relative PP efficiency[a]
Ferrocene	Neat	No		
"	Ar	Yes	0.43	0.4
Vinylferrocene	Neat	Yes	0.43	
"	Ar	Yes	0.43	1.0
"	He	Yes	0.43	0.04[b]
FCA	Neat	No		
"	Ar	Yes	0.45	1.5
DMAMF	Neat	Yes	0.40	
"	Ar	Yes	0.46	
BF	Neat	No		
"	Ar	No polymer		

a. At 10W power and 0.2 torr inert gas

b. Corrected for flow rate. Flow rate He/flow rate Ar = 1.55.

For ferrocene and FCA electroactive deposits were produced only by Ar PP although ESCA spectra for polymers formed by either method were similar. A possible explanation is that the films deposited by the neat method are more highly cross-linked and thus less permeable, or even impermeable to the electrolyte solution. Tentative evidence to support this proposal may be found in the 3400-2700 cm^{-1} region of the infra-red spectra of neat and Ar plasma polymerized ferrocene (Figure 4.2.5). The ratio of the aromatic (above 3000 cm^{-1}) to aliphatic C-H stretching mode band intensity is greater for the Ar deposit than the neat. Cross-linking at the carbon atoms of an intact ferrocene nucleus would decrease the ratio of aromatic to aliphatic C-H. An increase in ferrocene ring fragmentation would also decrease this ratio, but this seems less likely since the relative amounts of ferrocene and oxidized iron, determined by ESCA, were similar for the Ar and neat plasma polymers. The ESCA evidence is not unequivocal, however, since it is not possible to determine whether or not the oxidized iron signal arises from the same material or proportions of materials in the two deposits. Dong *et al* concluded that film cross linking was the reason that plasma deposits, which they obtained from hydroxy and aceto substituted ferrocenes, were non electroactive.[15] No spectroscopic evidence to show that these deposits contained intact ferrocene was reported.

The electrode potentials for the electroactive plasma polymers are all similar and are comparable to the value determined for ferrocene in solution (+0.42V). The electrode potential for Ar plasma polymerized FCA confirms the conclusion,

drawn from the ESCA and infra-red analyses, that the aldehyde function is eliminated in the plasma phase. An electrode potential of +0.69V was determined for FCA in solution.

Since the flow rate of inert gas may be easily controlled and measured, it is possible to estimate the relative deposition efficiencies for the Ar and He plasma polymers. The relative efficiencies given in Table 4.2.3 were derived from a comparison of first sweep CV peak areas corrected for deposition time and flow rate differences. Since only electroactive material is assessed by CV, any difference in the proportions of active and inactive material between the deposits will give rise to an error in the estimated relative efficiencies. It is also worth pointing out that as film thickness increases less of the active material may be 'sampled' by CV, this may cause a further error to the efficiency values in Table 4.2.3. It is clear, however, that deposition efficiencies for ferrocene, vinylferrocene and FCA are similar but the deposition efficiency for vinylferrocene is reduced by approximately one order of magnitude when the inert gas is changed from Ar to He. No efficiency estimation is given for DMAMF since voltammograms for this deposit were distorted (see Figure 4.2.8) and therefore unsuitable for derivation of Γ_{app} values.

All of the electroactive films show a continuous degradation of the ferrocene/ferricenium wave when repeatedly cycled between these two states. This decay has previously been observed for Ar plasma polymerized vinylferrocene.[9] Murray *et al* found that the extent of decay was proportional to the time spent in the ferricenium state and that the rate of

decay was decreased by prior storage of the modified electrode in air for periods of up to one month.[9,11]

4.2.4.2 Decay of ferrocene/ferricenium electroactivity

(a) Neat plasma polymers

Results

Figure 4.2.6 shows the decay of the ferrocene/ferricenium wave during continuous CV for deposits of neat plasma polymerized vinylferrocene ('thin'film), vinylferrocene ('thick' film) and DMAMF respectively. Not all the waves in Figure 4.2.6 represent consecutive CV cycles since the decay rate is slow enough to cause consecutive waves to almost superimpose as the decay proceeds. The peak current decay data for the 'thin' films of vinylferrocene gave linear second order plots (see Figure 4.2.7a). The 'thick' film of vinylferrocene and the DMAMF film gave linear first order plots (see Figures 4.2.7b,c). Table 4.2.4 summarizes the decay data.

Discussion

(i) Thin films of vinylferrocene plasma deposit

Second order decay of ferrocene/ferricenium electroactivity has previously been observed for monolayers of ferrocene covalently bound to an electrode surface using alkylaminesilane chemistry.[17] First and second order decay phenomena, depending upon experimental conditions (*vide infra*), have been reported by Rolison for Ar plasma polymerized vinylferrocene.[12]

In this study the decay was monitored by the decrease in CV peak current with time. The units of a second order rate

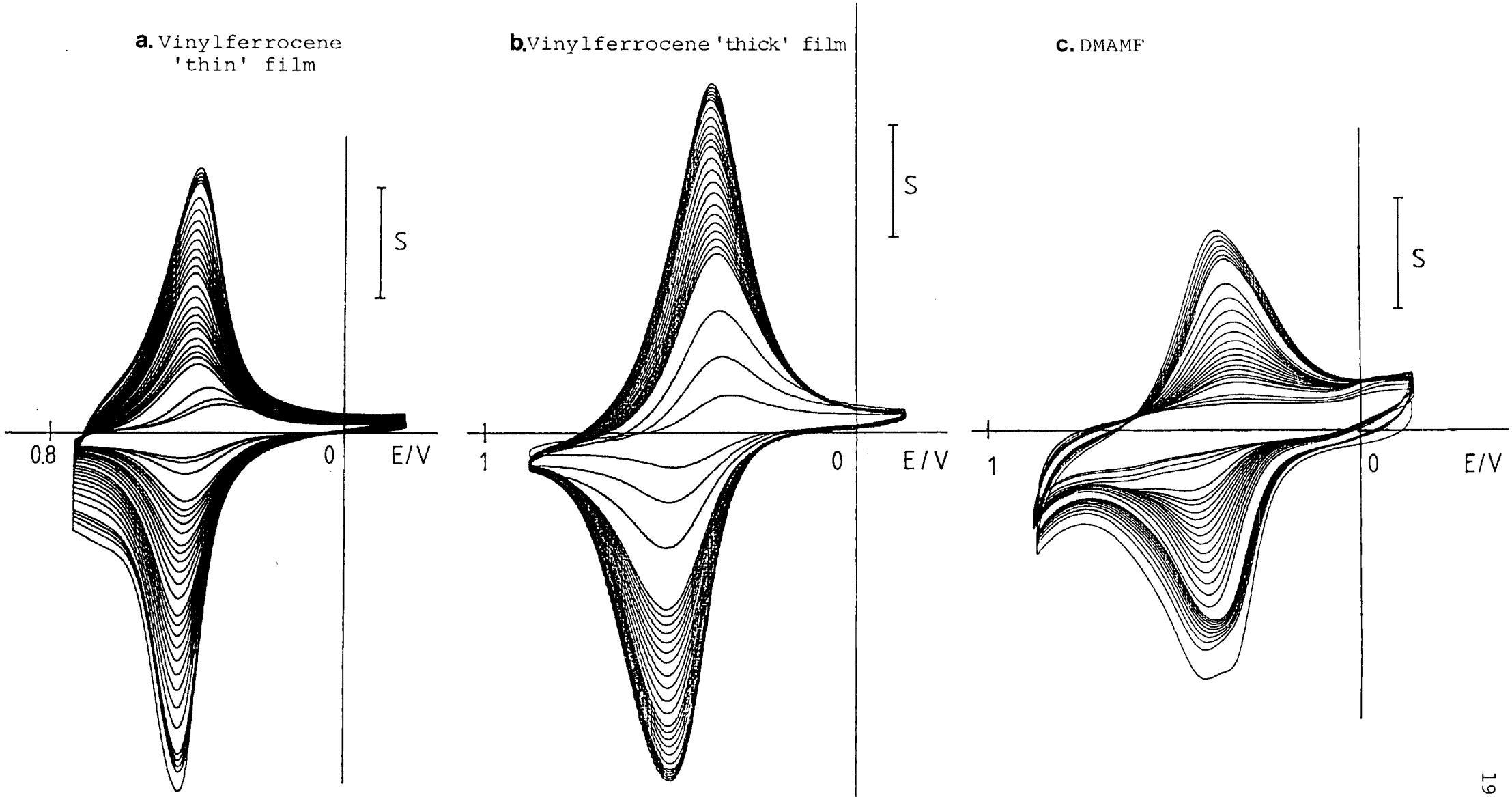

FIGURE 4.2.6 CV decay for neat plasma polymers at a sweep rate of 50mV/s.

(a) S = 40 $\mu A\ cm^{-2}$
(b) S = 80 $\mu A\ cm^{-2}$
(c) S = 20 $\mu A\ cm^{-2}$

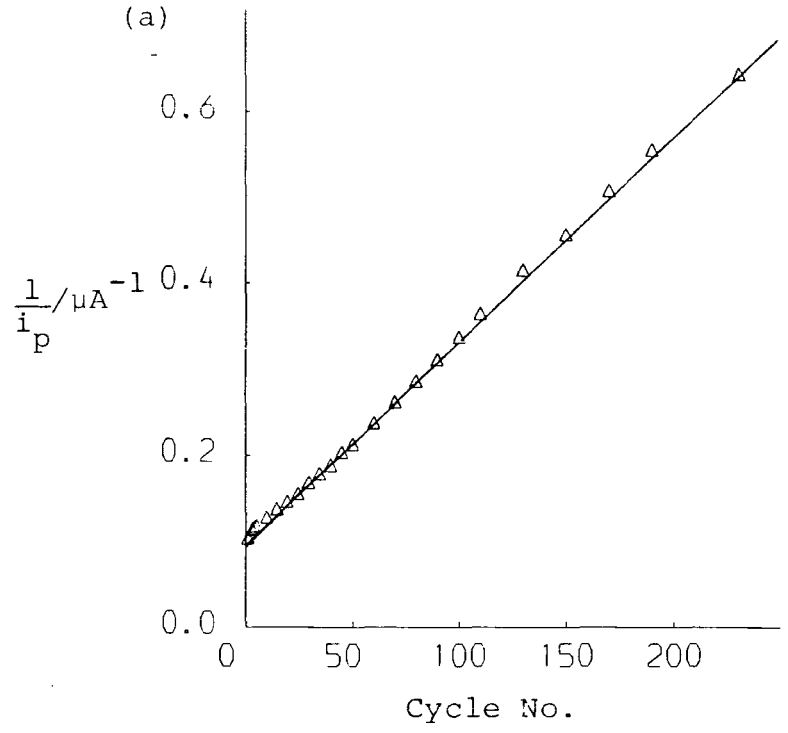

Second order plot for 'thin' film vinylferrocene

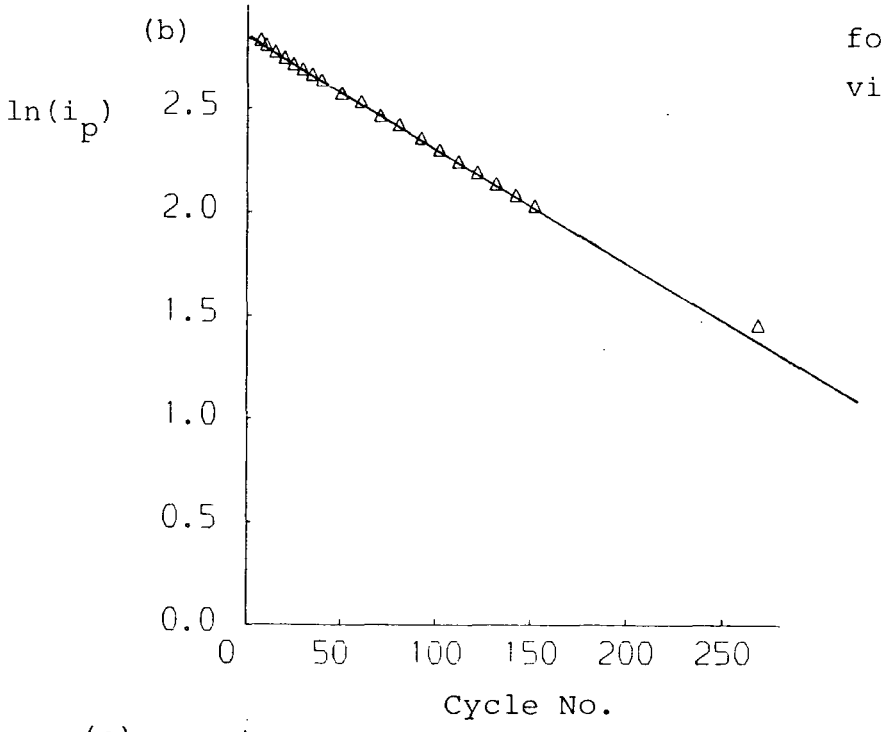

First order plot for 'thick' film vinylferrocene

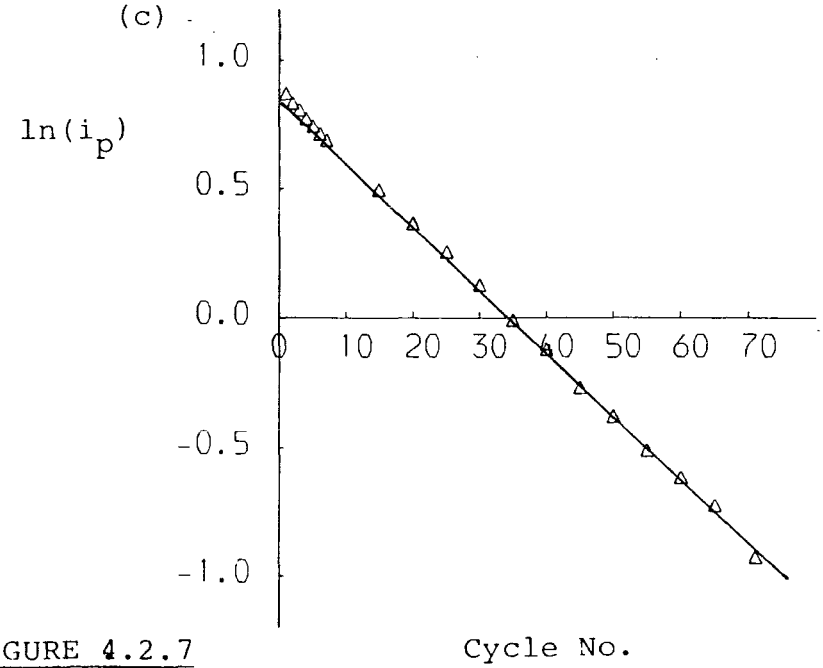

First order plot for DMAMF

FIGURE 4.2.7

TABLE 4.2.4 CV decay data for neat plasma polymerized vinylferrocene and DMAMF

Monomer	$\Gamma/10^{-9}$ mol cm^{-2}	peak splitting/ mV	sweep rate/ mV s^{-1}	Temp/^{o}C	kinetic decay order	½ life/ No.cycles		½ life/ time(mins) in ferricenium state[a]	
vinylferrocene	3.8	60	50	25	2nd	47[c]	44[d]	9.7[c]	9.1[d]
vinylferrocene	2.9	30	50	40	2nd	19	18	3.9	3.7
vinylferrocene	1.6	40	10	25	2nd	9.5	9.3	8.6	8.4
vinylferrocene	13.0[b]	110	50	25	1st	132	130	39.6	39.0
DMAMF	2.0	50	50	25	1st	32	28	10.2	9.0

a. This value allows for differences in $E^{\ominus}$ between films formed from different monomers and for any difference in anodic potential sweep limit between experiments.

b. This figure is an underestimate of Γ since the large peak splitting indicates that not all of the ferrocene sites in the film are oxidized during one anodic sweep.

c. Figures in left column taken from cycle number at which peak current had decayed by 50%.

d. Figures in right column derived from slope of 1st or 2nd order plot.

constant are thus $(\mu A)^{-1}cycle^{-1}$. Rolison used peak area and studied the decay by potentiostatting the films in the ferricenium state.[12] Second order rate constants were quoted in units of $cm^2mol^{-1}s^{-1}$. In either case the magnitude of the derived second order rate constant depends upon the size of the initial signal, *i.e.* upon film thickness. Derived second order rate constants for films of different thickness are thus not directly comparable. The 'true' second order rate constant, which has units $cm^3mol^{-1}s^{-1}$, is independent of film thickness. This value cannot be determined since the film thickness is unknown. For a second order process the half-life, $t_{\frac{1}{2}}$, is related to the second order rate constant, k_2, and the initial concentration, a_o, by the expression:

$$t_{\frac{1}{2}} = \frac{1}{k_2 a_o}$$

Since the initial concentration of ferrocene sites for a given plasma polymer should be independent of film thickness, and is likely to be similar for all the plasma polymers studied here, it is the half-life which is the directly comparable parameter and not the derived second order rate constant.

Table 4.2.4 shows that the half life, in numbers of CV cycles, is approximately five times greater at a sweep rate of 50mV/s than at 10mV/s. This result confirms the assertion that the extent of decay is proportional to the time spent in the oxidized state.

At 40°C the decay rate for thin films of neat plasma polymerized vinylferrocene is greater than at 25°C. Using derived second order rate constants normalized to the same

initial concentration of ferrocene sites an activation energy of 46 kJ mol^{-1} was obtained by use of the Arrhenius equation. This value is a crude estimate of the true activation energy since decay at only two temperatures was studied.

(ii) Thick film of vinylferrocene deposit

For a 'thick' film of neat plasma polymerized vinylferrocene ($\Gamma \geq 13.0 \times 10^{-9}$ mol cm^{-2}) the CV peak splitting is increased and the peaks are broadened compared to the 'thin' film. The electroactivity decays according to first order kinetics and the half-life is considerably greater than that for the 'thin' film.

The change in decay behaviour when film thickness is increased may be associated with incomplete oxidation of all the ferrocene sites within the film during one anodic sweep, which is suggested by the increased peak splitting. Rolison observed a change in decay behaviour for Ar plasma polymerized vinylferrocene from first to second order upon increasing the solution electrolyte concentration from 0.1 to 1.0M $LiClO_4$.[12] Film coverage was approximately constant at *ca.* $6\text{-}7 \times 10^{-9}$ mol cm^{-2} in Rolison's experiment.

(iii) DMAMF deposit

The film of neat plasma polymerized DMAMF gave CV peaks which, for the first few cycles, appeared to be composed of more than one component (see Figure 4.2.6). The peak current decay data gave a reasonably linear first order plot of comparable half life to that obtained for the 'thin' vinylferrocene deposits. For some films of neat plasma polymerized DMAMF the peak current grew (*sic*) over the first 2-3 cycles after which the usual decay was observed. The same phenomenon was observed for the 'thick' vinylferrocene deposit but was not found for any of the other electroactive deposits prepared by neat or inert gas plasma polymerization. This behaviour resembles that for the aged poly-$Fe(bpypyr)_3^{2+}$ modified electrode (see Chapter Three).

(b) Inert gas plasma polymers

Results and discussion

The electroactivity of all the films produced by inert gas plasma polymerization decayed upon repeated potential cycling between the ferrocene and ferricenium states. In no case could the activity loss phenomena be rationalized by simple kinetic laws. Considerable loss of electroactivity was observed over the first few cycles.

Cyclic voltammograms and plots of peak current against cycle number are shown in Figures 4.2.8 and 4.2.9. For the 10mV/s plots the initial peak current has been normalized to the same value as that for 50mV/s in order to show the increased decay rate (in number of cycles) at lower sweep rate more clearly. Although the decay patterns were qualitatively reproducible for films of the same plasma polymer prepared in different depositions, the variation in half lives obtained prevents any stability ordering of the different plasma polymers. Half lives shown in Table 4.2.5 correspond to the plots shown in Figures 4.2.9. It may be noted, however, that Ar plasma polymerized DMAMF gives less 'well-behaved' cyclic voltammograms and more rapid decay than the other deposits. In general the half lives, in numbers of cycles, although decreased at lower sweep rate are not reduced by as much as would be expected from the five fold increase in time spent in the oxidized state per cycle at 10mV/s compared to 50mV/s.

Rolison found first order decays for Ar plasma polymerized vinylferrocene when potentiostatted in the ferricenium state in 0.1M tetraalkylammonium electrolyte solution.[12]

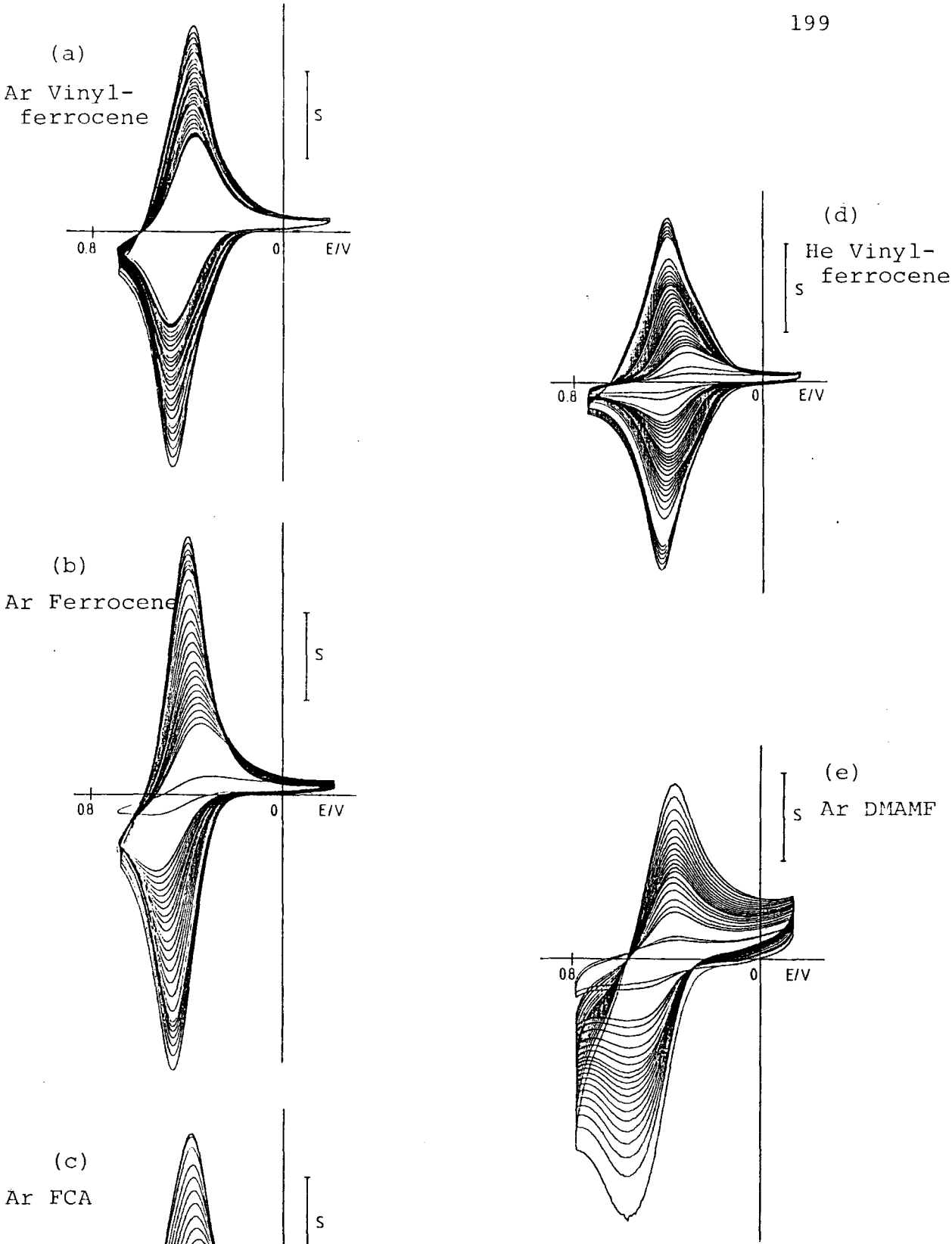

FIGURE 4.2.8 CV decay for inert gas plasma polymers at 50mV/s.

(a) s = 100 μA cm^{-2}

(b) s = 100 μA cm^{-2}

(c) s = 250 μA cm^{-2}

(d) s = 50 μA cm^{-2}

(e) s = 25 μA cm^{-2}

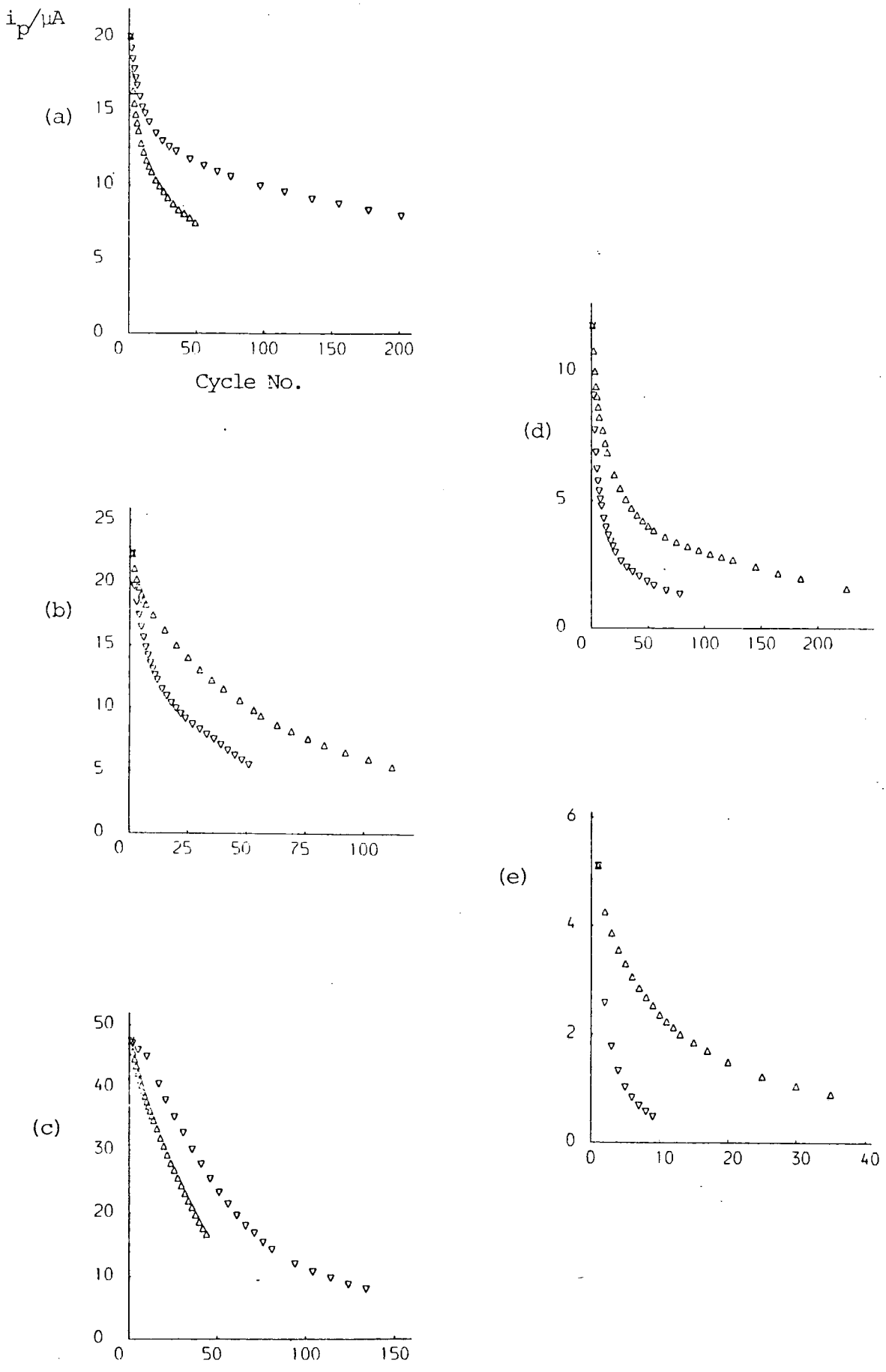

FIGURE 4.2.9 Peak current decay plots at 50 mV/s (upper curves) and 10 mV/s (lower curves) for the CVs shown in Fig. 4.2.8.

TABLE 4.2.5 CV decay data for inert gas plasma polymerized ferrocenes, 25°C

Monomer	Inert gas	$\Gamma/10^{-9}$ mol cm^{-2} a	peak splitting/ mV	sweep rate/ mV s^{-1}	½ life/ No. cycles	½ life/time (mins) in ferricenium state
Vinylferrocene	Ar	10.1	80	50	95	17
Vinylferrocene	Ar	12.2	30	10	23	21
Vinylferrocene	He	2.7	30	50	21	4.5
Vinylferrocene	He	2.2	25	10	5	5.3
Ferrocene	Ar	8.9	80	50	43	7.2
Ferrocene	Ar	15.4	25	10	15	16
FCA	Ar	35.2	140	50	50	9.7
FCA	Ar	54.1	50	10	31	30
DMAMF	Ar	-	190	50	9	1.9
DMAMF	Ar	-	120	10	∿2.5	2.6

a. In many cases this is an underestimate.

Potentiostatic decay (at +0.6V) was tested for Ar plasma polymerized ferrocene (see Figure 4.2.10). The decay data gave a reasonable first order plot (Figure 4.2.11) from which a half life of 8 minutes was obtained. Rolison found a half life of 8 minutes for Ar plasma polymerized vinylferrocene which had been aged for only one day. The effect of ageing on the stability of the modified electrodes was not investigated in this study.

The combined results suggest that in addition to the degradation observed for the neat plasma polymers some potential cycling induced loss or solubility of electroactive material occurs for the inert gas deposits for the following reasons:

(1) initial rapid loss of electroactivity on potential cycling;
(2) faster decay of electroactivity (in terms of time spent in the ferricenium state) at higher sweep rate;
(3) rational behaviour is observed for potentiostatic decay.

4.2.4.3 Conclusions

Although electroactive plasma deposits may be obtained from a variety of ferrocene monomers they invariably loose their electroactivity upon oxidative potential cycling or potentiostatting. It is apparent that this degradation is common to many ferrocene modified electrodes and is not peculiar to plasma polymers. Table 4.2.6 lists various ferrocene modified electrodes known to decay in this manner. A range of half lives for decay has been reported. The degradation of ferricenium electrochemically generated in acetonitrile solution has also been reported.[20,21,22] Since ferrocene modified electrodes have been used in glucose analysis[23] and have been proposed as candidates for components of

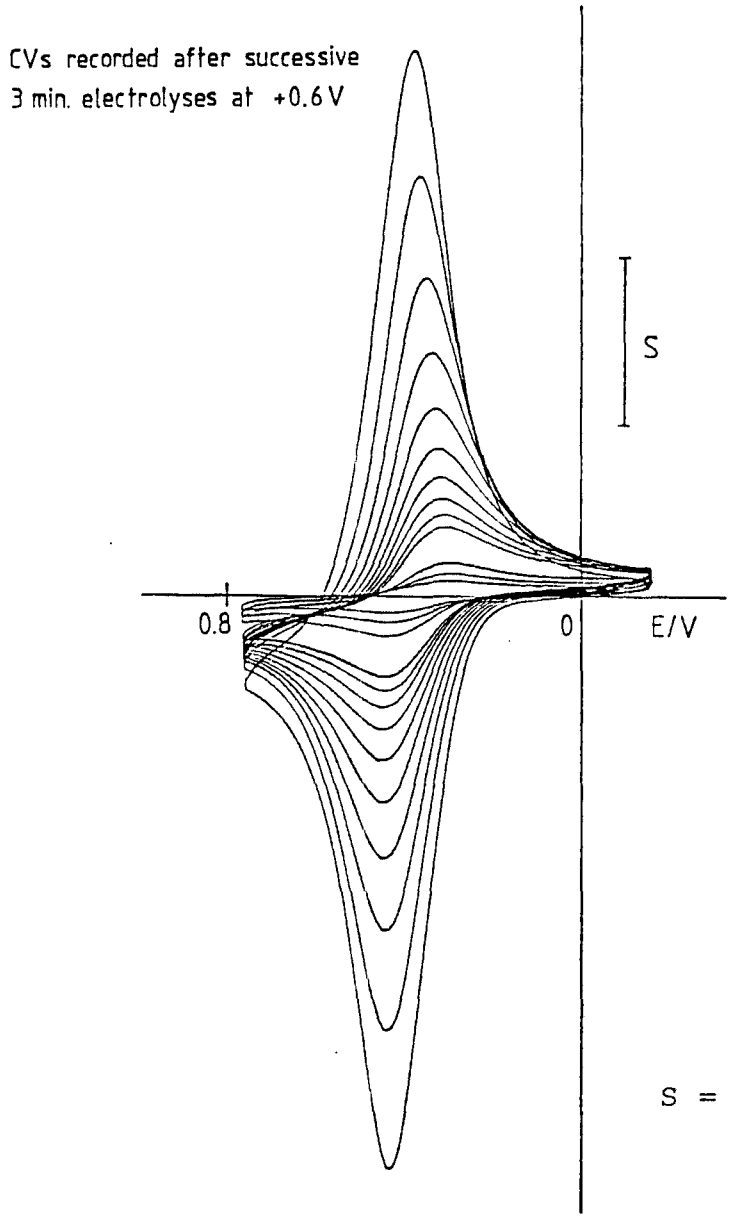

FIGURE 4.2.10 CV showing potentiostatic of Ar PP ferrocene

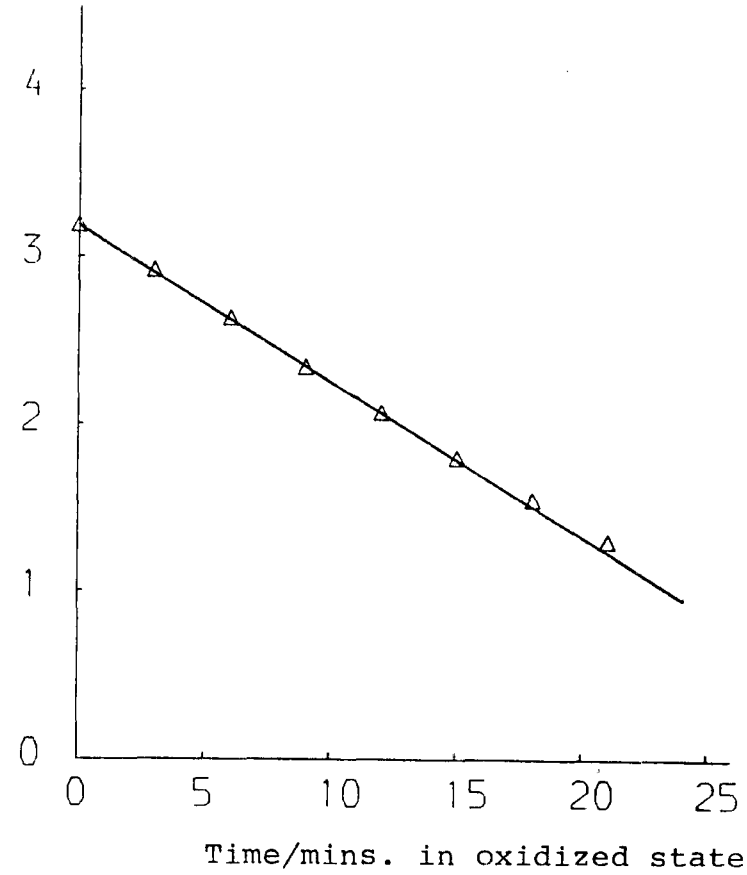

FIGURE 4.2.11 First order plot of i_p^{CV} peak current for potentiostatic decay.

cation detection electrodes,[24] further study of the decay mechanism is warranted.

TABLE 4.2.6 Ferrocene modified electrodes known to loose electroactivity upon oxidation

Ferrocene containing film	Reference
Neat plasma polymers	This work
Inert gas plasma polymers	9,11,12, this work
Radical initiation polymerized vinylferrocene	9,12
Silane bonded monolayers	17
Aminoferrocenes adsorbed onto carbon electrodes	18
Ferrocene partitioned into Nafion fluoropolymer	19
Electropolymerized pyrrole substituted ferrocene	This work, Chapter Two.

4.2.5 ESCA analysis of electrochemically degraded plasma polymer films

A platinum foil coated with neat plasma polymerized vinylferrocene, which had been cycled through the ferrocene/ferricenium wave 200 times in acetonitrile solvent and ClO_4^- electrolyte and finally returned to OV, was examined by ESCA. The C_{1s} and $Fe_{2p_{3/2}}$ spectra are shown in Figure 4.2.12. It is clear that an increase in the amount of oxidized iron compared to ferrocene environment iron has occurred over the pristine material. It is also evident, from the shoulder to the high binding energy side of the main C_{1s} peak, that oxid-

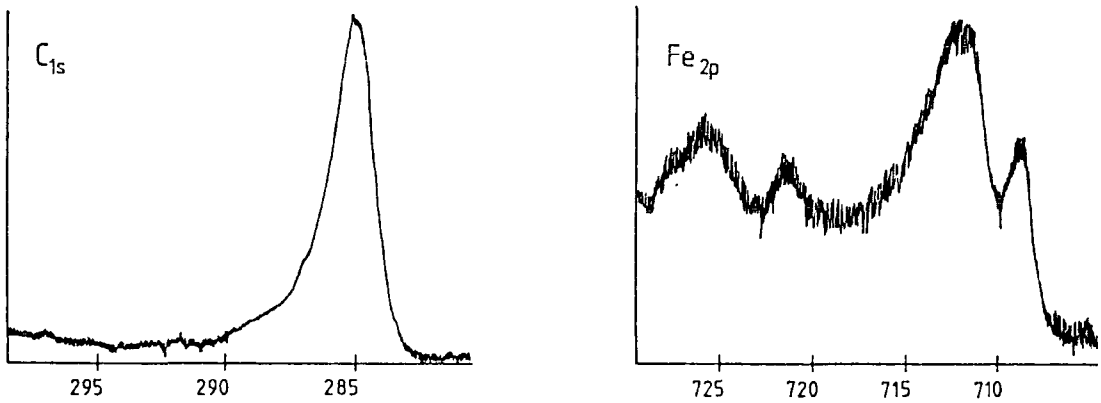

FIGURE 4.2.12 C_{1s} and Fe_{2p} ESCA spectra for CV degraded neat plasma polymerized vinylferrocene

ation of the carbon matrix has also taken place. Peak fitting the C_{1s} envelope in a manner analogous to that shown for pristine plasma polymerized BF (Figure 4.2.3) indicates that approximately 20% of the carbon atoms are bonded to oxygen in the degraded film. The overall film surface stoichiometry was $C_{19.3}Fe_1O_5$, no Cl was detected.

In a control experiment another platinum foil, coated in the same plasma discharge as the electrochemically cycled foil, was placed in a solution of 0.1M TBAP in acetonitrile for 2 hours. When examined by ESCA some increased iron oxidation (compared to the pristine material) was found but this was small compared to the increase for the electrochemically cycled electrode. It may, therefore, be concluded that electrochemical degradation of the redox active plasma polymers involves oxidation of both iron and carbon.

4.2.6 Photolysis of redox active plasma polymers

Evans *et al* have reported the photoassisted electrocatalytic reduction of tri- and tetrachloromethane at an electrode coated with neat plasma polymerized vinylferrocene.[4b] Broad band illumination at wavelengths greater than 284nm was used. The photostability of plasma polymerized, ferrocene containing films is thus of importance if such films are to be of long term use in photoassisted electrocatalysis.

Films of neat plasma polymerized DMAMF were irradiated in air for 2 hours at wavelengths of 290, 390, 490 and 590nm using a monochromated light source, with a band pass of 10nm, and an incident photon flux of *ca*. 4mW cm^{-2}. Films of neat plasma polymerized vinylferrocene were similarly irradiated at 290nm. Photoaccelerated oxidation of both polymers, which was most extensive at 290 and 390nm, was obvious from analysis of the C_{1s} and $Fe_{2p_{3/2}}$ spectra (compare Figure 4.2.12). In a control experiment, a film of neat plasma polymerized DMAMF which had been aged in darkness for one year showed less oxidation than freshly prepared films irradiated for 2 hours at 390 or 290nm.

4.2.7 Plasma codeposition from 4-vinylpyridine and vinylferrocene

Plasma codeposition from 4-vinylpyridine and vinylferrocene (neat) using 0.2 torr vinylpyridine gave a film which had a higher C/Fe surface elemental ratio than neat plasma polymerized vinylferrocene and which also contained nitrogen. This result shows that both carbon and nitrogen

from 4-vinylpyridine were incorporated into the codeposit. The overall surface stoichiometry was $C_{35}Fe_{2.1}N_1O_{3.2}$. The $Fe_{2p_{3/2}}$ ESCA spectrum was similar to those shown in Figure 4.2.2. The deposit showed ferrocene-like electroactivity with $E^{\ominus}$=0.43V, but again the electroactivity degraded with repeated potential cycling.

Doblhofer *et al* have prepared electroactive plasma codeposits from 4-vinylpyridine and $Fe(CO)_5$.[37] It thus seems likely that films with two types of electroactive centre could be prepared by plasma codeposition of vinylferrocene, 4-vinylpyridine and $Fe(CO)_5$.

4.2.8 Oxygen plasma deposition

Changing the plasma gas from Ar to oxygen and increasing the r.f. power from 10 to 25W produced a markedly different deposit from ferrocene. ESCA analysis revealed that the deposit contained C, Fe and O and that all of the iron was present in the +3 oxidation state. The C_{1s} spectrum showed extensive carbon oxidation and an overall surface stoichiometry of $C_{4.3}Fe_1O_{4.3}$ was obtained. Magnetic susceptibility analysis of a sample of this deposit on PTFE revealed that it was ferromagnetic. A previous study has indicated that γ-Fe_2O_3 may be produced under certain conditions by discharging ferrocene in an oxidizing atmosphere.[34]

4.3 Conclusions

Electroactive plasma polymer films have been prepared from a number of ferrocene monomers. All the plasma polymers

studied contained a significant amount of intact ferrocene but not all were electroactive. Electroactive films were degraded by repeated potential cycling to yield a film containing oxidized iron and carbon.

Plasma codeposition of vinylferrocene with 4-vinylpyridine does not impede the ferrocene electroactivity of the resulting film. Deposition using an oxygen plasma yields an oxidized, iron rich film.

4.4 Experimental

Plasma polymerizations were performed in a tubular, all-glass, grease-free vacuum line reactor of local design and *ca.* 1.5ℓ total capacity (see Figure 4.4.1). Flanged joints and cold traps were sealed with Viton 'O' rings, other connections were made with Cajon *ultra*torr couplings. Vacuum taps were sealed with PTFE stoppers. The line was evacuated with an Edwards ED2M2 $2\ell s^{-1}$ mechanical pump, a liquid nitrogen cold trap was used. The pumping system gave a base pressure of *ca.* $4x10^{-2}$ torr. An oil diffusion pump backed by a second mechanical pump was also connected to the line for the purpose of degassing liquid monomers prior to PP. Pressure measurements were made using a Pirani thermocouple gauge. Before each deposition with a new monomer the reactor was cleaned with a hard nylon brush using acetone, detergent and salt, washed thoroughly with distilled water and baked in an oven.

All PP experiments were performed with a dynamic flow of monomer or inert gas through the reactor, *i.e.* the reactor was open to the pumping system during PP.

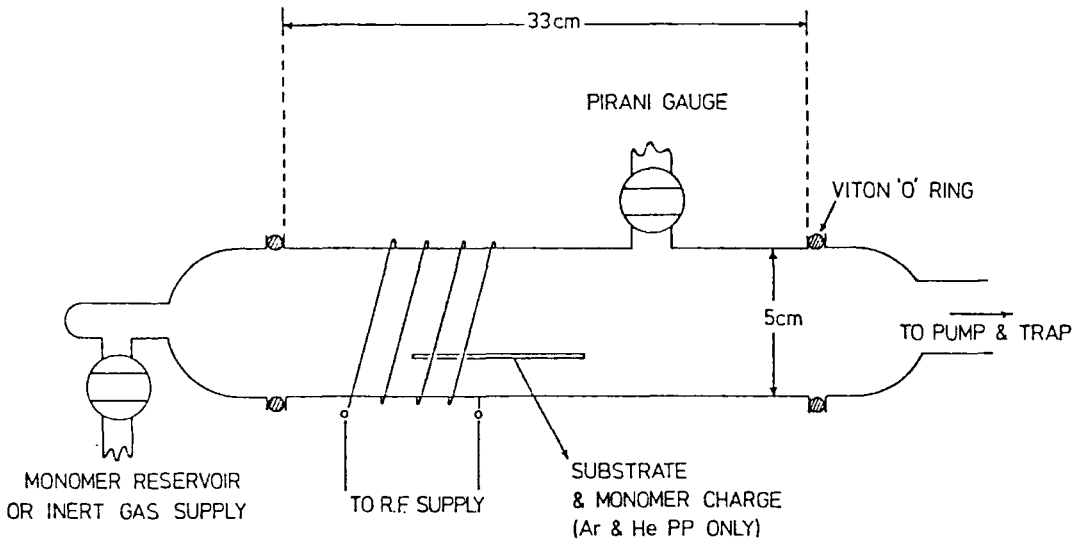

FIGURE 4.4.1 Schematic of plasma reactor

The r.f. generator (13.56MHz) and LC matching network, used to sustain the plasma, were of local construction. A Heathkit HM102 meter was used to measure the standing wave ratio and r.f. power. The r.f. power was inductively coupled to the reactor *via* an externally wound 9 turn copper coil.

Plasma polymers were deposited onto Al foil (for ESCA and ATR infra red analysis), 3.1mm diameter, Kel-F shrouded glassy carbon electrodes (ex BAS, for CV), platinum flag electrodes (for ESCA following CV) or polished KBr windows (for transmission infra red analysis). All deposition substrates were placed on a glass slide and positioned at the edge of the coil region nearest to the vacuum pump. The substrates were degreased with acetone before placement in the vacuum line and finally cleaned in the reactor with a 50W hydrogen plasma.

Other than DMAMF, which was degassed prior to use, monomers were used as received from the following commercial sources:

ferrocene (B.D.H.), vinylferrocene (Strem), FCA, DMAMF, BF (Aldrich).

Before attempting neat PP the section of the vacuum line between the monomer reservoir and the copper coil (see Figure 4.4.1) was heated to *ca.* 80^{o} using electrical heating tape. The coil region was also heated with a hot air gun to prevent condensation of the monomer onto the reactor walls or deposition substrate. Neat PP was achieved by warming the monomer reservoir, with a second hot air gun, and igniting the plasma when the pressure had risen to *ca.* 7.5×10^{-2} torr. PP was performed at 10W and for 1-5 minutes deposition time. Using the heated reservoir technique the monomer flow rates were eratic and no attempt to measure them was made. For the co-deposition experiment 4-vinylpyridine and vinylferrocene vapours were mixed at a 'T' junction before entering the discharge region.

For inert gas polymerizations a small charge (*ca* . 10mg) of monomer was placed *ca.* 1cm in front of the substrate to be coated and an inert gas plasma ignited at 0.2 torr (inert gas) and 10W power for 20 sec.-2 minutes. No part of the reactor was externally heated during these depositions. The inert gas pressure was controlled using an Edwards leak valve. The flow rates of Ar and He (B.O.C.) were determined, following the method of Yasuda,[35] by measuring the decrease in pressure with time immediately after closing the gas inlet to the vacuum line. Flow rates of 1.93×10^{-6} and 3.0×10^{-6} mol s^{-1} were determined for Ar and He respectively.

ESCA and CV analyses were performed as described in

Chapters Two and Three. ESCA spectra were recorded immediately after removal of the coated substrate from the plasma reactor. CVs were recorded after soaking the coated electrodes in dried acetonitrile for 15 minutes. All CVs were recorded in acetonitrile which was 0.1M in tetrabutylammonium perchlorate. A thermostatic water bath was used in the kinetic decay experiments.

Transmission infra red spectra were recorded on a Perkin-Elmer 580B double beam spectrometer equipped with a microcomputer workstation. The spectra were the average of at least 15 scans. Attenuation of Total Reflection (ATR) infra red spectra were recorded from samples deposited onto Al foil and using a KRS-5 internal reflection element. These spectra were recorded on a Nicolet 60 SX Fourier transform infra red spectrometer. The ATR spectrum of uncoated Al foil was subtracted from that of the coated foils.

REFERENCES - Chapter Four

1. A.Bradley and J. P. Hammes; J.Electrochem.Soc. 110, (1963),15.
2. R. Nowak, F.A. Schultz, M. Umana, H. Abruna and R.W.Murray, J.Electroanal.Chem., 94, (1978), 219.
3. a. Y. Osada, A. Bell and M. Shen, J.Polym.Sci.Polym.Lett. Ed., 16, (1978), 309.
   b. Y. Osada, Y. Iriyama, M. Takase and A. Mizumoto, Proc.Int'l Ion Engineering Congress, Kyoto,(1983), 1435.
4. a. M.F. Dautartas and J.F. Evans, J.Electroanal. Chem., 109, (1980), 301.
   b. M.F. Dautartas, K.F. Mann and J.F. Evans, J.Electroanal. Chem., 110, (1980), 379.
5. M.F. Dautartas, Ph.D. Thesis, University of Minnesota, Minneapolis, (1982).
6. P. Daum and R.W. Murray, J.Electroanal.Chem., 103,(1979), 289.
7. R.J. Nowak, F.A. Schultz, M. Umana, R. Lam and R.W. Murray, Anal.Chem., 52, (1980), 315.
8. M. Umana, D.R. Rolison, R. Nowak, P. Daum and R.W. Murray, Surface Science, 101, (1980), 295.
9. P. Daum, J.R. Lenhard, D. Rolison and R.W. Murray, J.Am. Chem.Soc., 102, (1980), 4649.
10. P. Daum and R.W. Murray, J.Phys.Chem., 85, (1981), 389.
11. D.R. Rolison, M. Umana, P. Burgmayer and R.W. Murray, Inorg.Chem., 20, (1981), 2996.
12. D.R. Rolison, Ph.D. Thesis, University of North Carolina at Chapel Hill, (1981).
13. D.R. Rolison and R.W. Murray, J.Electrochem.Soc.131, (1984), 337.

14. S-J. Dong and B-F. Liu, Acta Chimica Sinica, 40,(1982),1061.

15. S. Dong, B. Liu and J. Bi, Kexue Tongbao, 29, (1984), 1033.

16. S-J. Dong, B-F. Liu, G-J. Cheng, Y-S. Li and H. Chen, Acta Chimica Sinica, 42, (1984), 779.

17. J.R. Lenhard and R.W. Murray, J.Am.Chem.Soc., 100, (1978),7870.

18. N. Oyama, J.B. Yap and F.C. Anson, J.Electroanal.Chem., 100, (1979), 233.

19. I. Rubinstein, J.Electroanal.Chem., 176, (1984), 359.

20. J.W. Diggle and A.J. Parker, Electrochim.Acta, 18, (1973),975.

21. M. Sato, T. Yamada and A. Nishimura, Chem.Lett.,8, (1980),925.

22. W.P. Fehlammer and C. Moinet, J.Electroanal.Chem., 158, (1983), 187.

23. A.E.G. Cass, G. Davis, G.D. Francis, H.A.O. Hill *et al*, Anal.Chem., 56, (1984), 667.

24. M.W. Epenscheid and C.R. Martin, J.Electroanal.Chem., 188, (1985), 73.

25. M. Barber, J.A. Connor, L.M.Derrick, M.B. Hall and I.H. Hillier, J.Chem.Soc.Faraday Trans.II, 69, (1973), 559.

26. D.T. Clark and D.B. Adams, J.Chem.Soc.Chem.Commun. (1971),740.

27. A. Dilks, Chapter 5, p.352-354 in "Electron Spectroscopy: Theory, Techniques and Applications", vol.4, Ed.C.R.Brundle and A.D. Baker, Academic Press, London (1981).

28. K. Wandelt, Surface Science Reports, 2, (1982), 70.

29. P. Mills and J.L. Sullivan, J.Phys.D: Appl.Phys., 16, (1983), 723.

30. S.D. Phadke, Thin Solid Films, 48, (1978), 319.

31. E.R. Lippincott and R.D. Nelson, Spectrochimica Acta, 10, (1958), 307.

32. R.M. Silverstein, G.C. Bassler and T.C. Morrill, "Spectrometric Identification of Organic Compounds", 4th Edn., John Wiley, New York, (1981).

33. D.R. Hutton, Ph.D. Thesis, Durham University, (1983).

34. Matsushita Electrical Industrial Co.Ltd., Chemical Abstracts, 96:154287t, (1982), patent application.

35. H. Yasuda, "Plasma Polymerization", Academic Press, London, (1985).

36. T.N. Mzimela and E.W. Neuse, S.Afr.J.Chem., 34, (1981),47.

37. D. Doblhofer, W. Dürr and N. Jauch, Electrochimica Acta, 27, (1982), 677.

CHAPTER FIVE

PLASMA AND ELECTROCHEMICAL DEPOSITS DERIVED FROM PERFLUOROCYCLOPENTENE (PFCP)

5.1 Introduction

The plasma and electrochemical methods provide a means of polymerizing 'monomers' which do not possess the functional groups necessary for conventional polymerization methods. It is of interest, therefore, to compare the products obtained from plasma and electrochemical polymerization of the same monomer. Hernandez *et al*[29] have compared such products obtained from heterocyclic aromatic monomers. It was concluded that plasma polymers and 'undoped' electrochemical polymers, derived from the same monomer, had similar surface energies and stoichiometries.[29]

Certain differences between the two polymerization methods may be identified:

1. Plasma polymerization is a generally applicable technique whereas electrochemical polymerization of 'unconventional' monomers has mainly been limited to heterocyclic aromatic compounds.
2. The greater energies available in a plasma allow, in principle, for a wider range of polymer forming reactions and greater complexity of product compared to electrochemical polymerization.
3. Electrochemical polymers are usually doped (oxidized or reduced) and associated with a counter ion derived from the electrolyte used during preparation.

A priori, it might be anticipated that plasma and electrochemical polymerization are unlikely to produce similar products.

Described below is a comparison of deposits obtained by plasma discharge and cathodic electrolysis of one monomer, perfluorocyclopentene. The chemical shift range in the C_{1s} ESCA spectrum of fluorocarbon materials is a sensitive probe for functional group (CF, CF_2, CF_3) composition and should highlight any differences in the composition of products derived from the two methods.

5.1.1 Plasma polymerization (PP) of fluorocarbon monomers

In a series of publications Clark *et al* have demonstrated the utility of ESCA as a tool for the investigation of structure and bonding in plasma polymers.[1] Fluorocarbon monomers were studied, primarily because the molecular rearrangements, which most often accompany PP, are highlighted by the fluorine substituent induced chemical shifts in the C_{1s} spectrum of the resulting plasma polymers. PP of perfluorobenzene, for example, produces a deposit containing, C, CF, CF_2 and CF_3 functions which give rise to C_{1s} spectral components at progressively higher binding energies.[1c,i] PP of benzene will also involve molecular rearrangement but C, CH, CH_2 and CH_3 functions are indistinguishable to ESCA.

Clark *et al* have shown that perfluorinated aromatic compounds tend to retain the C/F stoichiometry of the monomer whereas perfluorinated alicyclic and aliphatic compounds eliminate fluorine as a prerequisite of PP.[1c,d,j] Clark and Shuttleworth studied the plasma polymer derived from perfluorocyclohexene;[1d,2] since this monomer is closely related to the one used in the present study further reference to this work is given below.

5.1.2 Electrochemistry and fluoropolymers

Silvester[3] has reported the formation of a black deposit on an electrode surface during the electrochemical reduction of perfluorocyclopentene (PFCP) in N, N´dimethyl-formamide (DMF)/tetraalkylammonium (R_4N^+) electrolyte solution. This deposit, which proved intractable to conventional spectroscopic analysis of the bulk material, is the subject of an investigation discussed in this chapter.

No preparations of electrode coatings formed by the electrochemical reduction or oxidation of other perfluorocarbon monomers have been reported.

Brewis *et al* have studied the electrochemical reduction of polytetrafluoroethylene (PTFE) using an electrode placed in contact with a film of the polymer immersed in DMF/R_4N^+ electrolyte solution.[4-7] Some of the results presented below suggest that the electrochemical reduction of PTFE and the cathodic deposition from PFCP have common features and so some of the investigations of Brewis *et al* are briefly reviewed here. It was found that electrochemical reduction of PTFE at potentials negative of -1.5V *versus* SCE produced a dark coloured layer on the surface of the PTFE film. The new phase spread in 'dendrites' to a distance of a few cm from the electrode and was typically a few μm thick. The material was found to be carbonaceous in nature and, by analogy to known chemical reductions of PTFE,[7] the following reduction scheme was proposed:

$$\text{-}(CF_2)\text{-}_n + 2ne^- \longrightarrow \text{-}(C)\text{-}_n + 2nF^-$$

The above reaction requires 4 electrons per C_2F_4 unit. Values in excess of 4 were consistently obtained by Brewis *et al* and it was proposed that further reduction of the $\{C\}_n$ matrix occurred, resulting in the formation of an intercalation compound:

$$\{C\}_n + R_4N^+ + e^- \rightleftharpoons C_n^- R_4N^+$$

The average value of excess charge amounted to one electron per 23 carbon atoms.[6] Cathodic formation of intercalation compounds in graphite electrodes had previously been demonstrated.[8-10] The appearance of the electrochemically reduced PTFE was similar to that of the graphite intercalation compounds and, as for the latter compounds, CV showed that the putative intercalation reaction was reversible.[6] It was emphasized, however, that the electrochemically defluoroinated PTFE layers were less structurally ordered than graphite and were better termed polymeric than graphitic. ESCA results, which show defluorination of treated PTFE, have been alluded to by Brewis *et al* but no spectra have been published.

PTFE may also be defluorinated by contact with a Lithium amalgam to give an intimate mixture of carbon and LiF.[11-13] ESCA was used to analyse defluorinated samples and revealed an increase in the C/F stoichiometry for the surface ($C_3Li_3F_1O_1$) compared to that obtained by bulk analysis ($C_1(LiF)_2$). The reactive nature of the carbonaceous film towards oxidation in air was also demonstrated by ESCA.[13]

5.2 Results and Discussion

5.2.1 Plasma polymer

5.2.1.1 ESCA analysis

Curve fitted C_{1s} spectra for plasma polymerized PFCP samples, prepared from glow discharges of the neat monomer vapour at 0.1 torr and over a range of r.f. powers, are shown in Figure 5.2.1. Considerable rearrangement of the monomer fluorocarbon structure is evident. F_{1s} spectra were symmetrically shaped, single component peaks centred at 689-690eV and similar to those previously reported for other plasma polymers derived from perfluorocarbon monomers.[1] †

The process of decomposition of the C_{1s} spectral envelope into components representing contributions from C, CF, CF_2 and CF_3 functions was developed by Clark *et al.* Component positions were assigned by reference to the experimentally determined binding energies of the various functions listed above in standard samples.[1c] C_{1s} envelopes were usually fitted to five Gaussian curves (excluding contributions from hydrocarbon and shake-up)[1]; these are listed (A-E) in Table 5.2.1. The separation, in eV, between the components used by various workers in the same laboratory studying fluorinated plasma polymers is also listed in Table 5.2.1. It may be noted that a range of chemical shifts has been used for components representing the same chemical function. The discrepancy probably arises for two reasons:

---

† The uncertainty in the F_{1s} binding energy is caused by the difficulty in locating the position of the hydrocarbon peak which is used as reference (*vide infra*).

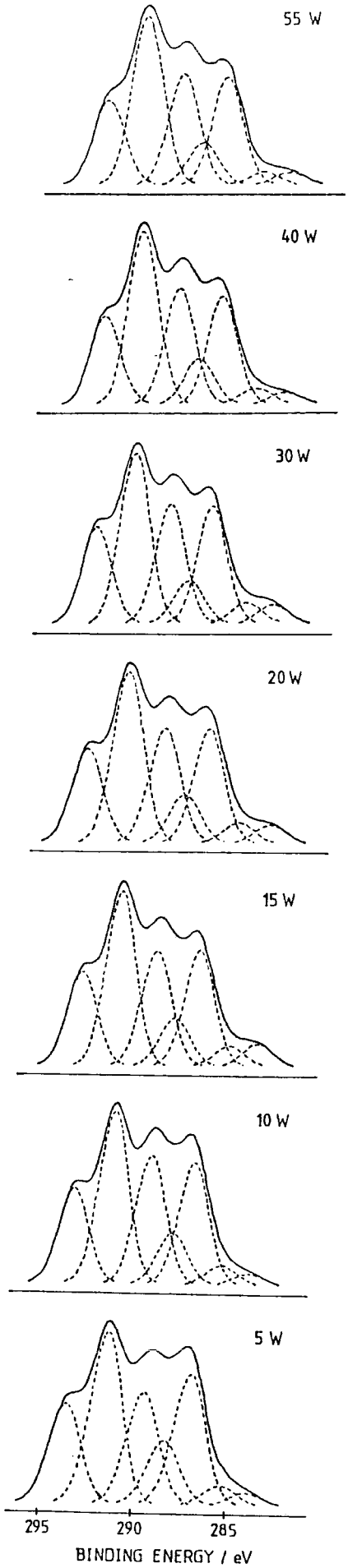

FIGURE 5.2.1 C_{1s} spectra for plasma polymerized PFCP samples prepared over a range of r.f. powers

TABLE 5.2.1 C_{1s} component peak separations in eV

Component	Assignment	peak separations with source reference				
		1c,2	1h	1k	14	this work
A	$C-CF_n$	1.5	1.8	1.5	1.6	1.4
B	CF	1.5	0.8	1.0	0.8	1.1
C	$CF-CF_n$	1.5	2.3	1.5	2.2	1.9
D	CF_2	2.0	2.2	2.0	2.4	2.1
E	CF_3					
		$\sum$=6.5	$\sum$=7.1	$\sum$=6.0	$\sum$=7.0	$\sum$=6.5

1. Plasma polymers are not regularly ordered materials and the components A-E must necessarily represent functional groups (C, CF *etc.*) in an average environment. This average environment is likely to change for different plasma polymers.

2. Even for the same plasma polymer different chemical shifts have been used to represent the same component. This suggests a degree of operator preference.

Functional group assignments for the components A-E are given in Table 5.2.1. The components B and C undoubtedly represent CF functions but the nature of their β substituents is uncertain. Whether component B represents CF bonded to unfluorinated carbon atoms only, or to CF as well, is not clear. Internal consistency must be

maintained. Thus, if B represents CF bonded to unfluorinated carbon only, then component A must be at least twice as large as B, since C-CF=C is the minimum conceivable bonding requirement for an isolated CF. This inequality of peak magnitudes is not always obtained[1] which leads to the conclusion that component C must represent CF bonded to CF_2 and CF_3 but not to CF. This latter conclusion requires the following inequality of component magnitudes:

$$2D(CF_2) + E(CF_3) > C(CF\text{-}CF_n).$$

From an inspection of published spectra it appears that in some cases the first inequality (A>2B) holds, in other cases the second, and in some cases both.[1] This variation is the cause of the uncertainty in the nature of the β substituents for the two CF components. In the PFCP plasma polymer spectra both of the aforementioned inequalities are obtained.

Occasionally 6 components have been used in the curve fitting procedure in order to discriminate between C-CF and $C\text{-}CF_n$.[1i]

Component position, determined from standard samples, and internal consistency are not the only constraints placed upon the analysis procedure. The F/C stoichiometry obtained from decomposition of the C_{1s} spectrum should agree with that determined from the $^{F_{1s}}/_{C_{1s}}$ peak area ratio. Table 5.2.2 gives F/C stoichiometries for plasma polymers produced over a range of r.f. powers and determined both from C_{1s} analysis and $^{F_{1s}}/_{C_{1s}}$ area ratio. Good agreement

TABLE 5.2.2 F/C stoichiometries for plasma polymerized PFCP

r.f. power/W	Incl. CH		Excl. CH	
	F/C 1	F/C 2	F/C 1 *	F/C 2†
5	1.34	1.31	1.41	1.38
10	1.35	1.35	1.42	1.42
15	1.35	1.30	1.45	1.40
20	1.36	1.30	1.45	1.39
30	1.36	1.30	1.43	1.36
40	1.39	1.34	1.46	1.40
55	1.36	1.37	1.43	1.44

*av. = 1.44 ± 0.02 †av. = 1.40 ± 0.03

F/C 1 is the stoichiometry obtained from C_{1s} component analysis.

F/C 2 is the stoichiometry obtained from the F_{1s}/C_{1s} area ratio.

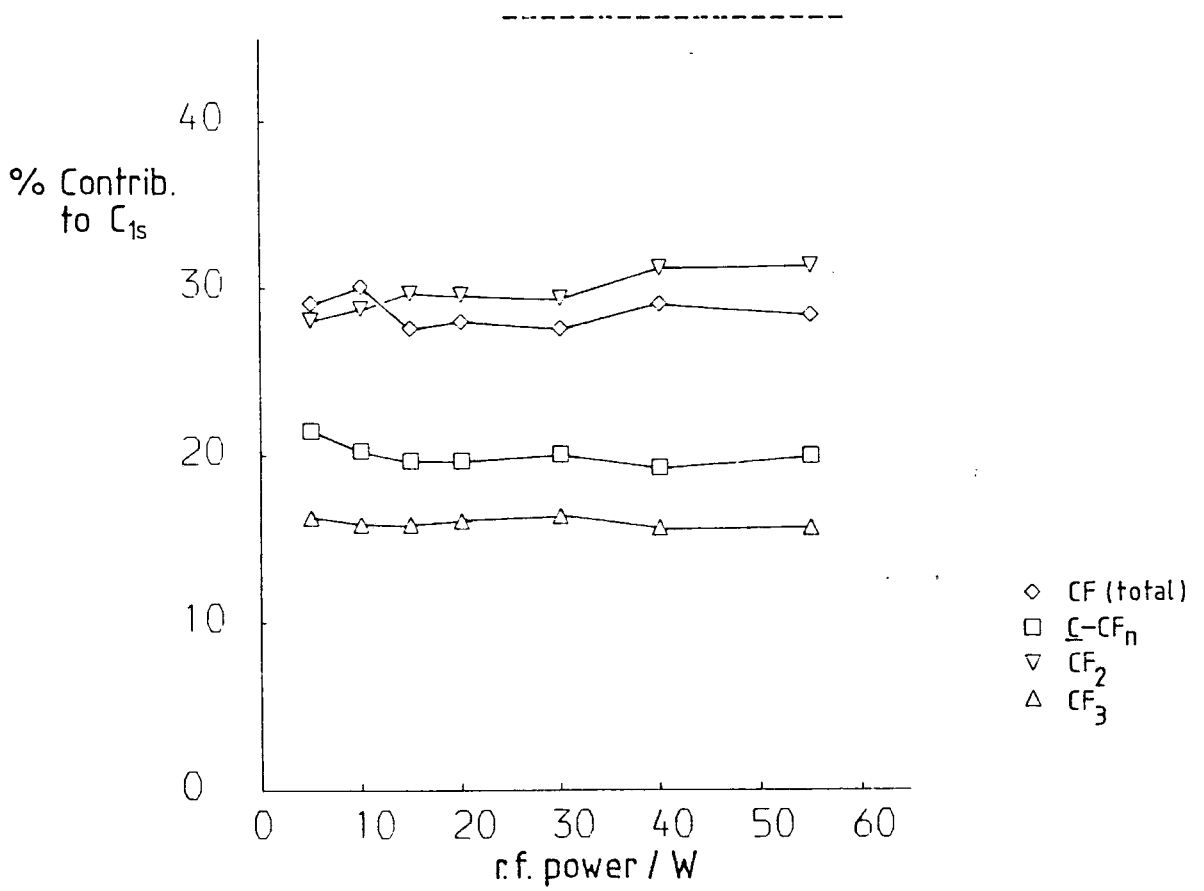

FIGURE 5.2.2 Variation in C_{1s} component contribution with r.f. power for plasma polymerized PFCP

between the two methods of calculation is found for all the samples, the average discrepancy being 3%. Following Shuttleworth,[1c,2] F/C stoichiometries excluding and including hydrocarbon are given. Figure 5.2.2 shows the variation in component contribution to the C_{1s} envelope with r.f. power. Components B and C have been summed to give a total CF contribution. Table 5.2.2 and Figure 5.2.2 show that both F/C stoichiometry and C_{1s} component analysis are essentially invariant over the power range 5-55W which represents a change in $W/_{FM}$[19] from 1.9×10^8 to 2.0×10^9 Jkg^{-1}. All the samples analyzed contained low levels of oxygen. The C/O stoichiometry varied randomly with r.f. power with an average value of *ca.* 50.

The relative sizes of the components A-E for plasma polymerized PFCP, *i.e.* $CF_2 > \underline{C}F\text{-}CF_n \simeq \underline{C}\text{-}CF_n > CF_3 > CF$, are the same as those found by Shuttleworth for glow-region plasma polymers formed from perfluorocyclohexene.[1c,2] If the average F/C stoichiometry of plasma polymerized PFCP is taken as 1.42 then 11% of the monomer fluorine has been eliminated in PP. Shuttleworth found an average F/C stoichiometry of 1.5 indicating a 10% elimination of fluorine from the monomer.[1c,2]

Gil'man *et al* have reported the PP of a number of perfluorocarbon monomers including PFCP in an electroded, 1 kHz a.c. glow-discharge.[15] F/C stoichiometries obtained using elemental analysis were consistently lower than those found by Clark *et al* using ESCA. Gil'man *et al* found F/C values of 1.09 and 1.15 for plasma polymerized PFCP and perfluorocyclohexene respectively. Although the different

experimental conditions used by Gil'man *et al* may produce deposits of different stoichiometry to those prepared in inductively coupled r.f. discharges, it should be emphasized that the necessary removal of a plasma polymer from the substrate to which it is often strongly adhered and the small amounts of material available, make elemental analysis a less than ideal tool for the study of plasma polymers.

The binding energies given in Figure 5.2.1 are approximate since the hydrocarbon peak, usually used as reference, is the smallest component in the C_{1s} envelope and therefore the most difficult to locate. Two Gaussian components were used to represent hydrocarbon contributions. The hydrocarbon component at higher binding energy probably arises from contamination lying on the surface of the plasma polymer since its intensity increased in relation to the other components at higher take-off angle (*i.e.* at greater surface sensitivity, see Appendix). The hydrocarbon component at lower binding energy probably arises from contamination on the surface of the substrate and lying underneath the plasma polymer. Hydrocarbon on the surface of the plasma polymer is likely to suffer from greater charging, and consequently appear at higher binding energy, since it is insulated from the conducting substrate by the plasma polymer. Two hydrocarbon components have previously been assigned in the C_{1s} spectra of plasma polymerized perfluoro-2-butyltetrahydrofuran.[1g]

5.2.1.2 Electrochemistry of electrodes coated with plasma polymerized PFCP

Platinum flag electrodes coated with plasma polymerized PFCP were potentiostatted at -1.5V in solutions of (a) 0.1M $LiClO_4/CH_3CN$ and (b) 0.1M tetrabutylammonium perchlorate (TBAP)/CH_3CN. Figure 5.2.3 shows that whereas a rising current-time plot is observed in TBAP solution, essentially no current flaws in $LiClO_4$ solution. Increasing the potential to -2.0V in $LiClO_4$ produced negligible increase in current. C_{1s} ESCA spectra for the coated electrodes after electrolysis are shown in Figure 5.2.4. The sample potentiostatted in $LiClO_4$ solution is identical to that for freshly prepared plasma polymerized PFCP. The C_{1s} spectrum for the electrode potentiostatted in TBAP solution is dominated by low binding energy components. Moreover an N_{1s} signal at *ca.* 402eV, a binding energy typical of R_4N^+, was found for this sample. C_{1s} spectra recorded at an increased take-off angle show an increase in the relative contribution of the low binding energy components for the sample treated in TBAP. This indicates that the plasma polymer was modified on its outermost surface only. Since the modified layer is thinner than the ESCA sampling depth the C_{1s} spectrum will contain contributions both from this modified layer and the underlying, unmodified plasma polymer. Therefore, peak area ratios may not be used to derive true stoichiometries for either phase. The apparent F/C stoichiometry was 0.6. That the decrease in apparent F/C ratio is caused, at least in part, by the incorporation of R_4N^+ ions is suggested by the N_{1s} spectrum (*vide supra*). From the ESCA spectra alone it is not possible to determine whether defluorination of the

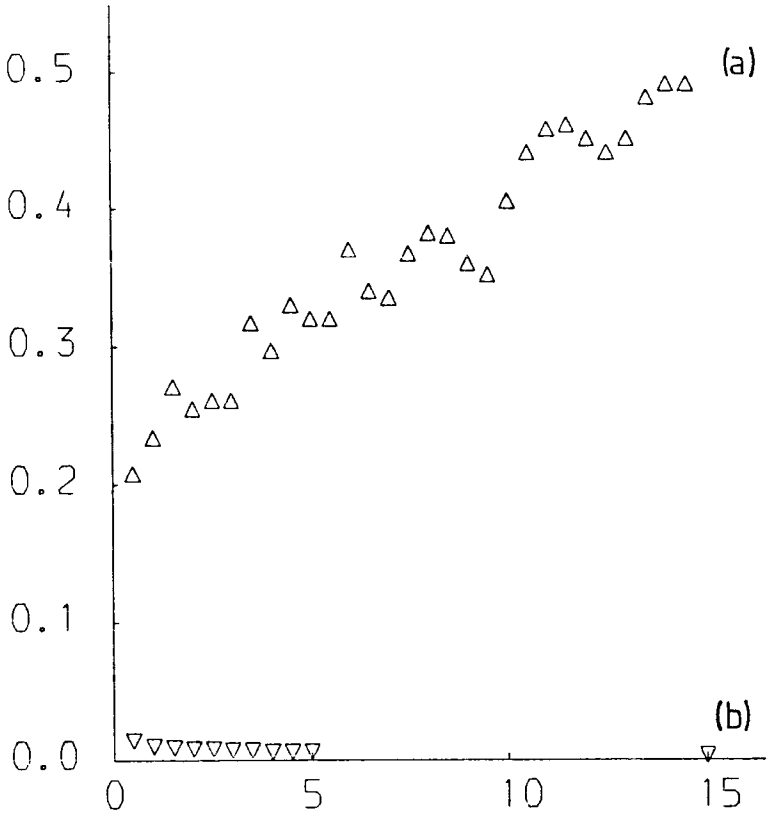

FIGURE 5.2.3 Current (mA, ordinate) *versus* time (mins., abscissa) for plasma polymer coated electrodes potentiostatted in (a) 0.1M/TBAP and (b) 0.1M $LiClO_4$ solutions

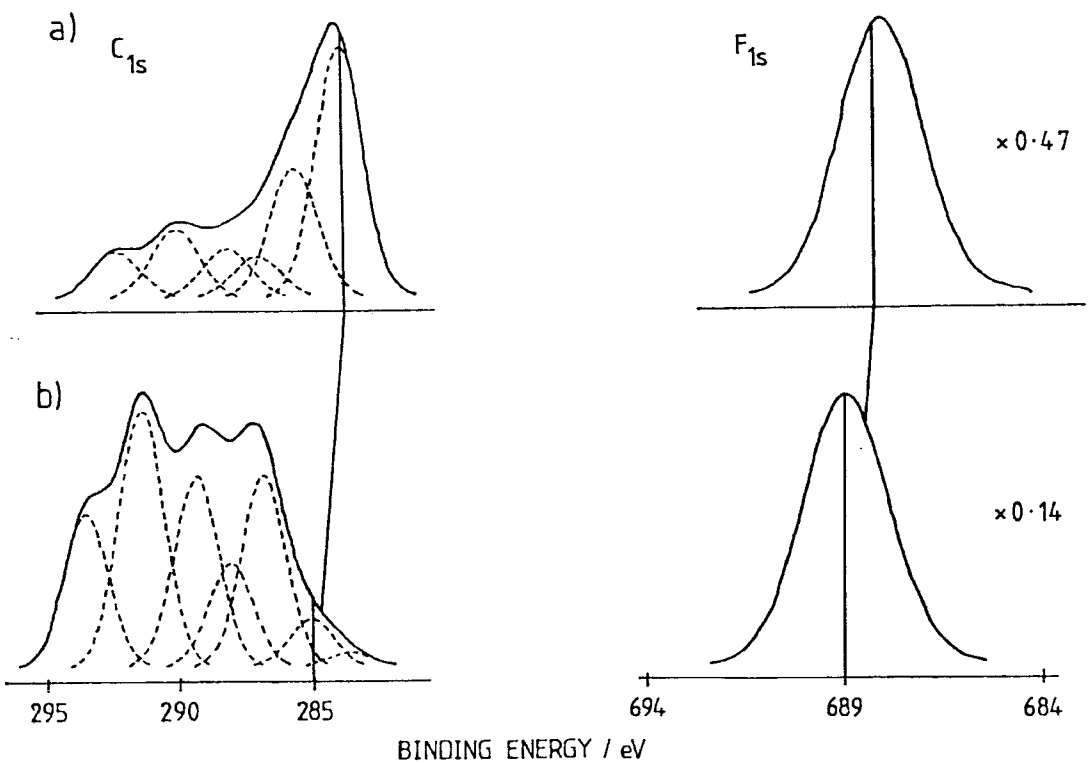

FIGURE 5.2.4 C_{1s} and F_{1s} ESCA spectra for plasma polymer coated electrodes potentiostatted in (a) 0.1M TBAP and (b) 0.1M $LiClO_4$ solutions

plasma polymer also contributes to this decrease. Defluorination is likely, however, since significant current flow (Figure 5.2.3) indicated that the plasma polymer was being reduced. By analogy to the electrochemical reduction of PTFE this might be expected to indicate defluorination.[6] Fluorinated carbanionic species are known to show a tendency to eliminate fluoride ion even when no conventional pathway is available.[16,17]

Similar inhibition of cathodic reductions in $LiClO_4$ solution compared to TBAP have been reported. Silvester found that monomeric PFCP formed an electrode deposit in TBAP/DMF but not in $LiClO_4$/DMF.[3] Van Tilborg *et al*[18] found that acetophenone could not be reduced in LiF/dry acetonitrile but that the addition of small amounts of R_4NF to the solution produced intense acetophenone reduction waves. Van Tilborg *et al* attempted to rationalize this anomaly in terms of increased carbonyl bond polarization when R_4N^+ electrolytes were used.

Cyclic voltammograms of plasma polymerized PFCP films at potentials positive of 0V were featureless in both electrolyte systems. When a gold electrode was used as substrate successive potential cycles showed increasing gold oxidation waves indicating imperfect passivation by the film or its removal from the electrode surface.

5.2.2 Electrodeposition from PFCP

5.2.2.1 Appearance of the deposits, microscopy

Electrode deposits were formed by controlled potential reduction, at -1.5V, of PFCP solutions in DMF which were saturated in tetramethylammonium bromide (TMAB), 0.1M in tetraethylammonium perchlorate (TEAP), 0.1M in TBAP or 0.1M in tetrahexylammonium iodide (THAI). Before drying the deposits formed from all electrolyte solutions appeared dark blue or black. After washing and drying only samples deposited from THAI solution were black. Deposits formed from TBAP solution were either blue or lustrous and bronze coloured. Those formed from TMAB solution were bronze. A sample of the deposit formed from TEAP solution and removed from the electrode onto semitransparent adhesive tape appeared blue in transmitted light but bronze in reflected light (see Figure 5.2.5). Bronze, blue and black colours have been reported for metal (M) intercalation compounds of graphite of varying intercalation ion density (see Table 5.2.3).[6]

Brewis *et al* report that the product of electrochemically reduced PTFE has a brassy lustre.[6]

Under otherwise constant electrolysis conditions the amount of material deposited on the electrode increased with increasing alkyl chain length of the electrolyte cation. From THAI solution deposits up to *ca.* 1mm thick could be grown. From TEAP solution films several μm thick could be formed. Deposits formed from TMAB solution did not completely cover the electrode but rather formed in islands several μm thick.

TABLE 5.2.3 Colours of graphite intercalation compounds[6]

Intercalation density	Colour
C_8 - C_{12} M	bronze
C_{24} - C_{30} M	violet or blue
C_{30+} M	black

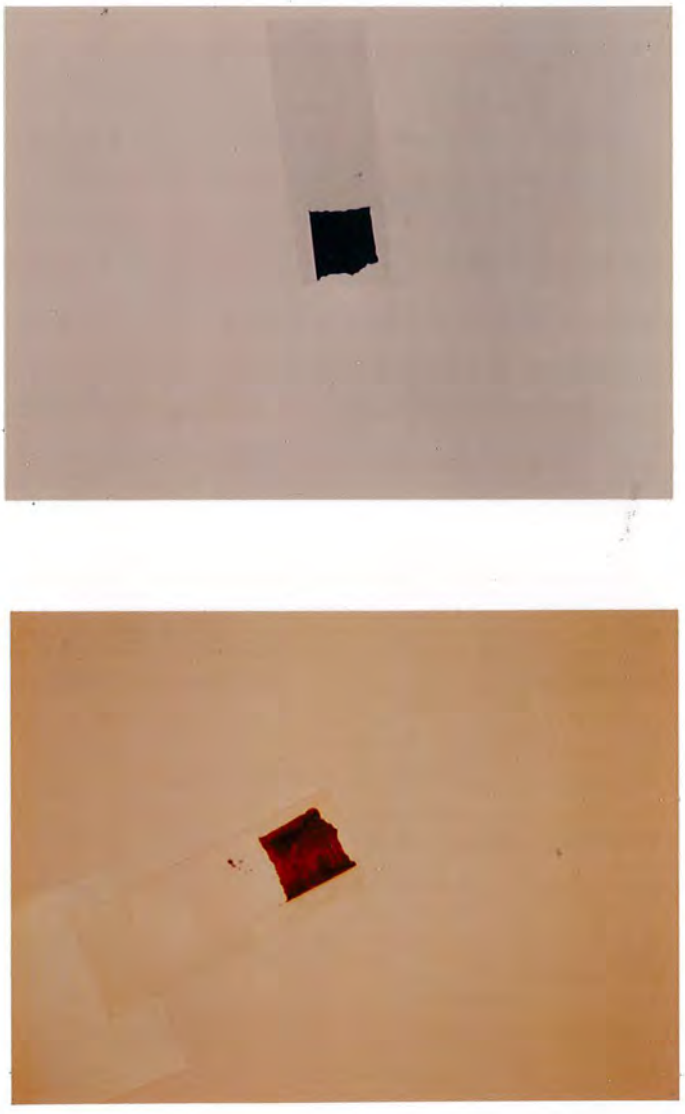

FIGURE 5.2.5 A sample of the deposit viewed in (a) transmitted light and (b) reflected light

It is likely that upon immediate removal from the electrolysis cell the deposits are swollen by solvent since:

(i) all the deposits, except those formed from THAI solution appeared considerably thicker when solvent wetted than when dry;

(ii) dried deposits formed from TMAB and TEAP solutions appeared bronze but appeared blue when solvent wetted. This dry/wet colour change was reversible and was not restricted to the use of DMF as wetting solvent.

Optical micrographs for deposits formed from the various electrolyte solutions onto gold flag electrodes are shown in Figure 5.2.6. The deposit formed from TMAB appears to form along macroscopic defects on the electrode surface. A scanning electron micrograph of the deposit formed from TEAP solution is also shown; the uneven topography is apparent. The deposit was conductive enough not to require gold coating in order to obtain the electron micrograph.

Scanning electron microscopy was also used to measure the film thickness of a deposit formed from TEAP solution onto a gold coated glass slide. The slide was fractured and the fracture edge thickness of the film determined to be 4μm ± 1μm. This value of film thickness was used to calculate a film conductivity of *ca.* $10^{-3}(\Omega cm)^{-1}$ from a linear plot of current against applied potential for other samples formed under identical conditions.

x 10

a

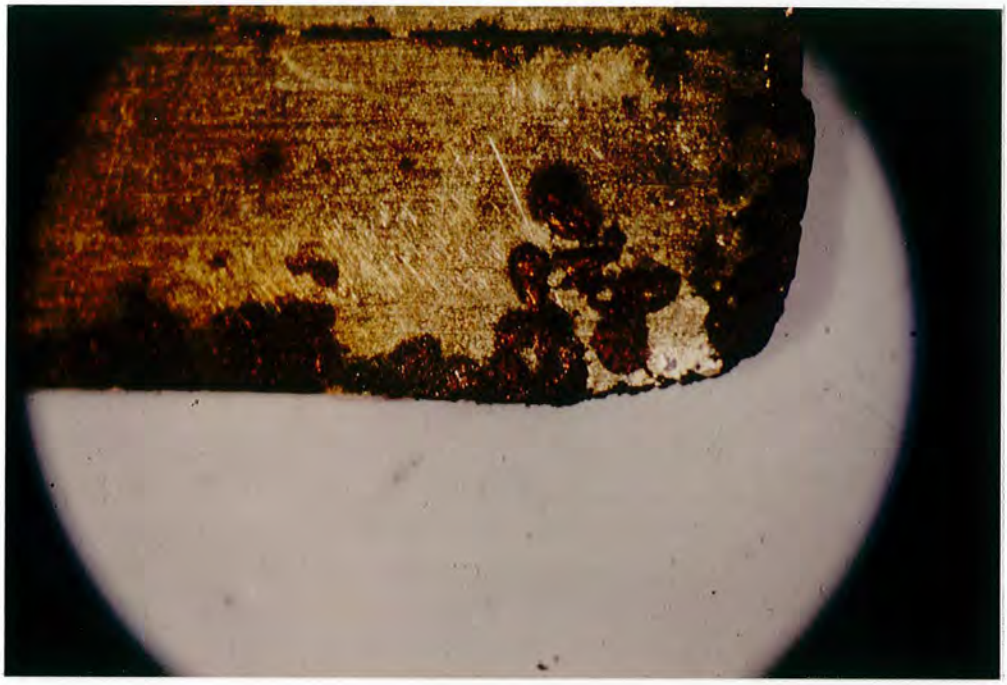

b

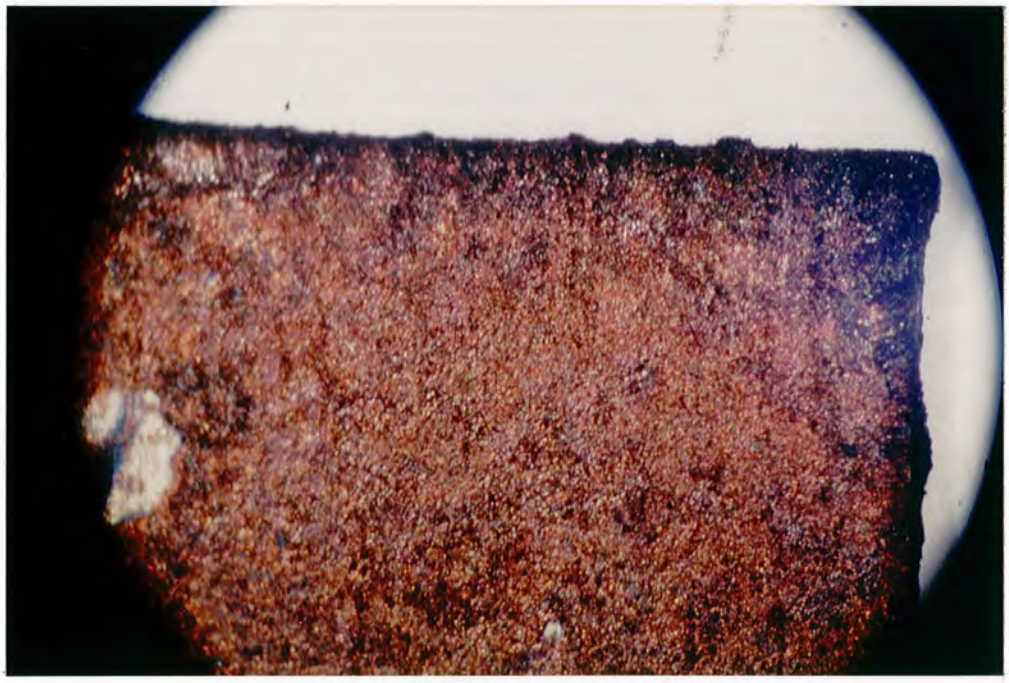

FIGURE 5.2.6 Optical micrographs for deposits formed from (a) TMAB, (b) TEAP, (c) TBAP and (d) THAI electrolytes solutions. A SEM of the sample formed from TEAP solution is also shown.

x10

c

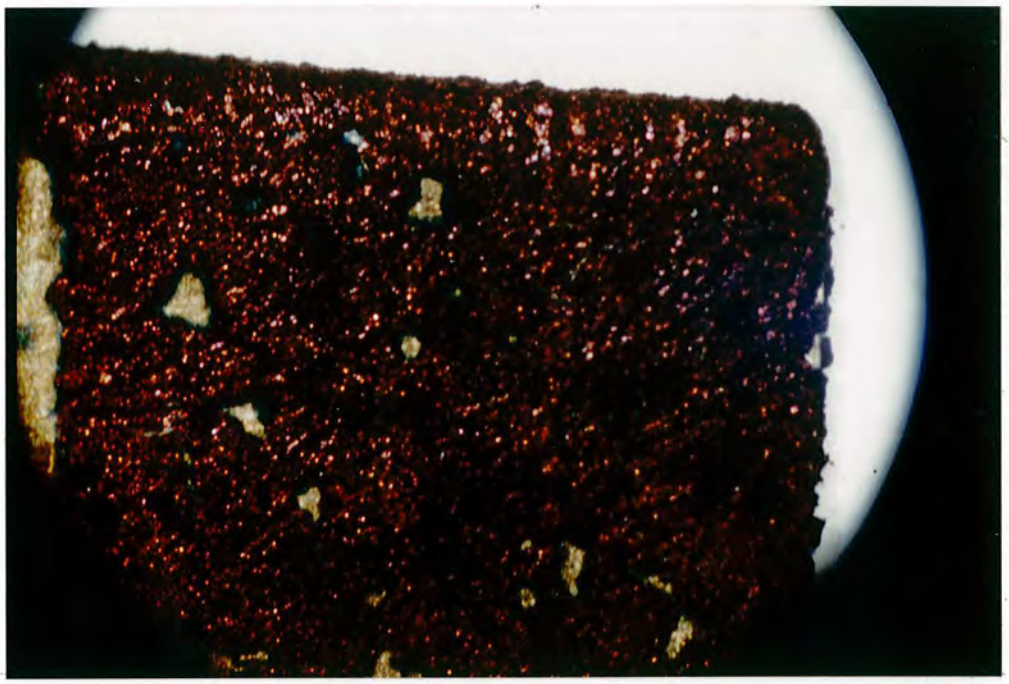

d

FIGURE 5.2.6 (contd.)

SEM

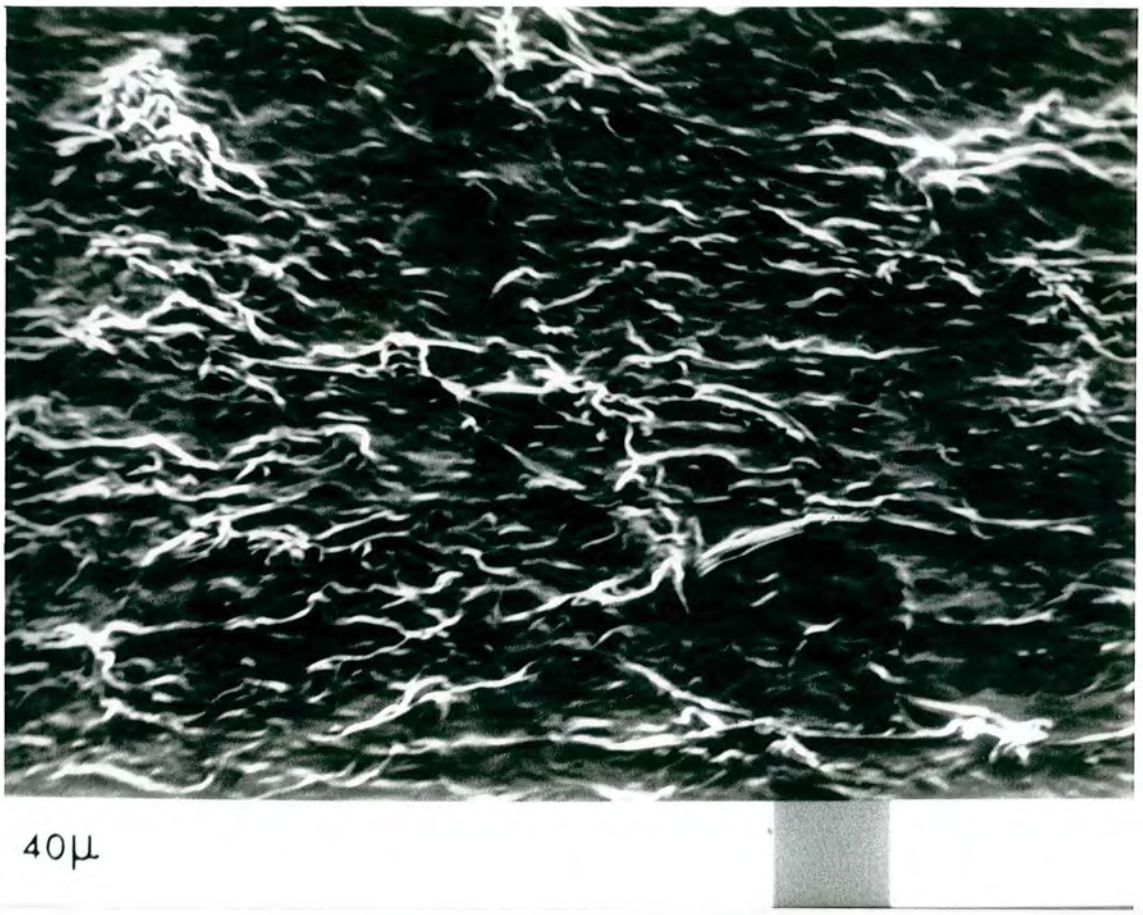

FIGURE 5.2.6 (contd.)

5.2.2.2 Elemental analysis

The results of elemental C, H, N microanalysis for a deposit formed from DMF/TEAP solution are shown in Table 5.2.4. The % F is obtained by deduction. ESCA shows that the surface C/O stoichiometry is *ca.* 10 (*vide infra*). The surface oxygen content is likely to be higher than the bulk and so the assignment of residual mass to fluorine is probably a valid procedure.

TABLE 5.2.4 Elemental microanalysis

	C	H	N	F[a]
% Mass found	44.3	2.33	1.66	51.7
Atomic Ratio	31.1	19.5	1	23.0

a. % F = 100-(%C + %H + %N)

If the tetraethylammonium ion was the only source of N and H in the deposit a H/N ratio of 20 would be expected, as found. If the tetraethylammonium is incorporated in the deposit 8 of the 31 C atoms in Table 5.2.4 derive from this ion leaving 23 derived from PFCP. This leaves a C/F ratio of unity implying that 3 fluorines are lost per monomer if all the carbon from PFCP is retained in the deposit. If the deposit is assumed to consist of a C_1F_1 matrix, derived from PFCP, associated or intercalated with $(CH_3CH_2)_4N^+$ ions, the intercalation density is one cation for every 23 matrix C atoms. This is the same intercalation density as that reported by Brewis *et al* for electrochemically reduced PTFE.[6]

5.2.2.3 ESCA analysis

Figure 5.2.7 shows C_{1s} spectra for electrode deposits produced by cathodic reduction of PFCP in DMF solutions containing TEAP, TBAP or THAI. Spectra for TMAB grown deposits are not shown since no sample which completely covered the electrode was obtained. It is clear that changing the electrolyte has an effect on the shape of the C_{1s} envelope for the resulting electrode deposit, this point is discussed below.

All the deposits contained nitrogen and gave N_{1s} spectra which were centred at *ca.* 402eV, a binding energy typical of tetraalkylammonium cations (see Chapter Two). For the remainder of the discussion it is assumed that all the nitrogen detected in the deposits arises from R_4N^+ ions. Although the N_{1s} spectra strongly suggest that this assumption is correct, they cannot be considered as unqualified proof of its validity.

All the samples gave F_{1s} peaks centred at *ca.* 688eV. The F_{1s} spectrum for a sample deposited from TEAP solution is typical of the rest and is shown in Figure 5.2.8. The binding energy is at least 1eV lower than that found for the plasma polymers derived from PFCP. A shift of the F_{1s} position to lower binding energy has previously been shown to be an indication of defluorination.[20] Clark and Abrahman have shown that the F_{1s} peak occurs at progressively lower binding energies with decreasing F/C stoichiometry for a series of plasma polymers.[1i] The F_{1s} peak position was found to be similar for deposits prepared from all four tetra-

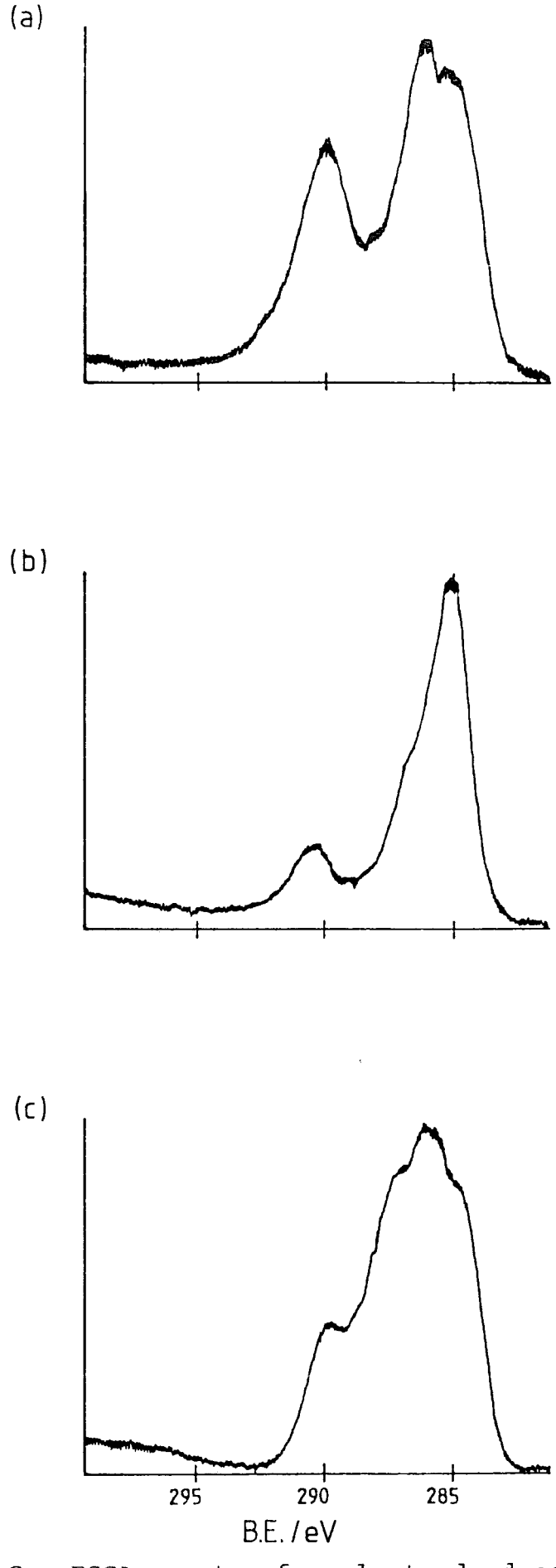

FIGURE 5.2.7 C_{1s} ESCA spectra for electrode deposits produced by cathodic reduction of PFCP in DMF solutions containing (a) TEAP, (b) TBAP and (c) THAI.

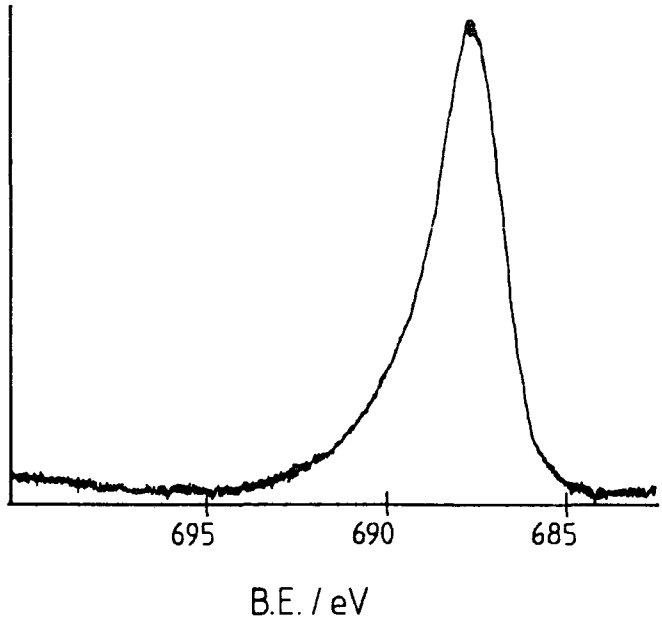

FIGURE 5.2.8 F_{1s} spectrum for a deposit formed from TEAP solution. The asymmetric peak shape is apparent.

alkylammonium electrolyte solutions, which suggests that a similar level of defluorination occurs in each case.

Table 5.2.5 lists C/F, C/N and C/O stoichiometries for deposits produced from TEAP, TBAP and THAI electrolyte solutions. For deposits formed from THAI solution the N_{1s} signal was so small that no accurate estimate of the C/N stoichiometry could be attempted. Moreover these deposits

TABLE 5.2.5 Surface stoichiometries

Electrolyte	C/F	C/N	C/O
TEAP[a]	1.9	25	10
TBAP[a]	2.8	30	10
THAI	4.2	-	1.6

a. Surface stoichiometries are average values derived from several samples.

contain more surface oxygen than fluorine and it must be concluded that for these samples most of the C_{1s} intensity which

occurs at binding energies greater than 285eV arises from oxygenated and not fluorinated carbon atoms. The reason for this unusually high oxygen content is not clear but the greater film thickness and its physical appearance (see Figure 5.2.6) further distinguish the THAI formed deposit from the others.

If for the TEAP and TBAP grown samples 8 and 16 carbon atoms respectively are associated with one nitrogen atom in a tetraalkylammonium cation then the residual carbon may be used to calculate a new C/F stoichiometry which should represent that of the material derived exclusively from PFCP. A value of 1.3 is obtained in each case. This is higher than that obtained by bulk elemental analysis of a TEAP deposit (Section 5.2.2.2); the discrepancy may be due to surface hydrocarbon contamination. Dousek *et al* also found an increased carbon content for the surface compared to the bulk for PTFE reduced by Lithium amalgam.[13]

The ratio of the residual carbon to total nitrogen should give the concentration of R_4N^+ ions in the deposit. Values of 17 and 14 matrix carbon atoms to one R_4N^+ ion are derived for the samples formed from TEAP and TBAP solution respectively. This is a higher cation incorporation level than found by elemental analysis (Section 5.2.2.2).

Both the C_{1s} and F_{1s} spectra (Figures 5.2.7,8) show skewed tails to the high binding energy side of the main peak(s). Asymmetry such as this is observed in the ESCA spectra of metals.[21,28]

Component analysis of the C_{1s} spectra is non-trivial for the following reasons:

(i) the peak shapes appear to be asymmetric and therefore not well represented by Gaussian curves;

(ii) although component analysis of highly fluorinated organic materials is well established[1] component analysis of lightly fluorinated materials is not routine. The same component positions that were used for plasma polymerized PFCP may not be used with confidence for the electrochemical deposit since the chemical shifts for the lightly fluorinated material are likely to be smaller. Dilks has shown that the $\underline{C}F_2$ peak for PTFE occurs at 292.2eV whereas the same component in polyvinylidenefluoride $+CF_2-CH_2+_n$ occurs at 290.8eV.[22]

(iii) $C-N^+$ and C-O functions are likely to occur at similar binding energies to $\underline{C}$-CF. More highly oxygenated carbon atoms are likely to give C_{1s} components at similar binding energies to CF.

Problems in curve fitting for some fluorographite samples were found by Clark *et al.*[30]

Despite these difficulties a crude attempt to curve fit the C_{1s} spectra of the deposits formed from TEAP and TBAP solutions is shown in Figure 5.2.9. Five Gaussian components centred at *ca.* 285.0, 286.7, 288.3, 290.0, 291.7eV were used. Signal intensity at 285.0, 290.0 and 291.7eV probably arises from CH or C, CF and CF_2 functions respectively. Signal intensity at *ca.* 286.7eV may arise from $C-\underline{C}F$, C-O or $C-N^+$, whilst that at *ca.* 288.3 may arise from CF or highly oxygenated carbon functions. The curve fitting procedure, though crude, illustrates two points:

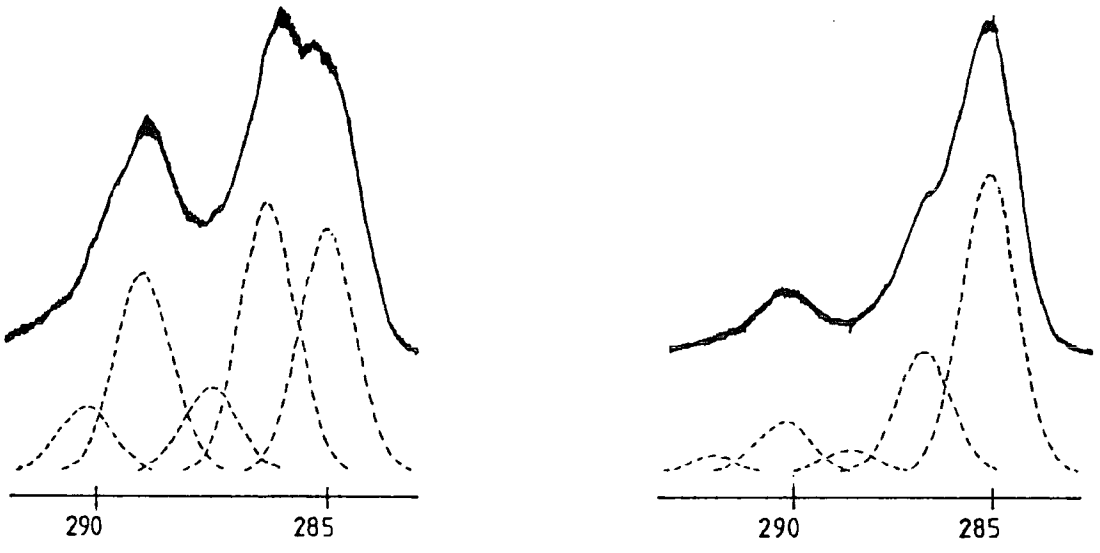

FIGURE 5.2.9 Curve fitted C_{1s} spectra for the deposits formed from (a) TEAP, (b) TBAP solutions

(i) for the deposit formed from TEAP solution the components at 285 and 286.7eV are of similar size. For the TBAP deposit the 285eV component is more than twice the size of that at 286.7eV. This increase would be expected if R_4N^+ cations are incorporated into the deposit;

(ii) although the C/F stoichiometry† may be *ca.* 1 it appears that CF is not the only fluorocarbon function present in the deposits. A significant proportion of CF_2 and by implication C not directly bonded to F is suggested.

The spectra obtained for deposits formed from TBAP and TEAP solutions were, within experimental error, invariant with deposition time over the range 2-10 minutes. Deposition over a 3 hour electrolysis in a stirred, two compartment 'H' cell resulted in a thinner deposit than that formed over a few minutes. Moreover the catholyte became intensely blue coloured suggesting that most of the product of extended electrolysis is soluble. This and the uncertainty in the monomer concentration caused by its high volatility (see Sec.5.3)

† For material derived from PFCP only, i.e. excluding R_4N^+ contributions.

prevent the determination of n, the number of electrons transferred in the deposition reaction, by exhaustive coulometry. The thin deposit formed by 3 hour electrolysis in TEAP solution had a C/F surface stoichiometry of *ca.* 5.

It was possible to produce electrode deposits by reduction of PFCP in CH_3CN/TEAP solution, but only on increasing the electrode potential to -1.7V. Even at -1.9V the amount of material deposited was less than that deposited from DMF solution at -1.5V and otherwise constant electrolysis conditions. The deposits produced from CH_3CN solution appeared similar to those formed from DMF and gave qualitatively similar C_{1s}, F_{1s} and N_{1s} spectra. The C/F stoichiometry was 2.1 whilst the C/N was *ca.* 24. These figures agree well with the values for deposits formed from DMF solution. It may thus be concluded that although deposition is inhibited in CH_3CN compared to DMF the chemical nature of the deposit appears unaffected.

As reported by Silvester[3] no visible deposit could be obtained by attempted cathodic reduction of PFCP in DMF/$LiClO_4$. Negligible current flow was recorded. When the electrode was washed, dried and examined by ESCA it was found to be covered by a coating containing C, F and Li thick enough to obscure the Pt_{4f} signal of the electrode itself. The C_{1s} spectrum was dominated by the 285eV component although some signal intensity at binding energies typical of CF and CF_2 functions was also observed. The C/F and Li/F stoichiometries were 0.88 and 0.86 respectively. The F_{1s} signal was essentially a single component peak centred at 685.8eV. A binding energy as low as this is typical of ionic fluoride.[13,14]

These results suggest that a thin film of approximately 1:1 LiF:partially fluorinated carbonaceous material is deposited. It is possible that the LiF passivates the electrode against further reduction of PFCP.

5.2.2.4 Thermal Stability

Figure 5.2.10 shows a thermogravimetric plot for a sample of the PFCP deposit formed from DMF/TBAP solution. Figure 5.2.11 shows a plot of C/F surface stoichiometry and percentage contribution to the total C_{1s} signal from the component at *ca.* 290.0eV (attributed to CF) against temperature for a sample of the same deposit heated inside the ESCA spectrometer. Little decomposition occurs at temperatures up to 150°C. Above this temperature fluorine is lost. The C/N stoichiometry remained almost constant at *ca.* 25 up to 250°C, at 300°C the C/N stoichiometry had approximately doubled. The C/O surface stoichiometry remained constant throughout the experiment at *ca.* 10 but after cooling and exposure to air it halved. Material remaining on the spectrometer probe tip after heating to 400°C was dull grey.

The sample used for the ESCA investigation of thermal stability was cathodically deposited directly onto the cleaned and polished surface of a copper probe tip. During ESCA analysis the copper probe tip was in electrical contact with the spectrometer and zero charging of the deposit was found. This result confirms the conclusion drawn from resistance measurements that these deposits are not electronic insulators.

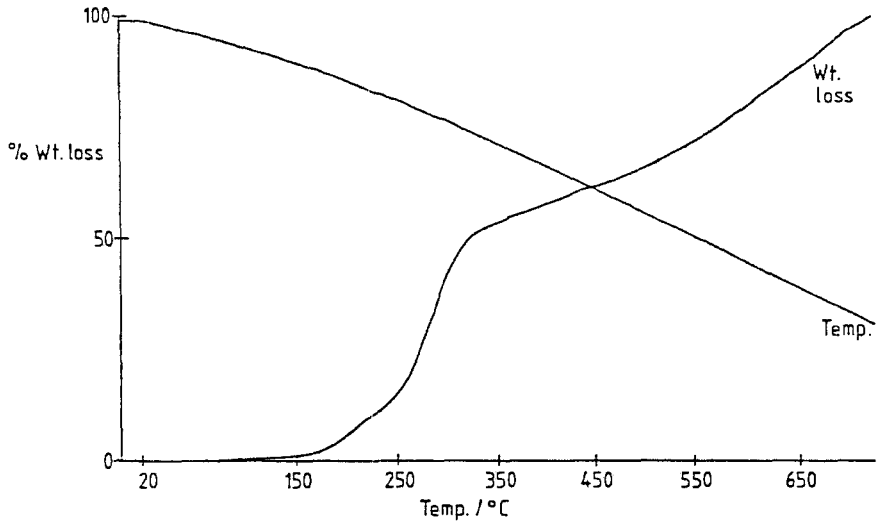

FIGURE 5.2.10 Thermogravimetric trace for a sample of PFCP deposit formed from DMF/TBAP solution.

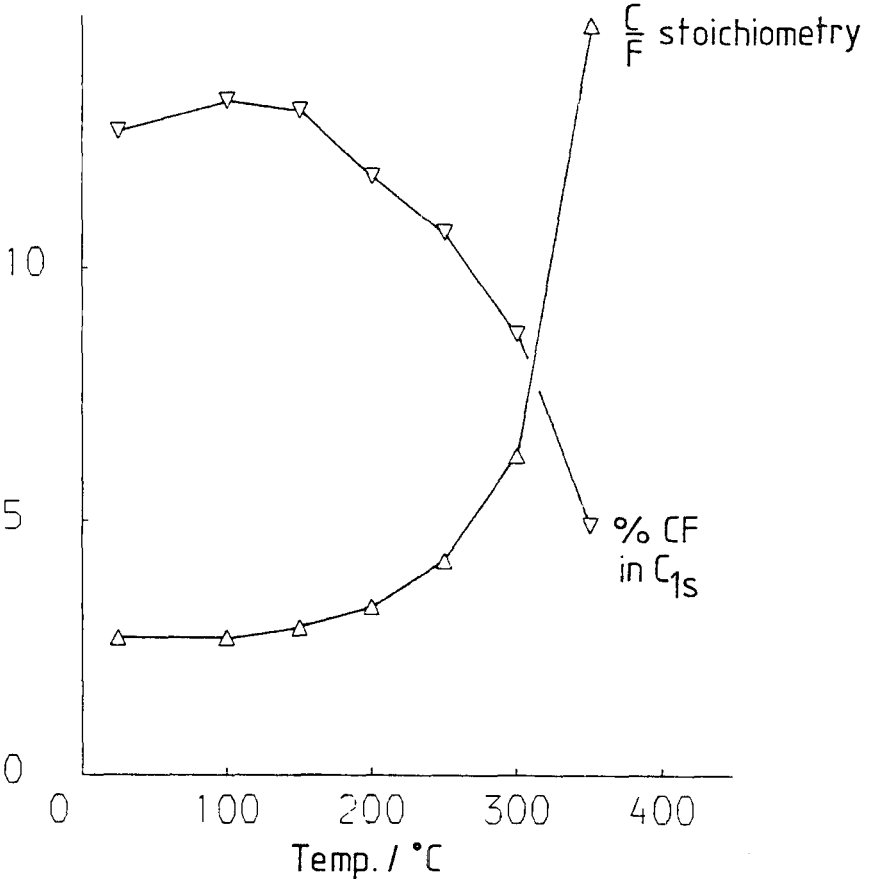

FIGURE 5.2.11 Temperature dependence of surface composition as determined by ESCA (see text)

5.2.2.5 Electrochemical experiments

(a) Cyclic Voltammetry

Silvester reported cathodic electrodeposition from PFCP solutions under potentiostatic conditions.[3] Figure 5.2.12 shows initial sweep cyclic voltammograms for cathodic electrodeposition from PFCP solutions in (a) DMF/TEAP, (b) DMF/TBAP and (c) DMF/THAI. An irreversible reduction peak is observed.

For the portions of the voltammograms between the points labelled a and b the cathodic current is greater on the reverse sweep than the forward; a and b are termed cross over points. Such features are typical in metal depositions from a salt solution onto a foreign cathode material.[23] Their occurrence in such systems is caused by the nucleation overpotential required to deposit the metal on the foreign electrode material.[23] As a result of this overpotential deposition continues (onto material already deposited) at potentials positive of that required to induce deposition on the bare electrode. For subsequent CV scans (Figure 5.2.13) the cross over features disappear further suggesting that they are caused by nucleation overpotential. Cross over points have been observed in the cyclic voltammograms of substituted pyrroles which form electrode coatings.[24]

Two features are noteworthy in the repeat scan CVs shown in Figure 5.2.13:

(i) the background current level between OV and *ca.* -1.OV increases with cycle number. This behaviour is analogous to the O to *ca.* + O.8V CV behaviour during polypyrrole electrodeposition and is probably caused by non-Faradaic charging of the growing film.

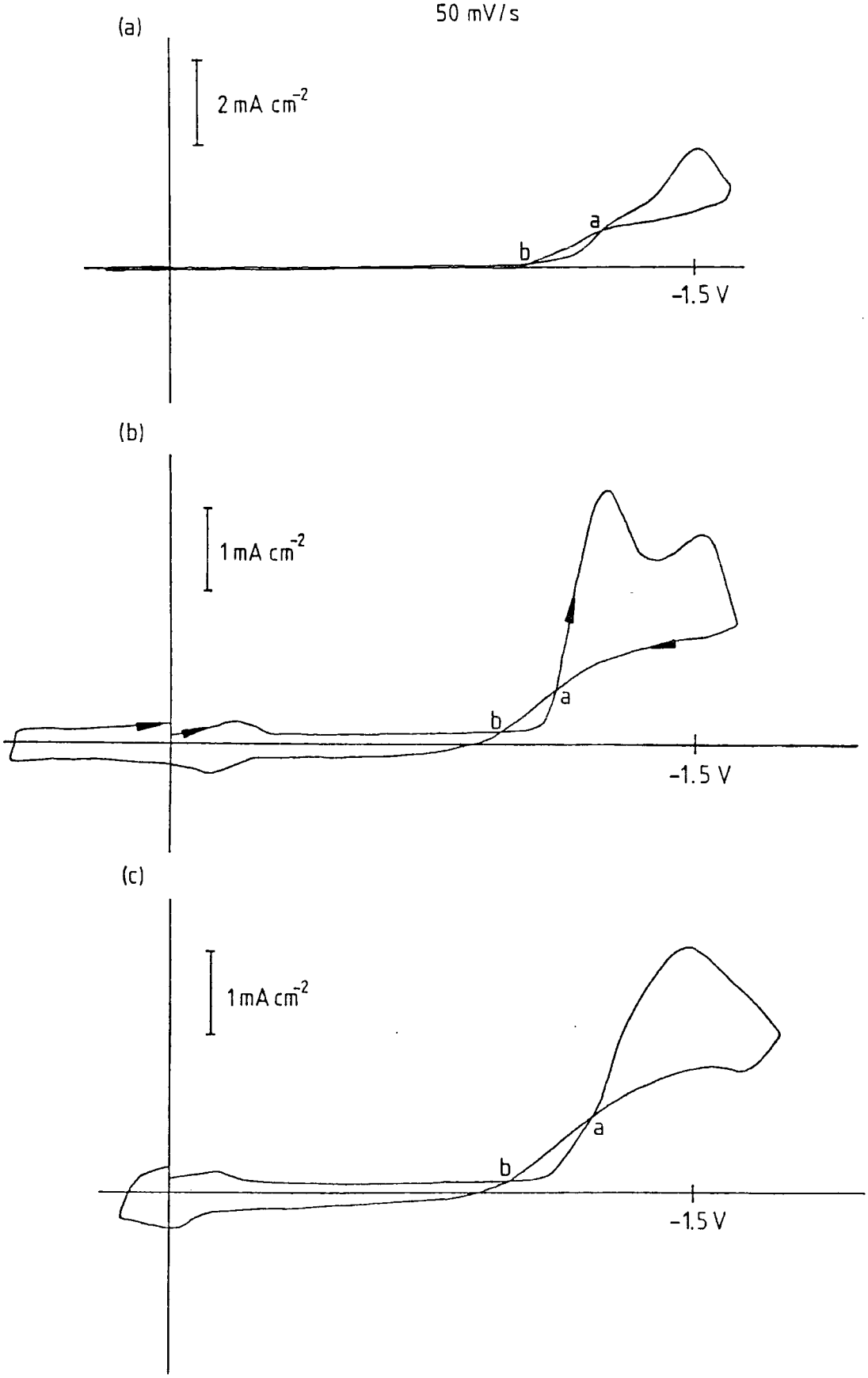

FIGURE 5.2.12 Cyclic voltammetric deposition from PFCP solutions

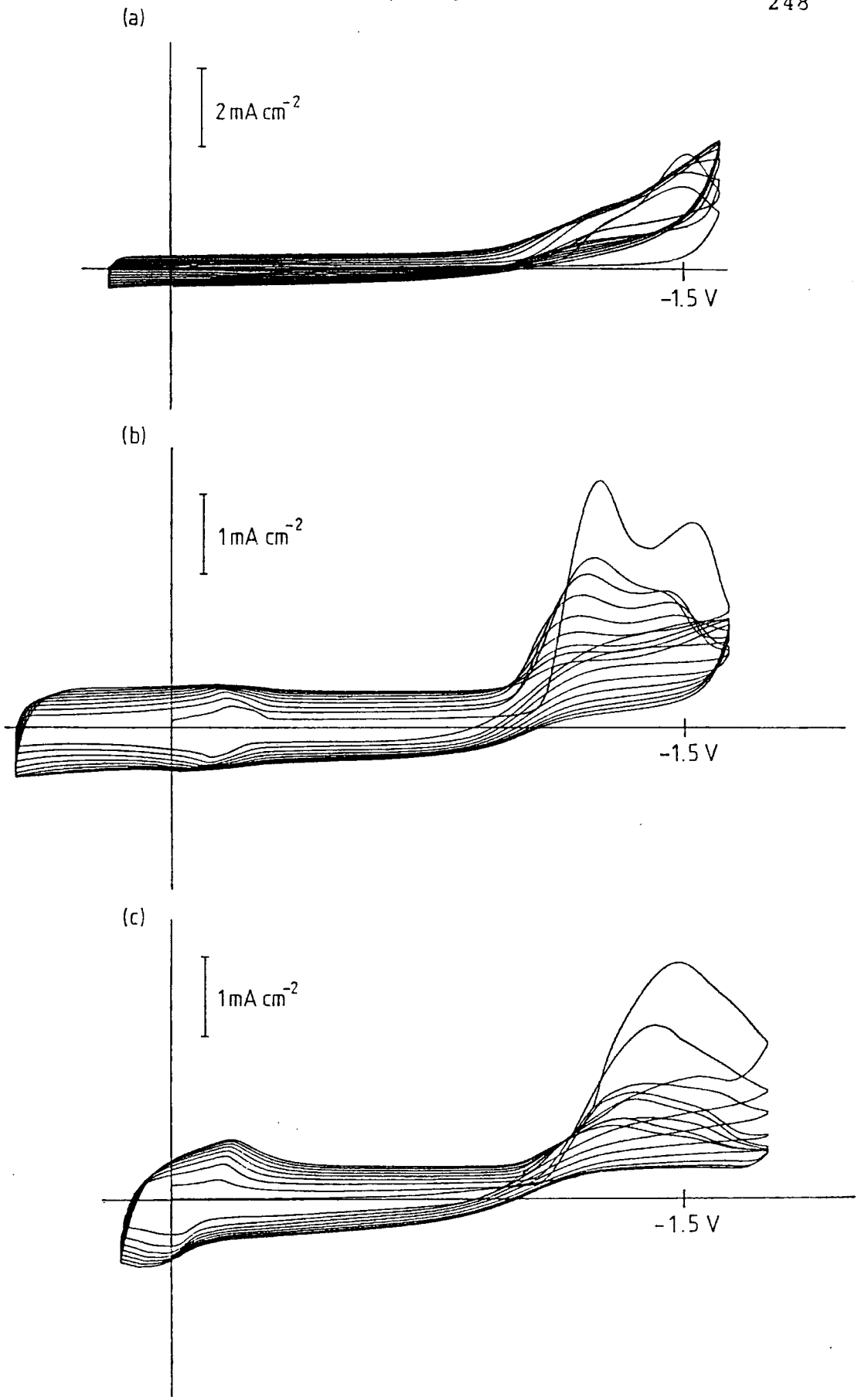

FIGURE 5.2.13 Cyclic voltammetric deposition from PFCP solutions

(ii) In the TBAP and THAI electrolyte systems a quasi-reversible wave fractionally negative of OV may be observed. It is possible that this feature is caused by a reversible intercalation reaction (*vide supra*). Similar features have been observed for both electrochemically reduced PTFE[6] and electrochemically intercalated graphite electrodes,[10] however the electrode potential in these cases is $\leq$ -1V. If this feature is due to a reversible intercalation reaction it is surprising that it is not observed in the TEAP electrolyte system. Furthermore the wave is not retained for a deposit grown in TBAP solution and then retested in a monomer free solution. Instead the CV shown in Figure 5.2.14 was obtained.

A cyclic voltammogram of perfluorocyclohexene in DMF/TBAP showed no increase in background current with cycling and no electrode deposit was formed.

When an electrode coated with a PFCP deposit was examined by CV in a ferrocene containing solution the ferrocene/ ferricenium wave was found to be of greater integrated peak

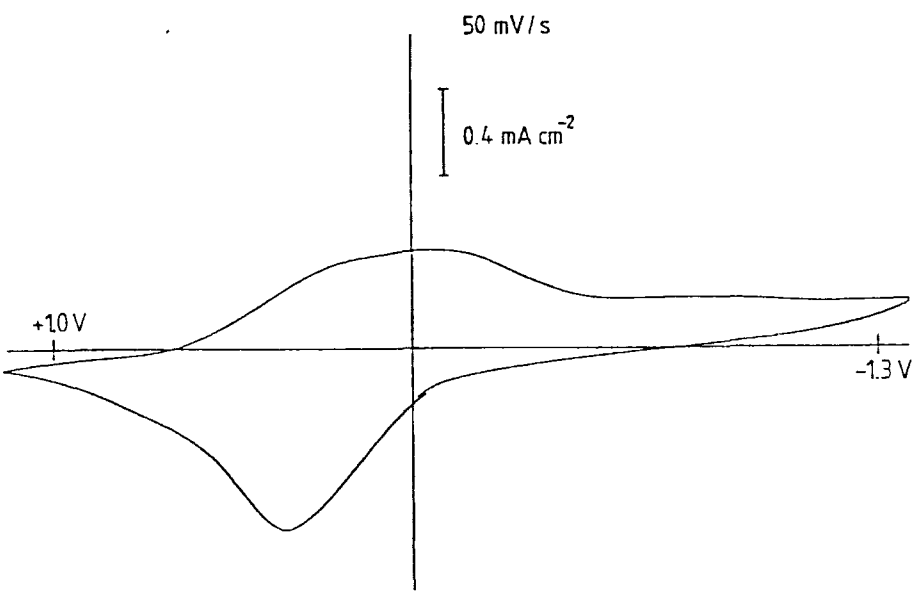

FIGURE 5.2.14 CV for PFCP deposit in inert solvent and electrolyte. Sweep rate = 50 mV/s.

current, allowing for contributions from the coating itself, than when using the naked electrode. The deposit may be porous to ferrocene but a larger peak current on the coated electrode suggests that the deposit is sufficiently electronically conducting to allow ferrocene oxidation on its outer surface which will be of greater area (see Figure 5.2.6) than the uncoated electrode.

(b) Chronoamperometry

Shown in Figure 5.2.15 are current-time (i-t) curves obtained for the cathodic deposition from PFCP solutions in DMF/TEAP and CH_3CN/TEAP, following the application of a $0 \rightarrow -1.7V$ potential jump. Similar curves were obtained for deposition from DMF/TBAP and CH_3CN/TBAP solvent/electrolyte systems. Table 5.2.6 gives the time taken for the current to peak following the voltage jump (t_{max}). The approximate charges contained under the peaks, using an estimated linear background subtraction, are also listed. Negligible current was observed to flow in the voltage jump experiment when DMF/$LiClO_4$ was used as solvent/electrolyte.

TABLE 5.2.6.

Solvent/electrolyte	t_{max}/S [a]	average peak area/ Coulombs [b]
DMF/TEAP	0.7 - 1.2	2.2×10^{-7}
CH_3CN/TEAP	8 - 12	1.1×10^{-7}
DMF/TBAP	1.6 - 2.5	1.6×10^{-7}
CH_3CN/TBAP	38 - 66	5.1×10^{-7}

a. The values indicate the range obtained by experimental repetition.

b. Electrode diameter = 1.5mm.

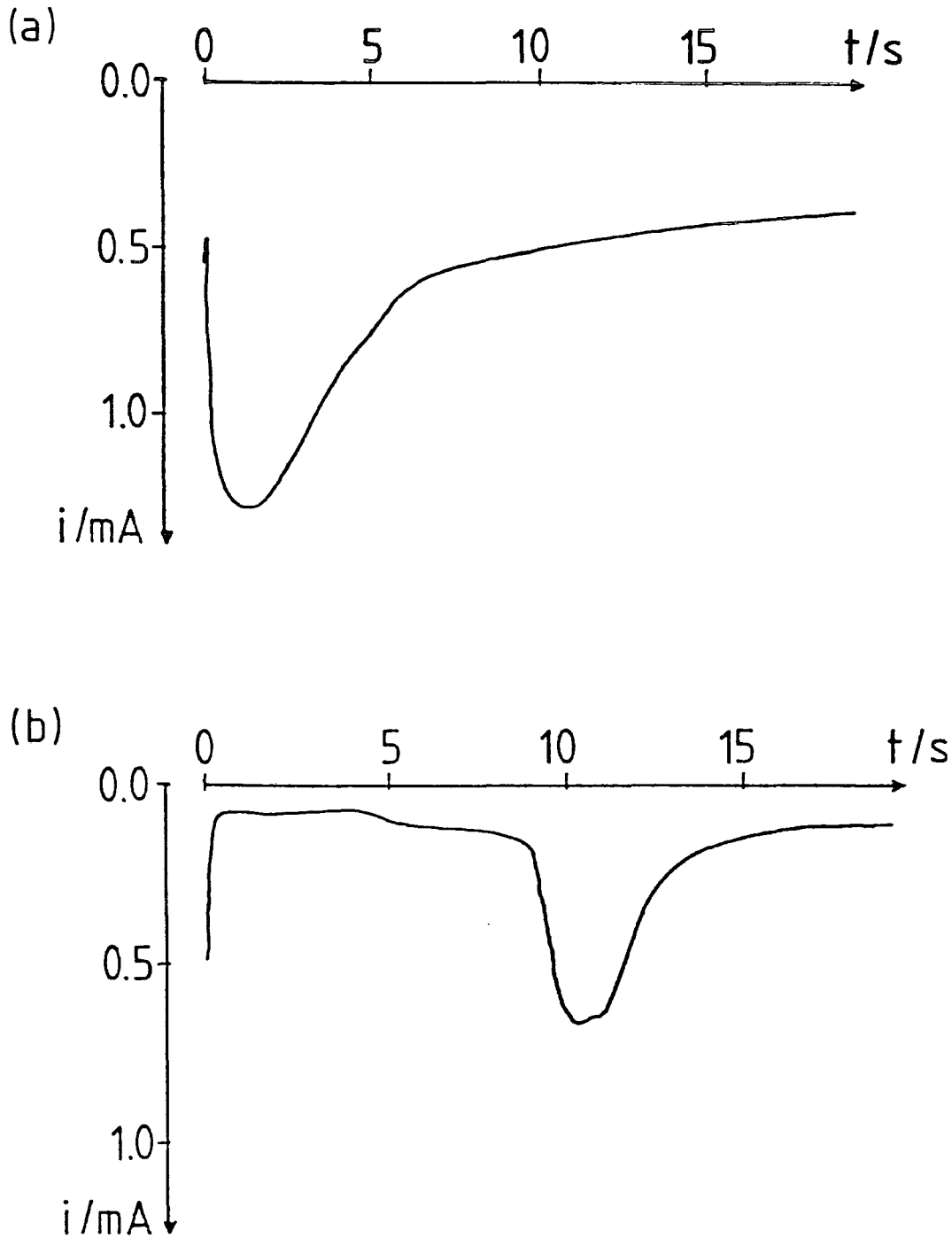

FIGURE 5.2.15 Current time (i-t) curves obtained for the cathodic deposition from PFCP solutions in (a) DMF/TEAP and (b) CH_3CN/TEAP, following the application of a 0→-1.7V potential jump.

The peaked i-t curves shown in Figure 5.2.15 resemble those obtained in electrocrystallization experiments where deposition of a new phase on the electrode surface involves nucleation.[25] An i-t curve with a less defined peak than those shown in Figure 5.2.15 has been attributed by Genies *et al* to nucleational film growth for polypyrrole.[26]

Electrochemical phase formation may be two dimensional (monolayer formation) or three dimensional and models to treat both cases have been presented.[25] It should be emphasized that all treatments of electrochemical phase formation consider single crystal electrodes whereas in the present study a polished gold electrode with a polycrystalline surface was used.

The magnitude of the charges given in Table 5.2.6 indicate that three dimensional nucleation is taking place. Inspection of an electrode after a single voltage jump experiment revealed the presence of a visible deposit.

Nucleation may be instantaneous, when the number of nuclei or growth centres does not increase during formation of the new phase, or progressive, when in the absence of coalescence the number of growth centres increases linearly with time.[25] Furthermore, true three dimensional electrocrystallization may be subject to lattice control or diffusion control. In the former case, the rate determining step is incorporation of material into the lattice whereas in the latter, it is diffusional mass transport to the electrode. Under diffusional control the occurrence of a peak in the i-t curve may be explained phenomenologically. At short times following the

voltage pulse, several independent growth centres each with an associated diffusional field will exist. As the surface area of each growth centre expands, the current will increase. Coalescence of the diffusional fields will eventually cause the current to decrease with time and at long times after the voltage pulse, the current may be approximated to that predicted by the Cottrell equation for semi-infinite diffusion to a continuous planar surface.

$$i = \frac{nFD^{\frac{1}{2}}C^{\infty}\mathbf{A}}{\pi^{\frac{1}{2}}\ t^{\frac{1}{2}}}$$

A theoretical treatment of three dimensional phase growth subject to lattice control using hemispheres as the model growth centres predicts that the peak current is *ca.* 1.3 times greater than the limiting current.[27] The traces shown in Figure 5.2.15 clearly indicate that for PFCP experiments the peak current exceeds the limiting current by a factor significantly greater than 1.3.

The number of electrons involved in the deposition reaction, n, was not, for the reasons previously stated, determined by exhaustive coulometry and remains unknown. If the C/F stoichiometry of unity†, derived from bulk elemental analysis, is accepted as correct for the electrode deposit and it is assumed that carbon is not eliminated in the deposition process then three fluorines are lost per monomer. If one electron is transferred for each fluorine lost and further reduction of the deposit in any putative intercalation reaction is ignored then a value for n of three is obtained. If any contribution to the charges listed in Table 5.2.6 due to non-Faradaic processes may be ignored then the apparent molar

† For material derived from PFCP only

coverage, Γ_{app}, corresponding to the i-t peak areas may be calculated from

$$\Gamma_{app} = \frac{Q}{nFA}$$

This calculation yields values ranging between $1.1 - 5.1 \times 10^{-7}$ mol cm^{-2}. The deposits formed in single voltage jump experiments appeared thicker than those obtained for the electroactive $Fe(bpypyr)_3^{2+}$ films for which typical molar coverages were of the order 10^{-8} mol cm^{-2}, (see Chapter 3).

The increased time required for the current to peak (t_{max}) in CH_3CN compared to DMF indicates that the solvent has a significant effect on the deposition process. One model for three dimensional phase formation subject to diffusion control suggests that t_{max} is related to the rate constant for phase formation by:[25]

$$t_{max} \propto \frac{1}{k} \quad \text{instantaneous nucleation}$$

$$t_{max} \propto \frac{1}{k^{\frac{1}{2}}} \quad \text{progressive nucleation}$$

Table 5.2.6 suggests that t_{max} for the CH_3CN/TBAP system may be *ca.* 25 times that for the DMF/TBAP system. This would correspond to a rate constant difference of 25 or 725 fold if either of the above proportionalities is valid.

5.2.2.6 Conclusions

The chemical compositions and morphologies of the plasma and electrochemical deposits derived from PFCP are grossly different. The composition of the plasma polymer agrees well with that which would be expected by

analogy to other plasma polymerized fluorocarbon monomers, particularly perfluorocyclohexene.

The electrochemical deposit is similar in many respects to electrochemically reduced PTFE, *viz.* similar colour, chemical composition and electrical conductivity. Despite the fact that ESCA analysis does not straightforwardly lead to functional group characterization, as it does for the plasma polymer, a change in chemical composition with variation of the electrolyte cation has been demonstrated for the electrochemical deposits. Nucleation during electrochemical deposition has also been demonstrated.

5.3 Experimental

5.3.1 Plasma Polymerization

The plasma reactor configuration was the same as that used for neat plasma polymerization of ferrocene monomers (Figure 4.4.1, Chapter Four). PFCP monomer was freeze-thaw degassed on a vacuum line prior to use. The monomer was pumped through the reactor during plasma polymerization; the pressure was set at 0.1 torr before ignition of the plasma by means of an Edwards leak valve connected to the monomer reservoir. Monomer flow rate, determined by the method described in Chapter Four, was 1.67×10^{-7} mole/s.

For ESCA analysis plasma polymers were deposited onto Al foil. Pt flag electrodes were used as deposition substrates when electrochemical experiments were performed prior to ESCA analysis. All plasma polymer samples were taken from the coil region of the reactor. Deposition time was 2 minutes. Smooth, colourless deposits were obtained.

5.3.2 Electrochemical experiments

Controlled potential electrolysis (at -1.5V unless otherwise stated) and cyclic voltammetry experiments were conducted using procedures and equipment described in Chapter Two. The equipment used for chronoamperometry experiments was described in Chapter Three. DMF (Aldrich) was of HPLC quality and transferred under a nitrogen atmosphere. Acetonitrile and electrolyte salts were dried by methods also described in Chapter Two. For ESCA and conductivity analysis deposits were formed onto Au or Cu flag cathodes from solutions which were *ca.* 0.1M in PFCP and 0.1M in supporting electrolyte. For chronoamperometric studies of deposition (at -1.7V) and cyclic voltammetric deposition a BAS gold disc (1.5mm diameter) cathode/working electrode was used; the PFCP concentration was *ca.* 0.05M whilst the supporting electrolyte concentration was 0.2M. PFCP concentrations are doubtless overestimated since the monomer is highly volatile and some of the measured volume of PFCP was observed to evaporate before injection into the electrolysis cell.

Controlled potential electrolyses were usually conducted for 2 minutes.

Before analysis deposits were washed with DMF and acetone and dried on a vacuum line. Conductivity measurements were recorded using the procedure described in Chapter Two.

For ESCA studies of thermal stability the deposit was electrically heated inside the spectrometer *via* feedthrough connections inside the shaft of the Kratos insertion probe.

Thermogravimetric analysis was made using a Stanton Redcroft TG-750.

Optical and scanning electron micrographs were taken using an Olympus stereomicroscope and a Cambridge Stereoscan 600 electron microscope respectively.

REFERENCES - Chapter Five

1. a. D.T. Clark and D. Shuttleworth, J.Polym.Sci.Polym. Chem.Ed., 16, (1978), 1093.

   b. D.T. Clark and D. Shuttleworth, *ibid*, 17, (1979),1317.

   c. D.T. Clark and D. Shuttleworth, *ibid*, 18, (1980), 27.

   d. D.T. Clark and D. Shuttleworth, *ibid*, 18, (1980), 407.

   e. D.T. Clark and M.Z. Abrahman, *ibid*, 19, (1981), 2129.

   f. D.T. Clark and M.Z. Abrahman, *ibid*, 19, (1981), 2689.

   g. D.T. Clark and M.Z. Abrahman, *ibid*, 20, (1982), 691.

   h. D.T. Clark and M.Z. Abrahman, *ibid*, 20, (1982), 1717.

   i. D.T. Clark and M.Z. Abrahman, *ibid*, 20, (1982), 1729.

   j. D.T. Clark and M.M. Abu-Shbak, *ibid*, 21, (1983), 2907.

   k. D.T. Clark and M.M. Abu-Shbak, *ibid*, 22, (1984), 1.

   l. D.T. Clark and M.M. Abu-Shbak, *ibid*, 22, (1984), 17.

2. D. Shuttleworth, Ph.D. Thesis, Durham University, (1978).

3. M.J. Silvester, Ph.D. Thesis, Durham University, (1981).

4. D.J. Barker, D.M. Brewis, R.H. Dahm and L.R.J. Joy; Electrochimica Acta, 23, (1978), 1107.

5. D.J. Barker, D.M. Brewis, R.H. Dahm and L.R.J. Hoy; Polymer, 19, (1978), 856.

6. R.H. Dahm, D.J. Barker, D.M. Brewis and L.R.J. Hoy, Chapter 11 in "Adhesion 4", Ed. K.W. Allen, Applied Science, London, (1980).

7. R.H. Dahm; Chapter 10 in "Surface Analysis and Pretreatment of Plastics and Metals", Ed. D.M. Brewis, Applied Science, London, (1982).

8. J.O. Besenhard and H.P. Fritz; J.Electroanal.Chem., 53, (1974), 329.

9. G. Eichinger and J.O.Besenhard; J.Electroanal.Chem., 72, (1976), 1.

10. J. Simonet and H. Lund; J.Electroanal.Chem., 75, (1977),719.

11. Z. Pelzbauer, J. Baldrian, J. Jansta and F.P. Dousek; Carbon, 17, (1979), 317.

12. F.P. Dousek, J. Jansta and J. Baldrian, Carbon, 18, (1980), 13.

13. L. Kavan, Z. Bastl, F.P. Dousek and J. Jansta, Carbon, 22, (1984), 77.

14. S.A. Johnson, Ph.D. Thesis, Durham University, (1985).

15. A.B. Gil'man, R.R. Shiffrina, V.K. Potapov, V.M. Kolotyrkin, V.E. Platonov, K.V. Dvornikova and G.G. Yakobson, J. Fluorine Chem., 28, (1985), 47.

16. M.M. Ahmad and W.J. Feast, Mol.Cryst.Liq.Cryst., 118, (1985), 417.

17. S.F. Campbell, R. Stephens and J.C. Tatlow, Tetrahedron, 21, (1965), 2997.

18. W.J.M. van Tilborg, C.J. Smit and R.A. van Santen, Recueil, 98, (1979), 526.

19. See Chapter 1 and H. Yasuda, 'Plasma Polymerization', Academic Press, London,(1985).

20. W.J. Brennan, Ph.D. Thesis, Durham University, (1984).

21. D. Briggs and J.C. Rivière, Chapter 3 in "Practical Surface Analysis by Auger and X-ray Photoelectron Spectroscopy", Eds. D. Briggs and M.P. Seah, John Wiley, Chichester, (1983).

22. a. A. Dilks, Ph.D. Thesis, Durham University, (1977).

b. A. Dilks, Chapter 5 in "Electron Spectroscopy: Theory Techniques and Applications", Vol.4, Eds. C.R. Brundle and A.D. Baker, Academic Press,London, (1981).

23. Southampton Electrochemistry Group, "Instrumental Methods in Electrochemistry", Ellis Horwood,Chichester, (1985).

24. M.G. Cross, D. Walton, N.J. Morse, R.J. Mortimer, D.R. Rosseinsky and D.J. Simmonds, J.Electroanal.Chem., 189, (1985), 389.

25. Chapter 9 in ref. 23.

26. E.M. Genies, G. Bidan and A.F. Diaz, J.Electroanal.Chem., 149, (1983), 101.

27. E. Bosco and S.K. Rangarajan, J.Electroanal.Chem., 134, (1982), 213.

28. G.E. McGuire, Chapter 1 in "Applied Electron Spectroscopy for Chemical Analysis", Eds. H. Windawi and F. Ho, John Wiley, New York, (1982).

29. R. Hernandez, A.F. Diaz, R. Waltman and J. Bargon, J.Phys.Chem., 88, (1984), 3333.

30. D.T. Clark and J. Peeling, J.Polym.Sci.Polym.Chem., Ed., 14, (1976), 2941.

APPENDIX A

ELECTRON SPECTROSCOPY FOR CHEMICAL APPLICATIONS (ESCA)

A.1 Introduction

The basis of the ESCA experiment is the kinetic energy distribution analysis of photoelectrons emitted from a sample as a result of irradiation, in vacuum, by a nearly mono-energetic beam ofsoft X-rays. The two most commonly used photon sources are $MgK\alpha_{1,2}$ (1253.6eV) and $AlK\alpha_{1,2}$ (1486.6eV) for which photoionization cross-sections are greatest for core-level (tightly bound) electrons.[5]

ESCA was developed into the analytical tool it has become following the pioneering work of Siegbahn *et al* in the 1950s and 1960s.[1,2] Siegbahn *et al* developed the first spectrometer to employ a magnetic, double focussing electron energy analyser capable of a resolution of a few parts in 10^4 over a wide energy range.[1a,2] As a direct consequence of this unprecedented resolution it was possible to observe, for the first time, that the kinetic energy of photoelectrons ejected from core levels was characteristic not only of the element from which they were ejected but also the chemical state of that element.

The application of ESCA to organic and polymeric materials has been pioneered by Clark *et al*.[3]

ESCA is also widely referred to as X-ray Photoelectron Spectroscopy (XPS). Several texts and reviews devoted to the subject exist.[4] The following discussion is not comprehensive but rather concentrates on certain aspects of ESCA referred to in preceding chapters.

A.2 Processes involved in ESCA (see Figure A.1)

A.2.1 Photoionization

As stated in the introduction, the irradiation of atoms in a molecule or lattice by soft X-rays causes ejection of electrons bound by an energy less than that of the X-ray photon. For an isolated molecule or atom the kinetic energy (KE) of an ejected electron is given by the equation[1a]

$$KE = h\nu - BE - Er \qquad \text{(eqn. A.1)}$$

where $h\nu$ is the photon energy

BE is the binding energy of the ejected electron

Er is the recoil energy of the molecule or atom.

Er may be neglected for commonly used X-ray sources.[1a]

The probability of photoionization varies both with $h\nu$ and with the element and orbital from which the electron is ejected.[5] Using MgKα X-rays the probability of photoionization from the core level (1s) of carbon is *ca.* 20 times greater than for valence levels (2s+2p).[5]

If photoionization occurred in isolation from other events then binding energies would be given by the expression

$$BE = -\varepsilon_i \qquad \text{(eqn. A.2)}$$

where $-\varepsilon_i$ is the orbital energy of the ejected electron.†

---

† The negative sign is used since an electron in an atomic or molecular orbital is considered to be at a lower energy than a free electron.

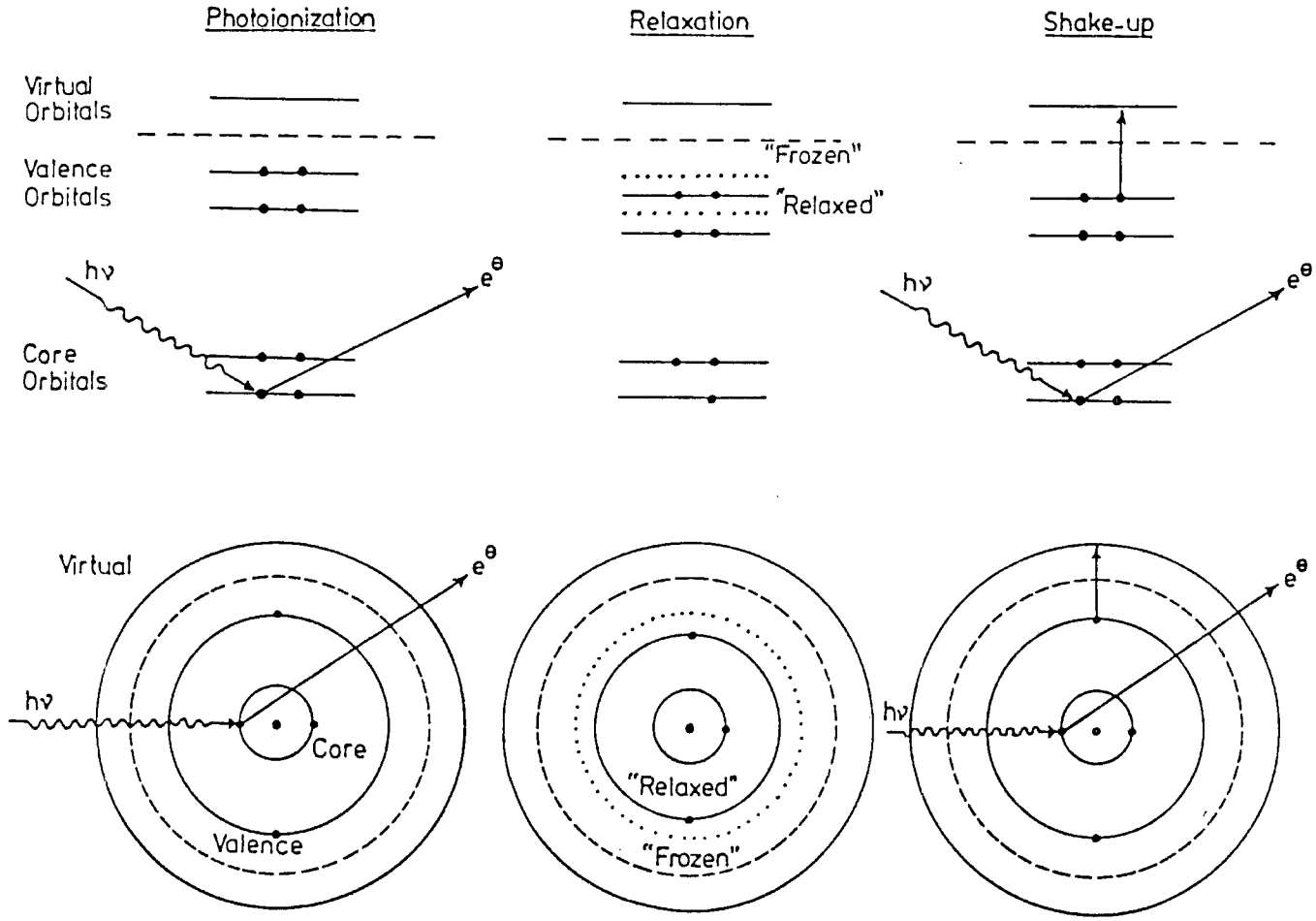

FIGURE A.1 Schematic of Photoionization, Relaxation and Shake-up

This is known as Koopmans' theorem[6] or the frozen orbital approximation. Calculated (LCAO-MO) orbital energies are generally greater than experimental binding energies. The major reason for this discrepancy is that electronic relaxation, which occurs in a timescale comparable to photoionization, is ignored in the frozen orbital approximation.

A.2.2 Relaxation

Removal of a core electron leads to a sudden increase in the effective nuclear charge experienced by the valence electrons. This causes a contraction of the valence electron shell to yield a more stable final core hole state than would result in the absence of this relaxation. Equation A.2 may be modified to allow for this stabilization

$$BE = -\varepsilon_i - RE \qquad \text{(eqn. A.3)}$$

where RE is the electronic relaxation energy.

An improvement over Koopmans' theorem is the ΔSCF method for calculation of binding energies.[7] In this method the binding energy is determined from the difference in calculated (LCAO-MO) heats of formation between the ground state and the final core hole state. The difference between the Koopmans' and ΔSCF binding energy is the relaxation energy (approximately).

A.2.3 Shake-up and shake-off processes

The sudden perturbation experienced by the valence electrons upon core level ionization gives rise to a finite probability for photoionization to be accompanied by simult-

aneous excitation of a valence electron, in addition to the relaxation process described above. Excitation to a higher bound state is known as "shake-up" whilst excitation to the continuum is referred to as "shake-off".[8] These processes result in an excited final core hole state and, because they occur in the same timescale as photoionization, satellite peaks may be observed at an energy

$$KE = h\nu - BE - \bar{E}$$

where $\bar{E}$ is the valence electron excitation energy.

For organic materials which contain localized unsaturation (*e.g.* polystyrene[8]) well defined, low energy, π-π^* shake-up peaks are observed. For solid samples higher energy shake-up peaks are swamped by the background signal caused by inelastically scattered photoelectrons. Clark[9] and Dilks[8] have shown that an investigation of shake-up structure in unsaturated hydrocarbon materials extends the scope of ESCA to the study of a class of compounds for which the chemical shift range is negligible.

In metals, and conductors generally, the form of the density of states curve above the Fermi level provides a continuous range of allowed one electron excitation energies.[10] Shake-up in metals results in an asymmetric tailing to the low KE side of the main peak and not in the occurrence of resolved satellite peaks.[10]

A.2.4 Relaxation of the core-hole state

Core-hole state lifetimes are typically 10^{-14}-10^{-17}s.[11] De-excitation of the core hole state occurs by the demotion of an electron from a valence level or less tightly bound core

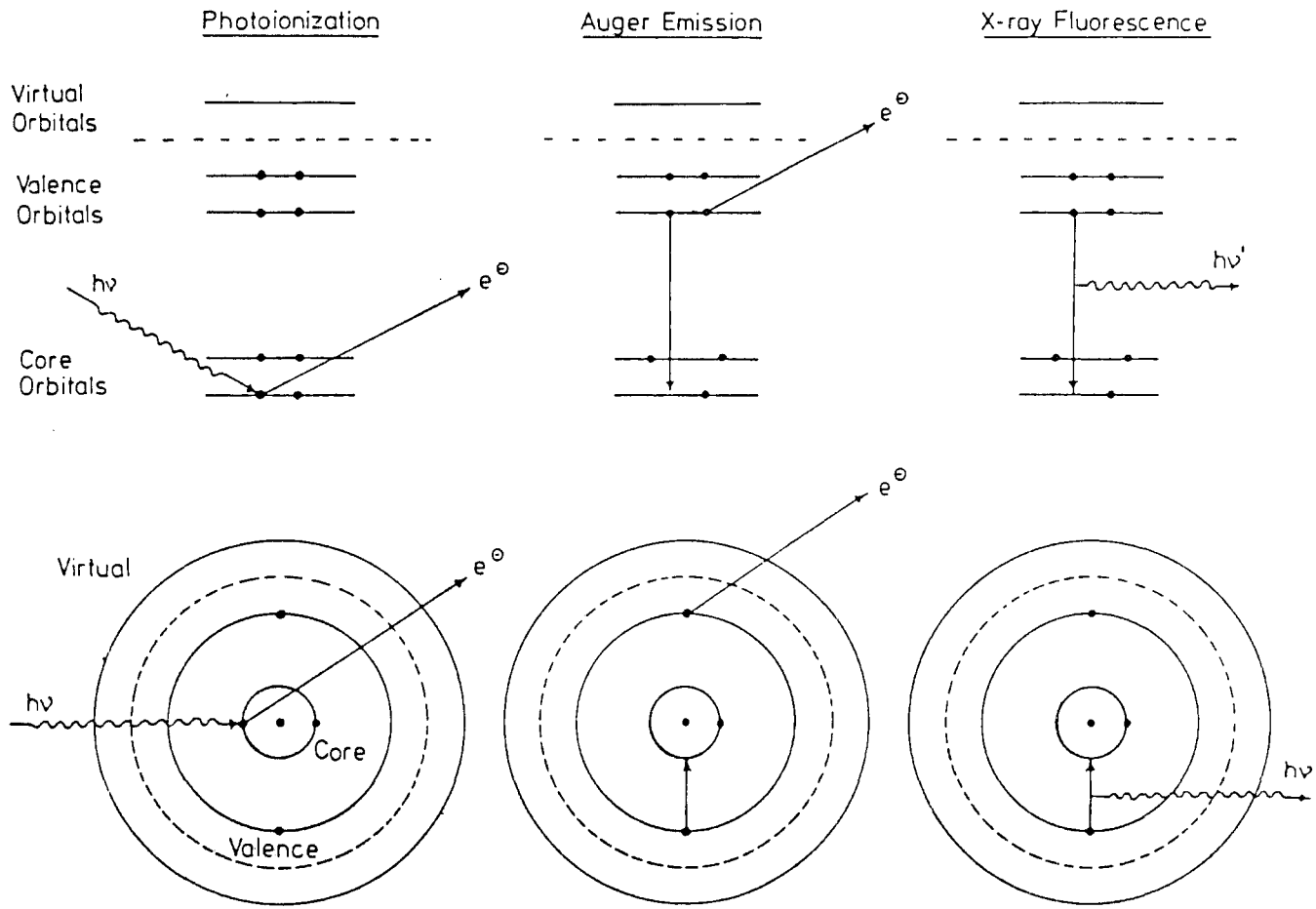

FIGURE A.2 Schematic of Photoionization, Auger Emission and X-ray Fluorescence

level to fill the vacancy created by photoionization. The demoted electron gives up its excess energy either as an X-ray quantum (X-ray fluorescence) or in the ejection of a second electron to yield a doubly ionized final state (the Auger process). Both de-excitation processes are delineated in Figure A.2. For a 1s core hole Auger emission is the most probable de-excitation process for light elements ($Z \leq 33$), whilst X-ray fluorescence is predominant for heavy elements.[1a]

A.3 Features of ESCA Spectra

A.3.1 Binding Energies, Calibration and Energy referencing

Core electrons are essentially localized on atoms and their binding energies are characteristic for the element with which they are associated.

For convenience binding energies are referenced to the Fermi level. An energy level diagram which represents the situation for an electronically conducting sample in electrical contact with the spectrometer is shown in Figure A.3. Electrical connection of a conducting sample to the spectrometer is analogous to earthing an electrical instrument. Charge flows to or from the sample until its Fermi level matches that of the spectrometer. Generally the spectrometer and sample will have different work functions (ϕ) and so the vacuum level of the sample will be displaced from that of the spectrometer by an amount $|\phi_{spec.} - \phi_s|$. This work function difference gives rise to an attractive ($\phi_{spec} < \phi_s$) or repulsive ($\phi_{spec} > \phi_s$) potential for electrons between the sample and the

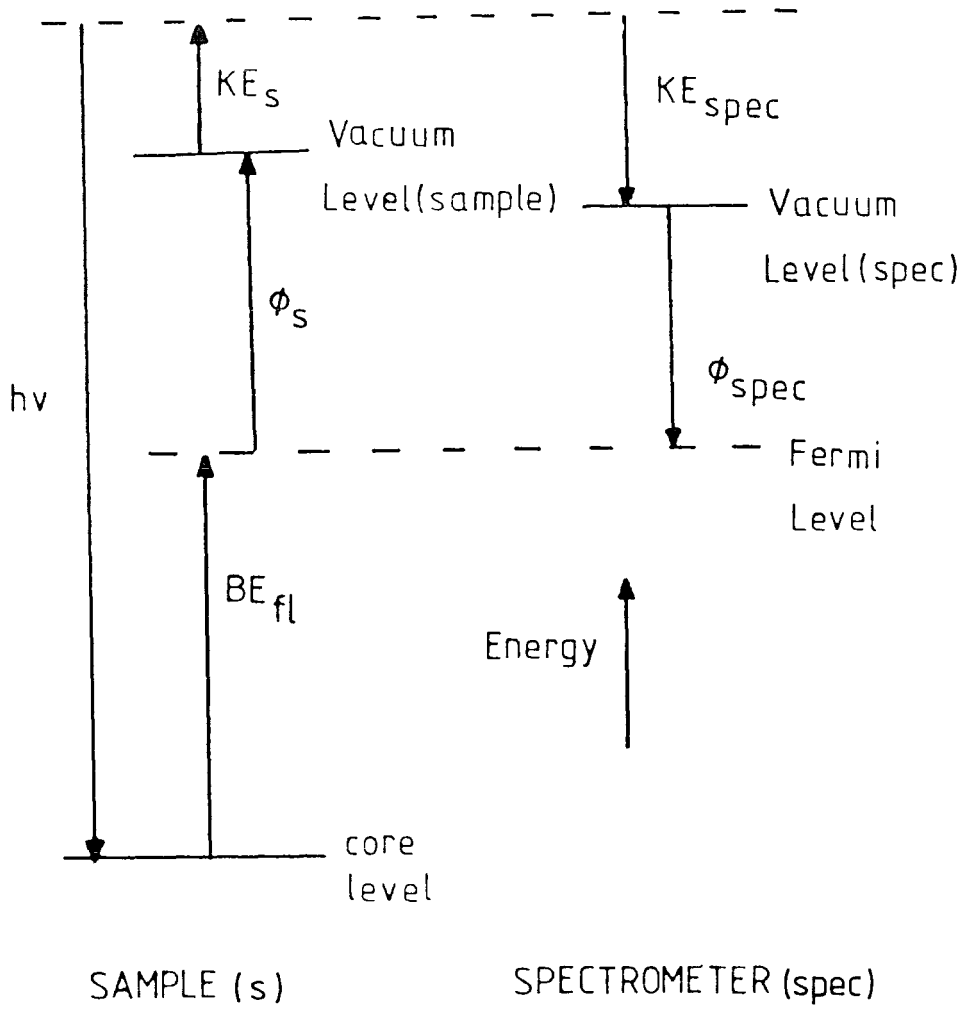

FIGURE A.3 Energy level diagram for a Conducting Sample in Electrical contact with the Spectrometer

spectrometer analyser.[12] The energy required to eject an electron with zero kinetic energy is $BE_{fl}+\phi_s$. This electron is accelerated towards or repelled from the analyser by an amount $(\phi_{spec} - \phi_s)$. The measured kinetic energy is therefore given by

$$KE = h\nu - BE_{fl} - \phi_s - (\phi_{spec} - \phi_s)$$

$$KE = h\nu - BE_{fl} - \phi_{spec} \qquad \text{(eqn. A.3)}$$

By referencing binding energies to the Fermi level a constant correction factor of ϕ_{spec} arises for all samples. The equivalent expression for binding energies referenced to the sample vacuum level is

$$KE = h\nu - BEvl - (\phi_{spec} - \phi_s)$$

It is clear from equation A.3 that it is not possible to calibrate the kinetic energy scale of an electron energy analyser by adjusting a single measured binding energy to the tabulated value since ϕ_{spec} is generally unknown. Instead the energy scale is calibrated to the binding energy separation of 2 core levels, using conducting samples. In the present studies a 284.4eV separation between $Au_{4f_{7/2}}$ and $Ag_{3d_{5/2}}$ was used as calibration standard.[13]

For insulating samples and conducting samples electrically isolated from the spectrometer, the resulting difference in Fermi levels invalidates eqn. A.3. Furthermore insulating samples become positively charged since electrons lost by photoionization are not replaced by conduction. This sample charging is partially offset by the flux of low energy secondary electrons emanating from the sample and spectrometer walls.[14] The result is the rapid attainment of an equilibrium sample charging of a few eV.[8] The appropriate form of equation A.3 for an insulating sample is

$$KE = h\nu - BE_{fl(spec)} - \Delta$$

where Δ accounts for work function and Fermi level differences as well as for sample charging. In practice the value of Δ is determined from a reference signal, usually hydrocarbon at 285.0eV. The hydrocarbon may be intrinsic to the sample or derive from extraneous surface contamination. Thin samples on gold substrates may be referenced to the $Au_{4f_{7/2}}$ peak at 84.0eV. Problems in binding energy referencing occur if a sample is unevenly or <u>differentially</u> charged.[18]

It should be noted that the magnitude of sample

charging varies with elemental composition. Materials rich in elements of high photoionization cross section (*e.g.* highly fluorinated polymers) will charge to a greater extent than those which are not (*e.g.* hydrocarbon polymers).[8]

A.3.2 Chemical Shifts

Although they are essentially localized, core electrons are sensitive to the valence electron distribution, which is dependent on the chemical state of the atom. Thus changes in the chemical environment of an atom give rise to shifts in core electron binding energies. An often quoted example is the C_{1s} core level spectrum of ethyl trifluoroacetate[2] (Figure A.4). Peak intensities are proportional to the number of carbon atoms in each environment.

Tables of binding energies and chemical shifts are available.[15] Whereas tabulated binding energies are sensitive to charge referencing and energy calibration differences, chemical shifts should be more reliable.

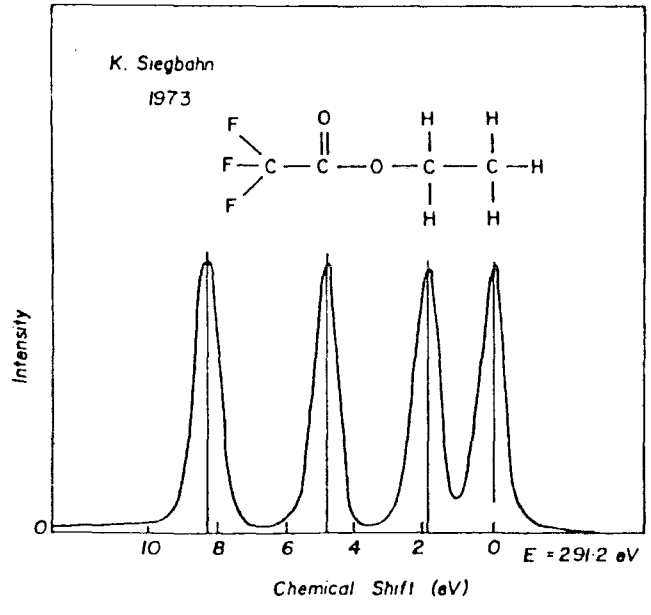

FIGURE A.4

A.3.3 Fine structure

(i) Spin-Orbit splitting

When photoionization takes place from a completely filled orbital of orbital quantum number (L) greater than 1 (*i.e.* not an s orbital) coupling between the resultant non-zero spin (S) and orbital (L) angular momenta leads to two possible values of total momentum (J). This coupling gives rise to a doublet structure in the ESCA spectrum[1a] (*e.g.* see Figure 4.2.1, Chapter Four). It should be noted that spin-orbit splitting is a final state effect, *i.e.* it is the presence of a single unpaired electron in a p, d or f orbital of the ionized state that leads to non-zero spin angular momentum and hence to spin-orbit splitting.[16]

The intensity ratio of the doublet components is given by the ratio of the degeneracies (2J+1) of the states (see Table A.1).

TABLE A.1

Orbital	Orbital Quantum No.	Total Quantum No.	Intensity Ratio
	L	$J = (L \pm S)$	(2J+1) : (2J+1)
s	0	$\frac{1}{2}$	singlet
p	1	$\frac{1}{2}$, $\frac{3}{2}$	1 : 2
d	2	$\frac{3}{2}$, $\frac{5}{2}$	2 : 3
f	3	$\frac{5}{2}$, $\frac{7}{2}$	3 : 4

(ii) Multiplet splitting

Multiplet splitting arises when interaction takes place between an unpaired electron created by photoelectron ejection and any unpaired electron already existing in the

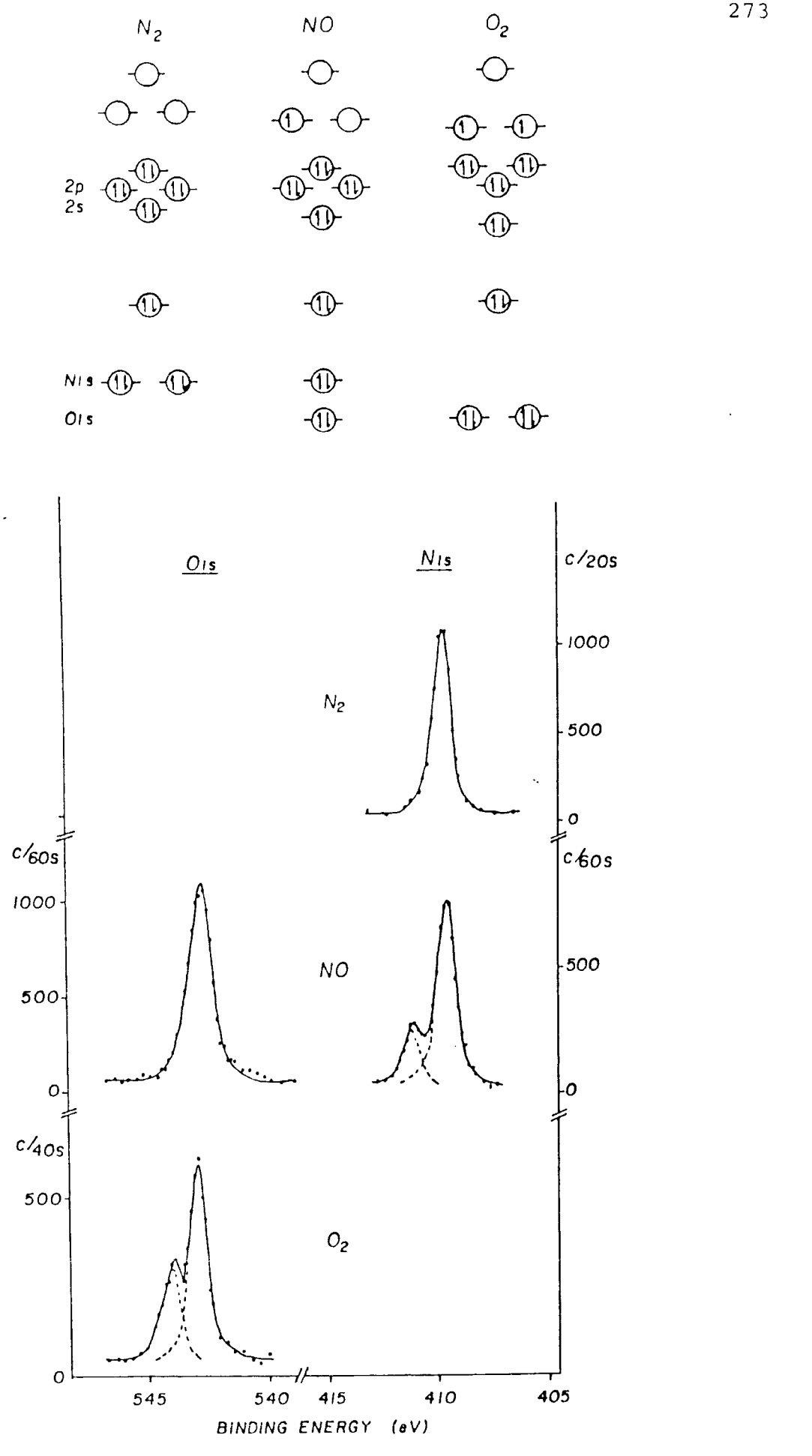

FIGURE A.5 Core Hole Spectra of N_2, NO and O_2 illustrating Multiplet Splitting

atom or molecule.[4c] The core level spectra of nitrogen, nitrous oxide and oxygen form an interesting example (Figure A.5).[1b] Nitrogen has an electron paired configuration and gives rise to a single photoionization peak. Nitrous oxide and oxygen both have unpaired electrons and show multiplet splitting in their core level spectra. The increased splitting of the N_{1s} signal compared to the O_{1s} signal for nitrous oxide indicates that most of the unpaired spin density is located on the nitrogen atom.

Multiplet splitting is frequently manifested as a peak broadening in the core level spectra of transition metal compounds[17] (*e.g.* Figure 2.4.1, Chapter Two).

A.4 Signal intensity

A.4.1 Homogeneous sample

Figure A.6 shows a schematic representation of the geometry of the ESCA experiment. The solid sample is assumed to be flat. The electron energy analyser entrance

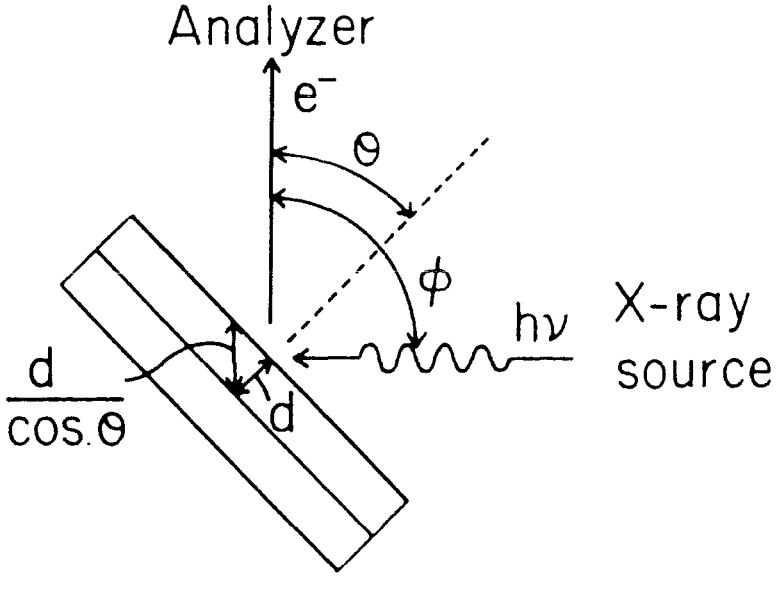

FIGURE A.6 Sample Geometry with respect to the Analyser and Photon Source

slit and the X-ray source subtend an angle ϕ at the sample surface. For the Kratos ES300 spectrometer used in this study ϕ is fixed at *ca.* 75^{o}. Detected photoelectrons emerge from the sample at an angle $(90-\theta)^{o}$ to its surface, θ is termed the electron take-off angle.

The detected intensity, I, of elastically scattered photoelectrons arising from a core level i in an infinitely thick sample is given by the differential equation

$$dI_i = F\alpha_i N_i k_i e^{-x/\lambda_i \cos\theta}\, dx \qquad \text{(eqn.A.4)}$$

where x is the distance into the sample measured normal to its surface. Since θ is usually non-zero x is modulated by $1/\cos\theta$ to allow for the increased distance a photoelectron must travel through the sample in the direction of the analyser.

F is the X-ray photon flux. F may be assumed to be unattenuated over the ESCA sampling depth which is defined by the mean free path of the photoelectrons (see A.4.3). F is a function of θ.

α_i is the photoionization cross section and represents the ionization probability for the core level i upon irradiation with X-ray photons. α_i varies with the core-level, the photon energy and ϕ. The photoionization cross sections for most core levels are within two orders of magnitude of each other which makes ESCA suitable for the study of all elements other than hydrogen and helium. Photoionization cross sections may be calculated[5] or determined experimentally.[2]

N_i is the number of atoms per unit area on which the core level is located. Although N_i is not directly related

to sample density it is generally the case that for similar materials of different density (*e.g.* low and high density polyethylene) I_i will be greater for the most dense material.[8]

k_i is a spectrometer factor which is related to the transmission characteristics of the electron lens/analyser system and the efficiency of the detector (electron multiplier). Both of these parameters vary with the kinetic energy of the photoelectrons (see Section A.5). In addition k_i may vary with θ (see Section A.4.2).

λ_i is the inelastic mean free path of the photoemitted electrons defined as the distance in the solid through which electrons will travel before $^1/_e$ of them have not suffered energy loss through inelastic collision. The mean free path of an electron depends upon its kinetic energy. For the energies involved in the ESCA experiment (KE>100eV)

$$\lambda_i \propto KE^{\frac{1}{2}}$$

approximately.[19]

Clark *et al* have measured mean free paths.[20,21] Typically for 500-1000eV electrons λ_i lies in the range 10-20 Å.

Integration of equation A.4

$$I_i^{\infty} = \int_0^{\infty} F\alpha_i N_i k_i e^{-x/\lambda_i \cos\theta} dx$$

gives

$$I_i^{\infty} = F\alpha_i N_i k_i \lambda_i \cos\theta \qquad \text{(eqn. A.5)}$$

(at fixed θ)

It should be noted that since F and k_i are functions of θ equation A.5 does not imply maximum signal intensity at a take-off angle of 0^o.

If subscripts i and j are used to represent different chemical elements (for the same or different core level) then at constant θ:

$$\frac{N_j}{N_i} = \frac{I_j^\infty}{I_i^\infty} \times \frac{\alpha_i k_i \lambda_i}{\alpha_j k_j \lambda_j}$$

N_j/N_i is the stoichiometric ratio of j and i in the sample. The term $\frac{\alpha_i k_i \lambda_i}{\alpha_j k_j \lambda_j}$ is a constant known as the instrumental sensitivity factor and this can be determined from standard compounds of known stoichiometry. For example, the sensitivity ratio of $Fe_{2p_{3/2}}$ to C_{1s} used in this study was determined from $K_3Fe(CN)_6$ and verified using samples of FeF_3 and PTFE.

A.4.2 Variation of signal intensity with electron take-off angle

Generally both the incident X-ray flux (F) and the spectrometer factor (k_i) depend upon θ. The X-ray source is divergent and Dilks has suggested that at small values of θ the top surface of the sample is eclipsed, from photons emanating from the part of the X-ray window below the axis about which θ varies, by the bottom surface of the sample and the probe-tip to which it is affixed.[8] This leads to a decrease in F as θ is decreased.

By means of an elegant experiment[22] Shuttleworth was able to show that, for an AEI ES200 spectrometer and using a sample of standard width, the edges of the sample fall

progressively further outside the solid angle of acceptance of the analyser as θ is reduced below a certain critical angle. Thus below this critical angle k_i will decrease with decrease in θ.

It was stated previously that at larger values of θ photoelectrons must travel further through the sample in order to be detected and this gives rise to the cosθ dependence of intensity in equation A.5. This increase in intensity as θ is decreased tends to offset the decreases mentioned above with the result that a maximum in signal intensity is found as θ is varied. For the C_{1s} core level this angle was found to be *ca.* 34° for an ES200 spectrometer.[8]

A.4.3 Vertically inhomogeneous samples, the substrate overlayer model

If a sample is vertically inhomogeneous, consisting of an overlayer (over) of thickness d and containing an element and core level i (*e.g.* C_{1s}) covering a substrate (subs) containing an element and core level $_j$ (*e.g.* Au_{4f}) as shown in Figure A.7 then integration of equation A.4 between appropriate limits gives:

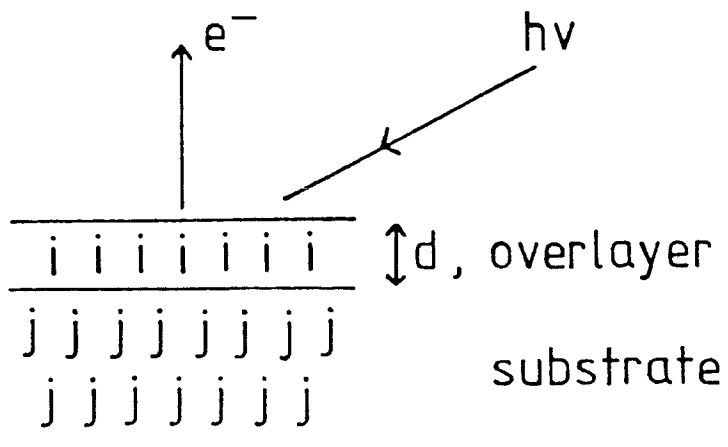

FIGURE A.7 Schematic of the Substrate-Overlayer Model

$$I_i^{over} = \int_o^d F\alpha_i N_i k_i e^{-x/\lambda_i \cos\theta} dx$$

$$I_i^{over} = F\alpha_i N_i k_i \lambda_i \cos\theta \ (1-e^{-d/\lambda_i \cos\theta}) \qquad \text{(eqn. A.6)}$$

and

$$I_j^{subs} = \int_d^\infty F\alpha_j N_j k_j e^{-x/\lambda_j \cos\theta} \ dx$$

$$I_j^{subs} = F\alpha_j N_j k_j \lambda_j \cos\theta e^{-d/\lambda_j \cos\theta} \qquad \text{(eqn. A.7)}$$

Dividing equations A.6 and A.7 by the form of equation A.5 appropriate for i or j gives

$$\frac{I_i^{over}}{I_i^{\infty}} = (1 - e^{-d/\lambda_i \cos\theta}) \qquad \text{(eqn. A.8)}$$

$$\frac{I_j^{subs}}{I_j^{\infty}} = e^{-d/\lambda_j \cos\theta} \qquad \text{(eqn. A.9)}$$

Thus by recording signal intensities for homogeneous samples of the overlayer and substrate materials which are effectively infinitely thick, as well as for the vertically inhomogeneous sample (Figure A.7), equation A.8 or A.9 may be used to calculate d if λ_i or λ_j is known. Alternatively if an independent method for determining the overlayer thickness, d, exists λ_i and λ_j may be calculated. Clark *et al* have used this method to calculate the inelastic mean free paths of C_{1s} and Au_{4f} photoelectrons ejected by MgKα and TiKα X-rays using films of polyparaxylylene deposited onto gold substrates.[20,21]

Equation A.9 also reveals that, for a vertically homogeneous sample, the contribution to the total signal intensity from a finite thickness layer decreases exponentially

with $\frac{d}{\cos\theta}$. For $\theta = 0^{o}$ substituting $d = \lambda_i$ into equation A.8 gives

$$\frac{I_i^{\lambda_i}}{I_i^{\infty}} = (1 - e^{-1}) = 0.63$$

This means that 63% of the total signal intensity derives from a depth equivalent to the electron mean free path. Similarly 86% of the signal arises from a depth $2\lambda_i$. The sampling depth for ESCA is defined as that depth from which 95% of the signal arises or $3\lambda_i$. A few hundred Angstroms therefore constitutes an effectively infinite sample thickness for the ESCA experiment. Since sampling depth is related to λ_i it is dependent upon the kinetic energy of the photoelectron ($\lambda_i \propto KE^{\frac{1}{2}}$). Thus non-destructive depth profiling may be performed in cases for which it is possible to study two core levels of the same element which have significantly different binding energies.[28] Alternatively if two X-ray sources of significantly different photon energy are available depth profiling using a single core level may be achieved.[21]

The electron take-off angle, θ, is generally non zero and so the <u>effective</u> sampling depth will be $3\lambda_i\cos\theta$. Thus the surface sensitivity of ESCA increases with θ. Variaton of electron take-off angle, which for the spectrometer used in this study is simply performed by rotation of the sample insertion probe, provides a generally applicable method of surface depth profiling.[28]

A.5 Electron energy analysis: sensitivity and resolution

The increase in sampling depth with electron kinetic energy gives rise to an increase in signal intensity with kinetic energy. However the signal intensity is also dependent upon the spectrometer factor, k, (equation A.5) which is, in turn, a function of kinetic energy. The form of this function depends both upon the construction of the spectrometer and its mode of operation.

After leaving the sample, photoelectrons enter a lens system which focusses them at the analyser entrance slit and retards their kinetic energies. Preretardation is used to improve resolution. The resolving power of a hemispherical analyser, of the type used in this study, is given by the expression[23]

$$\frac{\Delta E}{E_p} = \frac{0.63W}{R} \qquad \text{(eqn. A.10)}$$

where ΔE is the FWHM of a singlet peak and is known as the absolute resolution,

E_p is the pass energy of the analyser, *i.e.* the electron kinetic energy after preretardation,

W is the analyser slit width

R is the mean radius of the hemispheres.

It may be noted that, for a given analyser and slit width, resolution is improved by preretardation (E_p<KE).

Preretardation may be achieved by two methods of lens/analyser operation:

1. Fixed Retardation Ratio (FRR). Photoelectrons are retarded by a constant factor and transmission in the electron

lens is constant for all kinetic energies.[23] Thus E_p is directly proportional to KE (the energy with which the electrons leave the sample) and it may be deduced from equation A.10 that in FRR mode:

$$\text{resolution} \propto \frac{1}{KE}$$

hence

$$\text{sensitivity} \propto KE$$

If this sensitivity relationship is combined with the sampling depth dependence ($\propto KE^{\frac{1}{2}}$) and variations in electron detector efficiency with KE are neglected then in FRR:

$$\text{Signal intensity} \propto KE^{3/2}$$

2. Fixed Analyser Transmission (FAT). Photoelectrons are retarded to a constant E_p, the resolution is therefore independent of KE. Lens transmission is a function of KE, although not a simple one,[24] and the effect is to decrease sensitivity as KE increases. Thus in FAT mode

$$\text{resolution} = \text{constant}$$

$$\text{sensitivity} \downarrow \text{ as } KE \uparrow$$

Seah *et al* have reported the results of an investigation of the variation of observed signal intensity with KE for an ES300 spectrometer in both FRR and FAT operation modes.[24a,b]

The observed signal line shape is a convolution of several functions (the photon source, the core hole lifetime and spectrometer aberrations). Under the resolution conditions employed in the present study the standard lineshape is essentially Gaussian but with Lorentzian character in the tails. For insulators it has been shown that the assumption of a pure

Gaussian lineshape leads to only small errors in spectral analysis.[1b]

In the present study individual spectral envelopes were fitted exclusively with Gaussian components of constant FWHM at component positions which were, as far as possible, consistent with experimentally determined chemical shifts for standard compounds. Dilks has presented a logic flow chart for lineshape analysis.[8]

A.6 Instrumentation

A schematic of an ESCA spectrometer is shown in Figure A.8.

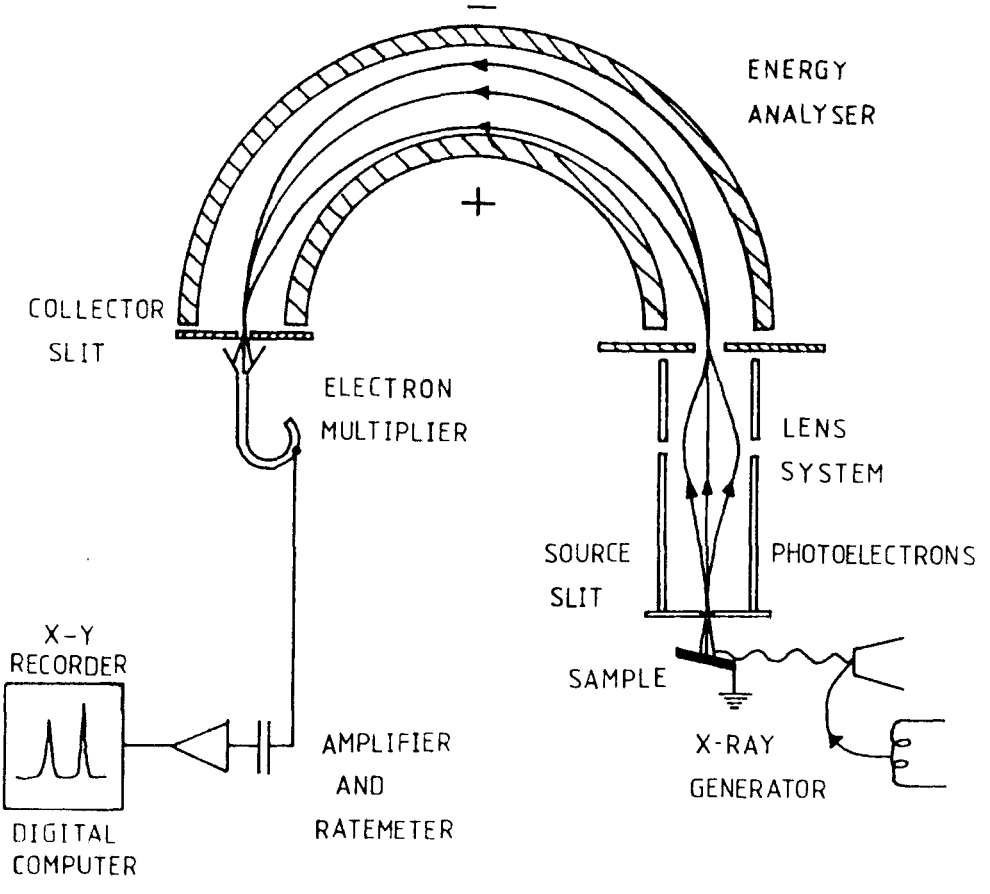

FIGURE A.8

The instrument used in the present study was a Kratos ES300. Specific discussions of this instrument have been presented[25,26] as have general accounts of ESCA equipment.[23] Table A.2 lists some of the operating parameters used and options available with the ES300.

TABLE A.2 Kratos ES300 operating parameters[a]

X-ray source	MgKα(1253.6eV)[b] / TiKα(4510eV)
Analyser type	Concentric hemispherical, electrostatic
Analyser operation mode	Fixed Retarding Ratio (FRR) / Fixed Analyser Transmission (FAT)
Calibration standard	$Au_{4f_{7/2}}$-$Ag_{3d_{5/2}}$ separation=284.4eV
Main pumping system	Turbomolecular
Typical operating pressure	1×10^{-3} torr

a. For a fuller discussion see refs. 25,26

b. The option underlined was used exclusively.

Data acquisition was computer controlled (LSI-11 mini-computer) and spectra were recorded onto floppy discs. Spectral manipulations (comparison or subtraction of spectra, background subtraction, *etc*) were performed using the Kratos DS300 software. Curve fitting was carried out manually using the DS300 graphics software.

A.7 Sample Handling

Unless otherwise stated in the relevant chapter solids were attached to a probe tip using insulating, double-sided adhesive tape.

Volatile solids and liquids were deposited onto a liquid nitrogen cooled probe tip under high vacuum conditions.

REFERENCES - Appendix

1. a. K. Siegbahn *et al*; "ESCA: Atomic Molecular and Solid State Structure Studied by means of Electron Spectroscopy", Almquist and Wiksells, Uppsala, (1967).

   b. K. Siegbahn *et al*; "ESCA Applied to Free Molecules", North-Holland, Amsterdam, (1969).

2. K. Siegbahn, Rev.Mod.Phys. 54, (1982), 709.

3. a. D.T. Clark, Chapter 17 in "Photon, Electron and Ion Probes of Polymer Structure and Properties", Eds. D. Dwight, R.J. Fabish and H.R. Thomas, ACS, Washington, (1981).

   b. Chapter 6 in ref. 4b.

   c. D.T. Clark, Chapter 16 in "Polymer Surfaces", Eds. D.T. Clark and W.J. Feast, John Wiley, New York,(1978).

4. a. "Electron Spectroscopy: Theory, Techniques and Applications", Vols. 1-4, Eds. C.R. Brundle and A.D. Baker, Academic Press, London, (1977, 1978, 1979, 1981).

   b. "Handbook of X-ray and Ultraviolet Photoelectron Spectroscopy", Ed. D. Briggs, Heyden, London (1977).

   c. P.K. Ghosh, "Introduction to Photoelectron Spectroscopy", John Wiley, New York, (1983), and references therein.

   d. "Practical Surface Analysis by Auger and X-ray Photoelectron Spectroscopy", Eds. D. Briggs and M.P. Seah, John Wiley, Chichester, (1983).

5. J.H, Scofield, J.Electron Spectrosc.Relat.Phenom., 8, (1976), 129.

6. T.A. Koopmans, Physica, 1, (1933), 104.

7. a. P.S. Bagus, Phys.Rev., 139A, (1965), 619.

   b. U. Gelius and K. Siegbahn, Faraday Discussions of the Chemical Society, 54, (1972), 257.

8. A. Dilks, Chapter 5 in ref. 4a, Vol.4.

9. D.T. Clark, Chapter 17 in "Molecular Spectroscopy", Ed. A.R. West, Heyden, London, (1977).

10. a. S. Doniach and M. Sunjic, J.Phys., C3, (1970), 285.

b. G.K. Wertheim and P.H. Citrin, Topics in Applied Phys., 26, (1978), 197.

11. D.T. Clark, in "Advances in Polymer Friction and Wear", Vol.5A, p.257, Ed. L-H. Lee, Plenum, New York, (1974).

12. p. 346 in ref. 4c.

13. Operator's Handbook, ES300 Spectrometer, Kratos Ltd.

14. M.F. Ebel and M. Ebel, J.Electron Spectrosc.Relat. Phenom., 3, (1974), 169.

15. C.D. Wagner, W.M. Riggs, L.E. Davis, J.F. Moulder and G.E. Muildenberg, "Handbook of X-ray Photoelectron Spectroscopy", Perkin-Elmer Corp,, Minnesota, (1979).

16. "Physical Methods and Molecular Structure 2", S304, Unit 20, Photoelectron Spectroscopy", The Open University, Milton Keynes, (1977).

17. D.T. Clark, H.S. Munro, P. Finocchiaro, E. Libertini and A. Recca, Polymer Commun., 25, (1984), 5.

18. D.T. Clark and J. Peeling, J.Polym.Sci.Polym.Chem.Ed., 14, (1976), 2941.

19. C. Fadley, Chapter 1 in Vol.2 of ref. 4a.

20. D.T. Clark and H.R. Thomas, J.Polym.Sci.Polym.Chem.Ed., 15, (1977), 2843.

21. D.T. Clark, M.M. Abu-Shbak and W.J.Brennan, J.Electron Spectrosc.Relat.Phenom., 28, (1982), 11.

22. D. Shuttleworth, Ph.D. Thesis, Chapter 8, Durham University (1978).

23. J.C. Rivière, Chapter 2 in ref. 4d.

24. a. M.P. Seah and M.T. Anthony, Surf.Interf. Anal. 6, (1984), 230.

b. M.P. Seah, M.E. Jones and M.T. Anthony, *ibid*, 242.

c. For a different opinion, see ref. 13.

25. D.R. Hutton, Ph.D. Thesis, Durham University, (1983).

26. W.J. Brennan, Ph.D. Thesis, Durham University, (1984).

27. P. Swift, Methodes Physiques d'Analyse, 8, (1972), 43.

28. D. Briggs, Chapter 3 in ref. 4d.

APPENDIX B

RESEARCH COLLOQUIA, SEMINARS AND LECTURES

A. Lectures and Seminars organised by the Department of Chemistry during the period 1982-1985 (* denotes Lectures attended)

13.10.82* Dr. W.J. Feast (Durham)
"Approaches to the Synthesis of Conjugated Polymers"

14.10.82 Prof. H. Suhr (Tubingen, FRG)
"Preparative Chemistry in Nonequilibrium Plasmas"

27.10.82* Dr. C.E. Housecroft (Oxford High School/Notre Dame)
"Bonding capabilities of butterfly-shaped Fe_4 units. Implications for C-H bond activation in hydrocarbon complexes"

28.10.82 Prof. M.F. Lappert, FRS. (Sussex)
"Approaches to Asymmetric Synthesis and Catalysis using electron-rich olefins and some of their metal complexes"

15.11.82* Dr. G. Bertrand (Toulouse, France)
"Curtius Rearrangement in Organometallic Series: A route for new hybridised species"

24.11.82 Prof. F.R. Hartley (R.M.C.S., Shrivenham)
"Supported Metal-Complex Hydroformylation Catalysts"

24.11.82* Prof. G.G. Roberts (Applied Physics, Durham)
"Langmuir-Blodgett films: Solid state polymerisation of diacetylenes"

8.12.32 Dr. G. Wooley (Trent)
"Bonds in transition metal-cluster compounds"

12. 1.83* Dr. D.C. Sherrington (Strathclyde)
"Polymer-supported phase transfer catalysts"

9. 2.83* Dr. P. Moore (Warwick)
"Mechanistic studies in solution by stopped flow F.T.-NMR and high pressure NMR line broadening"

21. 2.83 Dr. R. Lynden-Bell (Cambridge)
"Molecular motion in the cubic phase of NaCN"

2. 3.83* Dr. D. Bloor (Queen Mary College, London)
"The solid-state chemistry of diacetylene monomers and polymers"

8. 3.83* Prof. D.C. Bradley, FRS (Queen Mary College, London)
"Recent Developments in Organo-Imido-Transition Metal Chemistry"

9. 3.83* Dr. D.M.J. Lilley (Dundee)
"DNA, Sequence, Symmetry, Structure and Supercoiling"

11. 3.83* Prof. H.G. Viehe (Louvain, Belgium)
"Oxidations on Sulphur" and
"Fluorine substitutions in radicals"
(The W.K.R. Musgrave Lecture)

16. 3.83* Dr. I. Gosney (Edinburgh)
"New extrusion reactions: Organic synthesis in a hot-tube"

25. 3.83 Prof. F.G. Baglin (Nevada, USA)
"Interaction induced Raman Spectroscopy in Supracritical ethane"

21. 4.83 Prof. J. Passmore (New Brunswick, Canada)
"Novel selenium-iodine cations"

4. 5.83* Prof. P.H. Plesch (Keele)
"Binary ionisation equilibria between two ions and two molecules. What Ostwald never thought of"

10. 5.83 Prof. W. Burger (Munich, FRG)
"New reaction pathways from trifluoromethyl-substituted heterodienes to partially fluorinated heterocyclic compounds"

11. 5.83* Dr. N. Isaacs (Reading)
"The application of high pressures to the theory and practice of organic chemistry"

13. 5.83* Dr. R. de Koch (Michigan/Amsterdam)
"Electronic structural calculations in organo-metallic cobalt cluster molecules. Implications for metal surfaces"

13. 5.83 Dr. T.B. Marder (UCLA/Bristol)
"The Chemistry of Metal-carbon and metal-metal multiple bonds"

16. 5.83* Prof. R.J. Lagow (Texas, USA)
"The chemistry of polylithium organic compounds. An unusual class of matter"

18. 5.83* Dr. D.M. Adams (Leicester)
"Spectroscopy at very high pressures

25. 5.83 Dr. J.M. Vernon (York)
"New heterocyclic chemistry involving lead tetraacetate"

15. 6.83 Dr. A. Pietrzykowski (Warsaw/Strathclyde)
"Synthesis, structure and properties of Aluminoxanes"

22. 6.83 Dr. D.W.H. Rankin (Edinburgh)
"Floppy molecules - the influence of phase on structure"

5. 7.83* Prof. J. Miller (Camfinas, Brazil)
"Reactivity in nucleophilic substitution reactions"

5.10.83* Prof. J.P. Maier (Basel, Switzerland)
"Recent approaches to spectroscopic characterization of cations"

12.10.83 Dr. C.W. McLeland (Port Elizabeth, Australia)
"Cyclization of aryl alcohols through the intermediacy of alkoxy radicals and aryl radical cations"

19.10.83 Dr. N.W. Alcock (Warwick)
"Aryl tellurium (IV) compounds, patterns of primary and secondary bonding"

26.10.83* Dr. R.H. Friend (Cavendish, Cambridge)
"Electronic properties of conjugated polymers"

30.11.83* Prof. I.M.G. Cowie (Stirling)
"Molecular interpretation of non-relaxation processes in polymer glasses"

2.12.83* Dr. G. M. Brooke (Durham)
"The fate of the ortho-fluorine in 3,3-sigmatropic reactions involving polyfluoro-aryl and -hetero-aryl systems"

14.12.83* Prof. R.J. Donovan (Edinburgh)
"Chemical and physical processes involving the ion-pair states of the halogen molecules"

10. 1.84* Prof. R. Hester (York)
"Nanosecond Laser Spectroscopy of Reaction Intermediates"

18. 1.84* Prof. R.K. Harris (UEA)
"Multi-nuclear solid state magnetic resonance"

8. 2.84 Dr. B.T. Heaton (Kent)
"Multi-nuclear NMR studies"

15. 2.84 Dr. R.M. Paton (Edinburgh)
"Heterocyclic Syntheses using Nitrile Sulphides"

7. 3.84 Dr. R.T. Walker (Birmingham)
"Synthesis and Biological Properties of some 5-substituted Uracic Derivatives; yet another example of serendipity in Anti-viral Chemotherapy"

21. 3.84* Dr. P. Sherwood (Newcastle)
"X-ray photoelectron spectroscopic studies of electrode and other surfaces"

21. 3.84* Dr. G. Beamson (Durham/Kratos)
"EXAFS: General Principles and Applications"

23. 3.84* Dr. A. Ceulemans (Leuven)
"The Development of Field-Type models of the Bonding in Molecular Clusters"

2. 4.84* Prof. K. O'Driscoll (Waterloo)
"Chain Ending reactions in Free Radical Polymerisation"

3. 4.84* Prof. C.H. Rochester (Dundee)
"Infrared Studies of Adsorption at the Solid-Liquid Interface"

25. 4.84 Dr. R.M. Acheson (Biochemistry, Oxford)
"Some Heterocyclic Detective Stories"

27. 4.84 Dr. T. Albright (Houston, U.S.A.)
"Sigmatropic Rearrangements in Organometallic Chemistry"

14. 5.84 Prof. W.R. Dolbier (Florida, USA)
"Cycloaddition Reactions of Fluorinated Allenes"

16. 5.84 Dr. P.J. Garratt (UCL)
"Synthesis with Dilithiated Vicinal Diesters and Carboximides"

22. 5.84* Prof. F.C. de Schryver (Leuven)
"The use of Luminescence in the study of micellar aggregates" and
"Configurational and Conformational control in excited state complex formation"

23. 5.84 Prof. M. Tada (Waseda, Japan)
"Photochemistry of Dicyanopyrazine Derivatives"

31. 5.84 Dr. A. Haaland (Oslo)
"Electron Diffraction Studies of some organo-metallic compounds"

11. 6.84* Dr. J.B. Street (IBM, California)
"Conducting Polymers derived from Pyrroles"

19. 9.84* Dr. C. Brown (IBM, California)
"New Superbase reactions with organic compounds"

21. 9.84* Dr. H.W. Gibson (Signal UOP, Illinois)
"Isomerization of Polyacetylene"

19.10.84 Dr. A. Germain (Languedoc, Montpellier)
"Anodic Oxidation of Perfluoro Organic Compounds in Perfluoroalkane Sulphonic Acids"

24.10.84* Prof. R.K. Harris (Durham)
"N.M.R. of Solid Polymers"

28.10.84* Dr. R. Snaith (Strathclyde)
"Exploring Lithium Chemistry: Novel Structures, Bonding and Reagents"

7.11.84* Prof. W.W. Porterfield (Hampden-Sydney College, USA)
"There is no Borane Chemistry (only Geometry)"

7.11.84* Dr. H.S. Munro (Durham)
"New Information from ESCA Data"

21.11.84* Mr. N. Everall (Durham)
"Picosecond Pulsed Laser Raman Spectroscopy"

27.11.84* Dr. W.J. Feast (Durham)
"A Plain Man's Guide to Polymeric Organic Metals"

28.11.84 Dr. T.A. Stephenson (Edinburgh)
"Some recent studies in Platinum Metal Chemistry"

12.12.84 Dr. K.B. Dillon (Durham)
"^{31}P N.M.R. Studies of some Anionic Phosphorus Complexes"

11. 1.85 Emeritus Prof. H. Suschitzky (Salford)
"Fruitful Fissons of Benzofuroxanes and Isobenzimidazoles (umpolung of o-phenylenediamine)"

13. 2.85 Dr. G.W.J. Fleet (Oxford)
"Synthesis of some Alkaloids from Carbohydrates"

19. 2.85 Dr. D.J. Mincher (Durham)
"Stereoselective Synthesis of some novel Anthracyclinones related to the anti-cancer drug Adriamycin and to the Steffimycin Antibiotics"

27. 2.85 Dr. R.E. Mulvey (Durham)
"Some unusual Lithium Complexes"

6. 3.85 Dr. P.J. Kocienski (Leeds)
"Some Synthetic Applications of Silicon-Mediated Annulation Reactions"

7. 3.85 Dr. P.J. Rodgers (I.C.I. plc. Agricultural Division, Billingham)
"Industrial Polymers from Bacteria"

12. 3.85 Prof. K.J. Packer (B.P.Ltd./East Anglia)
"N.M.R. Investigations of the Structure of Solid Polymers"

14. 3.85* Prof. A.R. Katritzky F.R.S. (Florida)
"Some Adventures in Heterocyclic Chemistry"

20. 3.85 Dr. M. Poliakoff (Nottingham)
"New Methods for detecting Organometallic Intermediates in Solution"

28. 3.85* Prof. H. Ringsdorf (Mainz)
"Polymeric Liposomes as Models for Biomembranes and Cells?"

24. 4.85* Dr. M.C. Grossel (Bedford College, London)
"Hydroxypyridone dyes - Bleachable one-dimensional Metals?"

25. 4.85 Major S.A. Shackelford (U.S. Air Force)
"In Situ Mechanistic Studies on Condensed Phase Thermochemical Reaction Processes: Deuterium Isotope Effects in HMX Decomposition, Explosives and Combustion"

1. 5.85 Dr. D. Parker (I.C.I. plc, Petrochemical and Plastics Division, Wilton)
"Applications of Radioisotopes in Industrial Research"

7. 5.85* Prof. G.E. Coates (formerly of University of Wyoming, U.S.A.)
"Chemical Education in England and America: Successes and Deficiencies"

8. 5.85 Prof. D. Tuck (Windsor, Ontario)
"Lower Oxidation State Chemistry of Indium"

3. 5.85 Prof. G. Williams (U.C.W. Aberystwyth)
"Liquid Crystalline Polymers"

9. 5.85 Prof. R.K. Harris (Durham)
"Chemistry in a Spin: Nuclear Magnetic Resonance"

14. 5.85 Prof. J. Passmore (New Brunswick, U.S.A.)
"The Synthesis and Characterisation of some Novel Selenium-Iodine Cations, aided by ^{77}Se N.M.R. Spectroscopy"

15. 5.85 Dr. J.E. Packer (Auckland, New Zealand)
"Studies of Free Radical Reactions in aqueous solution using Ionising Radiation"

17. 5.85 Prof. I.D. Brown (McMaster University, Canada)
"Bond Valence as a Model for Inorganic Chemistry"

21. 5.85 Dr. D.L.H. Williams (Durham)
"Chemistry in Colour"

22. 5.85 Dr. M. Hudlicky (Blacksburg, U.S.A.)
"Preferential Elimination of Hydrogen Fluoride from Vicinal Bromofluorocompounds"

22. 5.85 Dr. R. Grimmett (Otago, New Zealand)
"Some Aspects of Nucleophilic Substitution in Imidazoles"

4. 6.85 Dr. P.S. Belton (Food Research Institute, Norwich)
"Analytical Photoacoustic Spectroscopy"

13. 6.85 Dr. D. Woolins (Imperial College, London)
"Metal - Sulphur - Nitrogen Complexes"

14. 6.85 Prof. Z. Rappoport (Hebrew University, Jerusalem)
"The Rich Mechanistic World of Nucleophilic Cinylic Substitution"

19. 6.85 Dr. T.N. Mitchell (Dortmund)
"Some Synthetic and NMR - Spectroscopic Studies of Organotin Compounds"

26. 6.85 Prof. G. Shaw (Bradford)
"Synthetic Studies on Imidazole Nucleosides and the Antibiotic Coformycin"

12. 7.85* Dr. K. Laali (Hydrocarbon Research Institute, University of Southern California)
"Recent Developments in Superacid Chemistry and Mechanistic Considerations in Electrophilic Aromatic Substitutions; a Progress Report"

B. Lectures Organised by Durham University Chemical Society during the period 1982-1985 (* denotes lectures attended)

14.10.82* Mr. F. Shenton (County Analyst, Durham)
"There is death in the pot"

28.10.82 Prof. M.P. Lappert, F.R.S. (Sussex)
"The Chemistry of Some Unusual Subvalent Compounds of the Main Group IV and V Elements"

4.11.82* Dr. D.H. Williams (Cambridge)
"Studies on the Structures and Modes of Action of Antibiotics"

11.11.82 Dr. J. Cramp (I.C.I. plc)
"Lasers in Industry"
(Joint Lecture with the Society of Chemical Industry)

25.11.82* Dr. D.H. Richards, P.E.R.M.E. (Ministry of Defence)
"Terminally Functional Polymers - their Synthesis and Uses"

27. 1.83 Prof. D.W.A. Sharp (Glasgow)
"Some Rodox Reactions in Fluorine Chemistry"

3. 2.83* Dr. R. Manning (Dept. Zoology, Durham)
"Molecular Mechanisms of Hormone Action"

10. 2.83 Sir G. Allen, F.R.S. (Unilever Ltd.)
"U.K. Research"

17. 2.83* Prof. A.G. MacDiarmid (Pennsylvania)
"metallic Covalent Polymers (SN)x and (CH)x and their Derivatives"(R.S.C. Centenary Lecture)

3. 4.83* Prof. A.C.T. North (Leeds)
"The Use of a Computer Display System in Studying Molecular Structures and Interactions"

20.10.83* Prof. R.B. Cundall (Salford)
"Explosives"

3.11.83* Dr. G. Richards (Oxford)
"Quantum Pharmacology"

10.11.83* Prof. J.H. Ridd (U.C.L.)
"Ipso-Attack in Electrophilic Aromatic Substitution"

17.11.83* Dr. J. Harrison (Sterling Organic)
"Applied Chemistry and the Pharmaceutical Industry"
(Joint Lecture with the Society of Chemical Industry)

24.11.83* Prof. D.A. King (Liverpool)
"Chemistry in 2-Dimensions"

1.12.83* Dr. J.D. Coyle (The Open University)
"The Problem with Sunshine"

26. 1.84* Prof. T.L. Blundell (Birkbeck College, London)
"Biological Recognition: Interactions of Macromolecular surfaces"

2. 2.84* Prof. N.B.H. Jonathan (Southampton)
"Photoelectron Spectroscopy - A Radical Approach"

16. 2.84* Prof. D. Phillips (The Royal Institution)
"Luminescence and Photochemistry - A Light Entertainment"

23. 2.84* Prof. F.G.A. Stone F.R.S. (Bristol)
"The Use of Carbene and Carbyne Groups to Synthesise Metal Clusters"
(The Waddington Memorial Lecture)

1. 3.84* Prof. A.J. Leadbetter (Rutherford Appleton Labs.)
"Liquid Crystals"

8. 3.84* Prof. D. Chapman (Royal Free Hospital School of Medicine, London
"Phospholipids and Biomembranes: Basic Science and Future Techniques"

28. 3.84 Prof. H. Schmidbaur (Munich, F.R.G.)
"Ylides in Coordination Sphere of Metal: Synthetic, Structural and Theoretical Aspects"
(R.S.C. Centenary Lecture)

18.10.84* Dr. N. Logan (Nottingham)
"N_2O_4 and Rocket Fuels"

23.10.84* Dr. W.J. Feast (Durham)
"Syntheses of Conjugated Polymers. How and Why?"

8.11.84 Prof. B.J. Aylett (Queen Mary College, London)
"Silicon - Dead Common or Refined?"

15.11.84* Prof. B.T. Golding (Newcastle-upon-Tyne)
"The Vitamin B_{12} Mystery"

22.11.84* Prof. D.T. Clark (I.C.I. New Science Group)
"Structure, Bonding, Reactivity and Synthesis as Revealed by ESCA"
(R.S.C. Tilden Lecture)

29.11.84* Prof. C.J.M. Stirling (University College of North Wales)
"Molecules taking the Strain"

6.12.84* Prof. R.D. Chambers (Durham)
"The Unusual World of Fluorine"

24. 1.85* Dr. A.K. Covington (Newcastle-upon-Tyne)
"Chemistry with Chips"

31. 1.85* Dr. M.L.H. Green (Oxford)
"Naked Atoms and Negligee Ligands"

7. 2.85* Prof. A. Ledwith (Pilkington Bros.)
"Glass as a High Technology Material"
(Joint Lecture with the Society of Chemical Industry)

14. 2.85* Dr. J.A. Salthouse (Manchester)
"Son et Lumiere"

21. 2.85 Prof. P.M. Maitlis, F.R.S. (Sheffield)
"What Use is Rhodium?"

7. 3.85* Dr. P.W. Atkins (Oxford)
"Magnetic Reactions"

(C) Research Conferences attended (* indicates Poster presentation)

July 1983*	SERC Summer School on Surface Physics, University of York
September 1984	British Association for the Advancement of Science Annual Conference, University of East Anglia (Norwich)
April 1985	Polymer Surfaces and Interfaces, University of Durham
September 1985*	IUPAC Congress, UMIST (Manchester)

(D) First Year Induction Course, October 1982

This course consists of a series of one hour lectures on the services available in the department.

1. Departmental organisation
2. Safety matters
3. Electrical appliances and infrared spectroscopy
4. Chromatography and Microanalysis
5. Atomic absorptiometry and inorganic analysis
6. Library facilities
7. Mass spectrometry
8. Nuclear magnetic resonance spectroscopy
9. Glassblowing technique.